Nuclear emulsion detectors for colliders, dark matter search and medical physics

Giuliana Galati

Università di Bari Aldo Moro & INFN Bari

Nuclear emulsion detectors for colliders, dark matter search and medical physics

Giuliana Galati
Università di Bari Aldo Moro & INFN Bari

HOW DO THEY WORK

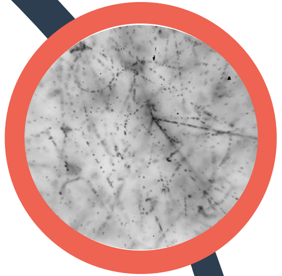

THEIR ORIGINS

OPERA

SND@LHC

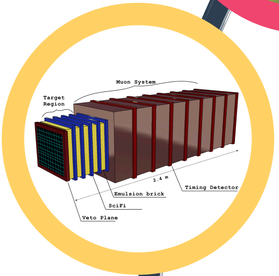

MUON RADIOGRAPHY

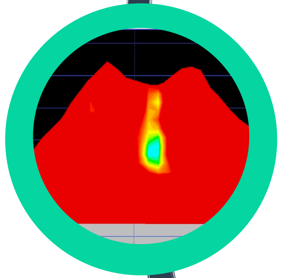

FOOT

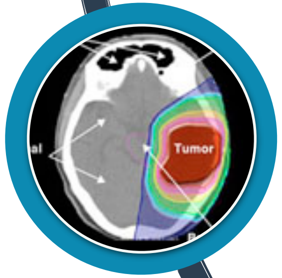

NEWSDM

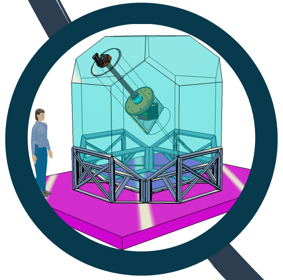

HOW DO THEY WORK

Main difference w.r.t. photographic films

- The ratio of silver halide to gelatine is up to ten times larger in nuclear emulsions (higher sensitivity)
- Nuclear emulsion is typically from 10 to 100 times thicker (3D reconstruction)
- Developed silver grains are smaller and more uniform

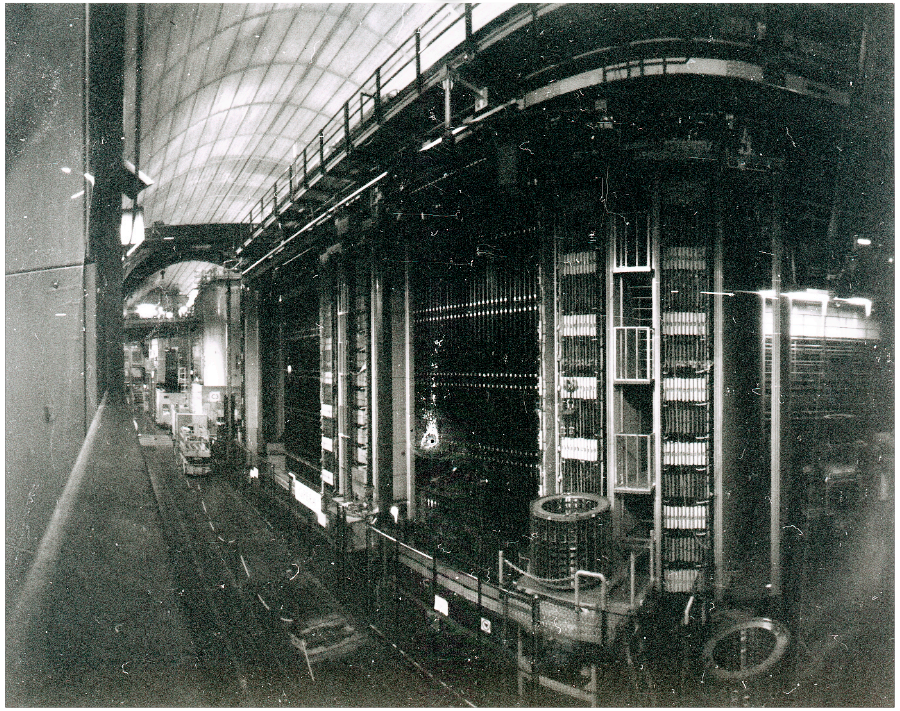

Image taken using OPERA emulsion film with pinhole handmade camera by Donato Di Ferdinando

Detection principle

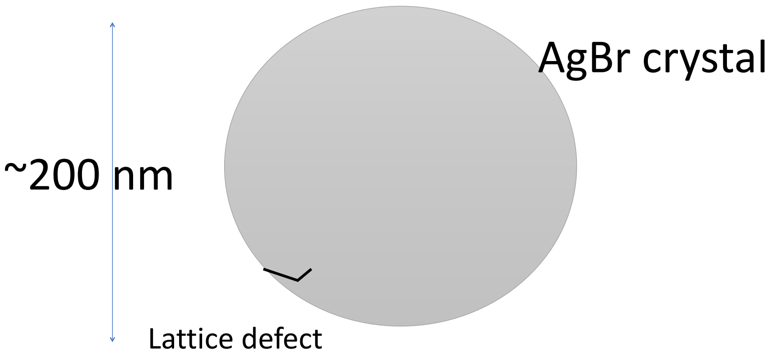

Detection principle

1. Ionization induced by a particle
    - 2.6 eV band gap

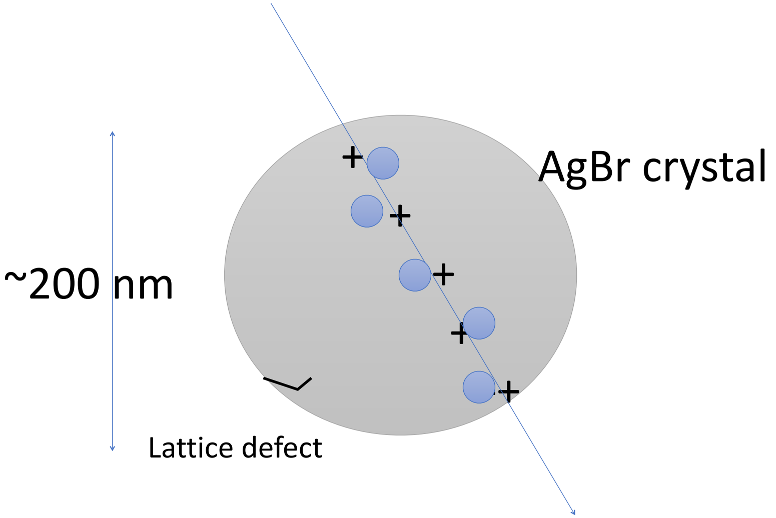

Detection principle

1. Ionization induced by a particle
   - 2.6 eV band gap

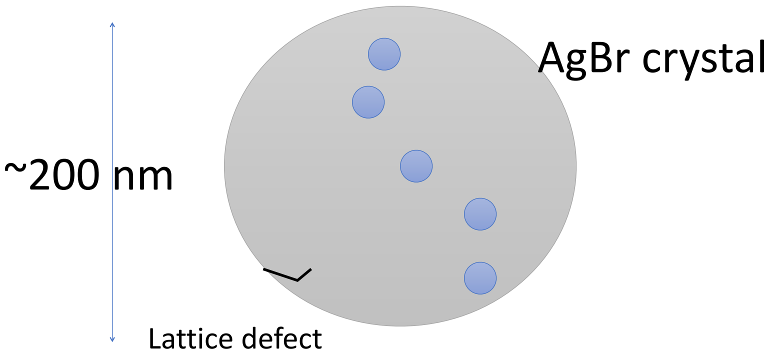

Detection principle

1. Ionization induced by a particle
   - 2.6 eV band gap
2. Electrons trapped at a lattice defect on the crystal surface
   - Attract interstitial silver ions
   - Produce a "latent image" = Ag_n

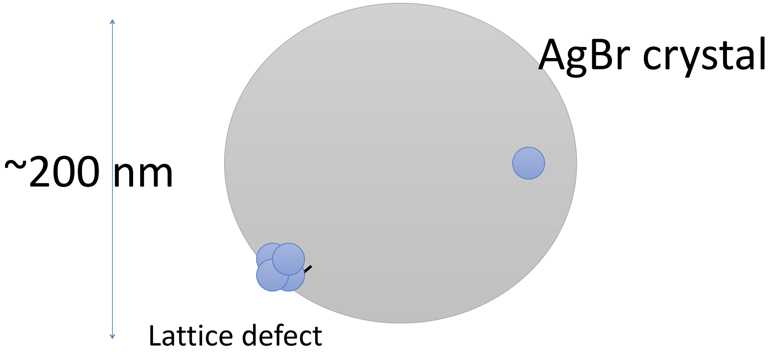

Detection principle

1. Ionization induced by a particle
   - 2.6 eV band gap
2. Electrons trapped at a lattice defect on the crystal surface
   - Attract interstitial silver ions
   - Produce a “latent image” = Ag_n

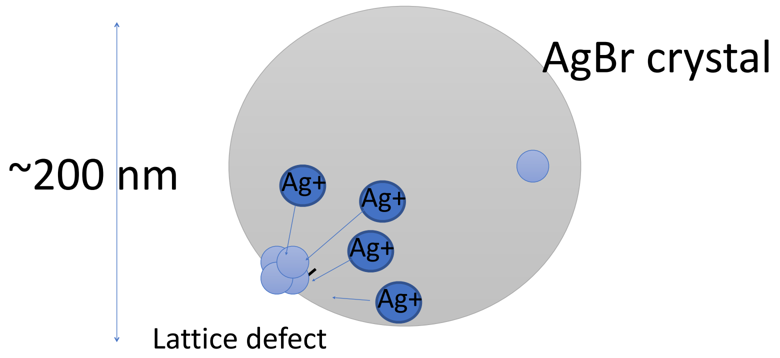

Detection principle

1. Ionization induced by a particle
   - 2.6 eV band gap
2. Electrons trapped at a lattice defect on the crystal surface
   - Attract interstitial silver ions
   - Produce a “latent image” = Ag_n

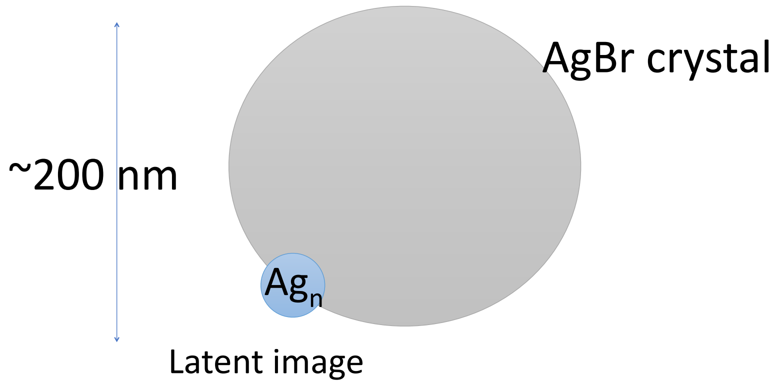

Detection principle

1. Ionization induced by a particle
   - 2.6 eV band gap
2. Electrons trapped at a lattice defect on the crystal surface
   - Attract interstitial silver ions
   - Produce a “latent image” = Ag_n
3. Chemical amplification of signal
   - Development →silver filaments
   - 10^7 - 10^8 amplification

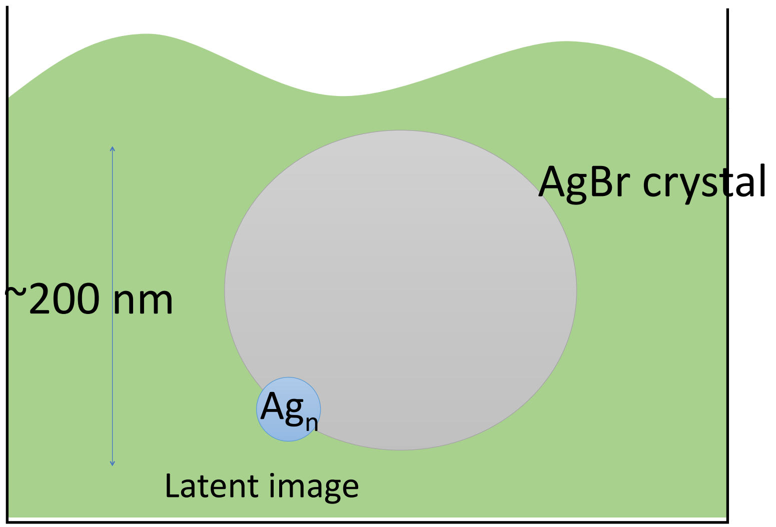

Detection principle

1. Ionization induced by a particle
   - 2.6 eV band gap
2. Electrons trapped at a lattice defect on the crystal surface
   - Attract interstitial silver ions
   - Produce a “latent image” = Ag_n
3. Chemical amplification of signal
   - Development →silver filaments
   - 10^7 - 10^8 amplification

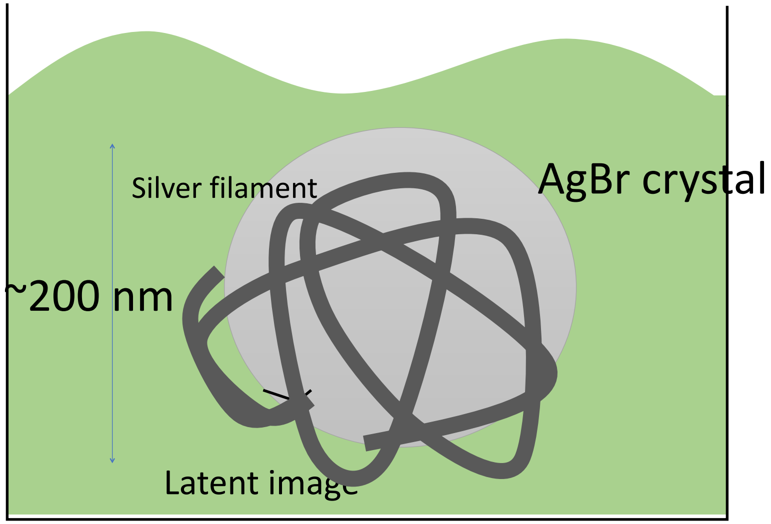

Detection principle

1. Ionization induced by a particle
   - 2.6 eV band gap
2. Electrons trapped at a lattice defect on the crystal surface
   - Attract interstitial silver ions
   - Produce a "latent image" = Ag_n
3. Chemical amplification of signal
   - Development →silver filaments
   - 10^7 - 10^8 amplification
4. Dissolve crystals

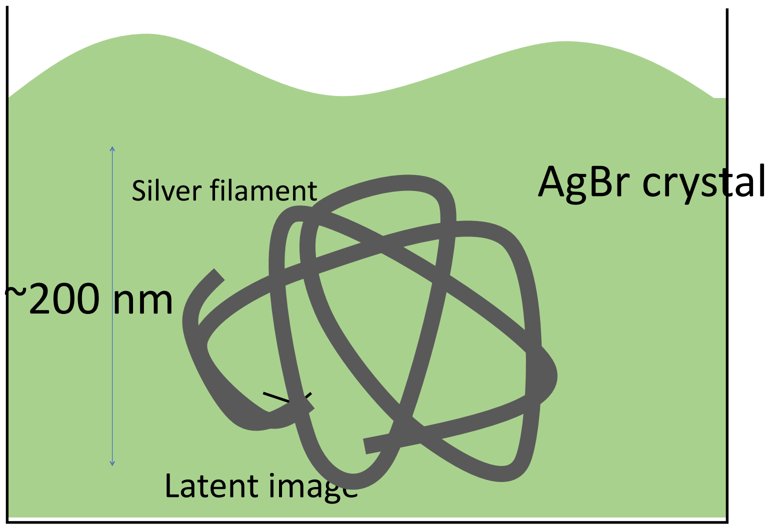

Detection principle

1. Ionization induced by a particle
   - 2.6 eV band gap
2. Electrons trapped at a lattice defect on the crystal surface
   - Attract interstitial silver ions
   - Produce a "latent image" = Ag_n
3. Chemical amplification of signal
   - Development →silver filaments
   - 10^7 - 10^8 amplification
4. Dissolve crystals
5. Observe it at optical microscopes

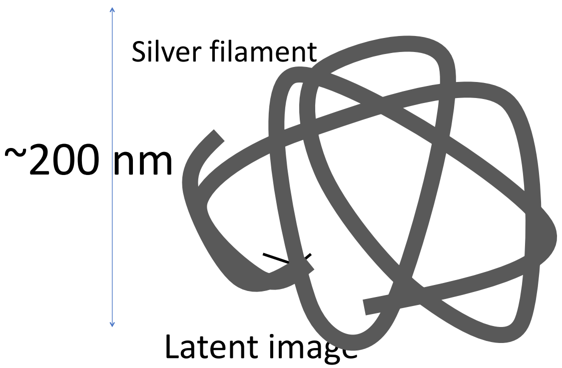

Detection principle

1. Ionization induced by a particle
   - 2.6 eV band gap
2. Electrons trapped at a lattice defect on the crystal surface
   - Attract interstitial silver ions
   - Produce a “latent image” = Ag_n
3. Chemical amplification of signal
   - Development → silver filaments
   - 10^7 - 10^8 amplification
4. Dissolve crystals
5. Observe it at optical microscopes

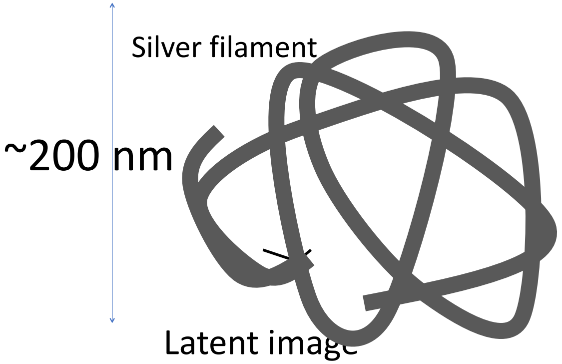

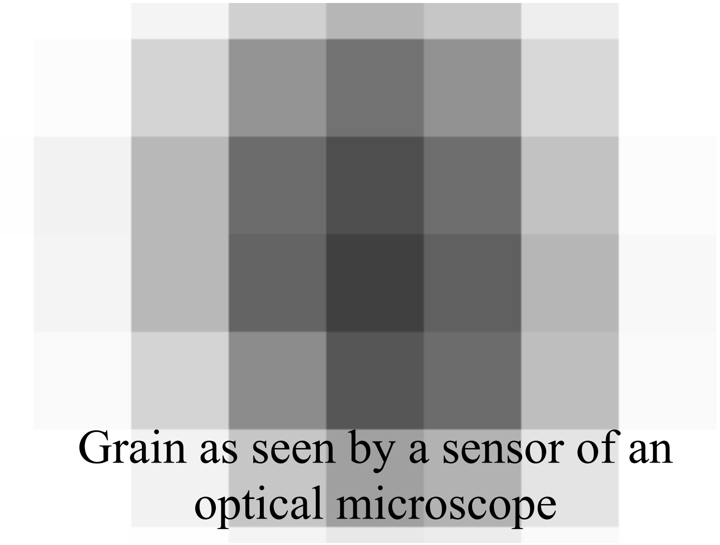

Grain as seen by a sensor of an optical microscope

Nuclear Emulsion chemical composition

- Standard emulsions composition: AgBr + gelatin
- Gelatine provides a 3D substrate to locate the crystals of silver halide and prevent them to migrate during the chemical development: keep the original position

OPERA films

Element	Mass fraction
Ag	0.3834
Br	0.2786
I	0.0081
C	0.13
N	0.0481
O	0.1243
H	0.024
S	0.001
Si	0.001
Na	0.001
K	0.0005

Grain dimension: ~ 200 nm

Nano Imaging Tracker (NIT)

Constituent	Mass Fraction	
AgBr-I	0.78	→ sensitive elements
Gelatin	0.17	→ retaining structure
PVA	0.05	→ to stabilise the crystal growth

Element	Mass Fraction	Atomic Fraction
Ag	0.44	0.10
Br	0.32	0.10
I	0.019	0.004
C	0.101	0.214
O	0.074	0.118
N	0.027	0.049
H	0.016	0.410
S	0.003	0.003

Grain dimension after development: $\sim 20 - 45$ nm

Detection principle

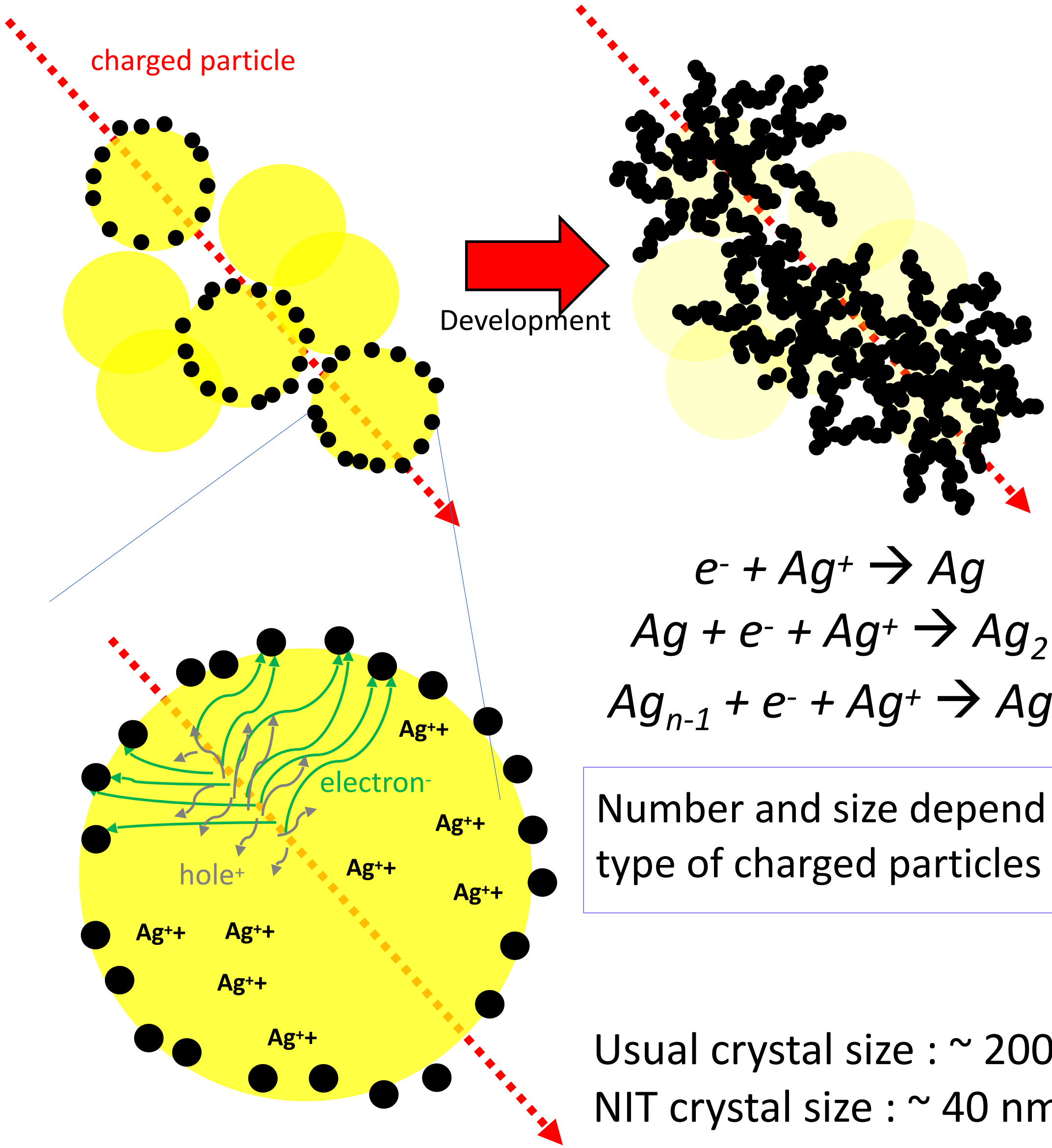

$$e^- + Ag^+ \rightarrow Ag$$
$$Ag + e^- + Ag^+ \rightarrow Ag_2$$
$$Ag_{n-1} + e^- + Ag^+ \rightarrow Ag_n$$

Number and size depend on the type of charged particles (dE/dx)

Usual crystal size : ~ 200 nm
NIT crystal size : ~ 40 nm

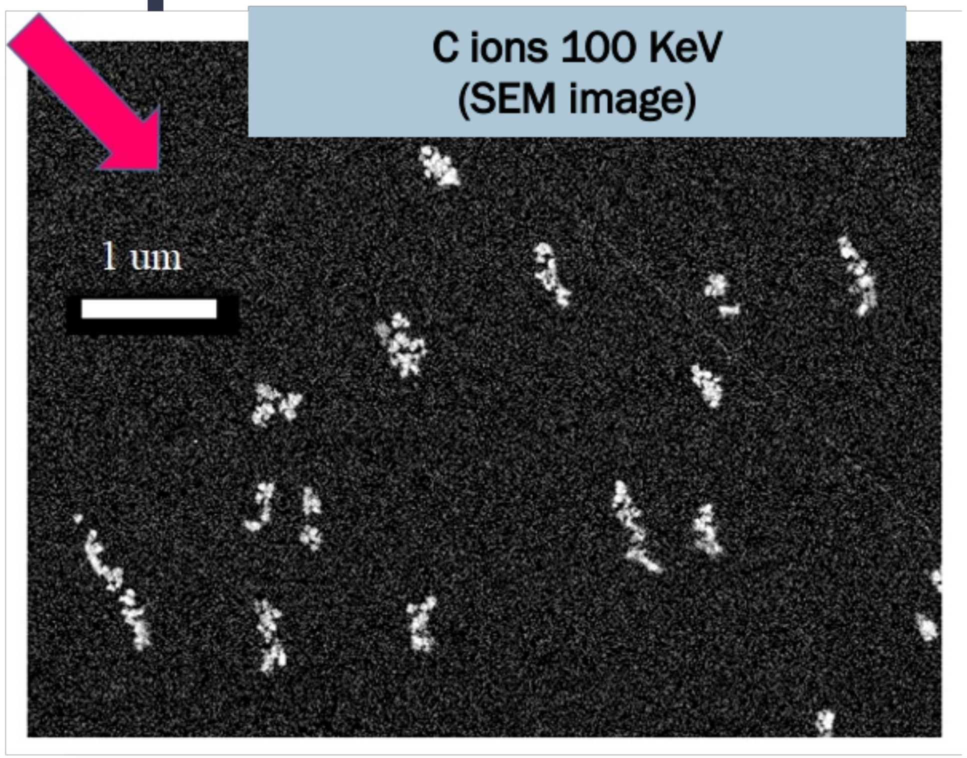

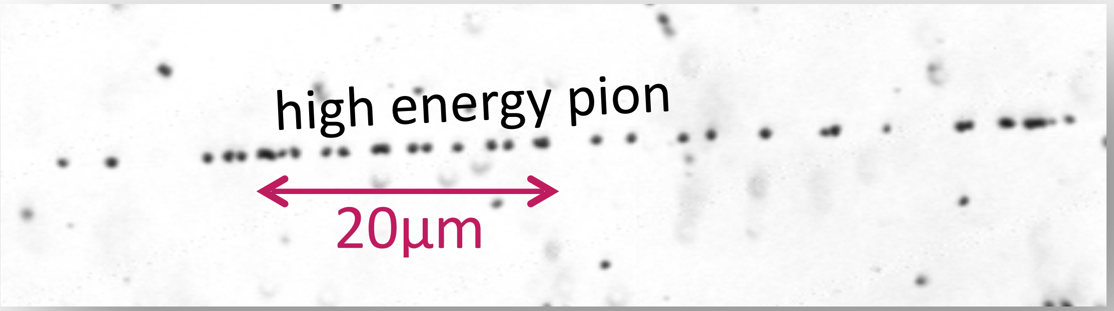

Production process

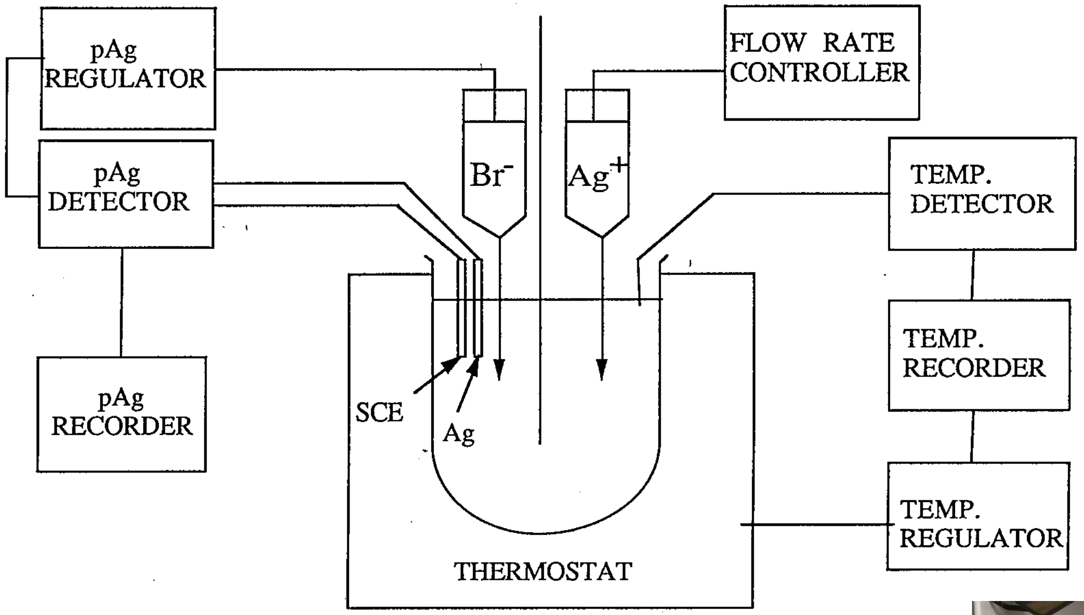

Gelatin aqueous solution

$AgNO_3 + KX \rightarrow AgX + KNO_3$ in an aqueous gelatin solution

K can be replaced by Na

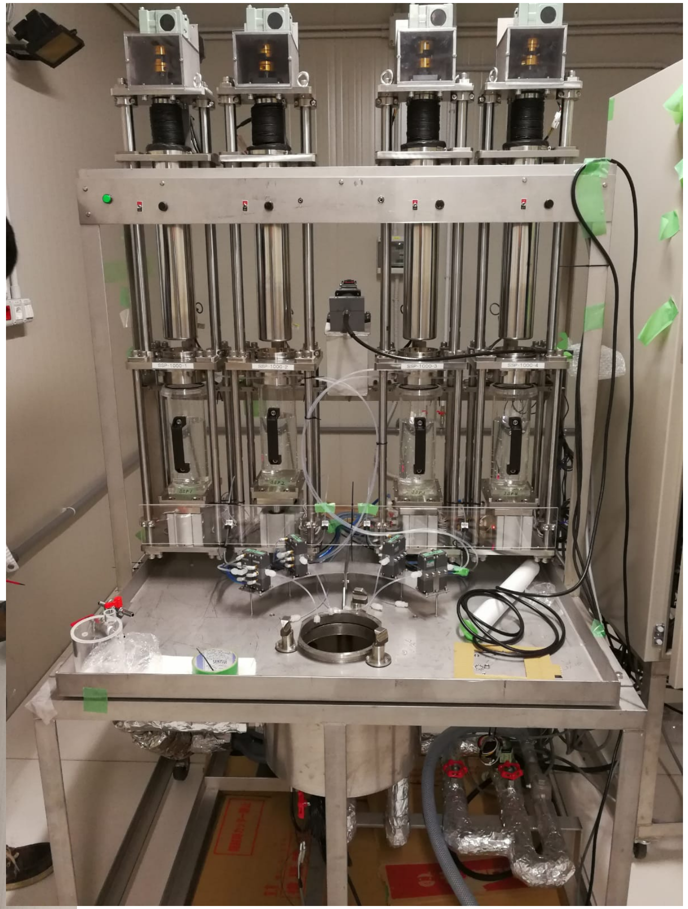

Production machine installed underground at Gran Sasso (Italy)

Production process

Crystal formation

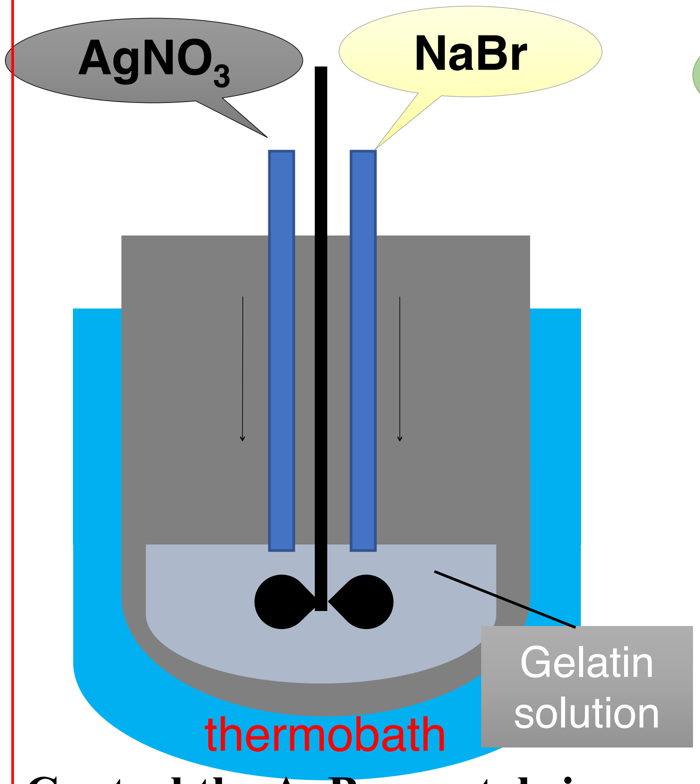

Control the AgBr crystal size
Temperature, insertion speed
Concentration of chemical, pAg control, rotation speed

wash/salt reduction

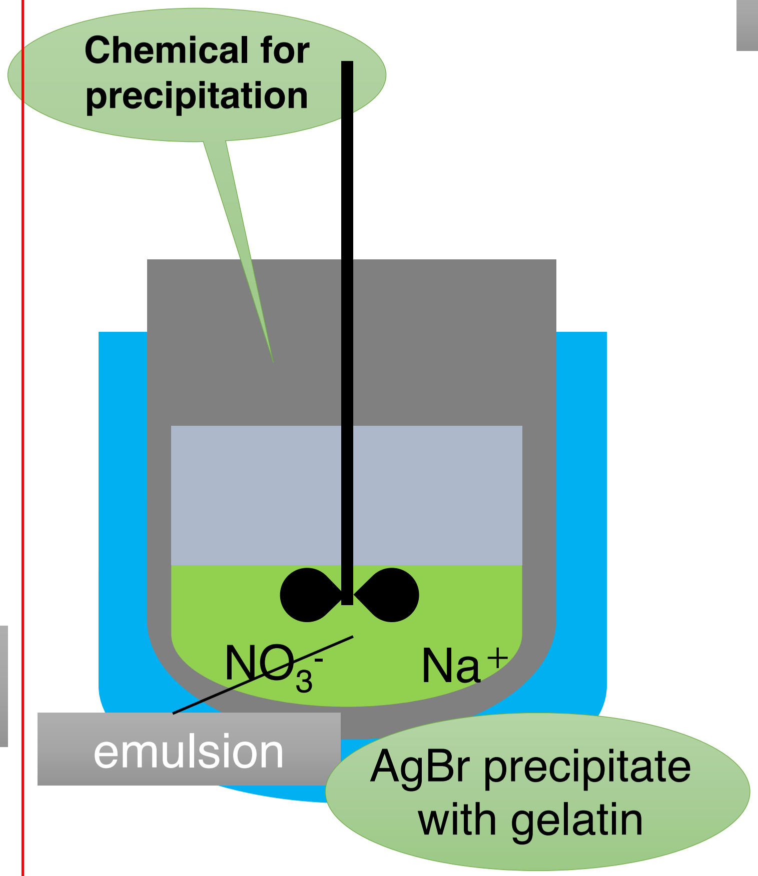

Apply

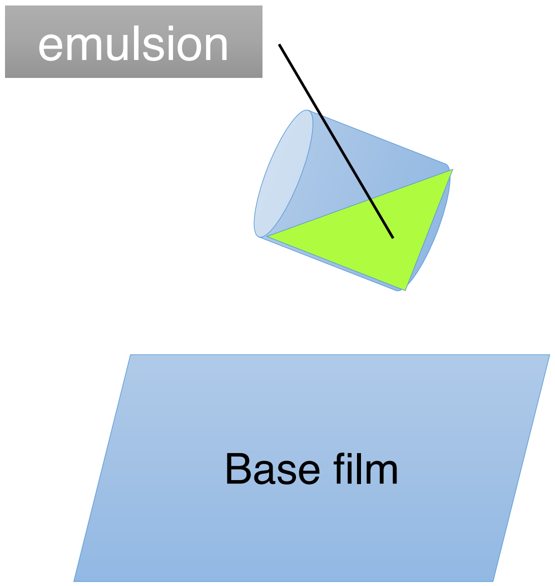

Control of dry condition

Temperature, humidity, Thickness etc.

Production process

Crystal formation

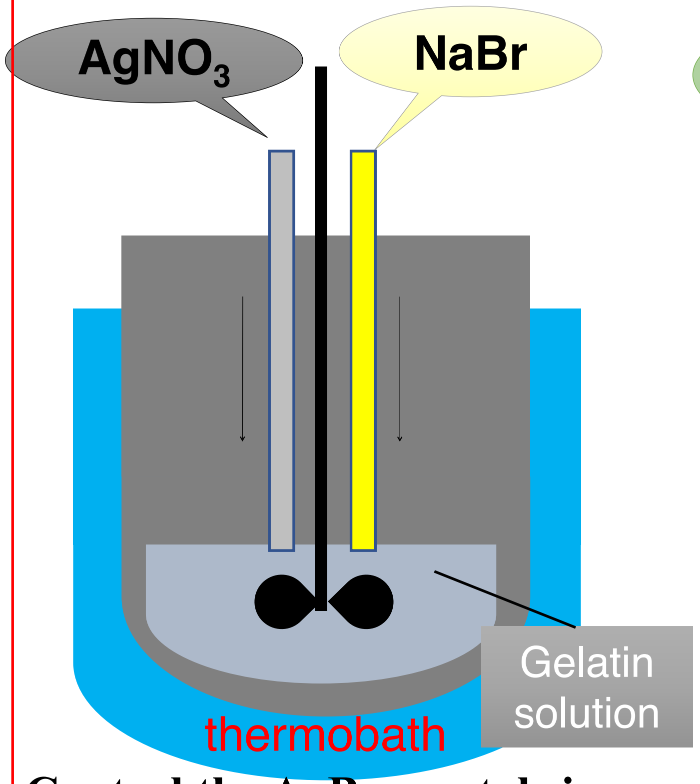

Control the AgBr crystal size
Temperature, insertion speed
Concentration of chemical, pAg control, rotation speed

wash/salt reduction

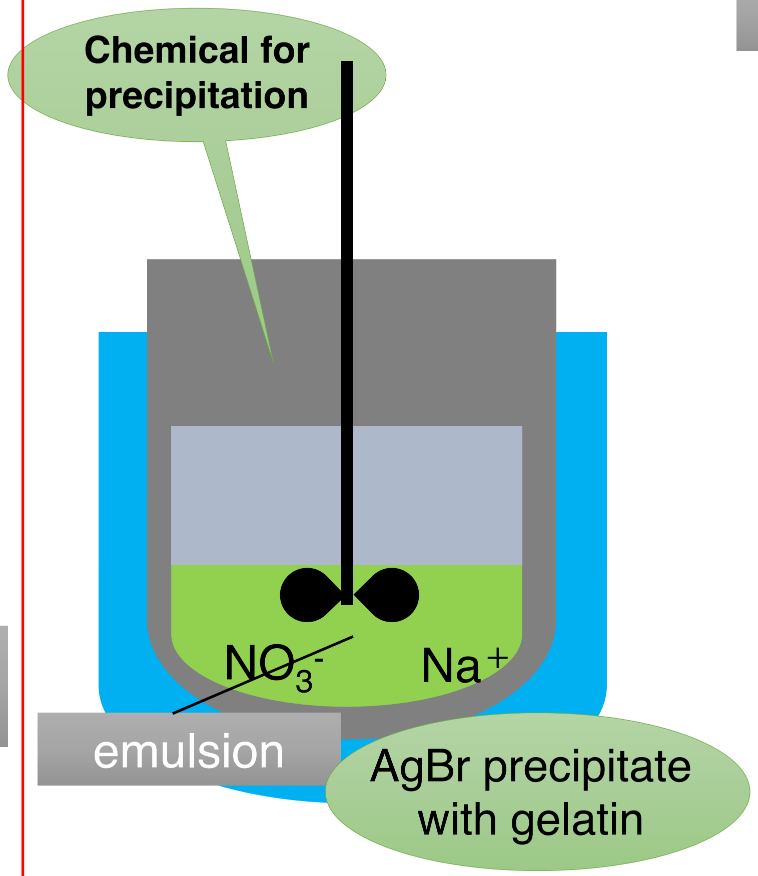

Apply

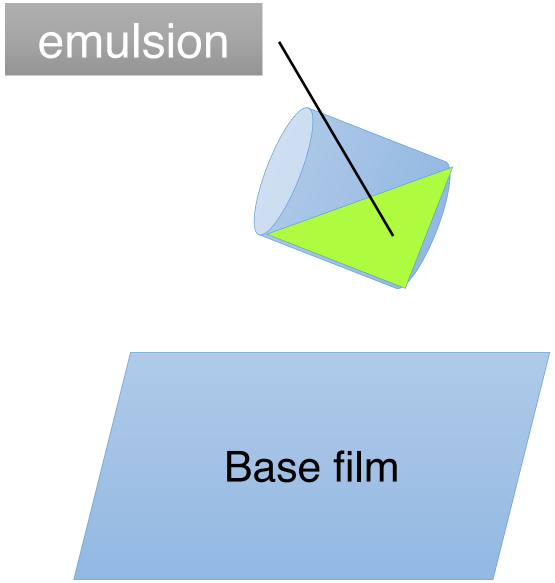

Control of dry condition

Temperature, humidity,
Thickness etc.

Production process

Crystal formation

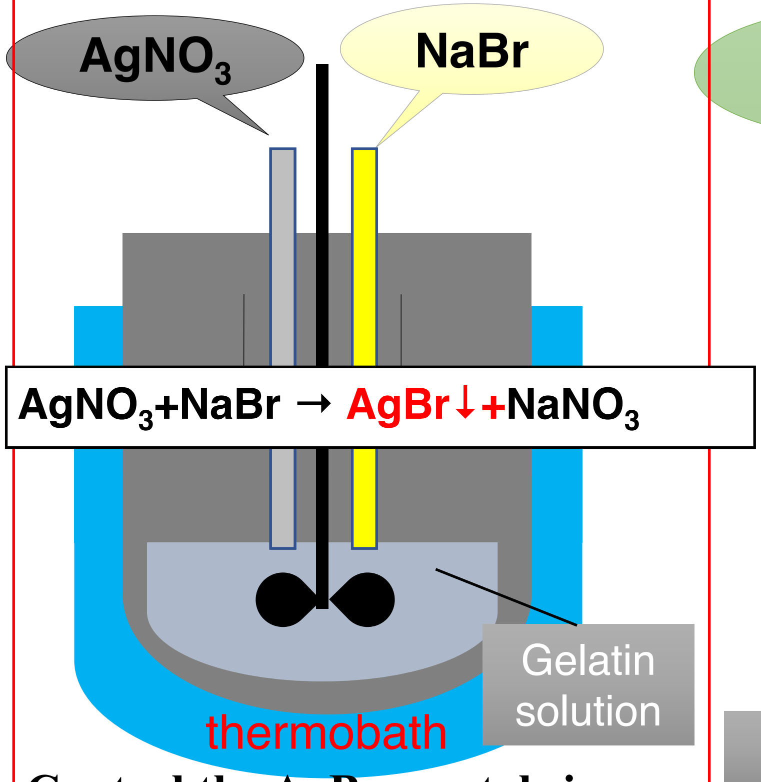

Control the AgBr crystal size
Temperature, insertion speed
Concentration of chemical, pAg control, rotation speed

wash/salt reduction

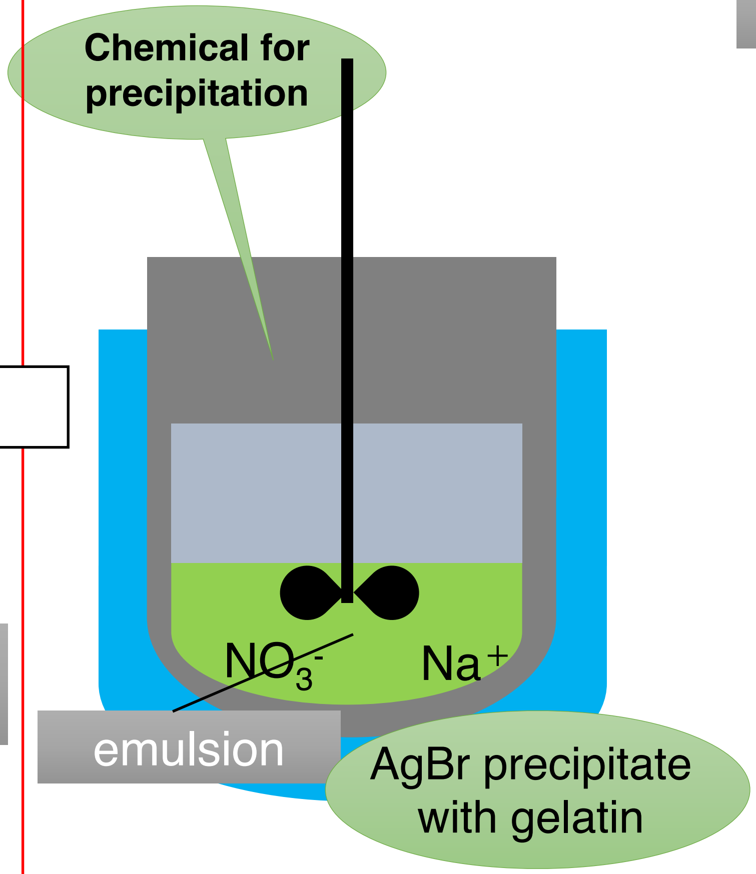

Apply

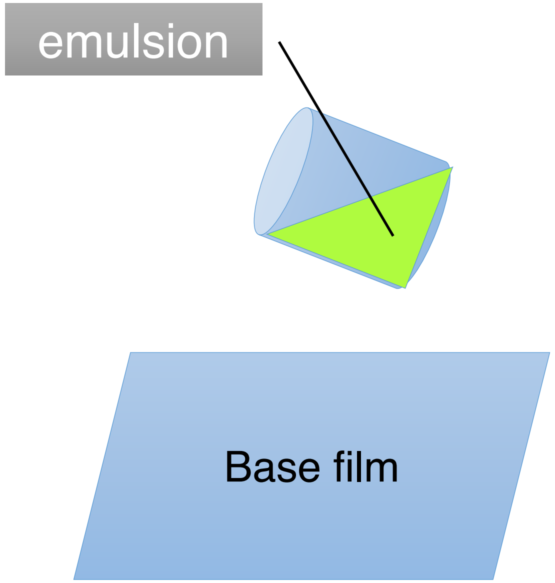

Control of dry condition

Temperature, humidity, Thickness etc.

Production process

Crystal formation

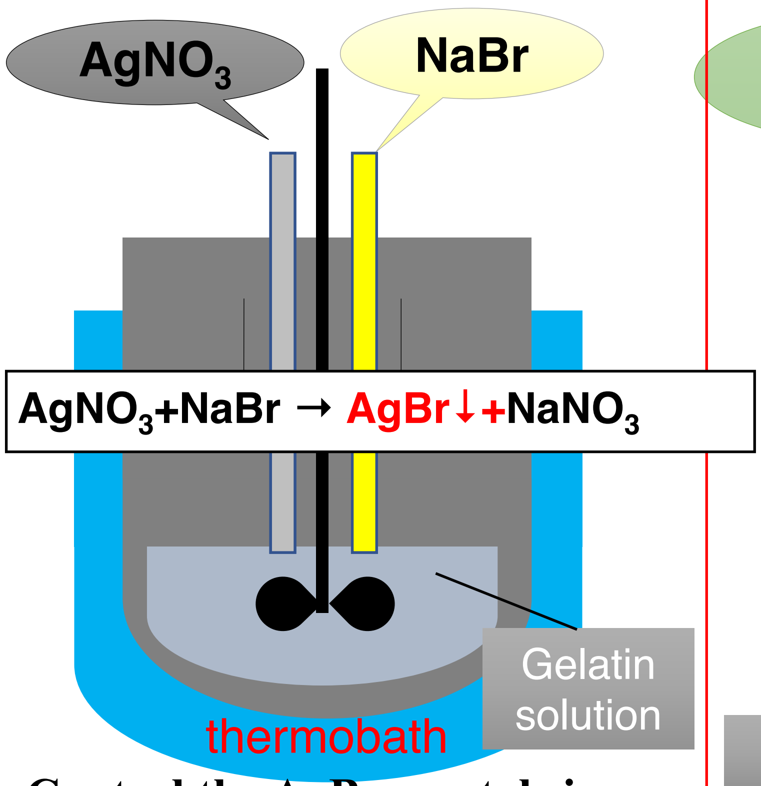

Control the AgBr crystal size

Temperature, insertion speed
Concentration of chemical, pAg control, rotation speed

wash/salt reduction

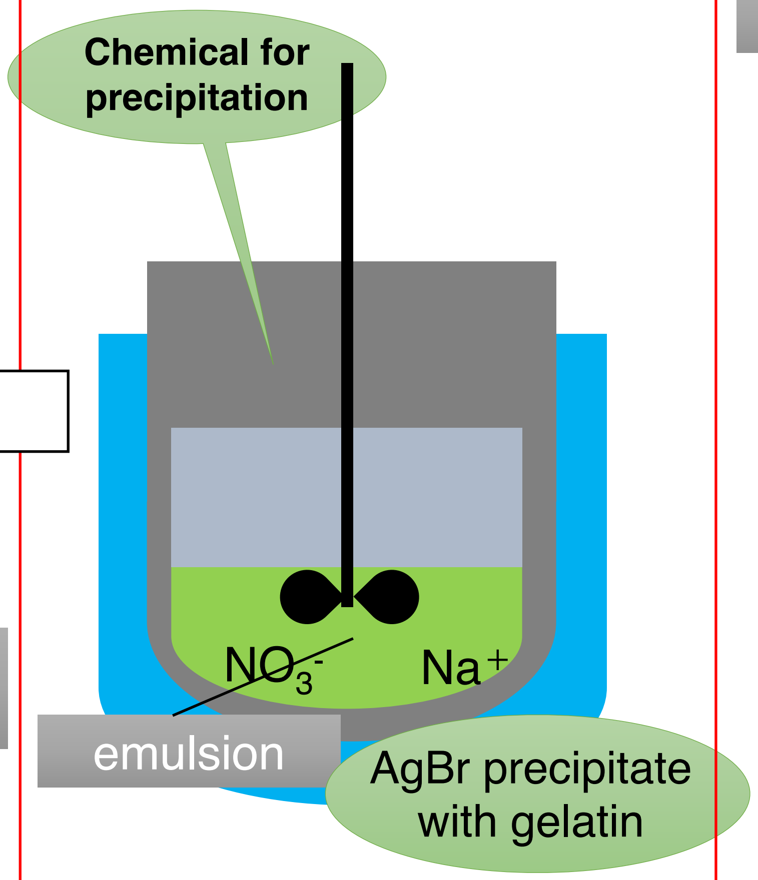

Apply

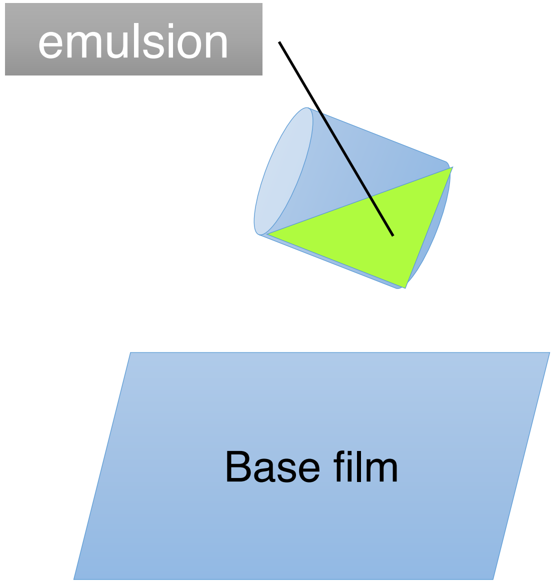

Control of dry condition

Temperature, humidity,
Thickness etc.

Production process

Crystal formation

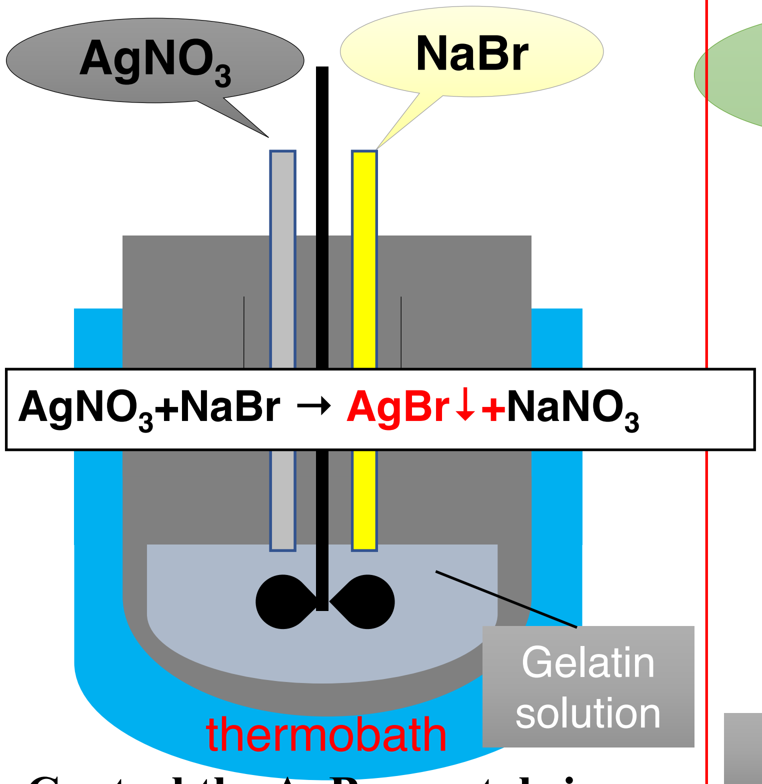

Control the AgBr crystal size
Temperature, insertion speed
Concentration of chemical, pAg control, rotation speed

wash/salt reduction

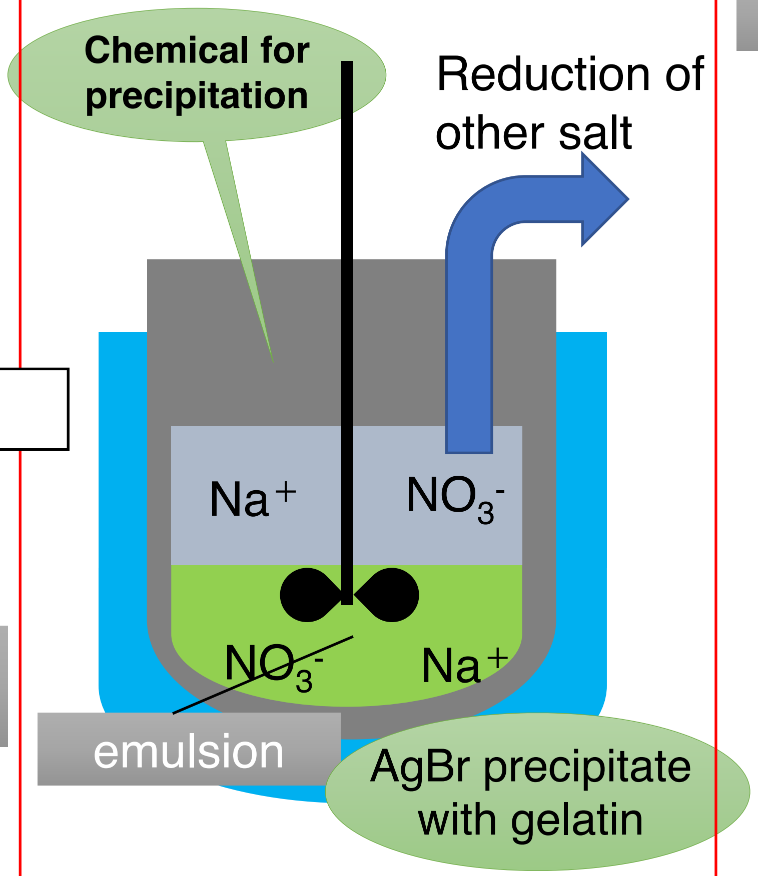

Apply

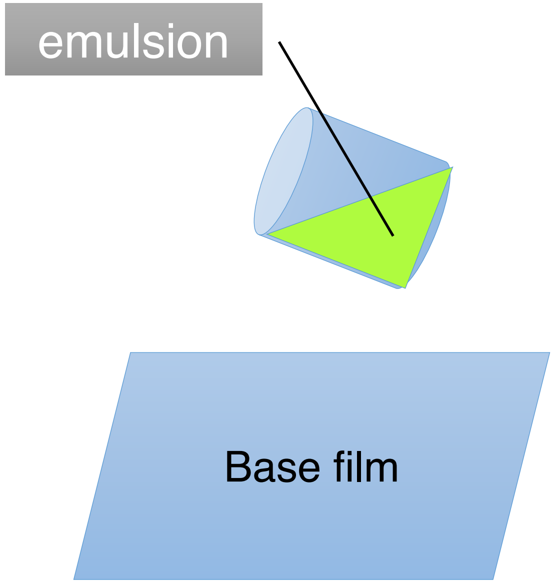

Control of dry condition

Temperature, humidity,
Thickness etc.

Production process

Crystal formation

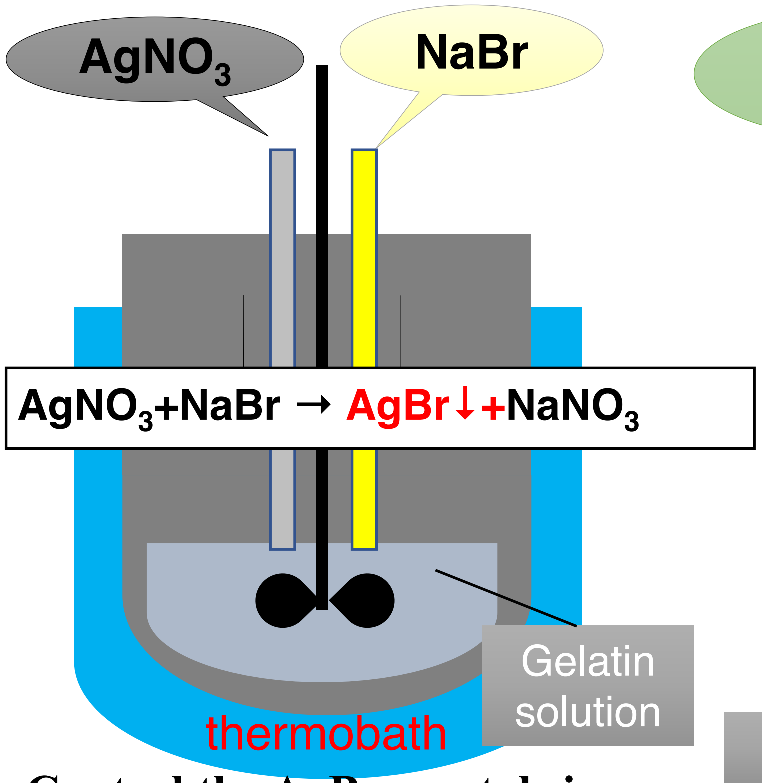

Control the AgBr crystal size
Temperature, insertion speed
Concentration of chemical, pAg control, rotation speed

wash/salt reduction

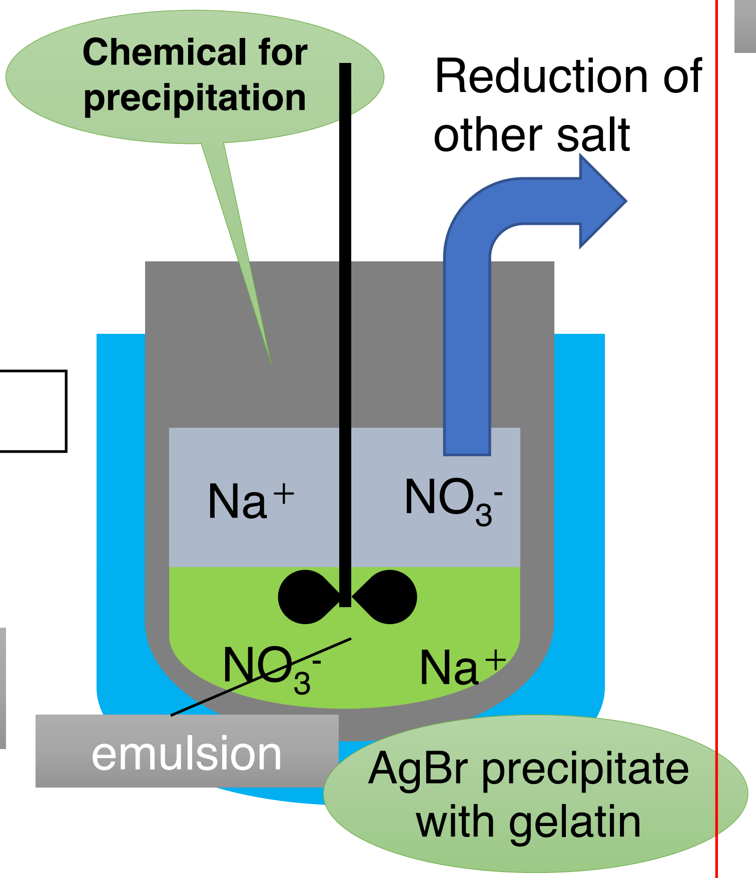

Apply

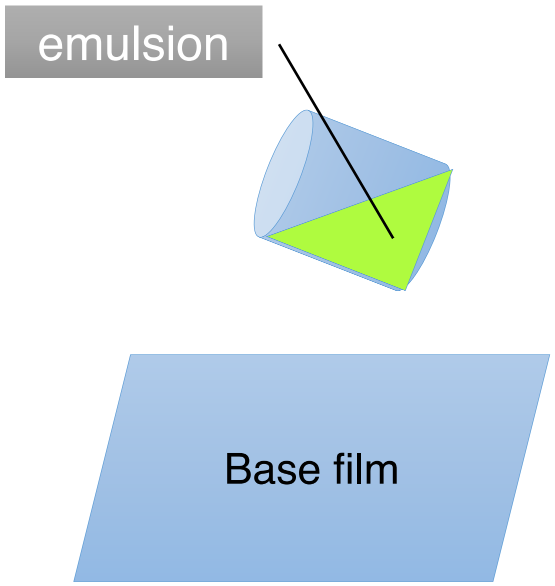

Control of dry condition

Temperature, humidity, Thickness etc.

Production process

Crystal formation

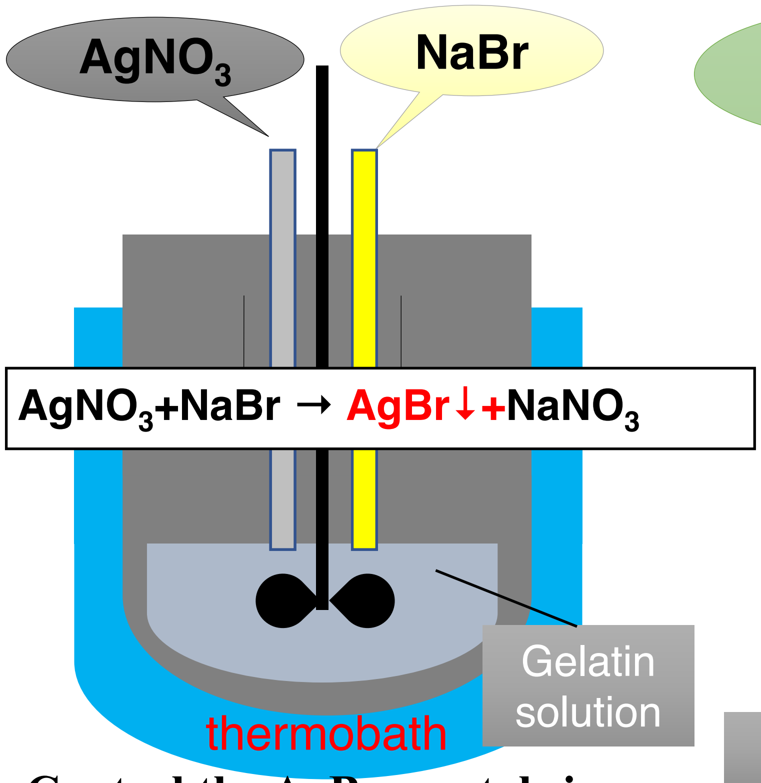

Control the AgBr crystal size
Temperature, insertion speed
Concentration of chemical, pAg control, rotation speed

wash/salt reduction

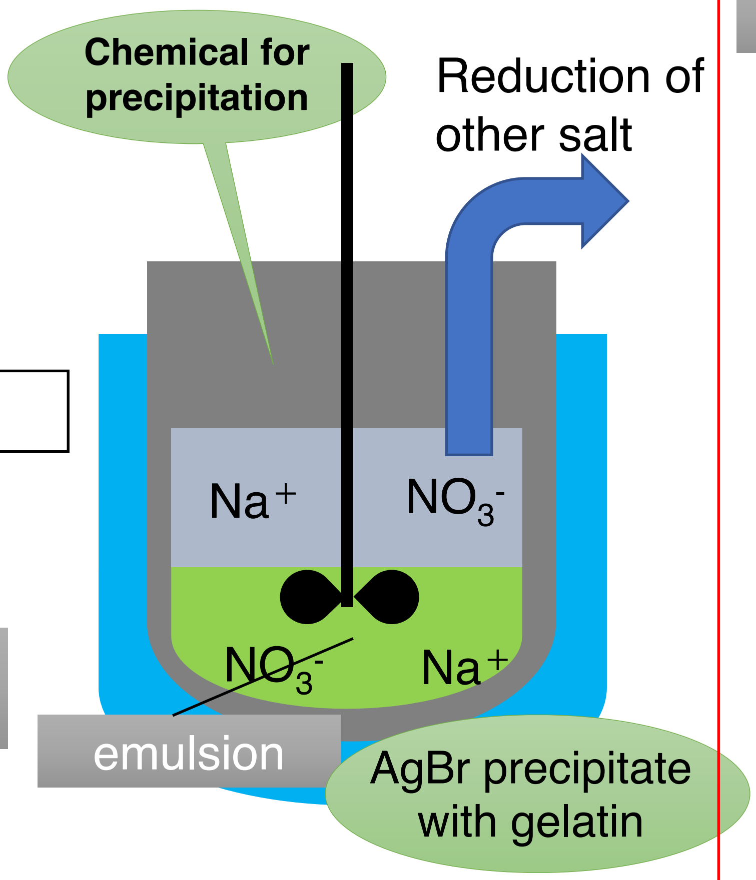

Apply

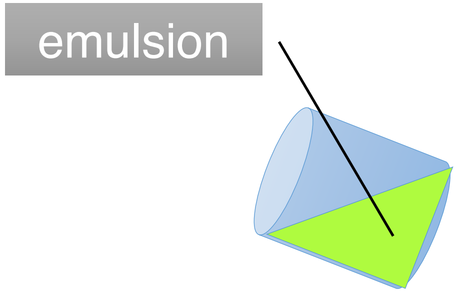

Nuclear Emulsion

Control of dry condition

Temperature, humidity, Thickness etc.

Film production

Control of AgBr crystal size, density

Desalination

Reduction of Na, NO_3

Sensitization

Au+S sensitization
→ tuning of the sensitivity (grains/μm at a given dE/dx)

Nuclear emulsions development

- Develop
- Stop
- Fix
- Wash
- Glycerine

- Dry

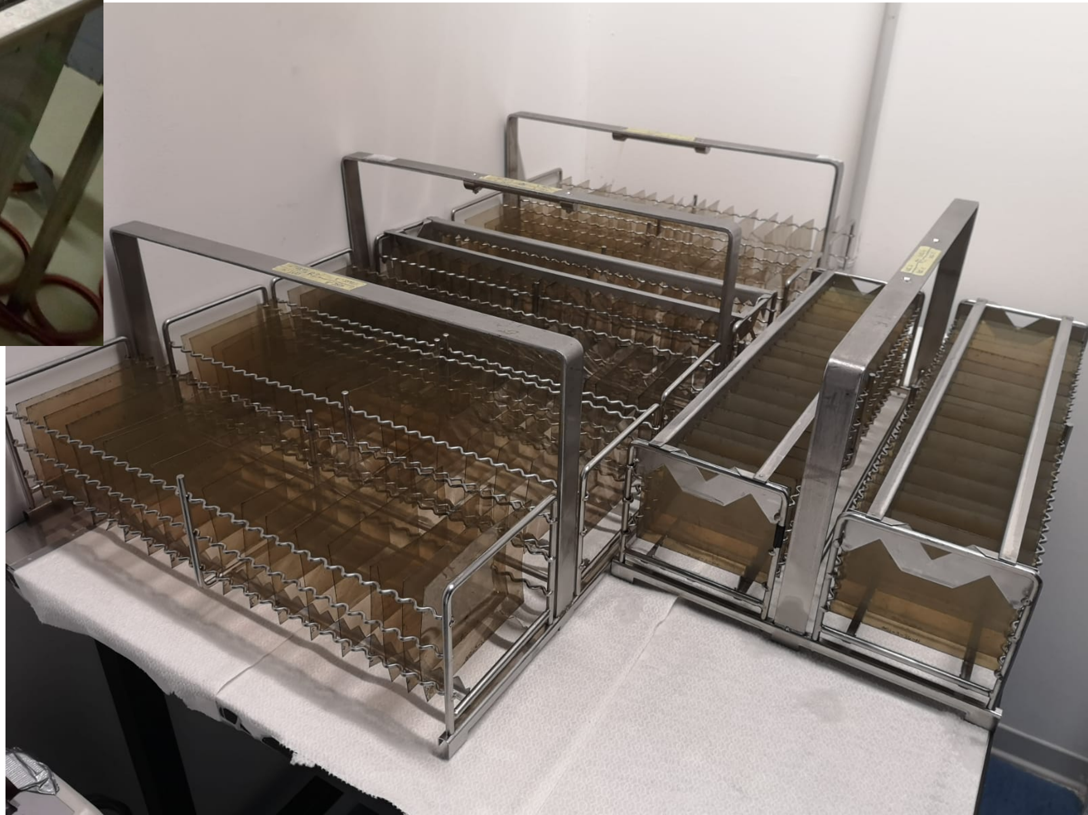

Emulsions in a particle physics experiment

Used to instrument the target region of experimental apparatus in order to study the properties of the incoming particles and/or the interaction products

Two techniques:

- “Bulk”: target fully made of emulsion films (visualizer detector), **old fashion**
- Emulsion Cloud Chamber (ECC): target made of passive material interleaved with nuclear emulsions acting as trackers with micrometric resolution (vertex detector with additional performance depending on the structure), **modern way**

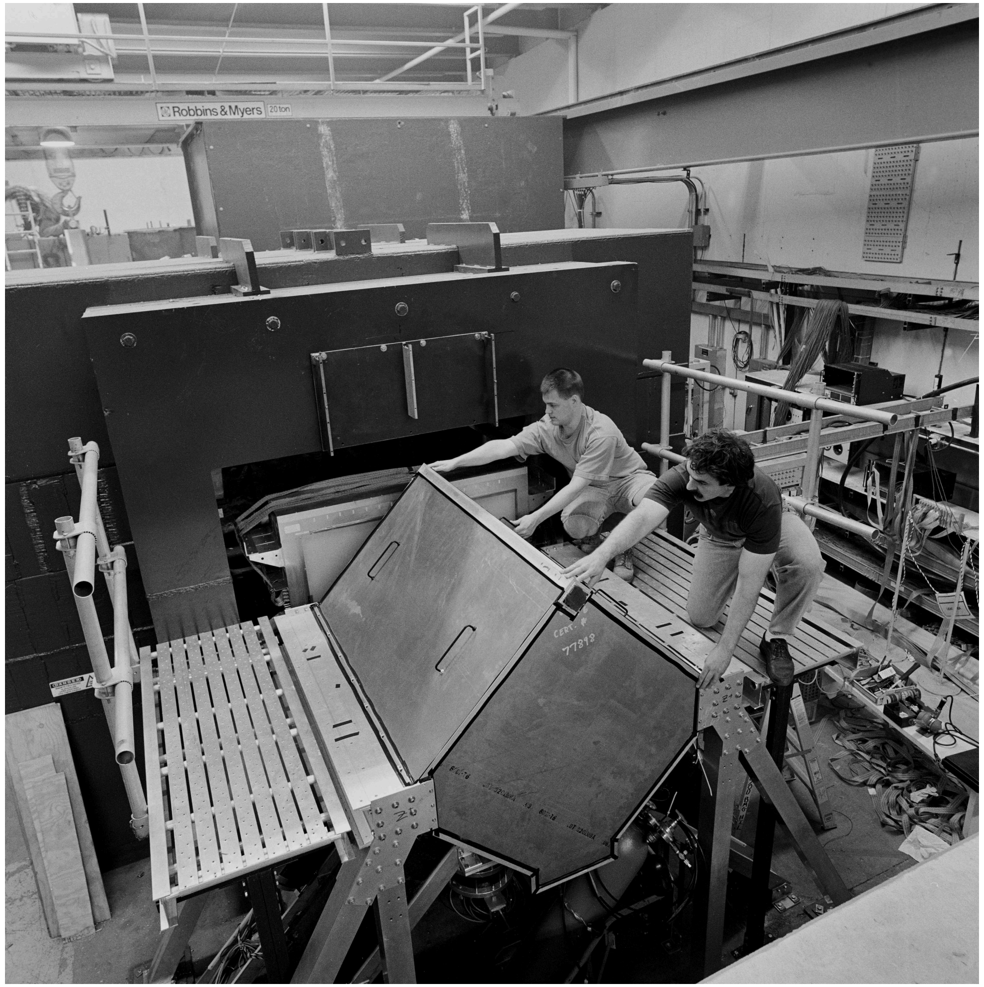

Fermilab DONUT experiment discovers ν_τ

Bulk emulsions

Particles || to the emulsions

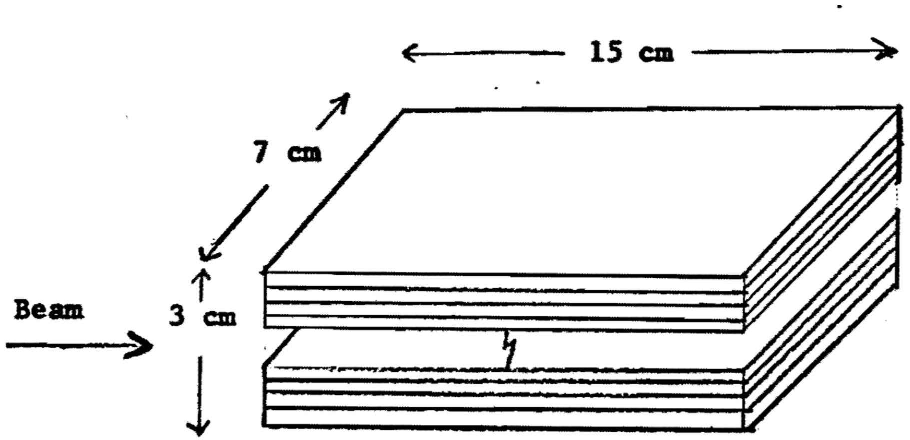

Particles ⊥ to the emulsions

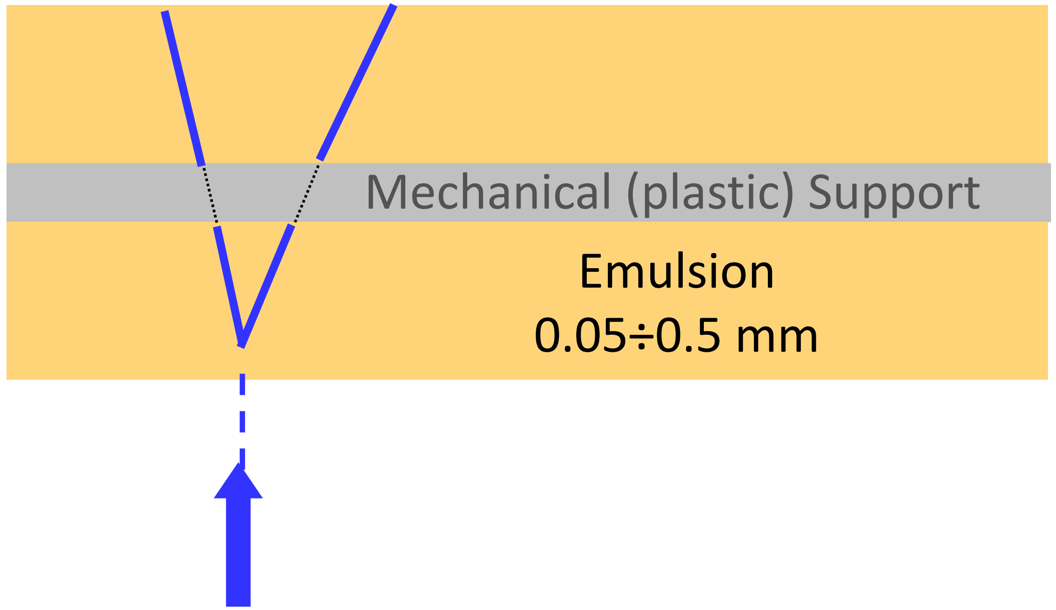

90/95% sensitive volume

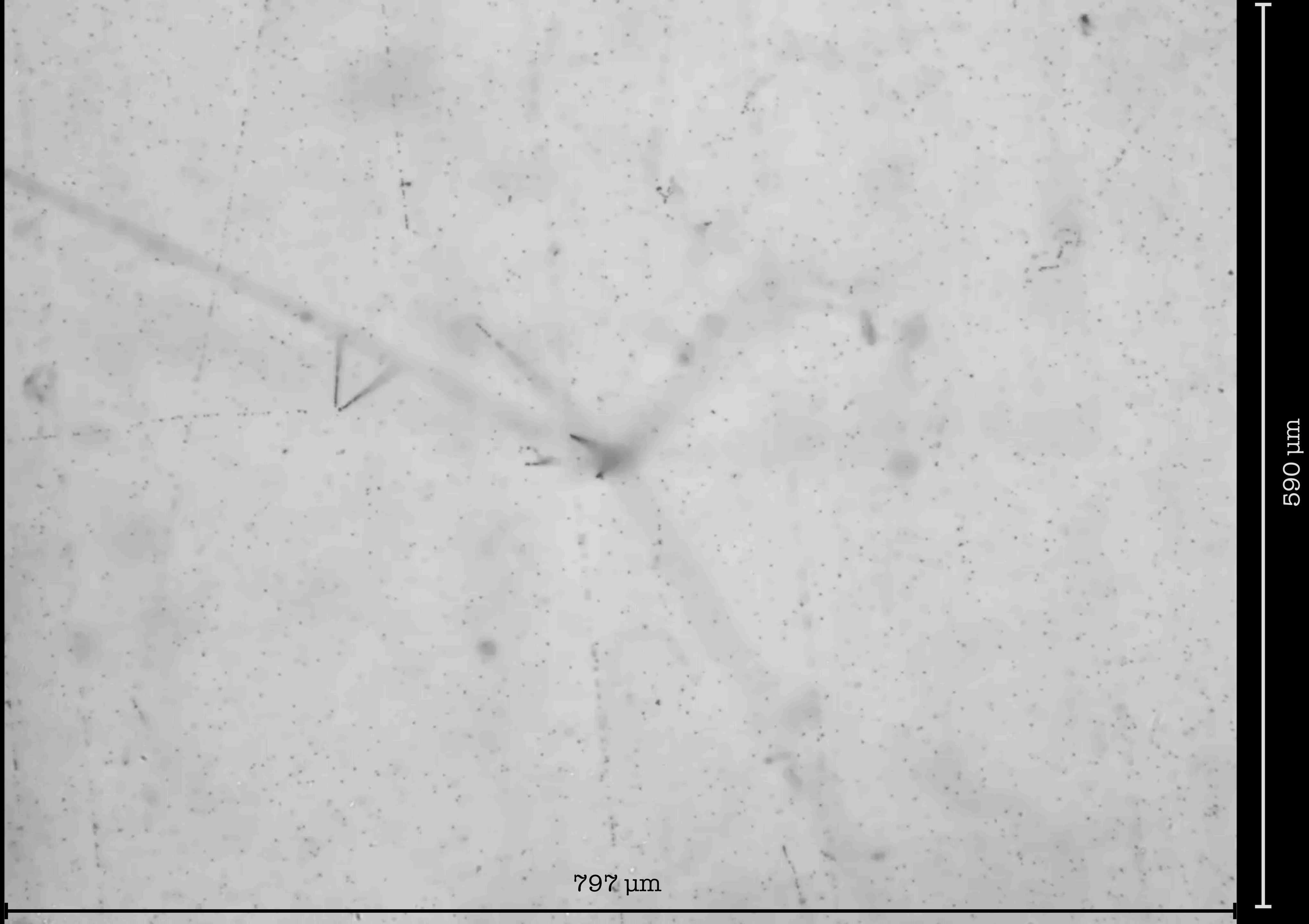
797 µm
590 µm

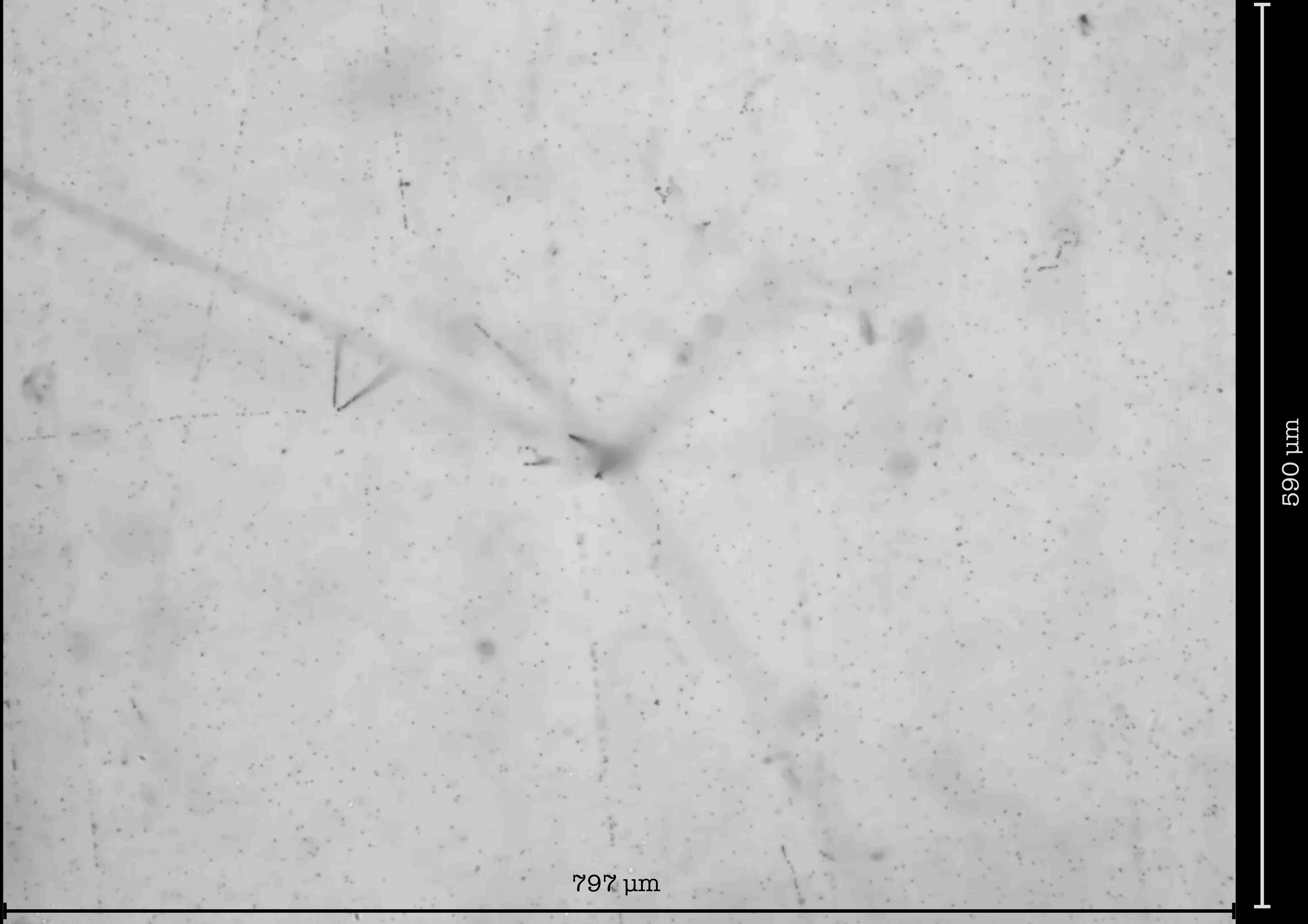
797 µm
590 µm


400 µm
300 µm


400 µm
300 µm

Emulsion Cloud Chamber

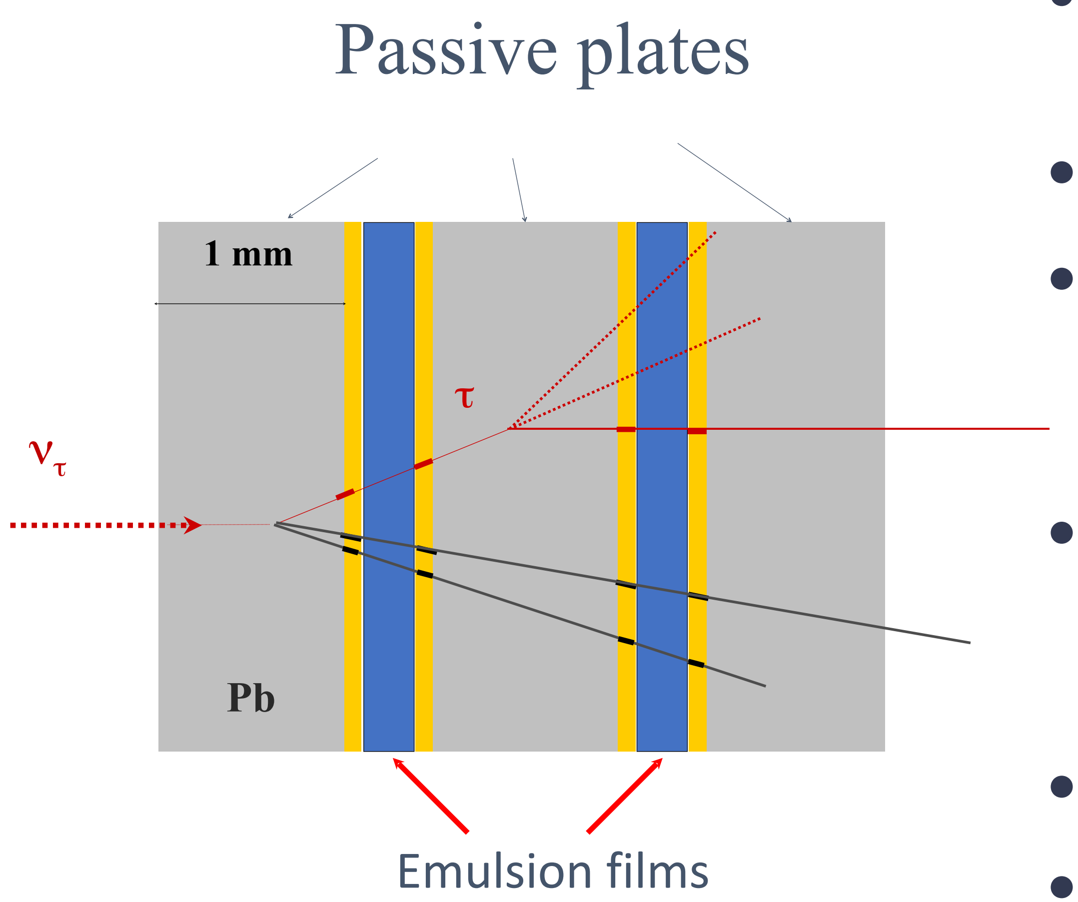

- Nuclear emulsions interleaved with passive material
- Particles ⊥ to emulsions
- Higher interaction probability: compact and relatively cheap target with large masses (low fluxes and/or cross-sections)
- Momentum measurement through the detection of the multiple Coulomb scattering in passive materials
- Electromagnetic shower identification
- Hybrid setup is used to provide the time stamp and to restrict the analysis region, when needed

ECC tracks' reconstruction

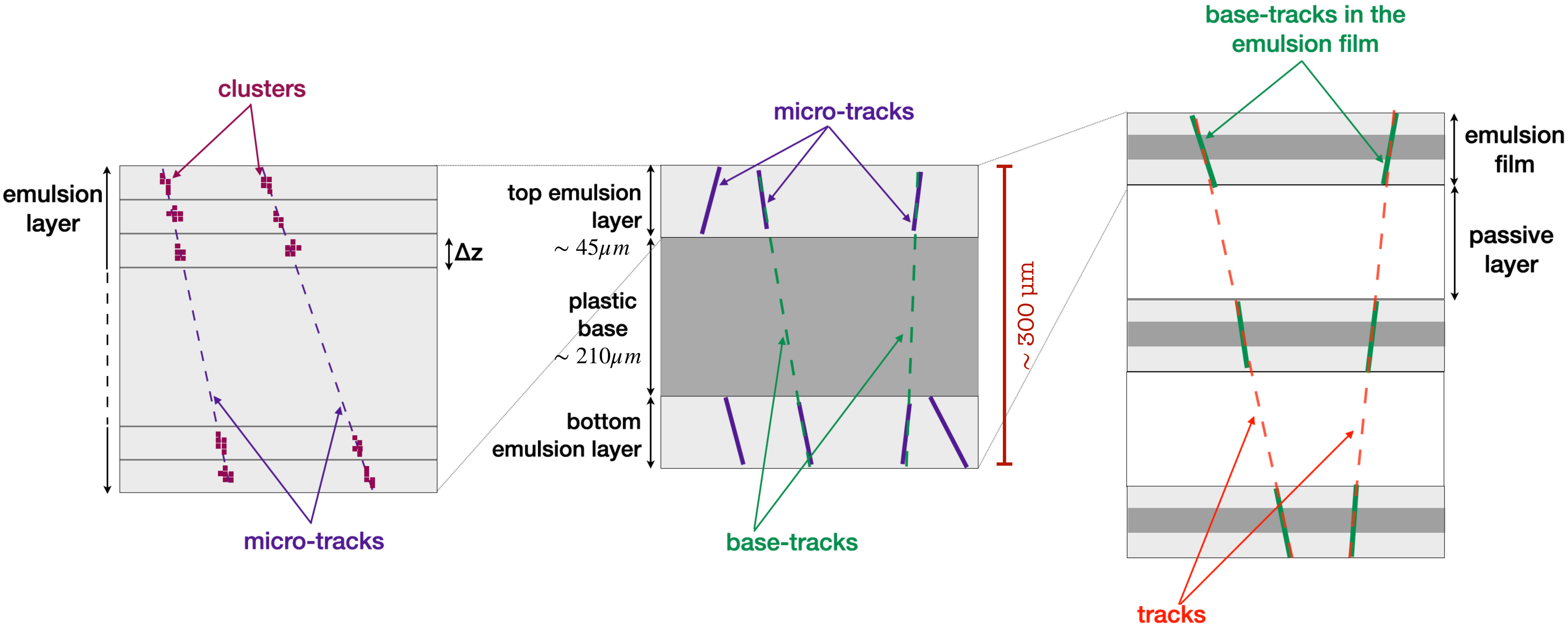

ECC tracks’ reconstruction

ECC tracks' reconstruction

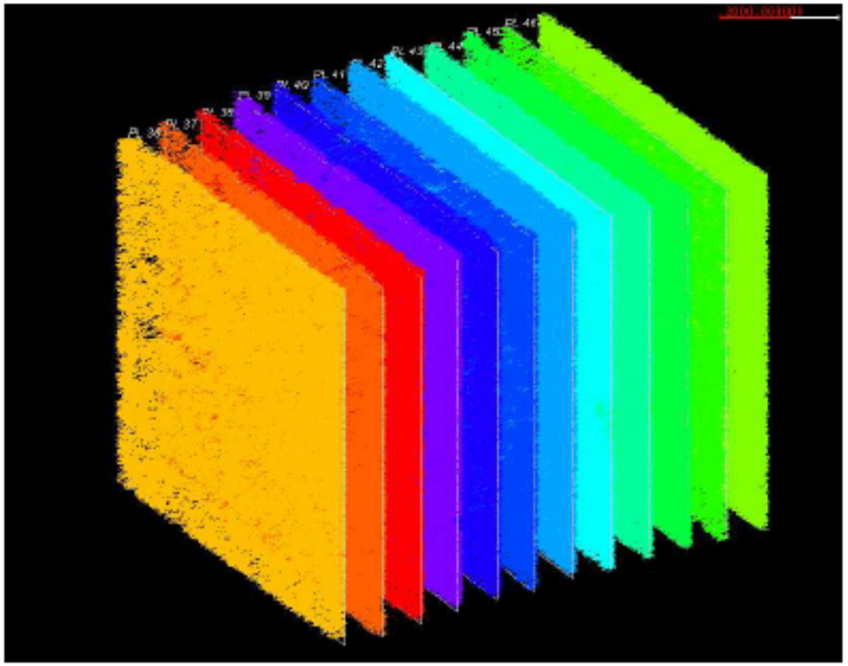

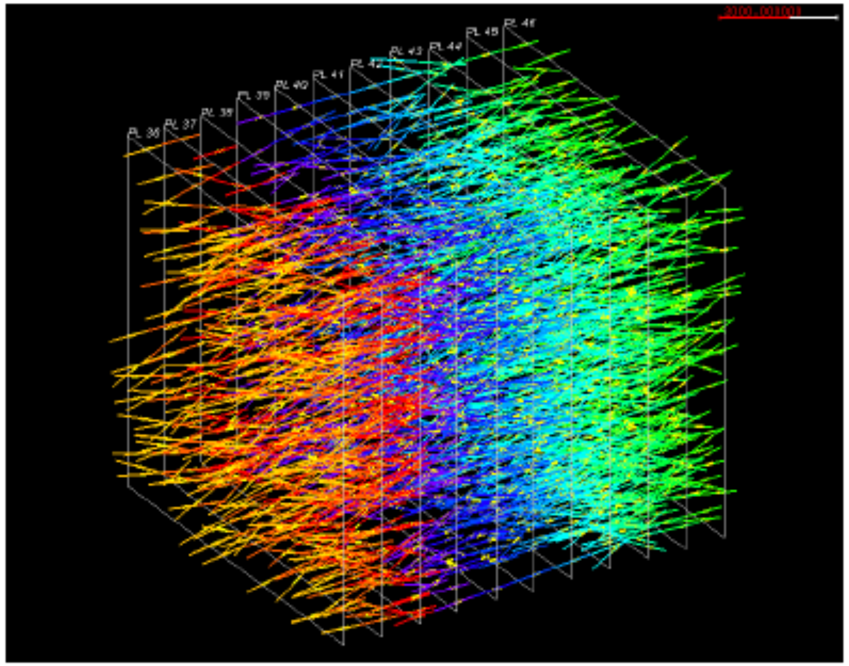

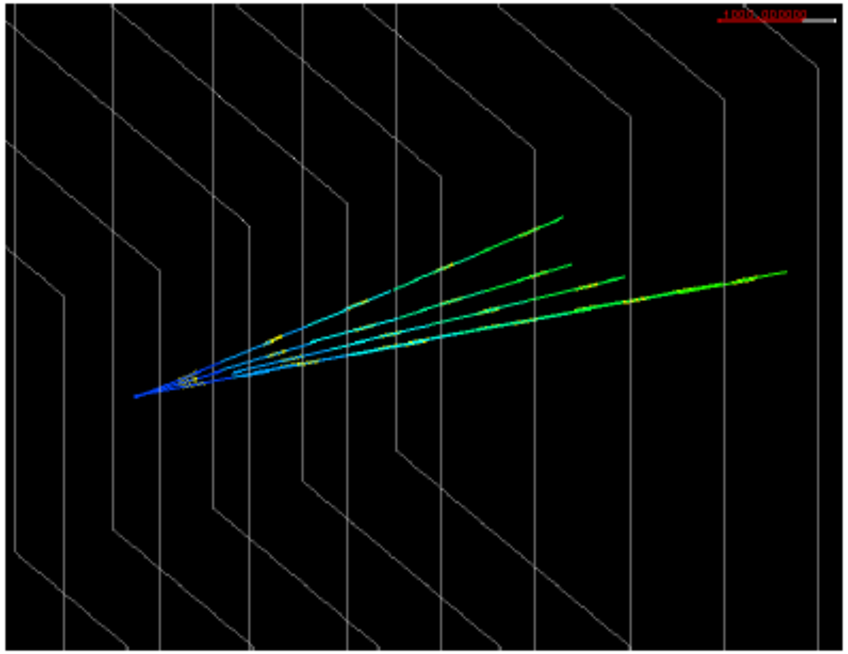

AT THE ORIGINS OF NUCLEAR EMULSIONS

Nuclear emulsion technology: the birth

- 1896 **Bequerel** (Nobel Prize in 1903) discovers the radioactivity by observing the blackening of photographic films due to uranium salts: he accidentally placed a uranium ore on top of a photographic plate. After several experiments, he concluded that this was due to uranium emission different from X-rays
- 1910 **Kinoshita** observes tracks of α particles
- 1925 **Marietta Blau** optimised nuclear emulsions for detecting low-energy protons
- Important developments of the emulsion sensitivity in 1930s and 1940s thanks to the Bristol group led by **Powell** who developed films sensitive to electrons (Nobel Prize in 1950)

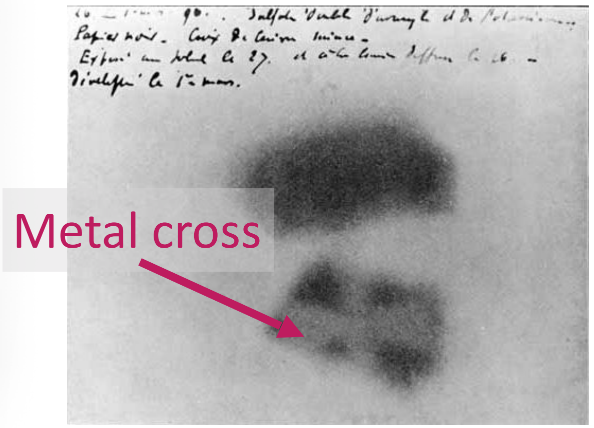

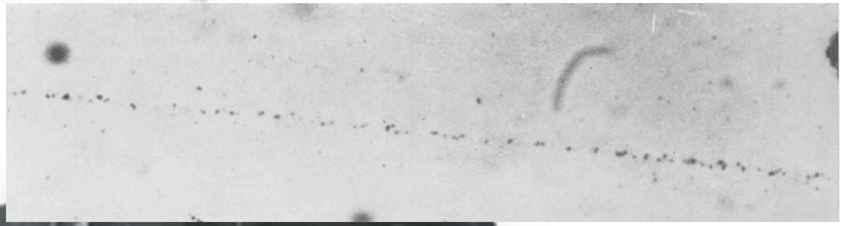

Nuclear emulsion technology: developments

- After the Second World War, very active collaboration between academic groups and photographic industries (Kodak, Ilford)
- 1970s and 1980s: With the development of electronic detectors, emulsions are less used
- Revolution in the readout technique in the late 1980s. In the 1990s fully automated optical microscopes for the readout provide a revival of the technology

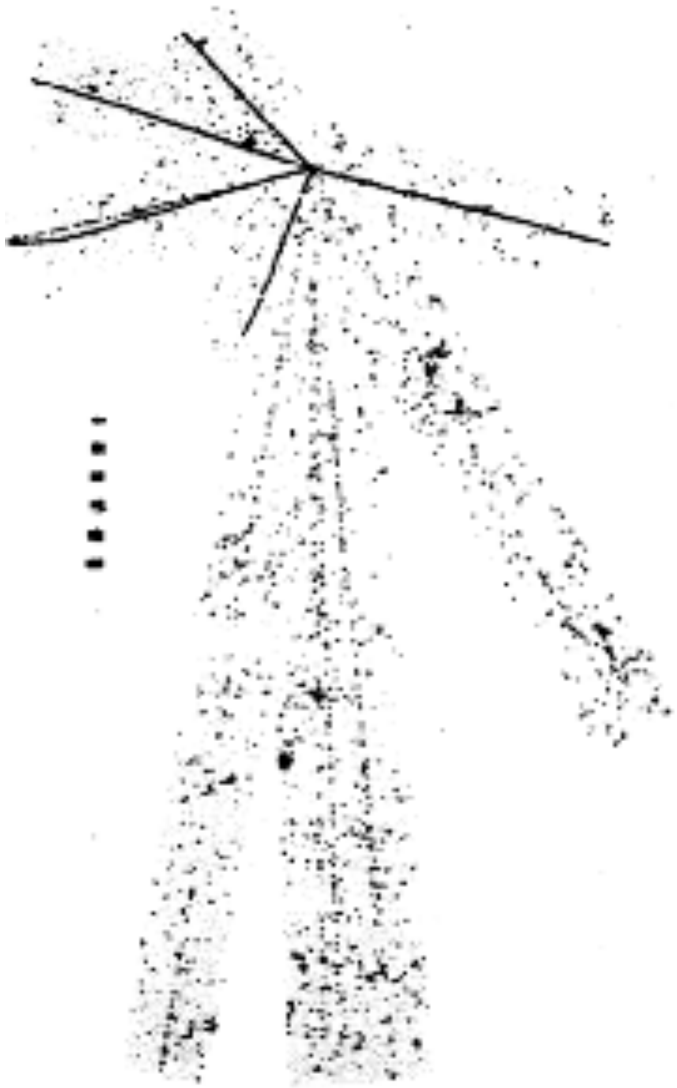

Nuclear emulsion technology: current era

- 2000s: the era of the OPERA experiment, the largest ever emulsion experiment with an industrial production of films by the Fuji Film Company (110000 m^2)
- 2010: technology established and OPERA provides its unique results. Faster scanning system are developed
- Present: New era with nanometric films for nanometric accuracy: breakthrough in the readout technologies.
  Thanks to ultra-fast scanning systems and nanometric accuracy new enterprises are possible: NEWSdm, SHiP and SND and other experiments

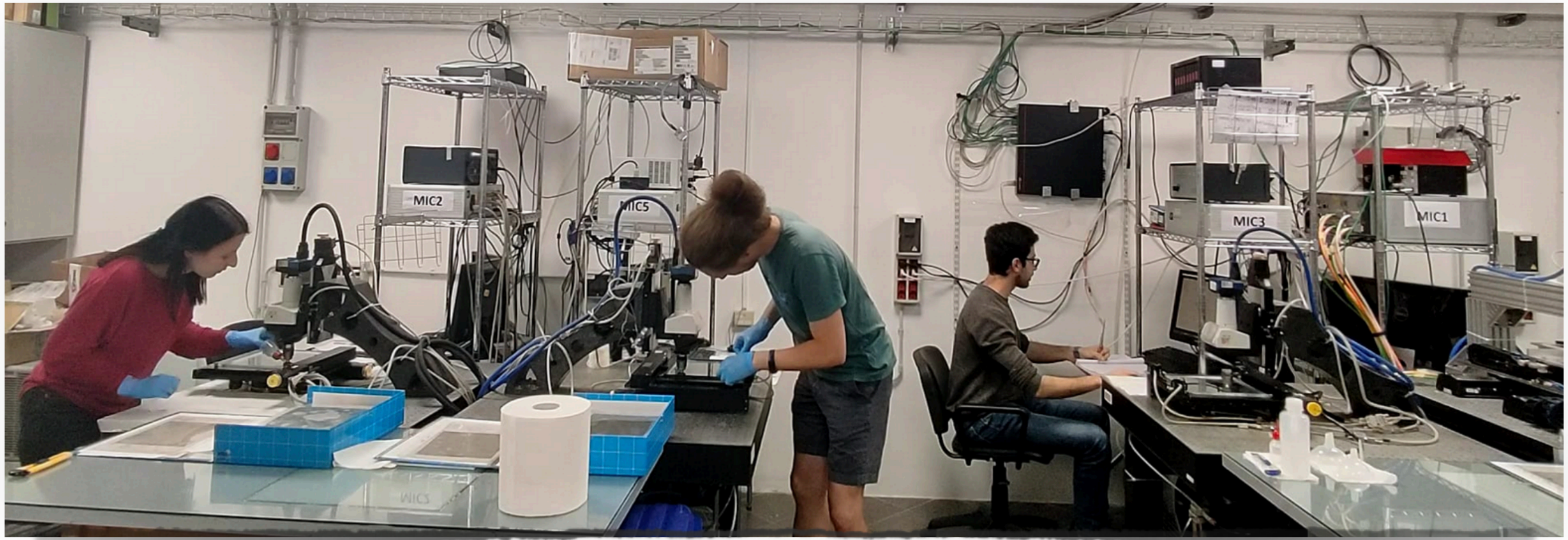

Nuclear emulsions scanning lab in Naples

The Discovery of the Pion

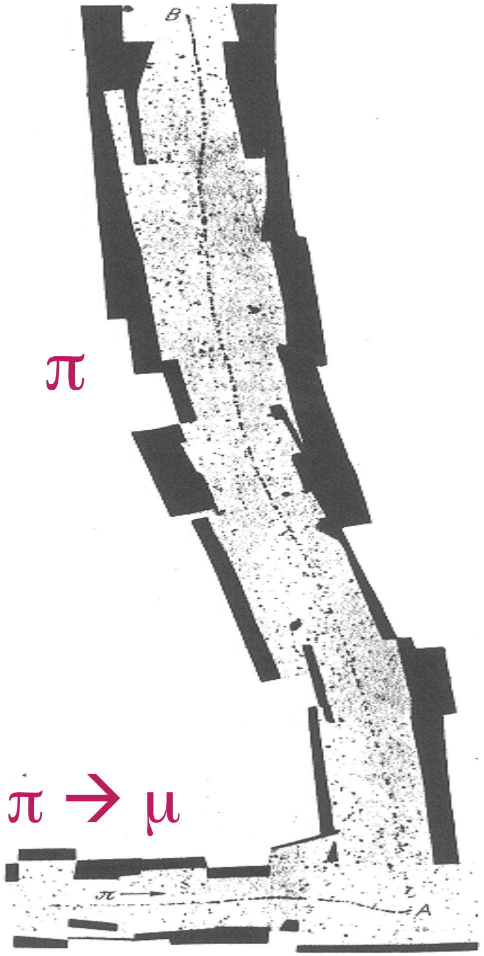

- Cosmic ray study on an airplane at about 9km of altitude and at Pic du Midi
- 600 μm thick emulsion with a new kind of gelatine to register the passage of ionizing particles
- Powell used these emulsions to solve the mystery of the Yukawa meson in 1947
- Powell got the Nobel Prize in 1950. The Committee underlined the simplicity of the detector used.

Lattes, Muirhead, Occhialini and Powell,
OBSERVATIONS ON THE TRACKS OF SLOW MESONS IN PHOTOGRAPHIC EMULSIONS, Nature 159 (1947) 694.

First observation of “charmed” hadrons

A possible decay in flight of a new type particle

Niu et al., Prog.Theor.Phys.46 (1971) 1644-1646.

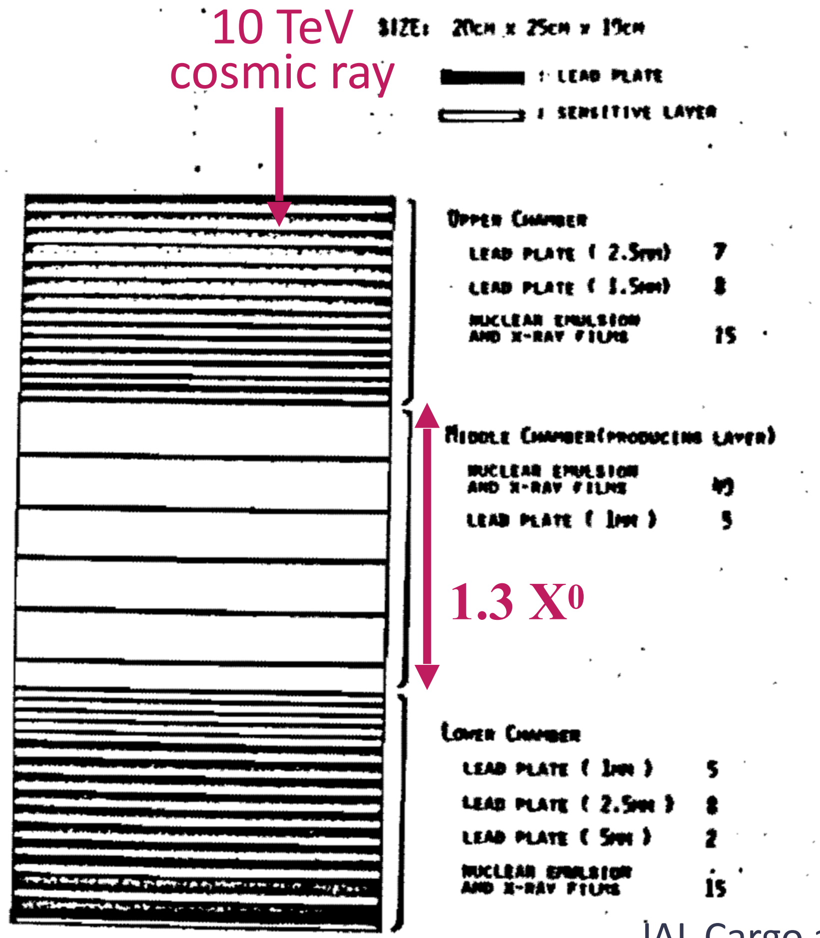

3 years earlier!

JAL Cargo airplane
from Aug to Dec 1969
~500 hours

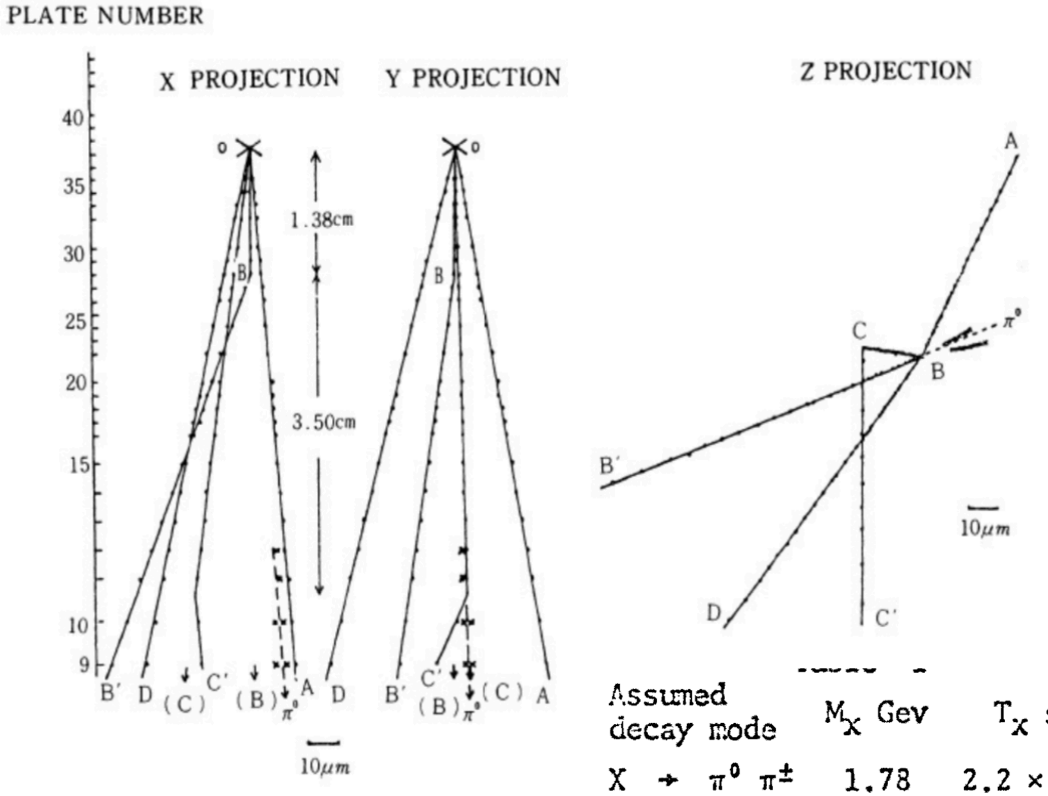

Assumed decay mode	M_X Gev	T_X sec.
$X \to \pi^0 \pi^\pm$	1.78	2.2×10^{-14}
$X \to \pi^0 p$	2.95	3.6×10^{-14}

Discovery of a narrow resonance in e^+e^- annihilation, PRL 33 (1974) 1406-1408

First observation of “beauty” hadron decay

Two particles with “beauty” quark content are produced and decay (10^{-12} s) producing “charmed” particles that in turn decay

Volume 158B, number 2 PHYSICS LETTERS 8 August 1985

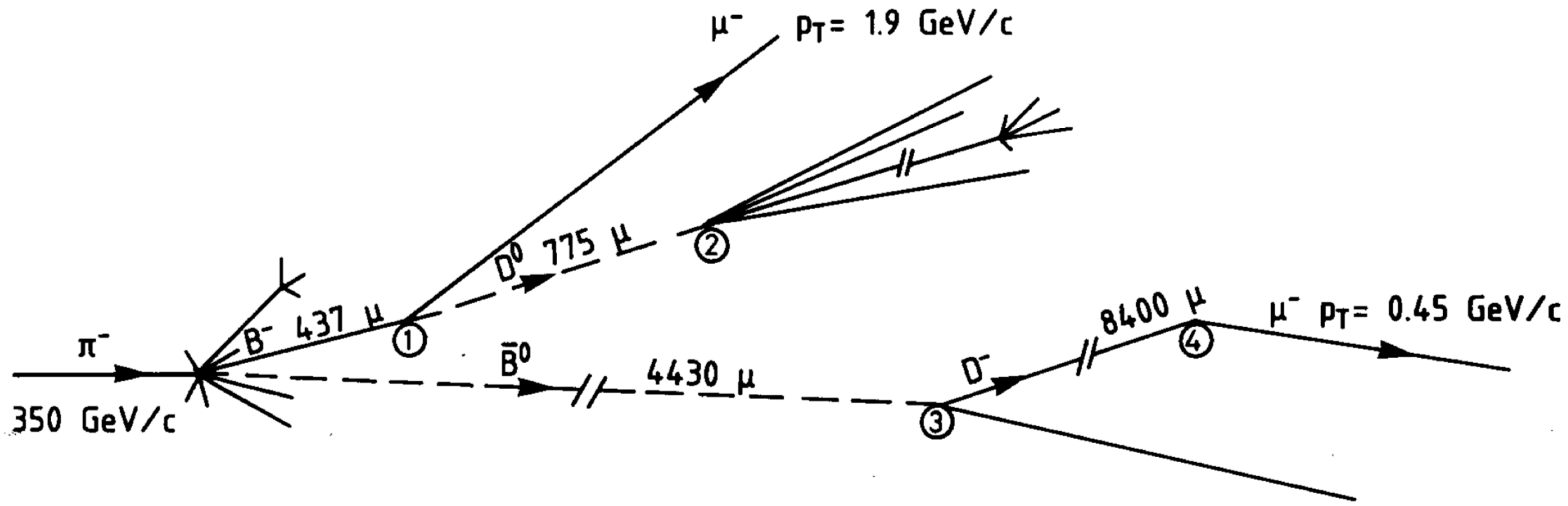

$$L = \beta\gamma c\tau \sim \gamma c\tau$$

$$\gamma \sim \frac{1}{\langle\theta\rangle}$$

$$c\tau \sim L\langle\theta\rangle$$

Petrera, Romano, NIM 174 (1980) 61
Direct Observation of the decay of Beauty particles into charm particles, PLB 158 (1985) 186, WA75 experiment at CERN

Diffractive Ds production in CHORUS

Phys. Lett. B435 (1998) 458, CHORUS experiment at CERN

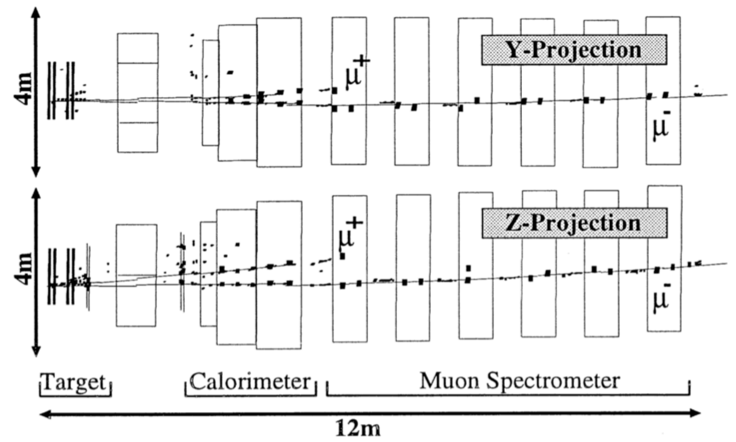

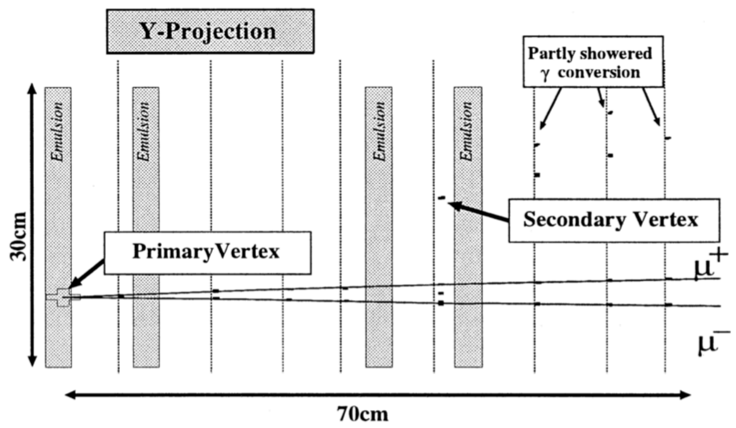

800 kg emulsion target

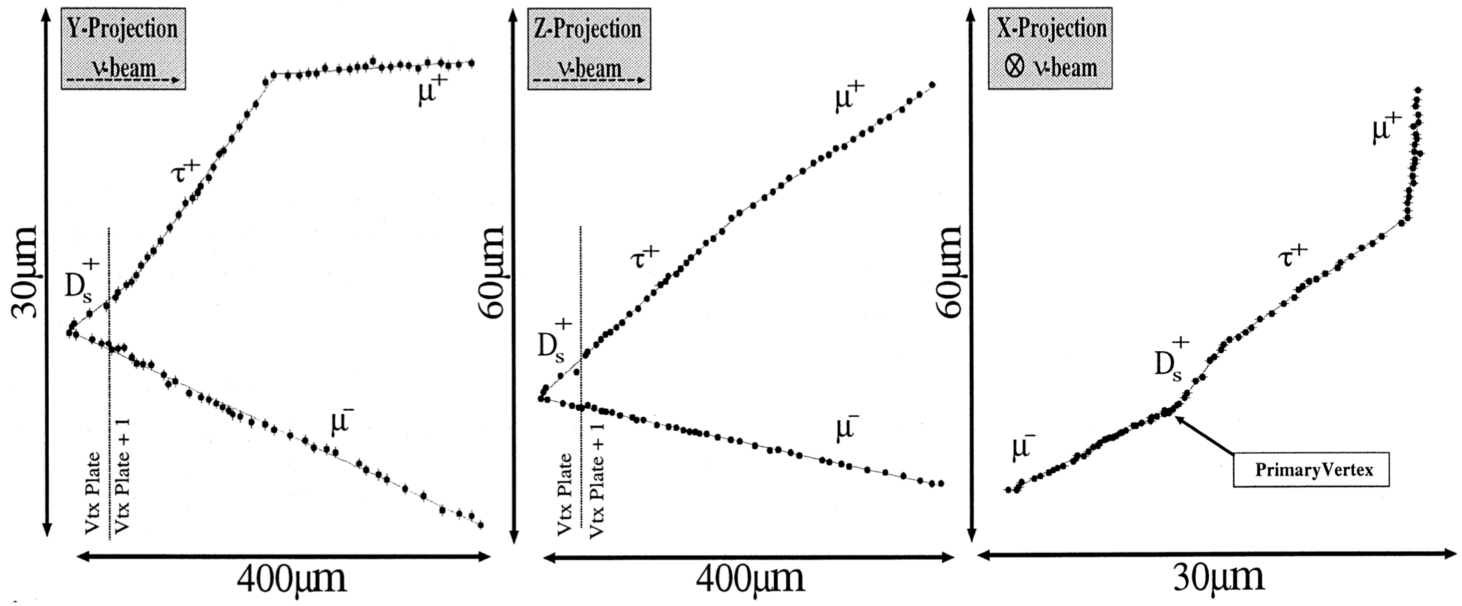

$$\nu_\mu\, n \longrightarrow \mu^- D_s^{+*} n$$
$$\quad \hookrightarrow D_s^+ \gamma$$
$$\quad\quad \hookrightarrow \tau^+ \nu_\tau$$
$$\quad\quad\quad \hookrightarrow \mu^+ \nu_\mu \bar{\nu}_\tau$$

First observation of the associated charm production in neutrino CC interactions

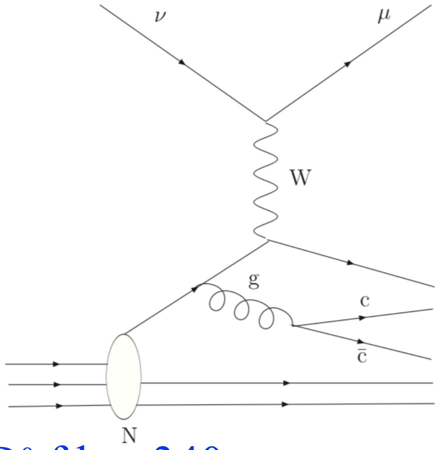

D^0 f.l. = 340 μm

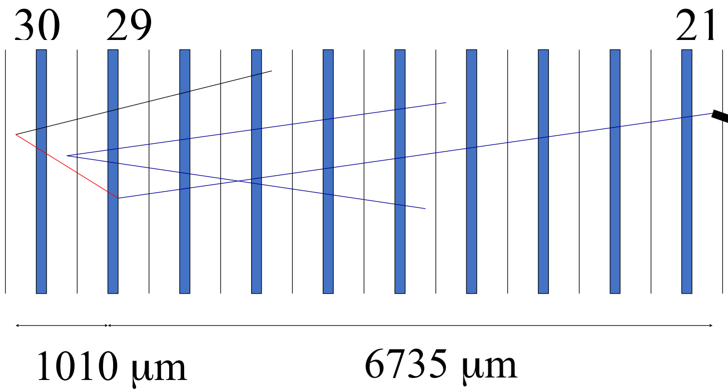

$N_s = 2$

$N_h = 6$

B.G. = 0.04±0.01

1st vertex

ϑ_{kink} = 420 mrad

f.l. = 1010 μm

2ry vertex

ϑ_2 = 310 mrad

f.l. = 7560 μm

$p\beta = 500^{+180}_{-110}$ MeV/c

dE/dx → proton

P = 0.78 GeV/c

$P_\perp >$ **330 MeV/c**

List of particles measured at primary and secondary vertices

Particle ID	θ_Y (rad)	θ_Z (rad)	$\tau = L\langle\theta\rangle/c$
μ^-	0.009	0.104	
C^0	−0.047	−0.055	2.8×10^{-13} s
Particle 1	−0.102	0.020	1.4×10^{-12} s
C^0 daughter	0.267	0.188	
C^0 daughter	−0.139	−0.054	
Particle 2	−0.495	−0.120	

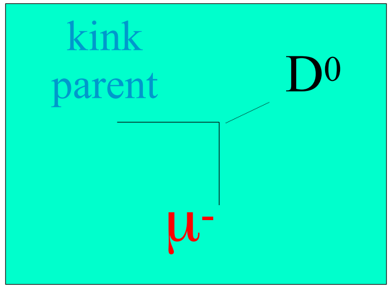

transverse plane

Phys. Lett B 539 (2002) 188, CHORUS Experiment at CERN


PEACE
THE STARS AND STRIPES
210241

The τ / θ paradox

$$\tau^+ \rightarrow \pi^+\pi^+\pi^- \qquad\qquad \theta^+ \rightarrow \pi^+\pi^0$$

The τ / θ paradox

$$\tau^+ \rightarrow \pi^+\pi^+\pi^- \qquad \theta^+ \rightarrow \pi^+\pi^0$$

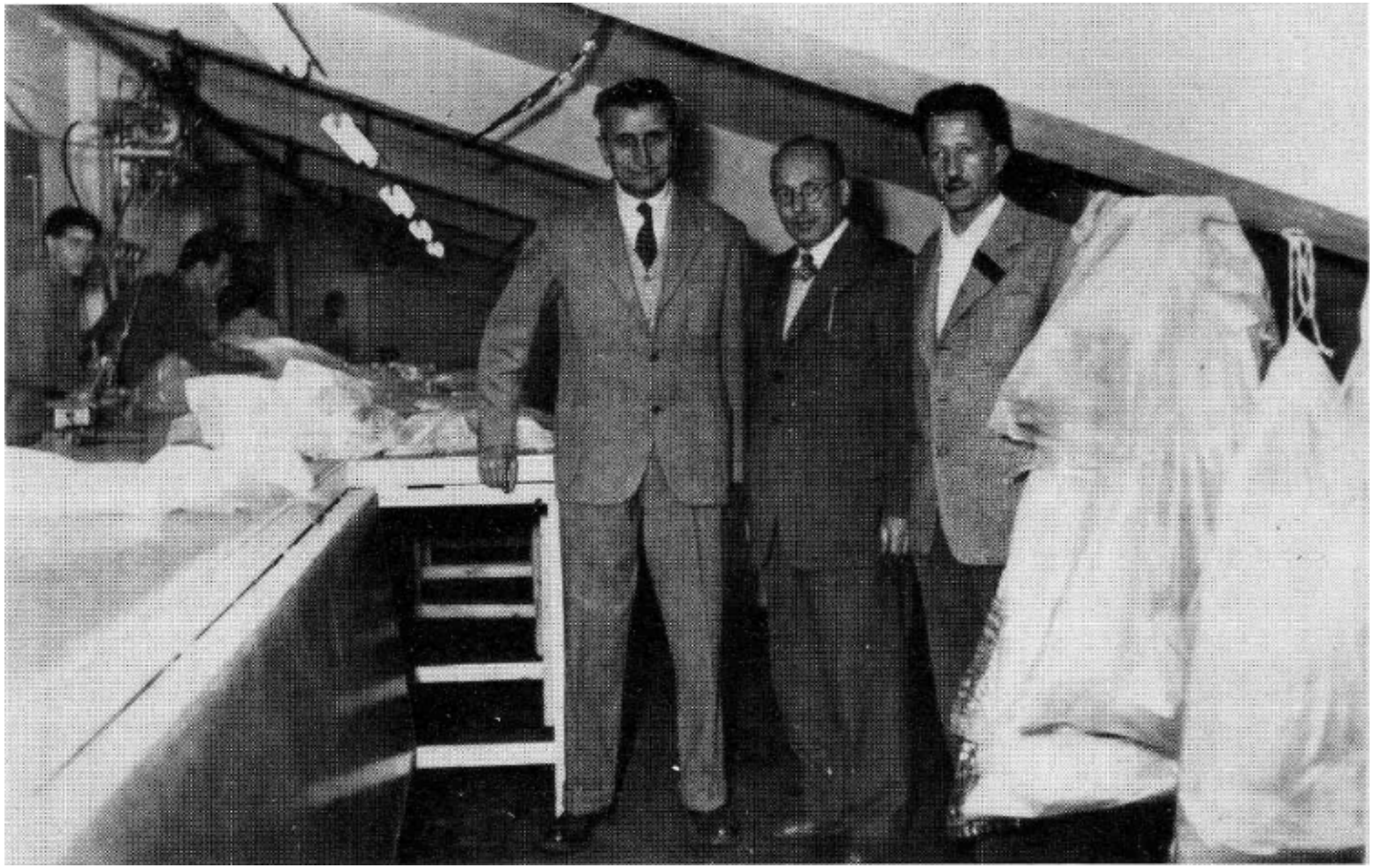

Antonio Rostagni (left) and Michelangelo Merlin (right) with an English collaborator supervising the construction of the G-Stack weather balloon in the attic of the Physics Institute of Padua

G-Stack

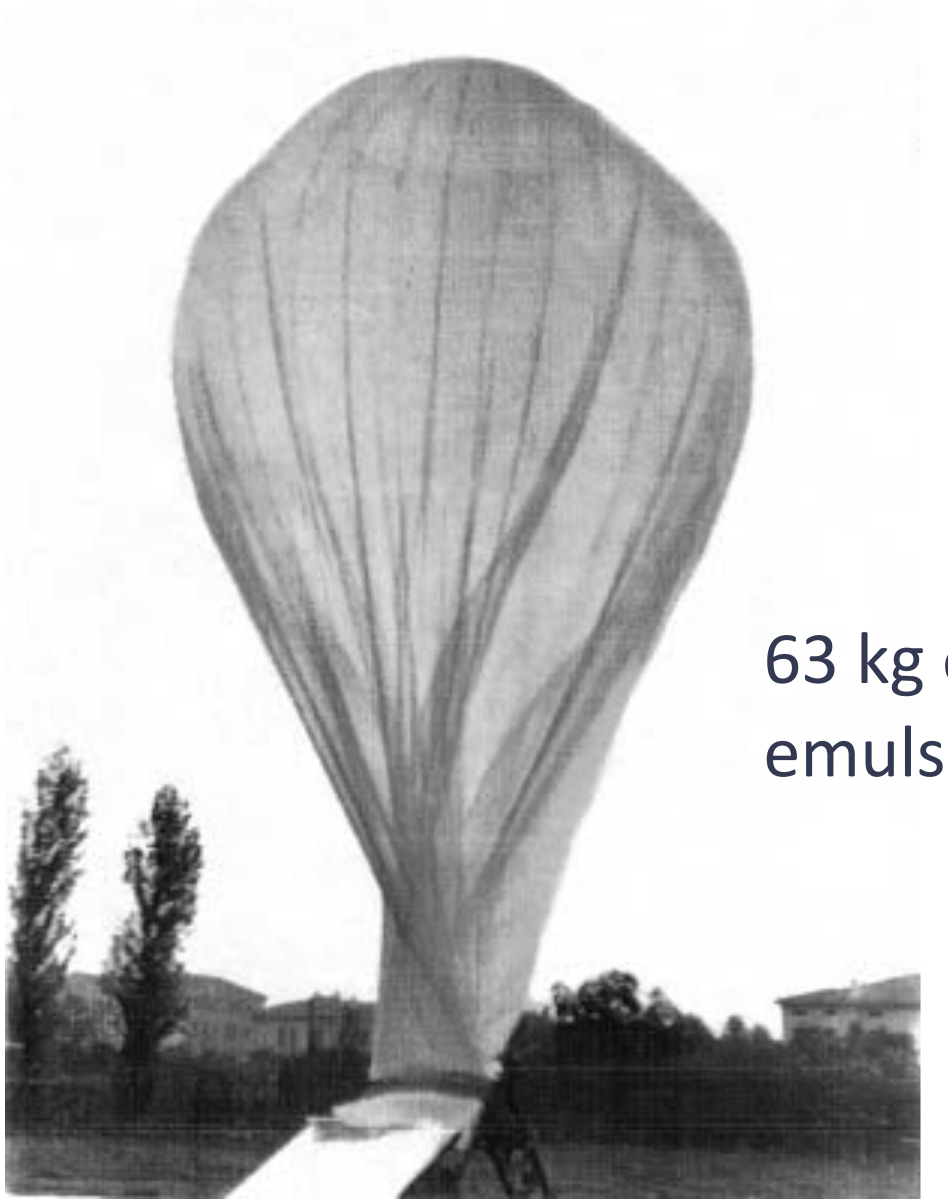

63 kg of nuclear emulsions!

OPERA

WANTED

FOR CRIMES AGAINST PHYSICS

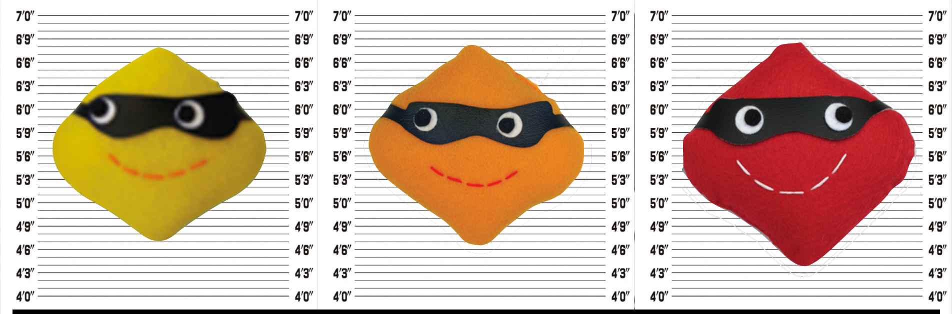

PHYSICS DEPARTMENT

NEUTRINOS ν

Discovery of the neutrino(s)

1930 - W. Pauli «invented a particle that cannot be detected»

1956 - Experimental discovery of the electron neutrino (Nobel Prize 1995)

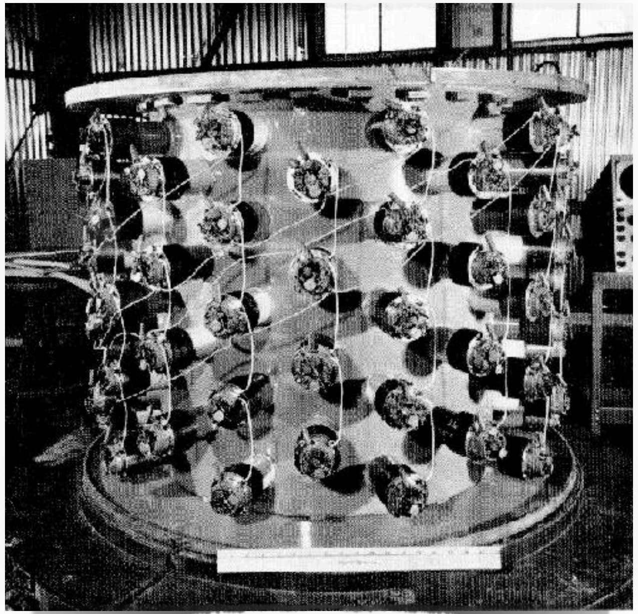

1962 - Discovery of muon neutrino

1991 - Indirect evidence that there are only 3 types of neutrinos

2000 - Discovery of tau neutrino

Discovery of the neutrino(s)

1930 - W. Pauli «invented a particle that cannot be detected»

1956 - Experimental discovery of the **electron** neutrino (Nobel Prize 1995)

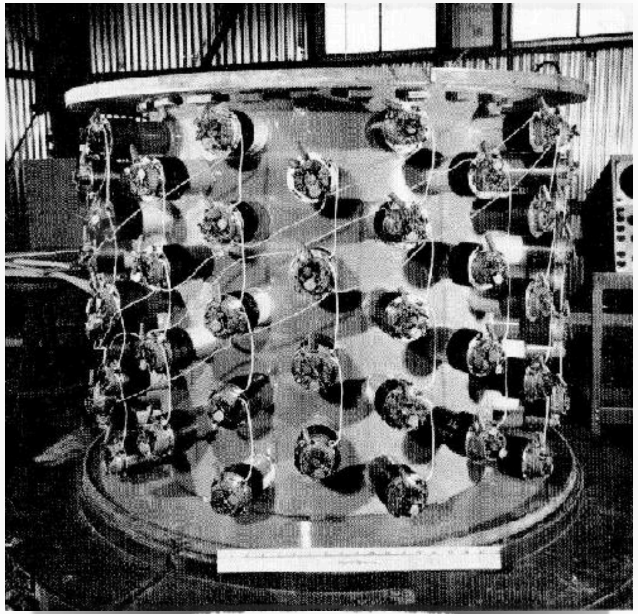

1962 - Discovery of **muon** neutrino

1991 - Indirect evidence that there are only 3 types of neutrinos

1998 - HELP: Missing neutrinos from the Sun!

2000 - Discovery of **tau** neutrino

Super-Kamiokande

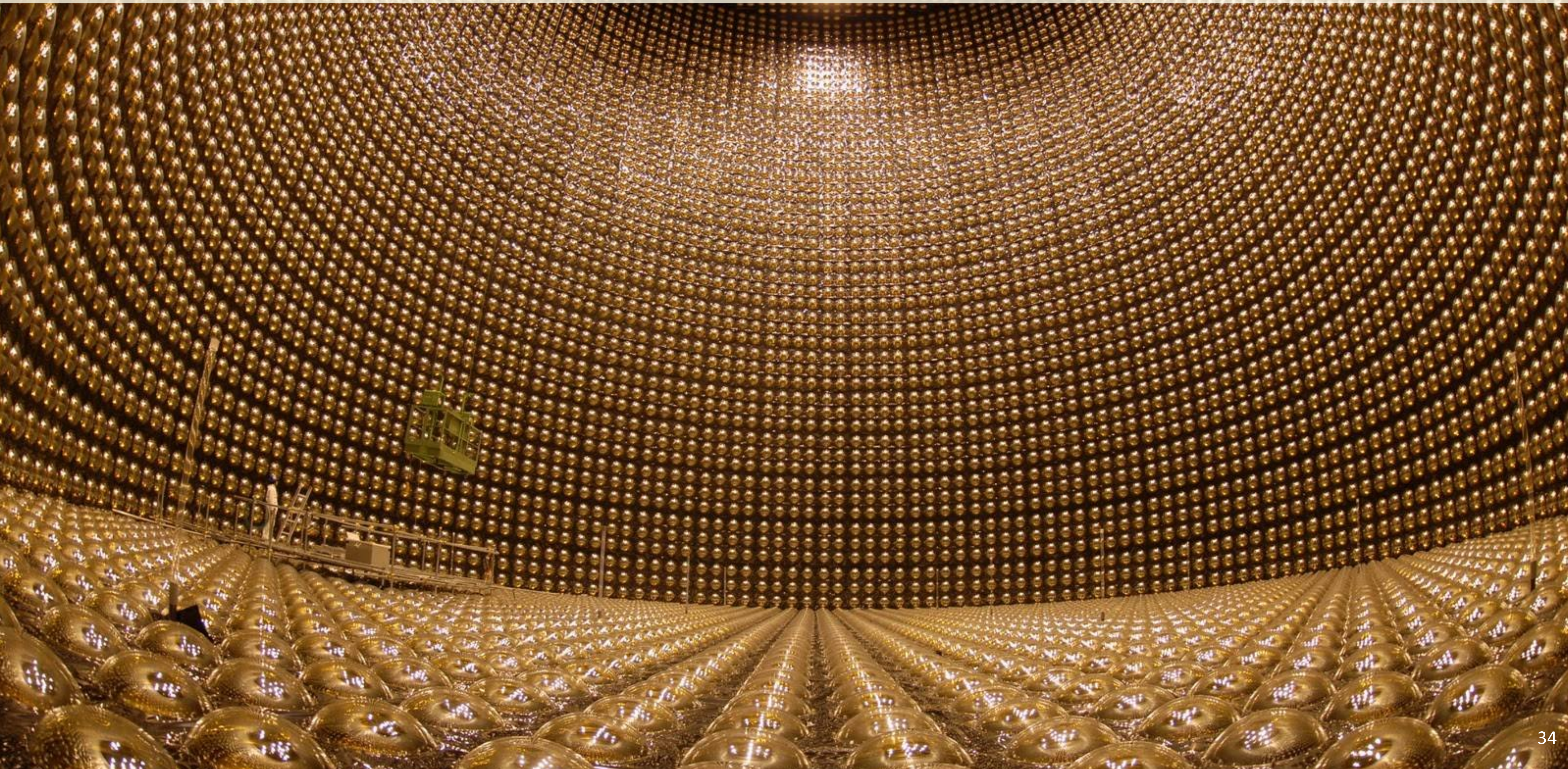

Super-Kamiokande

1000 meters underground

50 kton of pure water

13000 detectors

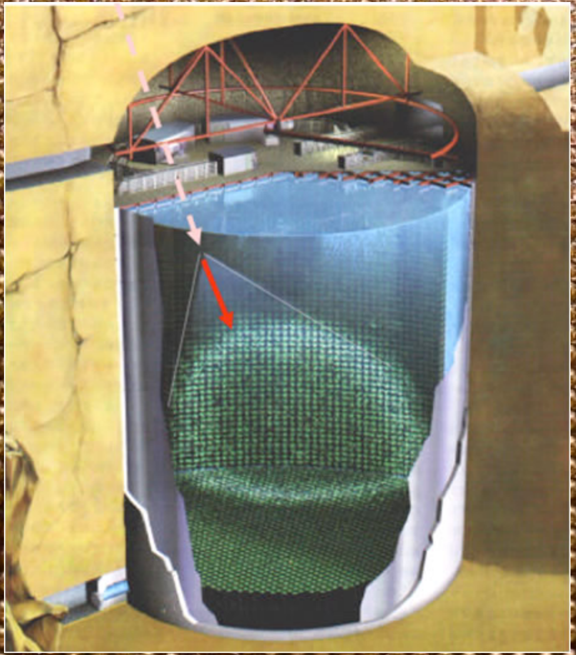

Super-Kamiokande

1000 meters underground

50 kton of pure water

13000 detectors

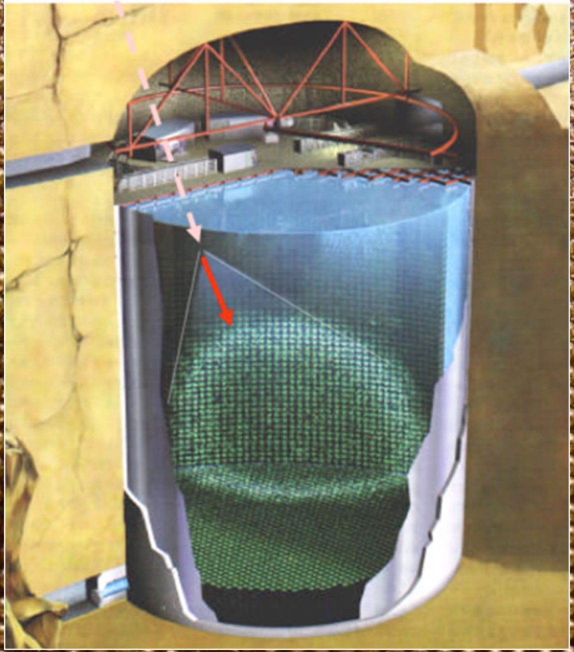

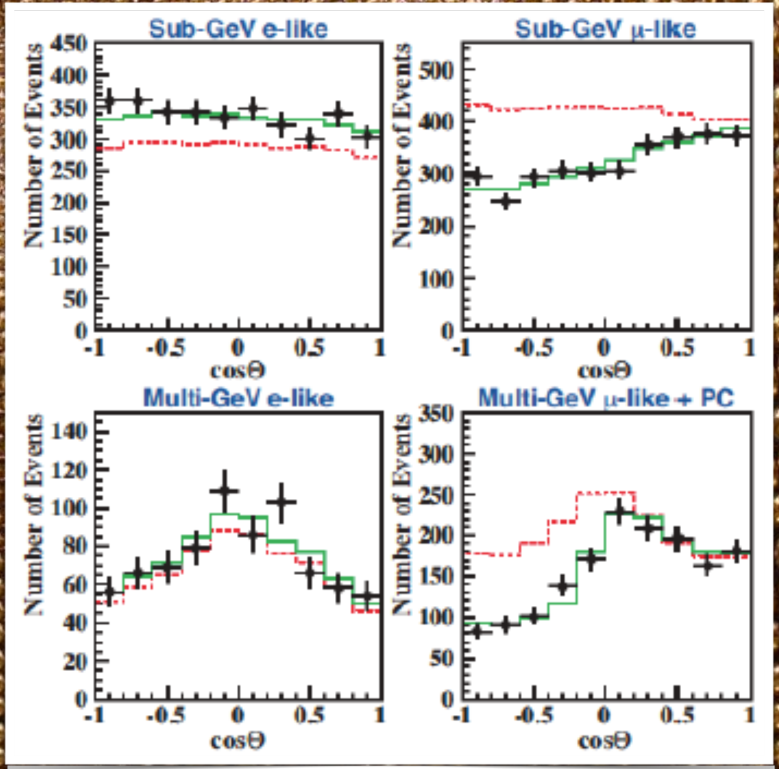

non-oscillated expected flux
best fit for $\nu_\mu \to \nu_\tau$ oscillation
data

What happened to the missing neutrinos?

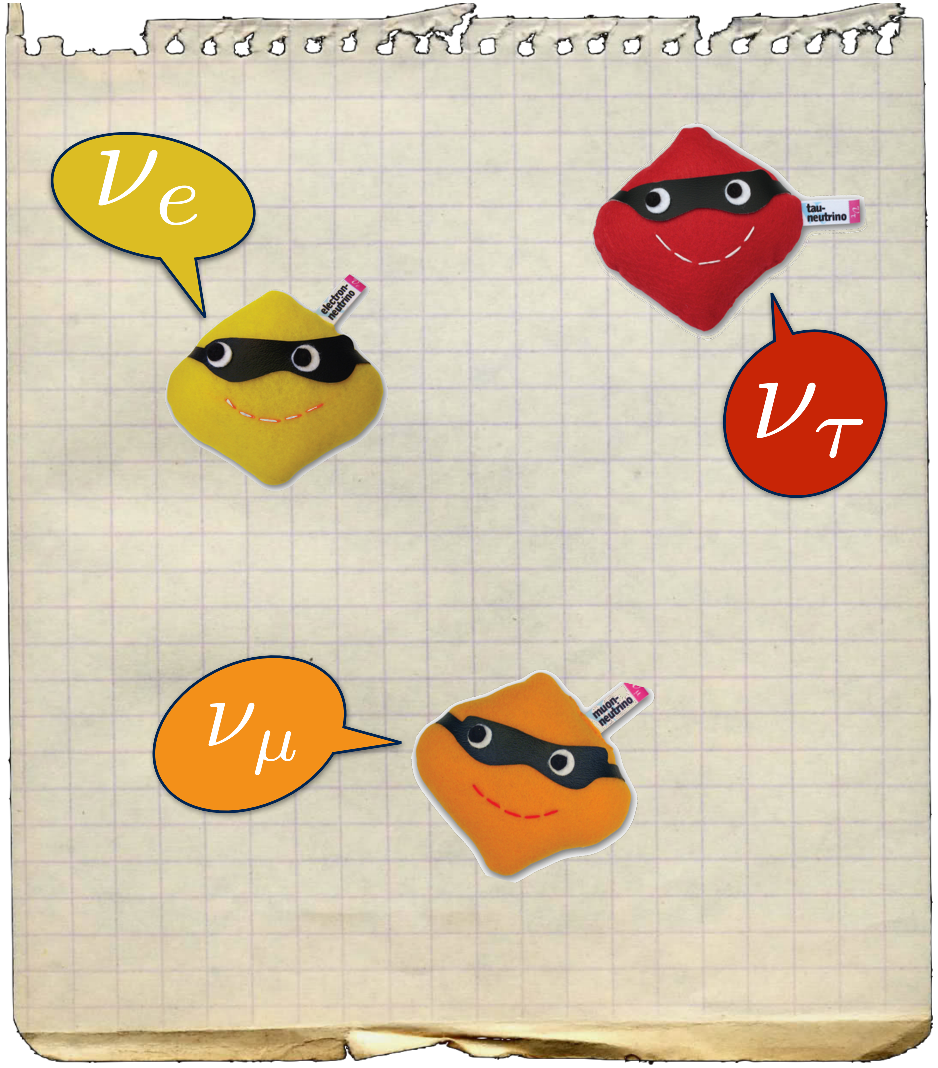

What happened to the missing neutrinos?

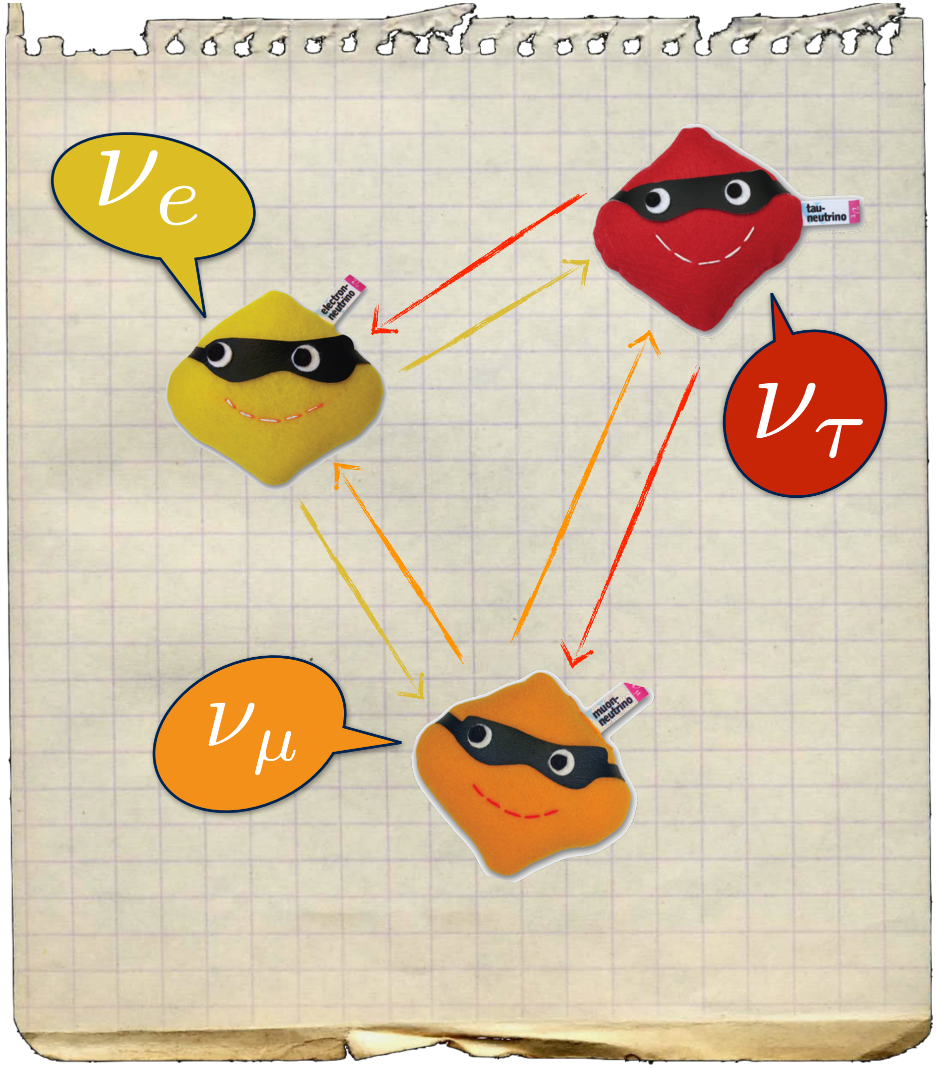

What happened to the missing neutrinos?

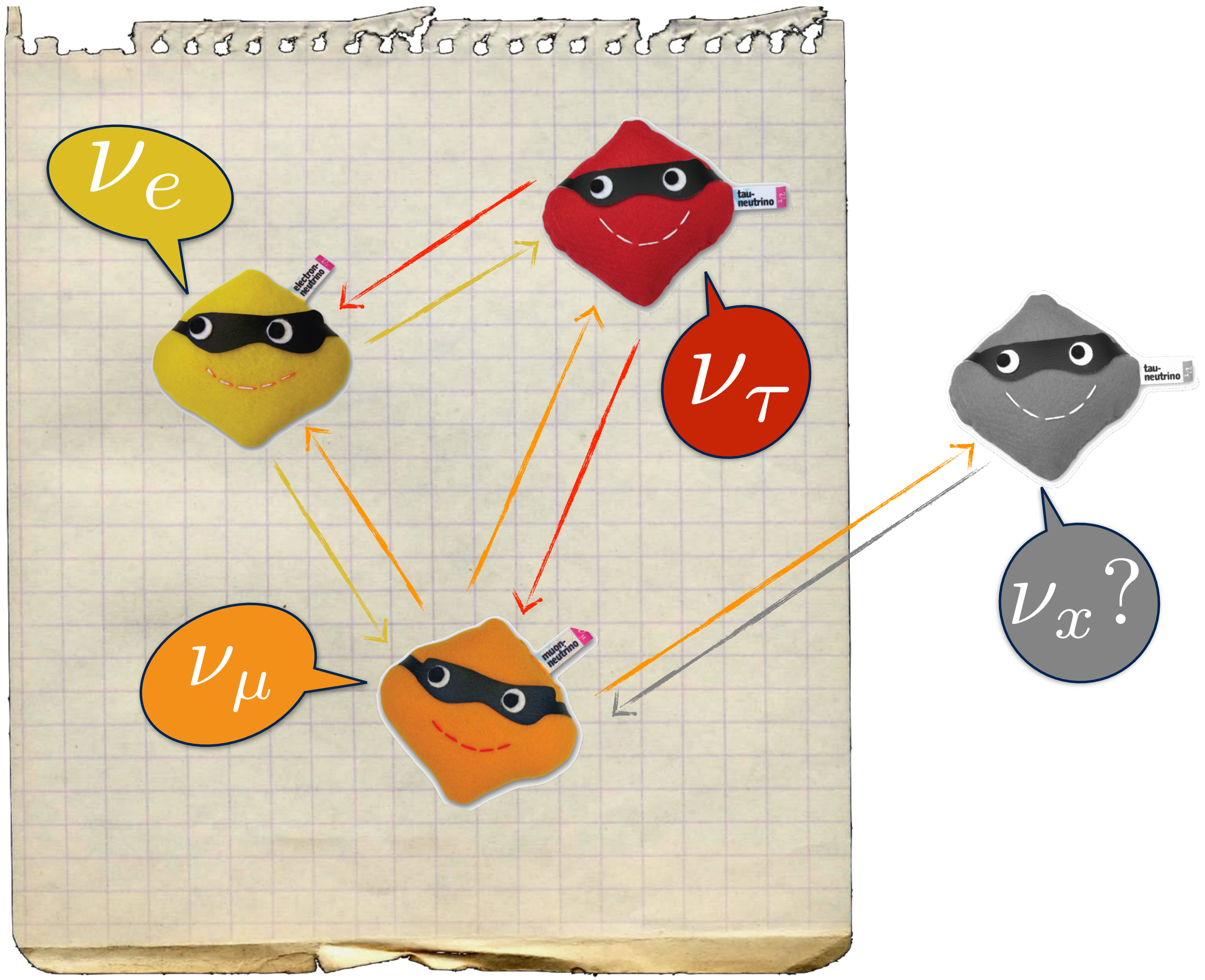

Neutrino oscillations

1957 - Bruno Pontecorvo hypothesizes that neutrinos can **oscillate**

$\Longrightarrow$ If the neutrino oscillates then it has **mass**!

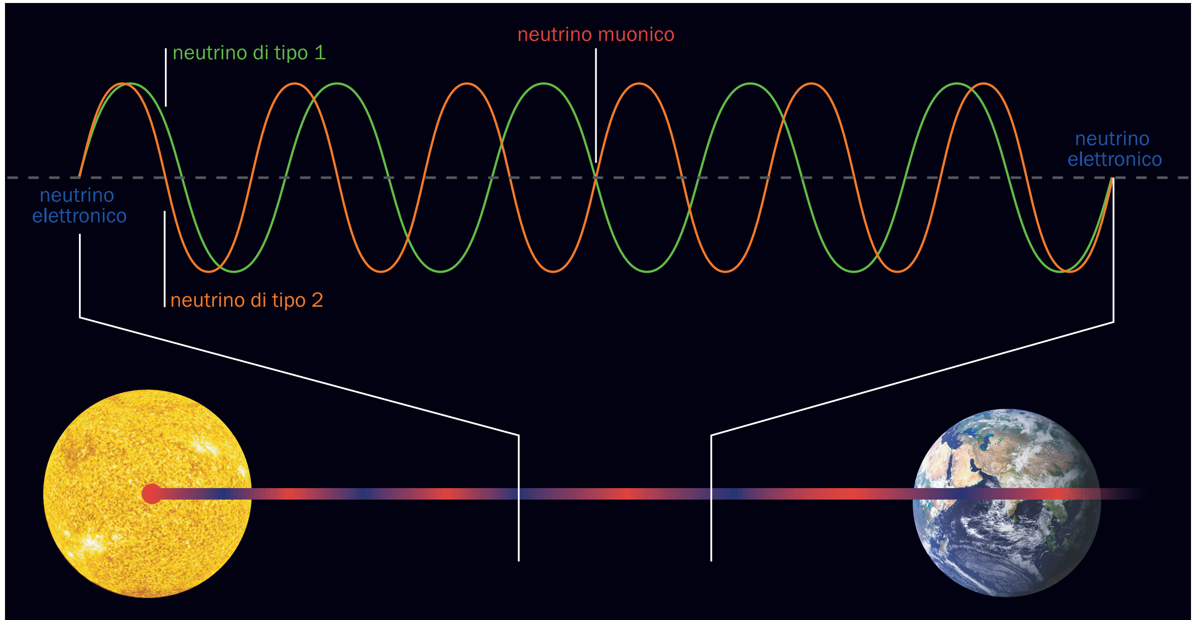

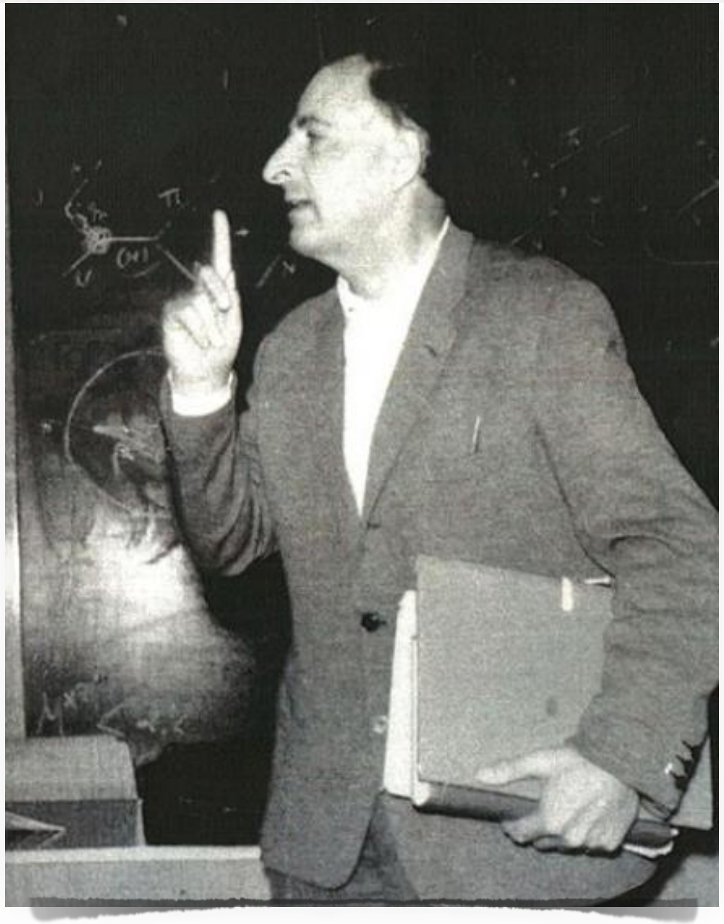

The largest camera in the world

- Small neutrino cross-section and beam divergence: massive active target (~ 1.2 kton target with 30 ton emulsions)
- Detect τ-lepton production and decay: micrometric space resolution

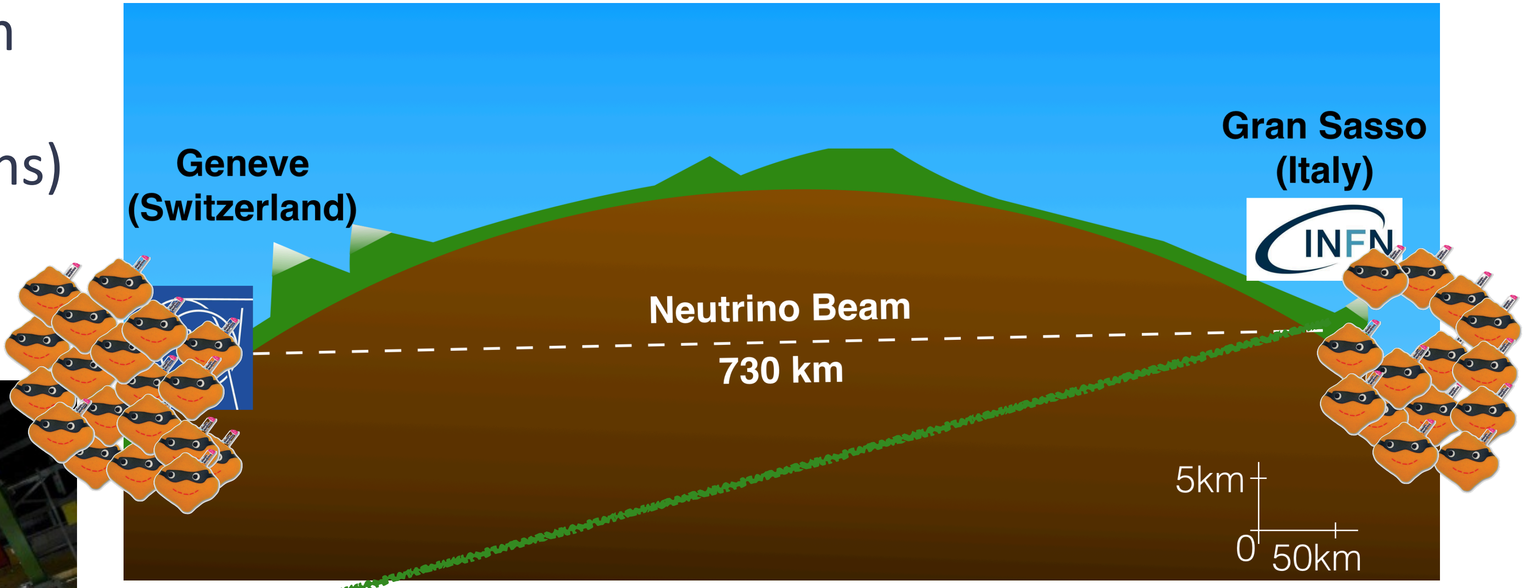

4000 tons

9 million nuclear emulsions

110000 m² of emulsion films

The largest camera in the world

- Small neutrino cross-section and beam divergence: massive active target (~ 1.2 kton target with 30 ton emulsions)
- Detect τ-lepton production and decay: micrometric space resolution

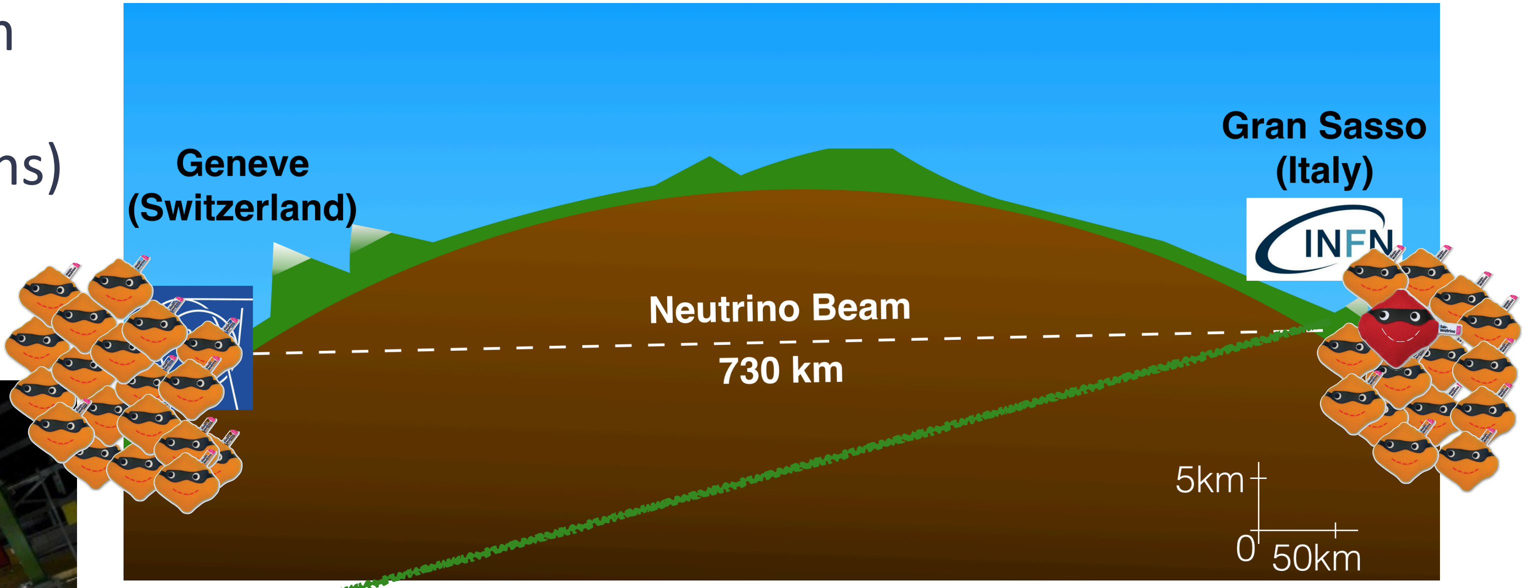

4000 tons

9 million nuclear emulsions

110000 m² of emulsion films

The largest camera in the world

SM1 SM2

ν

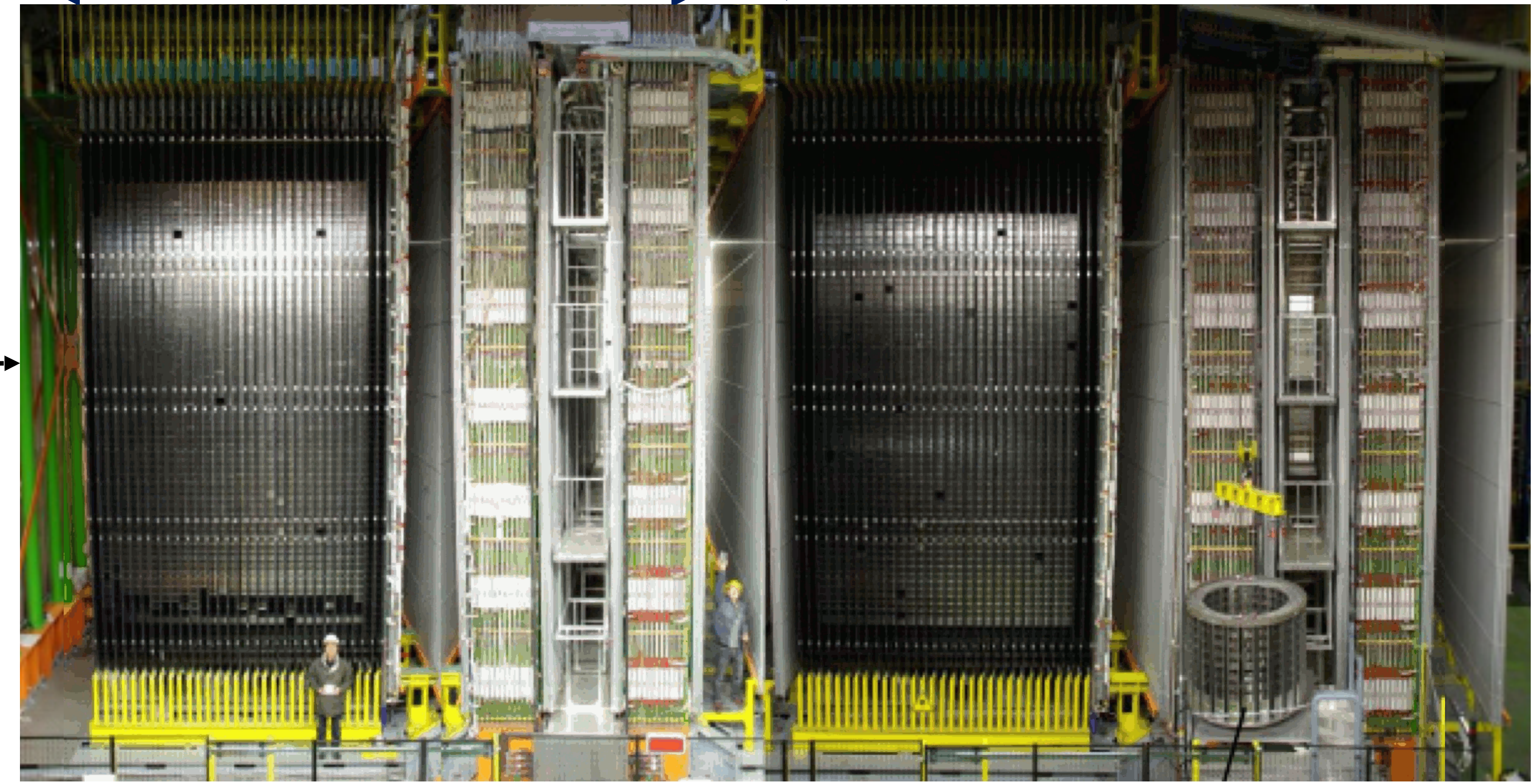

1400 meters underground: **Gran Sasso National Laboratories**

(reduction of cosmic ray flux by a factor of 10^6)

The largest camera in the world

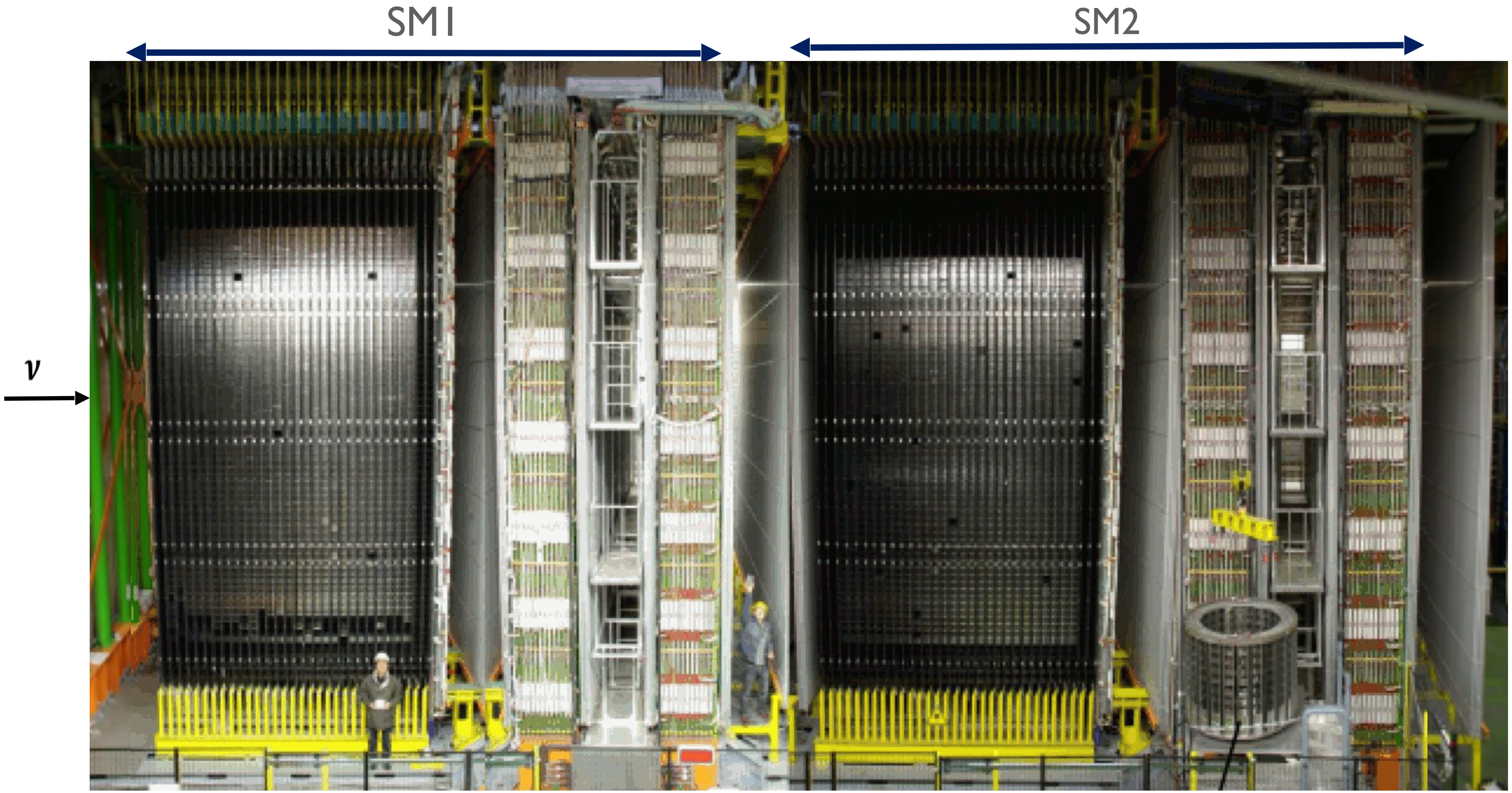

1400 meters underground: **Gran Sasso National Laboratories**

(reduction of cosmic ray flux by a factor of 10^6)

The largest camera in the world

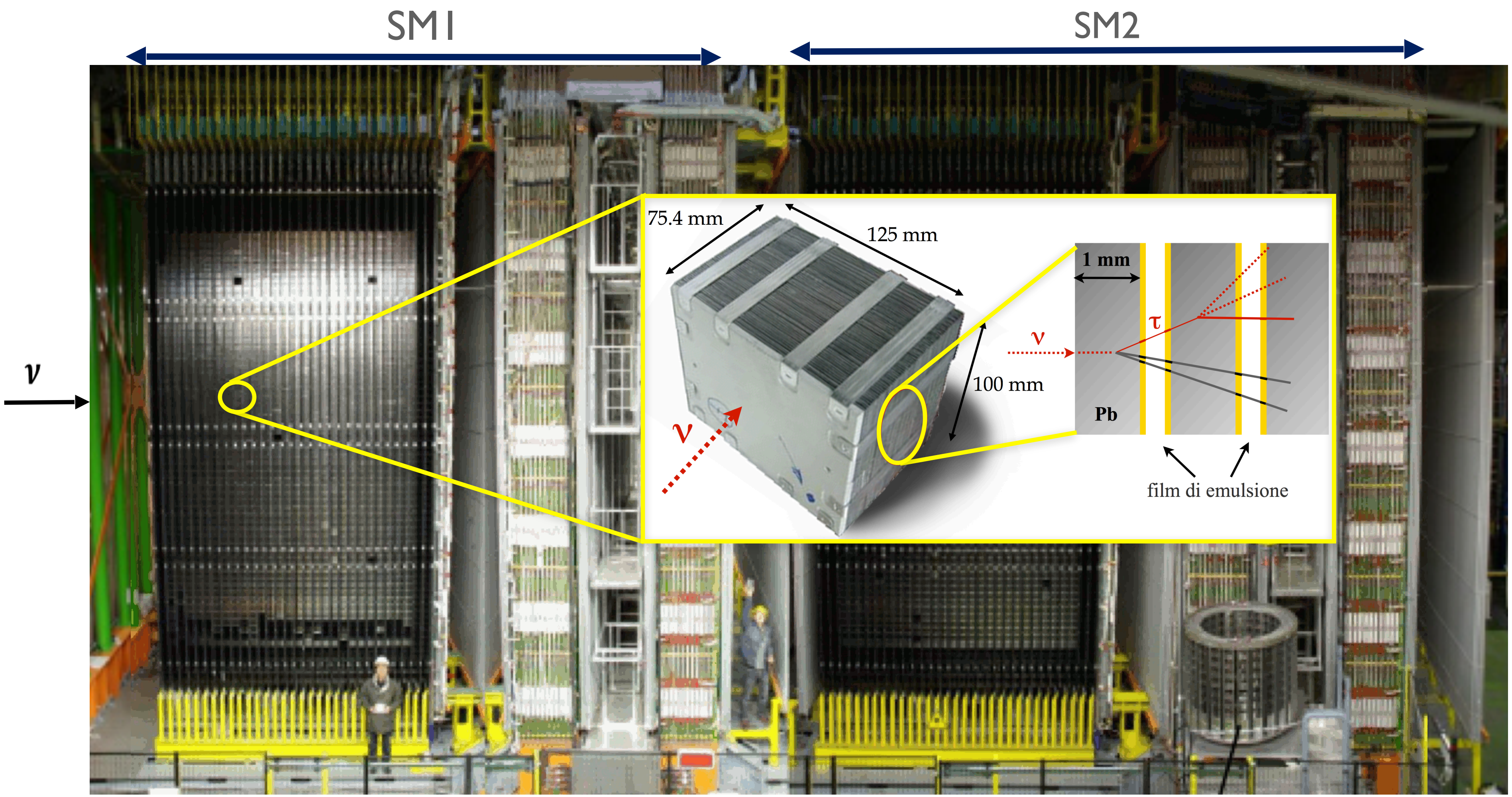

1400 meters underground: **Gran Sasso National Laboratories**

(reduction of cosmic ray flux by a factor of 10^6)

Bricks: the heart of the detector

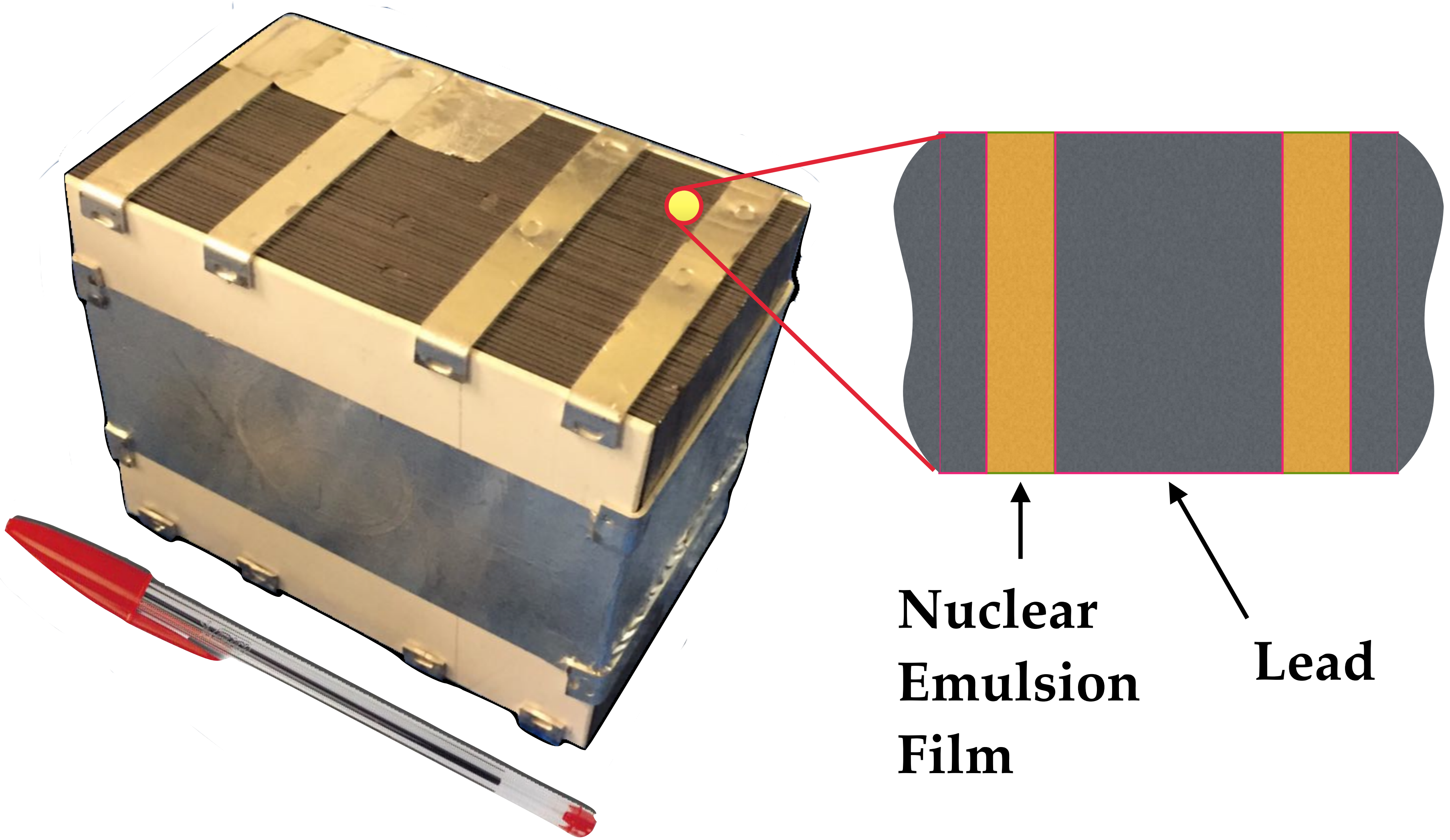

Bricks: the heart of the detector

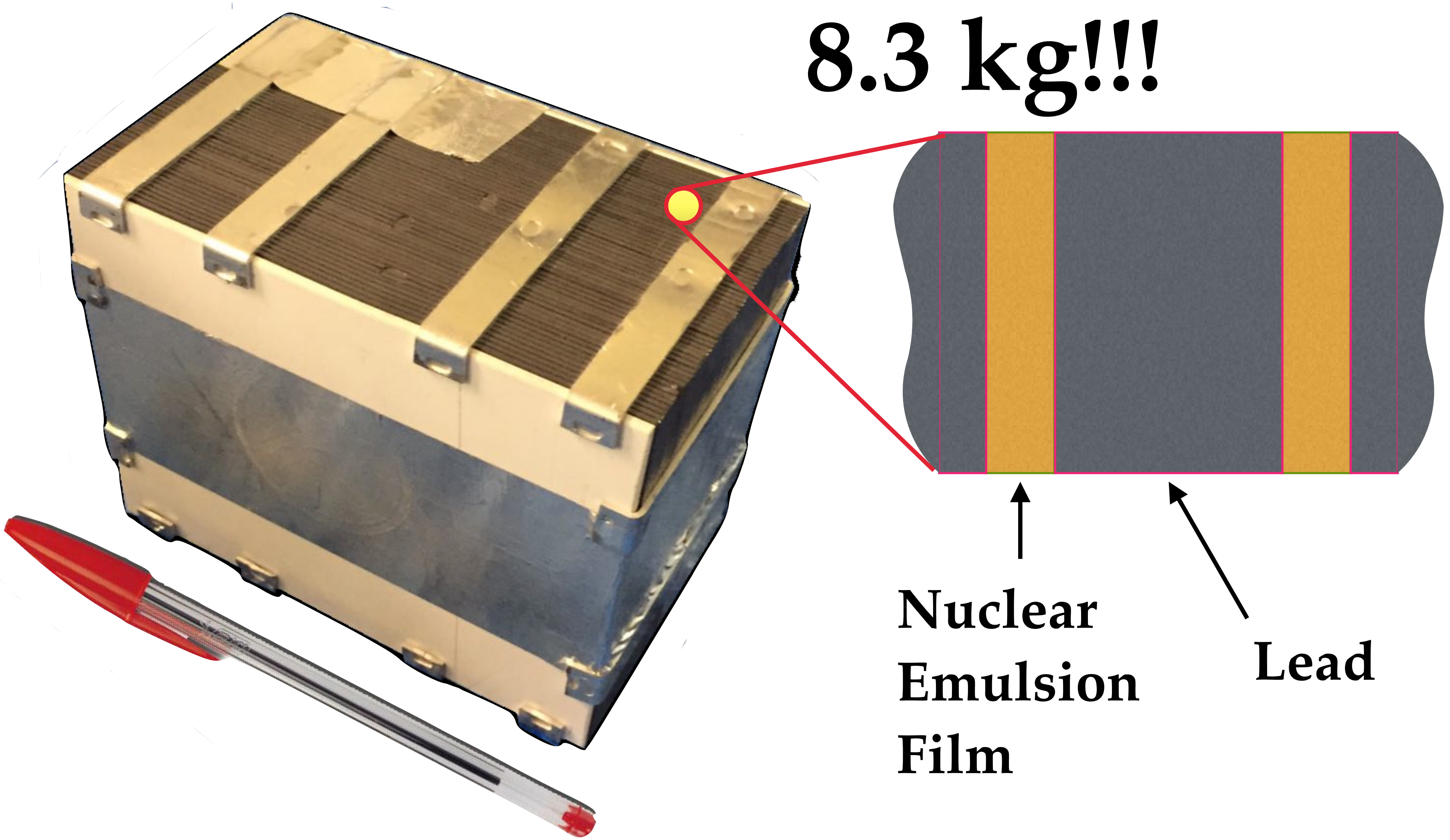

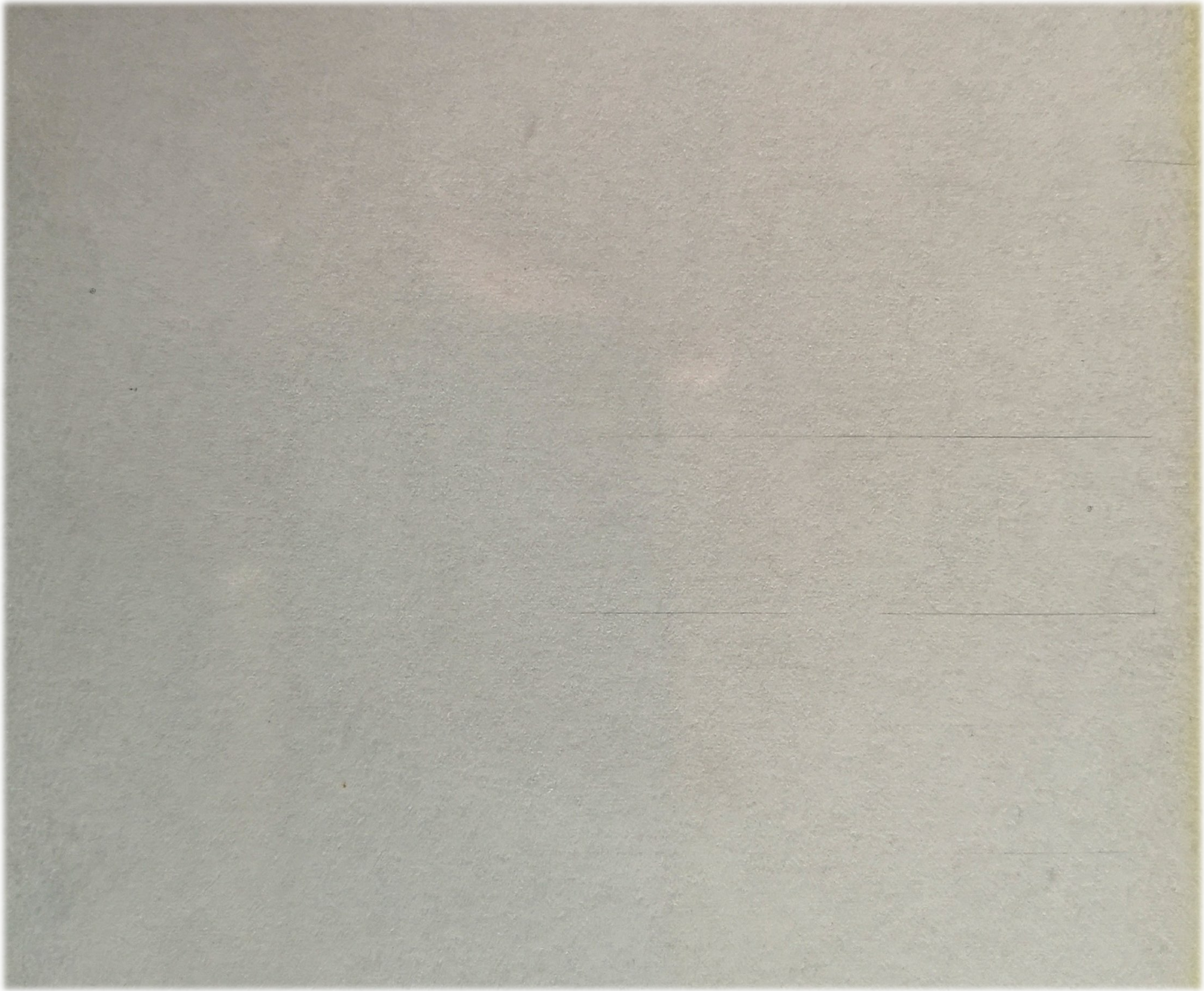

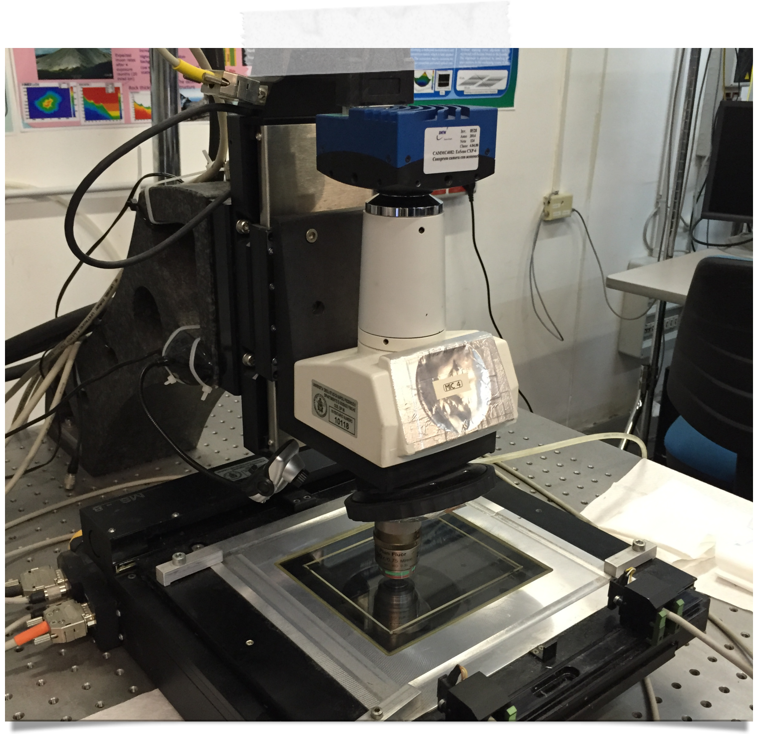

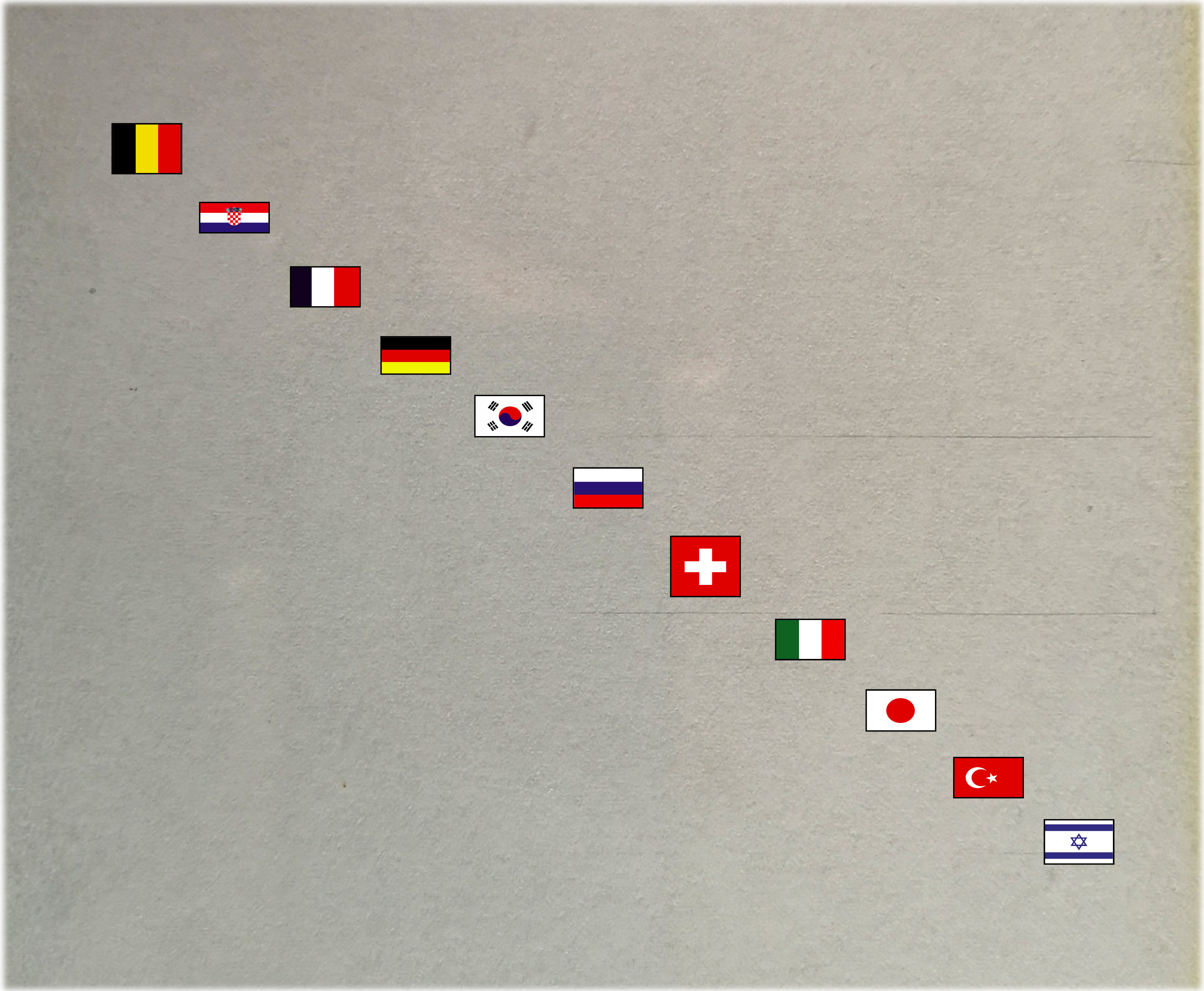

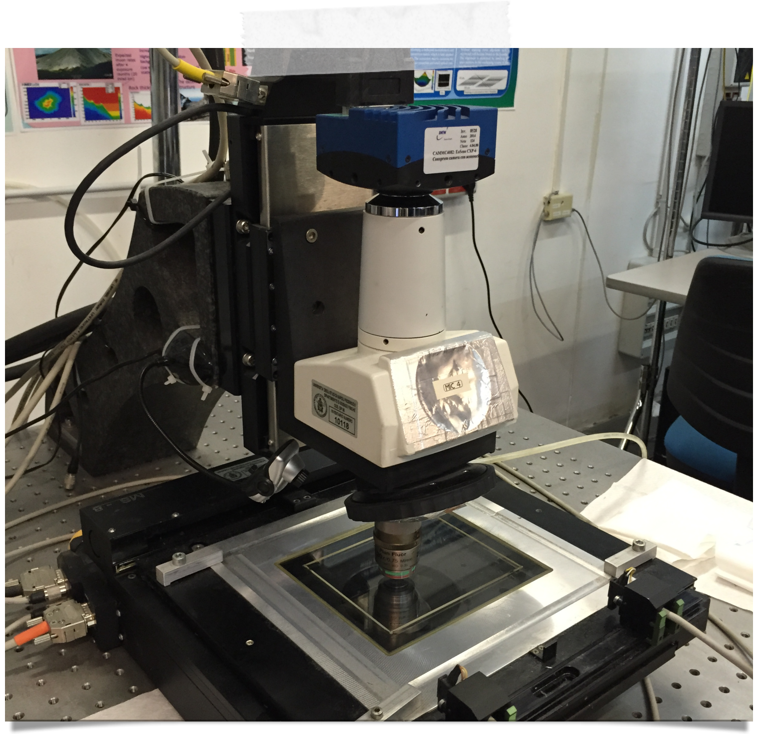

The OPERA experiment

The OPERA experiment

- Electronic detectors to provide the“time stamp”, preselect the interaction brick and reconstruct μ charge/momentum

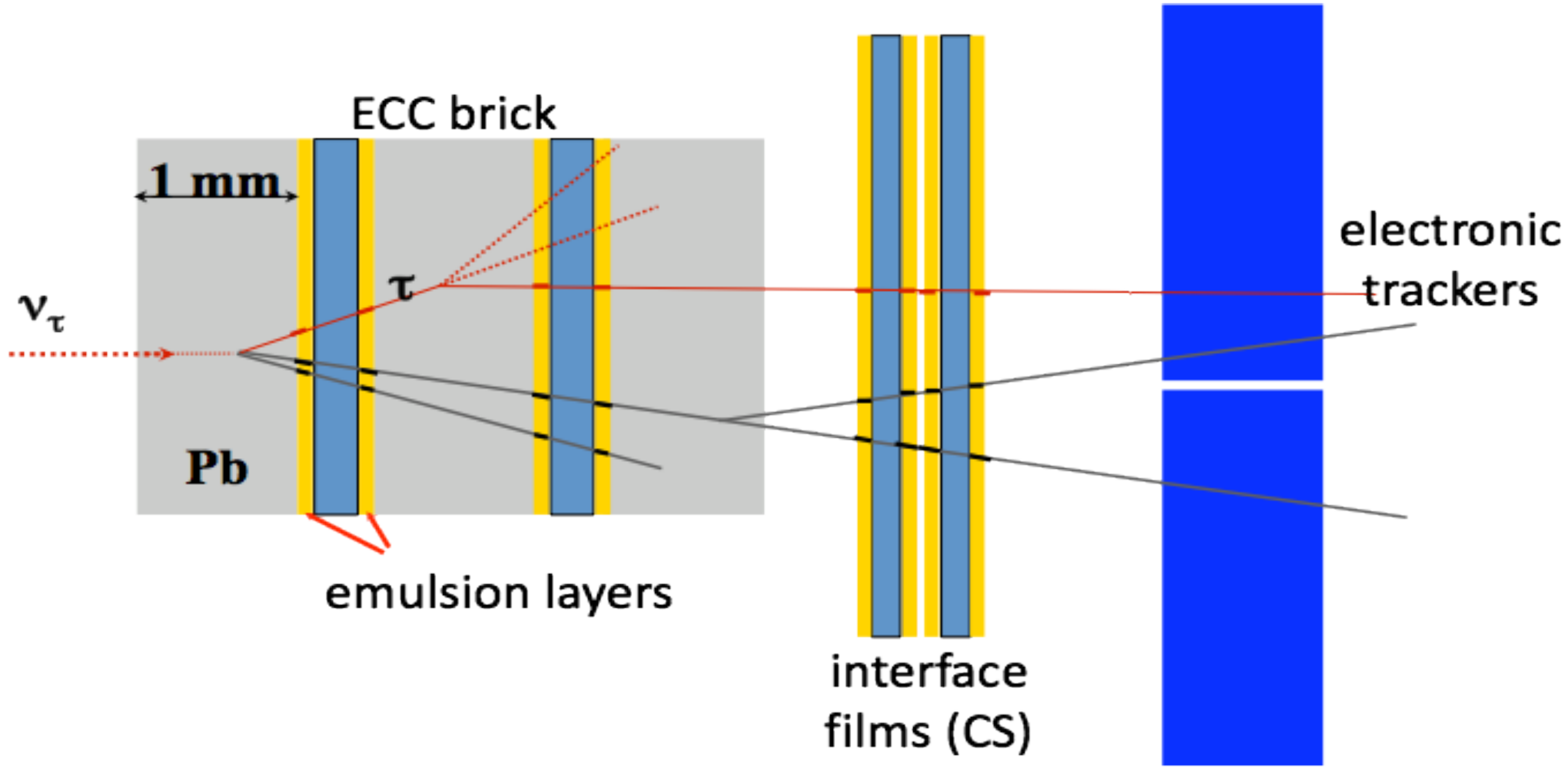

Interface emulsion films

- High signal/noise ratio for event trigger and scanning time reduction

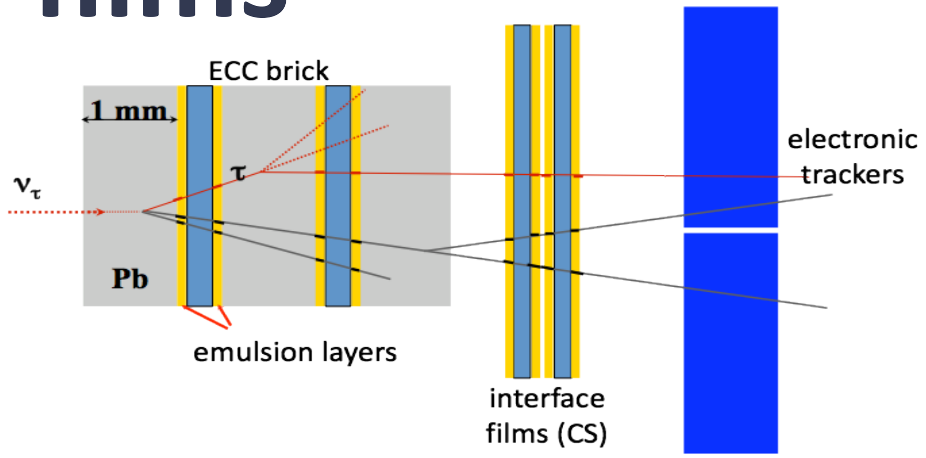

ν_μ

XZ projection

ν_μ

YZ projection

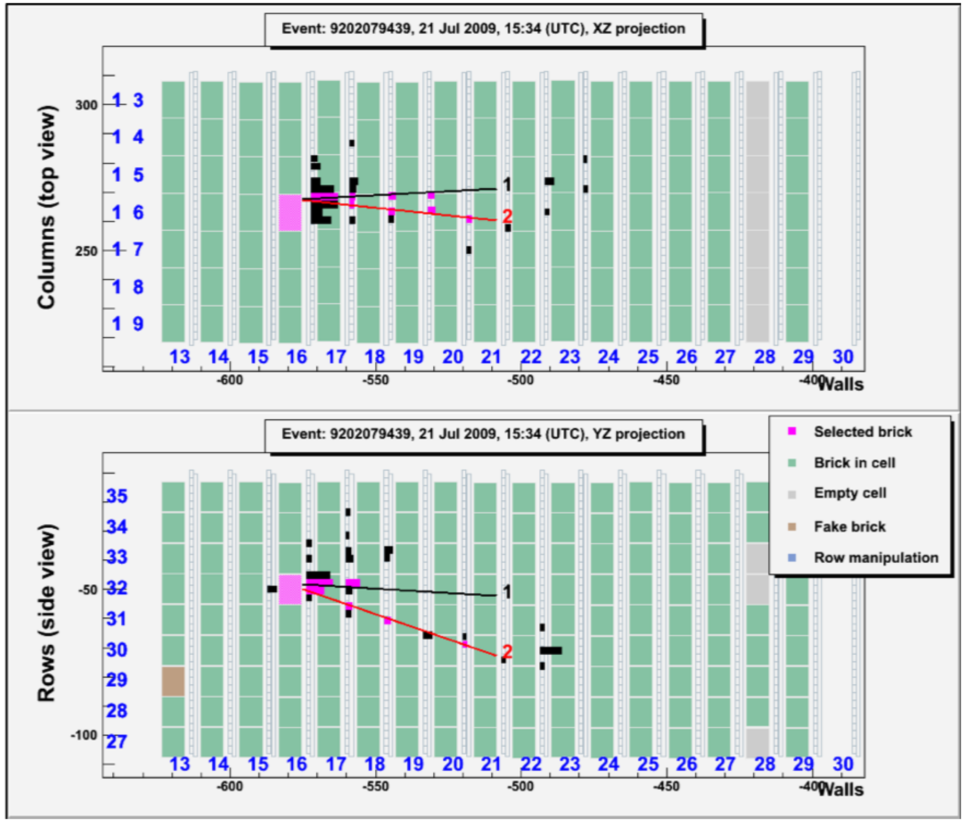

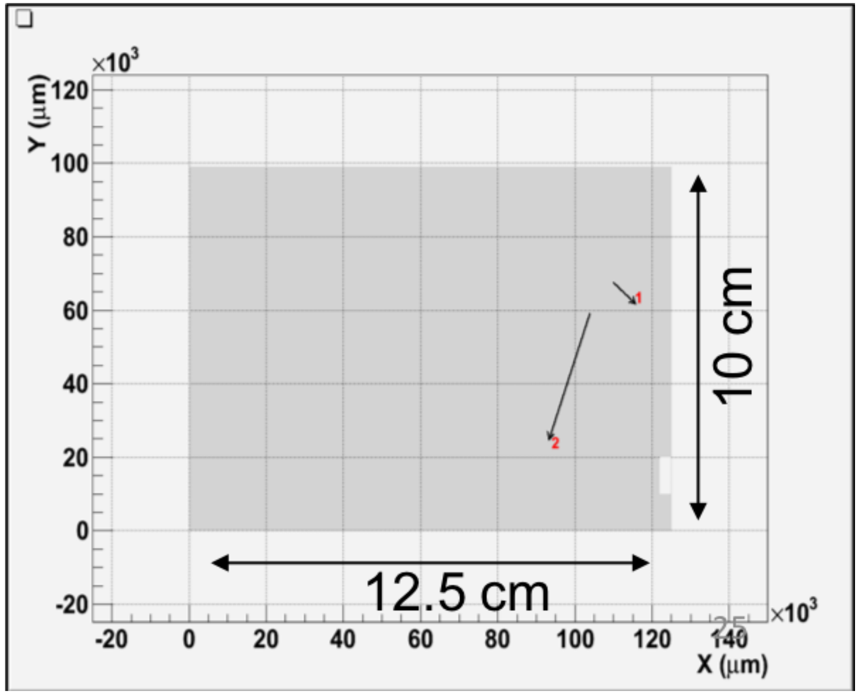

Interface emulsion films

Example of electron neutrino

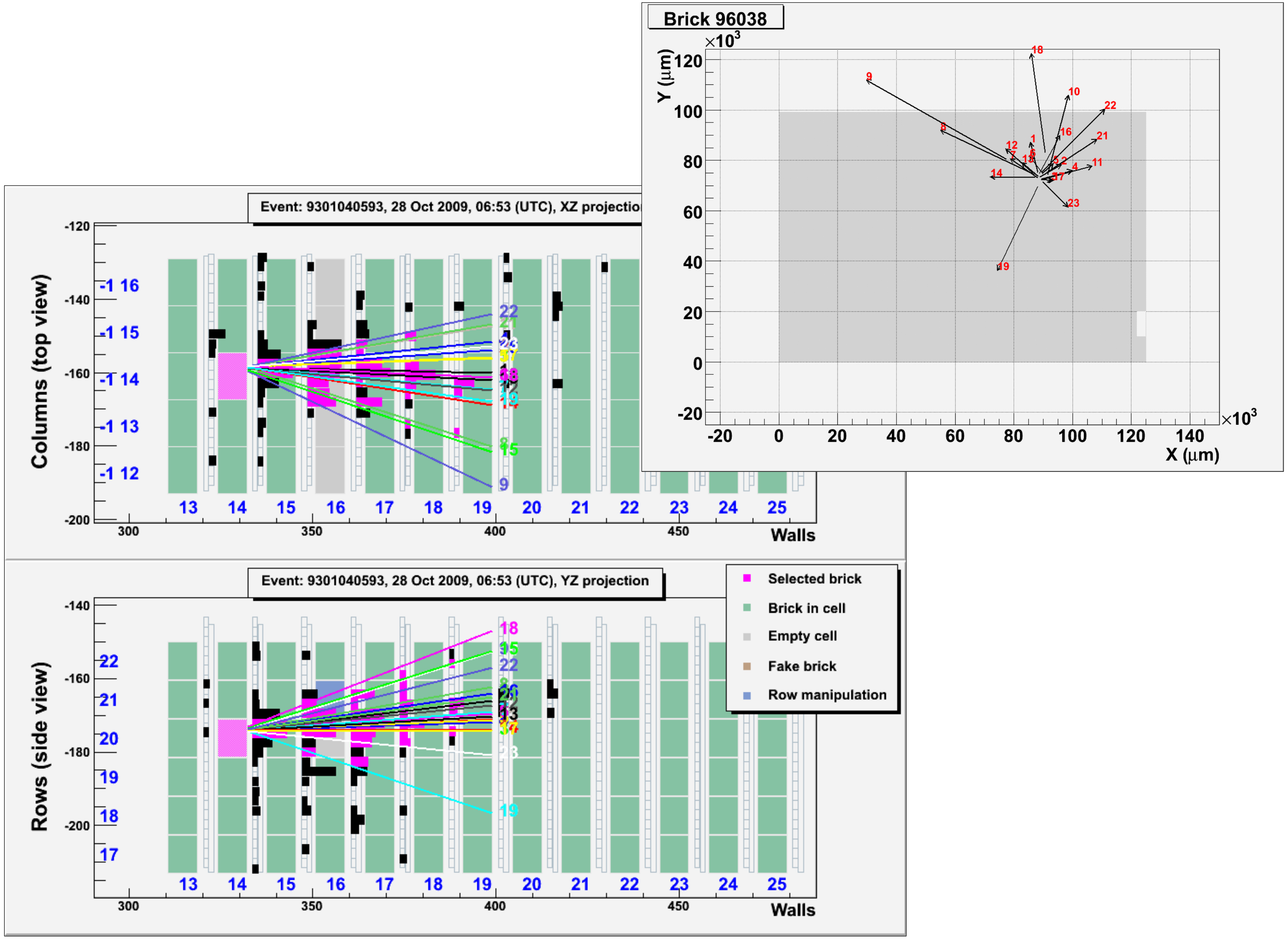

Interface emulsion films

Example of electron neutrino

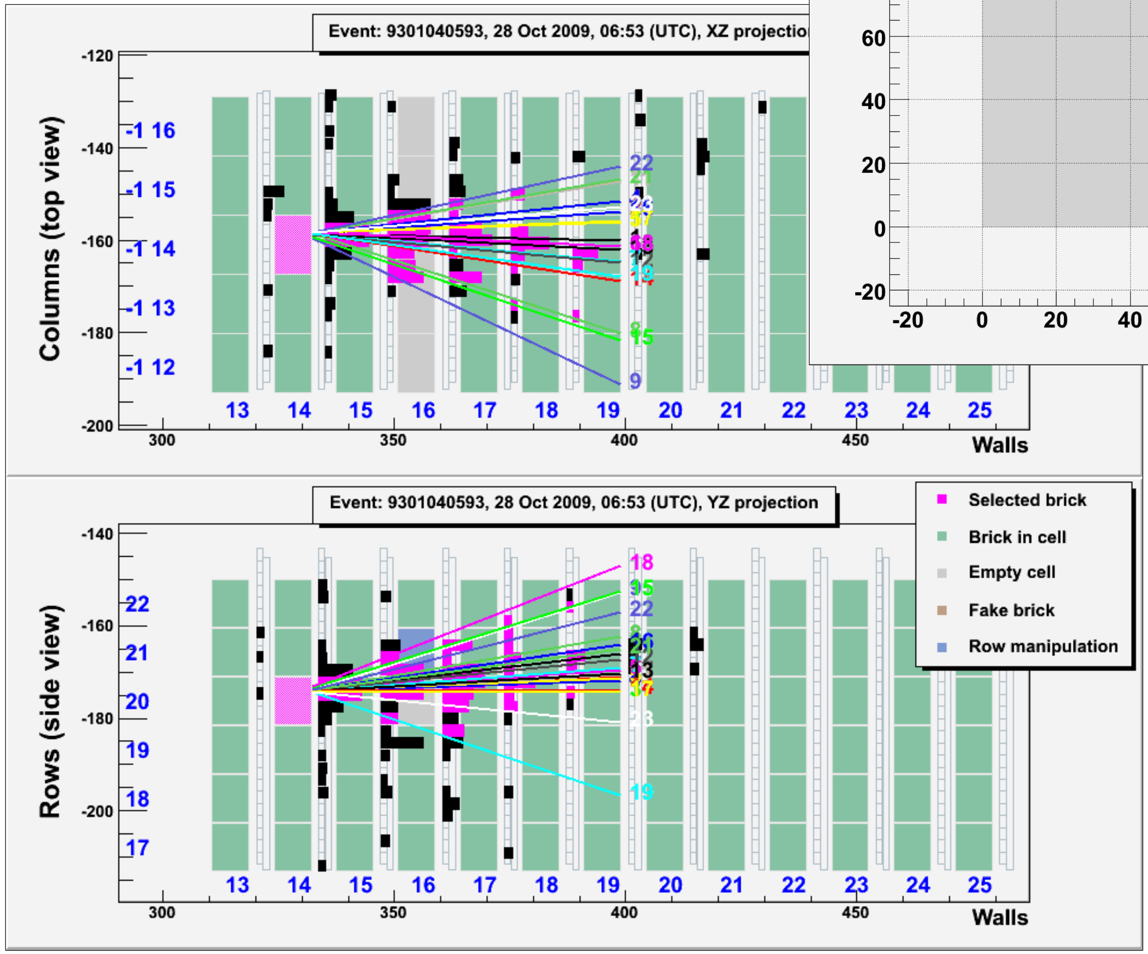

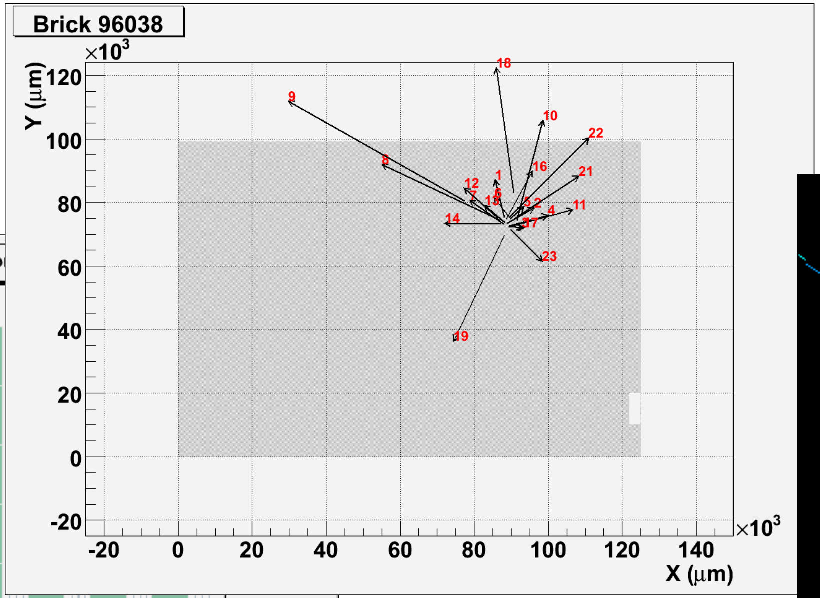

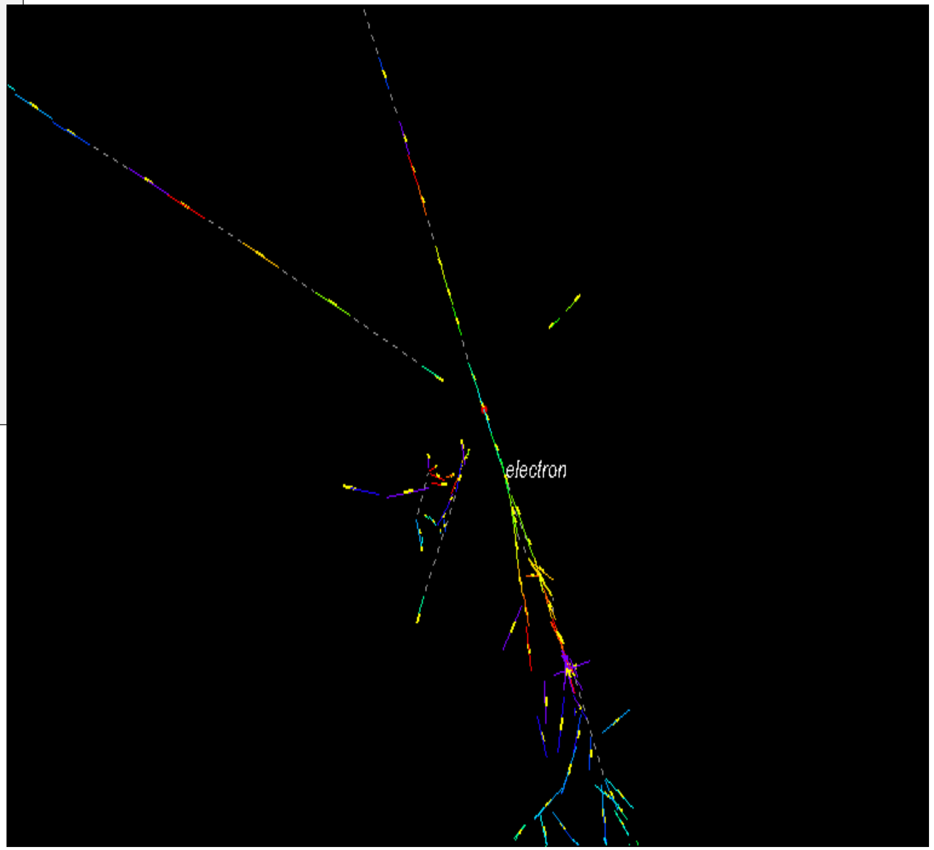

Track follow-up and vertex finding

- Track follow-up film by film:
  - Brick exposure at the surface laboratory to cosmic-rays for alignment
  - Definition of the stopping point

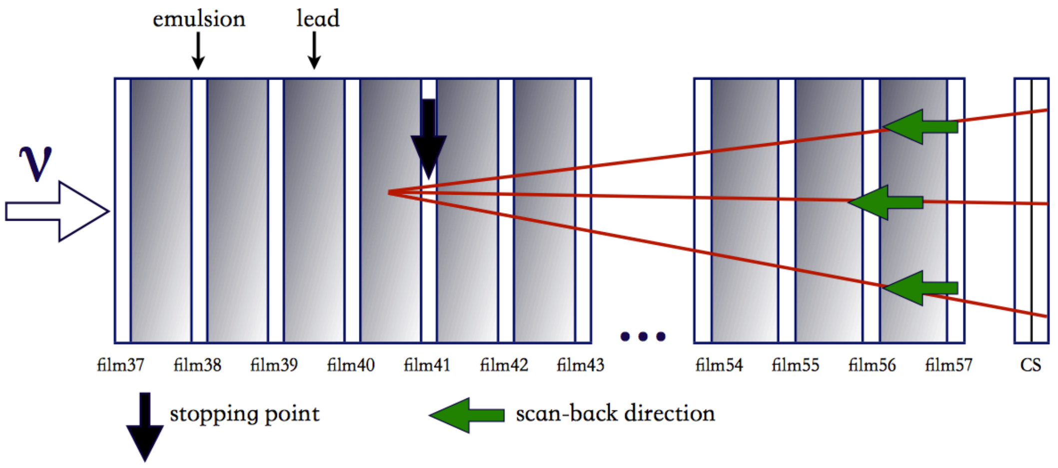

- Volume scan: ~1-2 cm³ around the stopping point

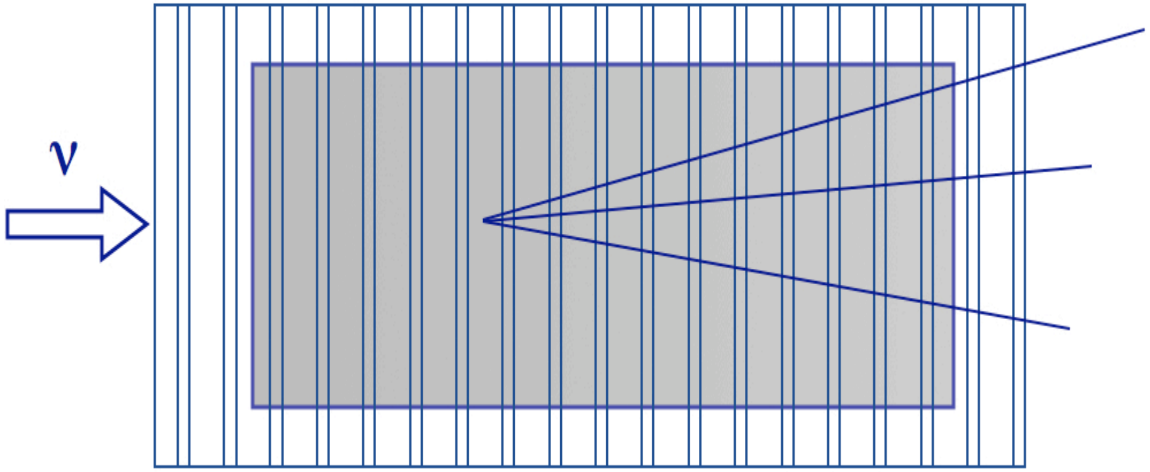

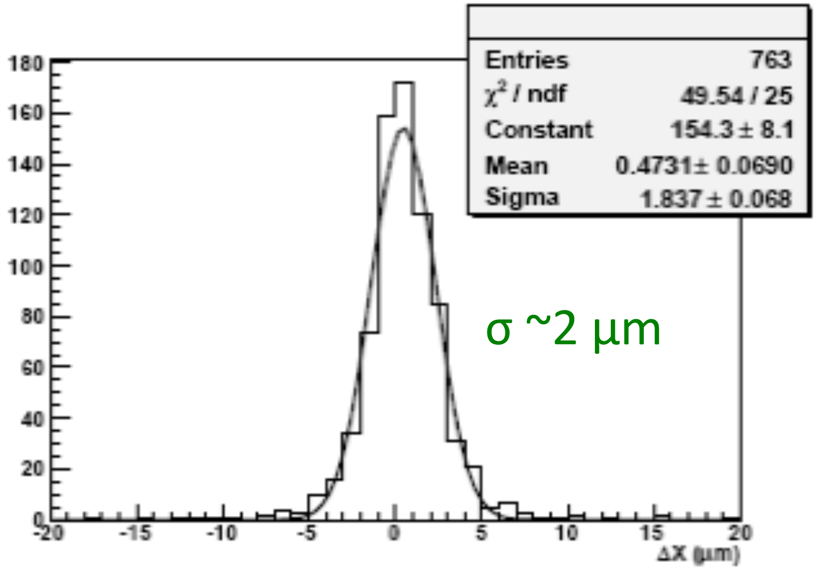

Location of neutrino interactions

- Basetracks: 3D vector data, micrometric precision

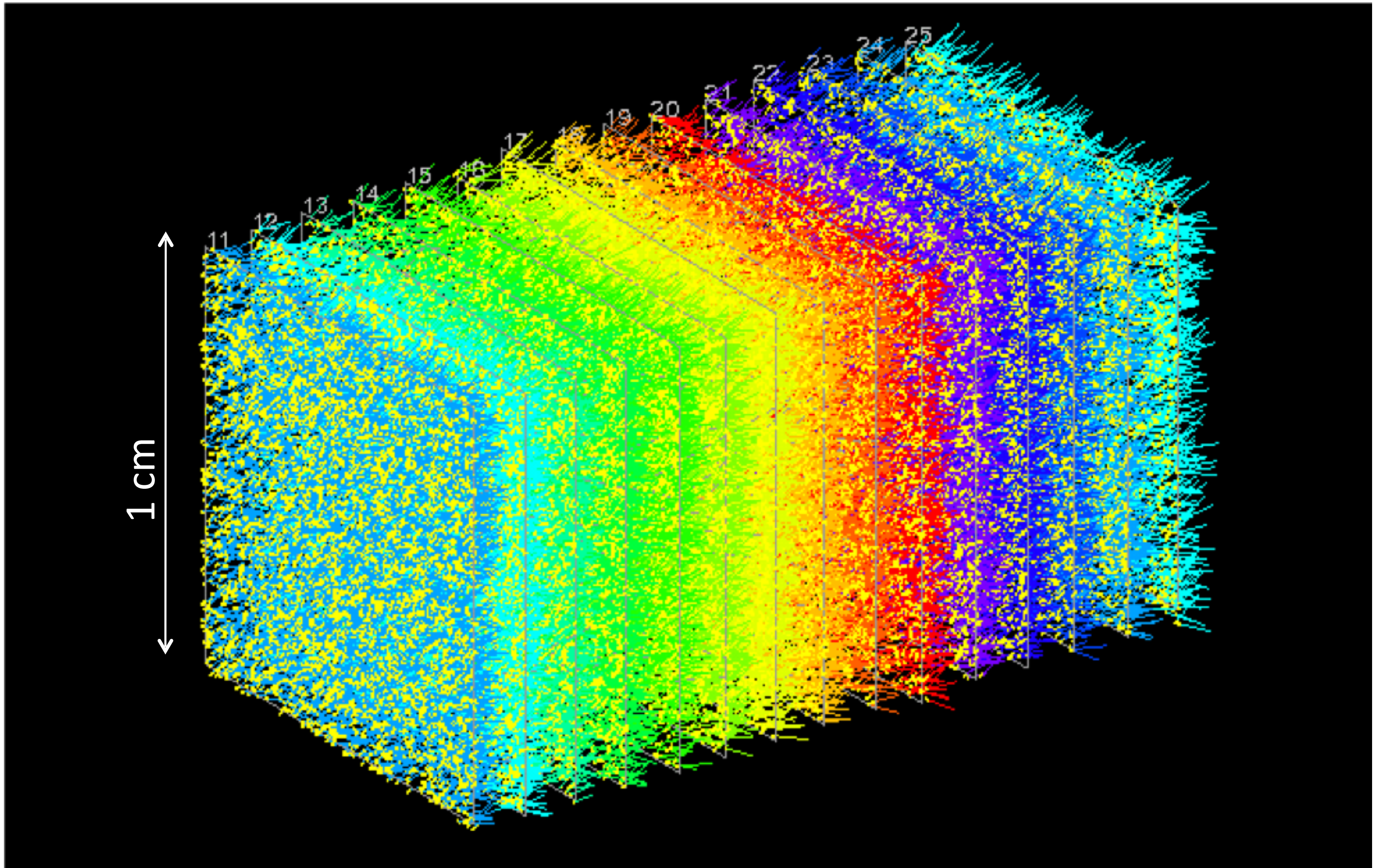

Location of neutrino interactions

- Aligned basetracks: tracks

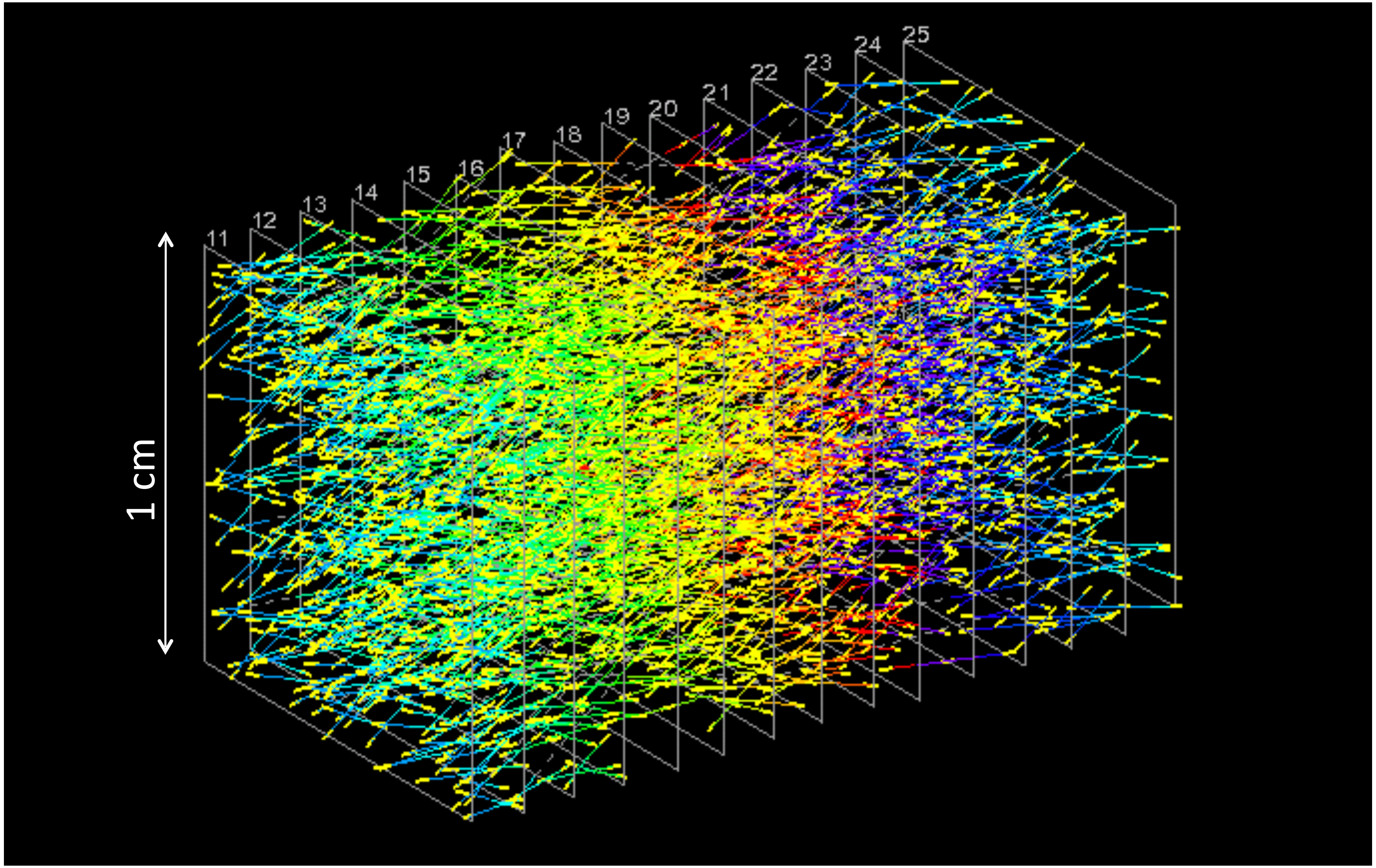

Location of neutrino interactions

- Converging tracks: vertex reconstruction

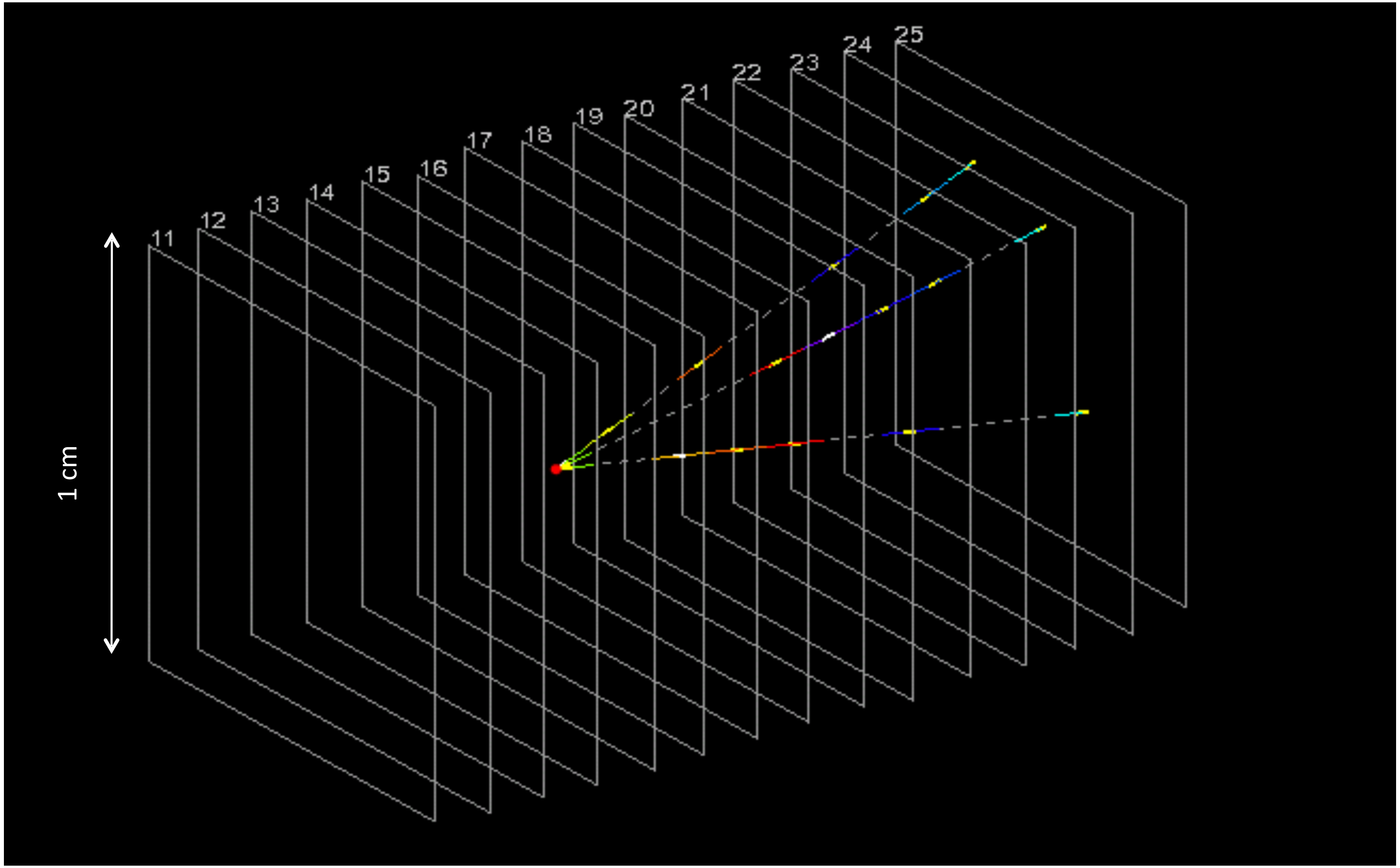

Location of neutrino interactions

- Converging tracks: vertex reconstruction

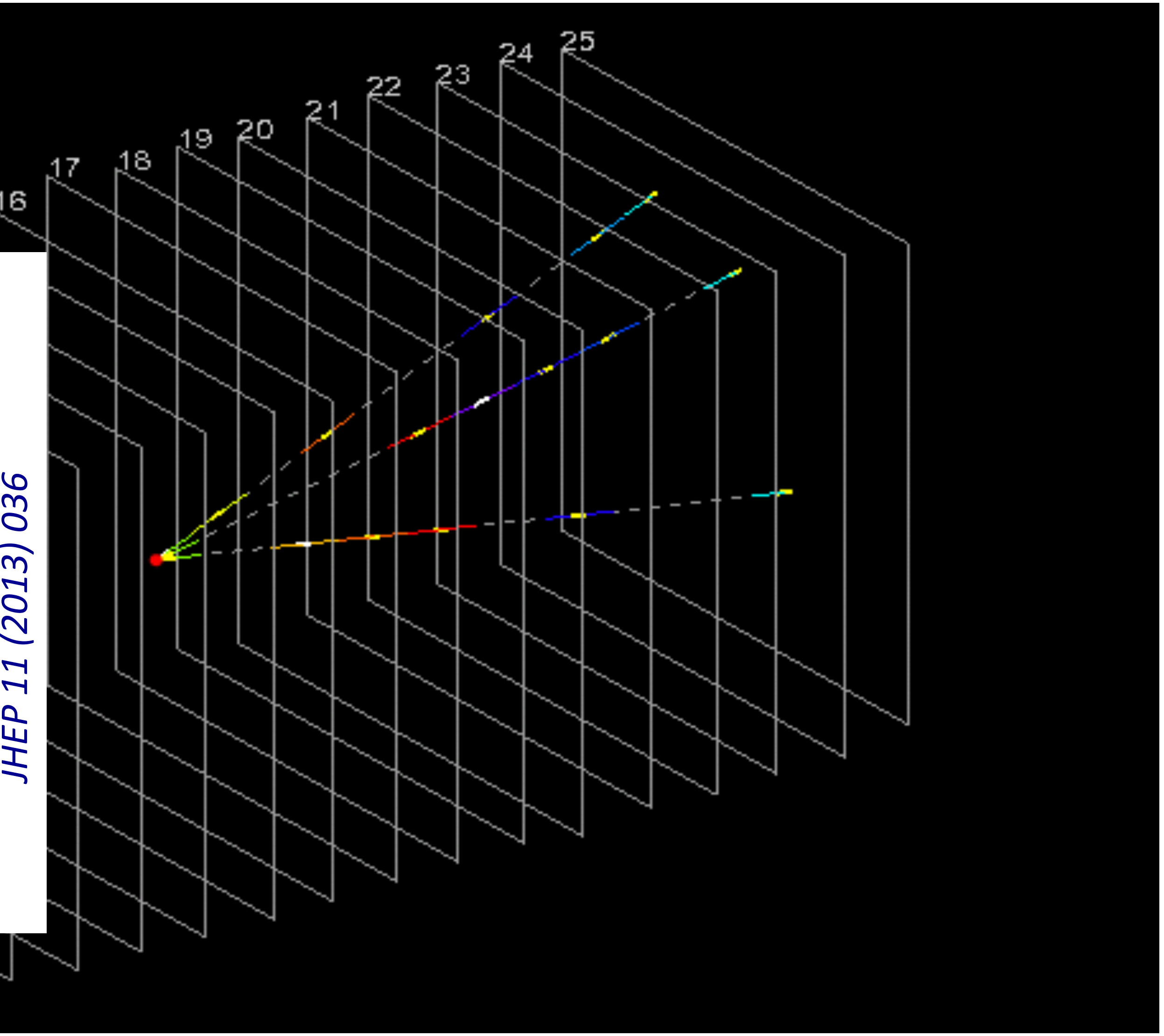

Event location efficiency versus energy

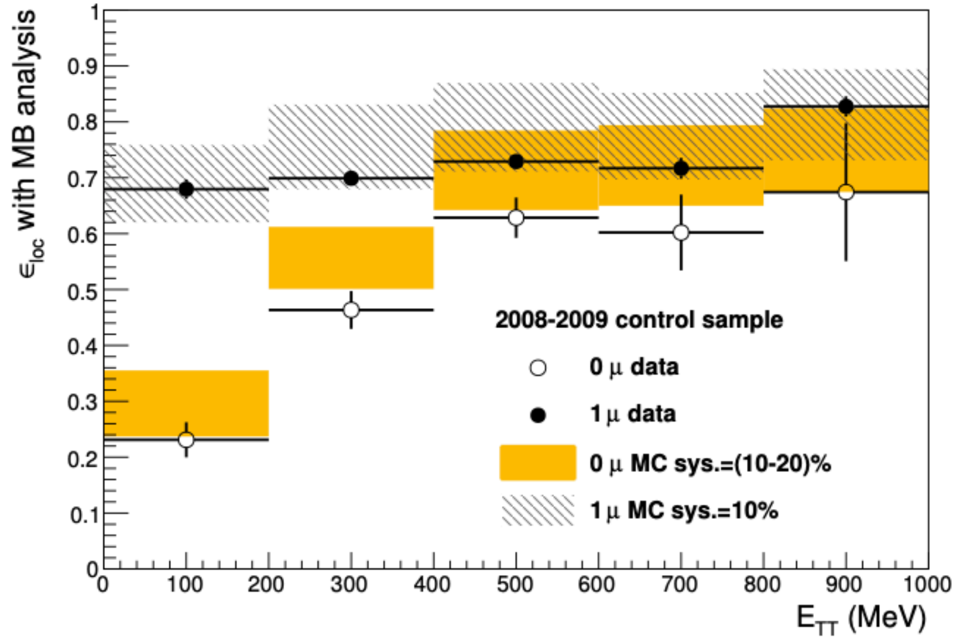

JHEP 11 (2013) 036

Recognize neutrinos

Recognize neutrinos

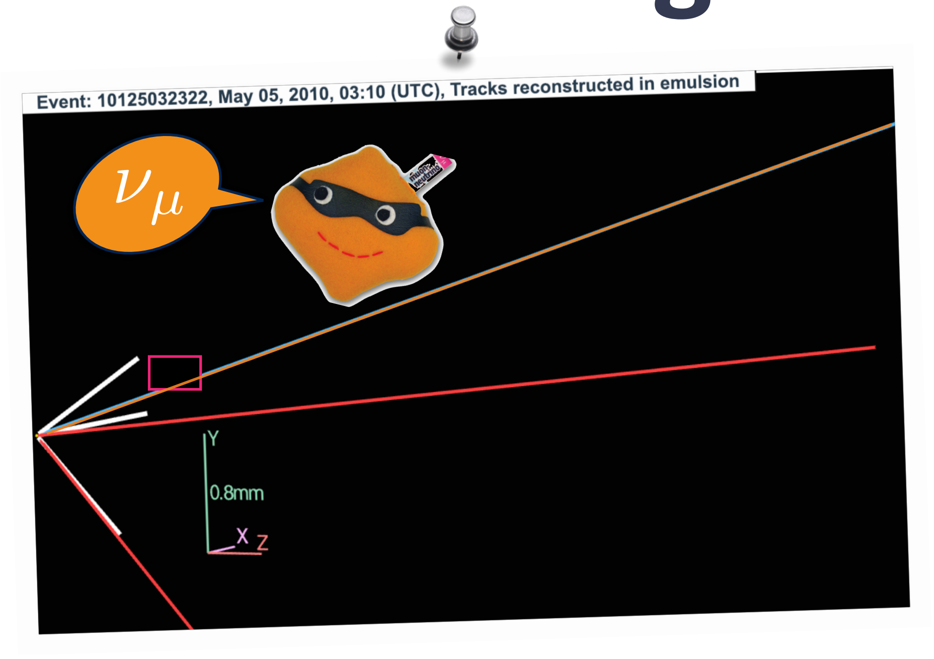

Recognize neutrinos

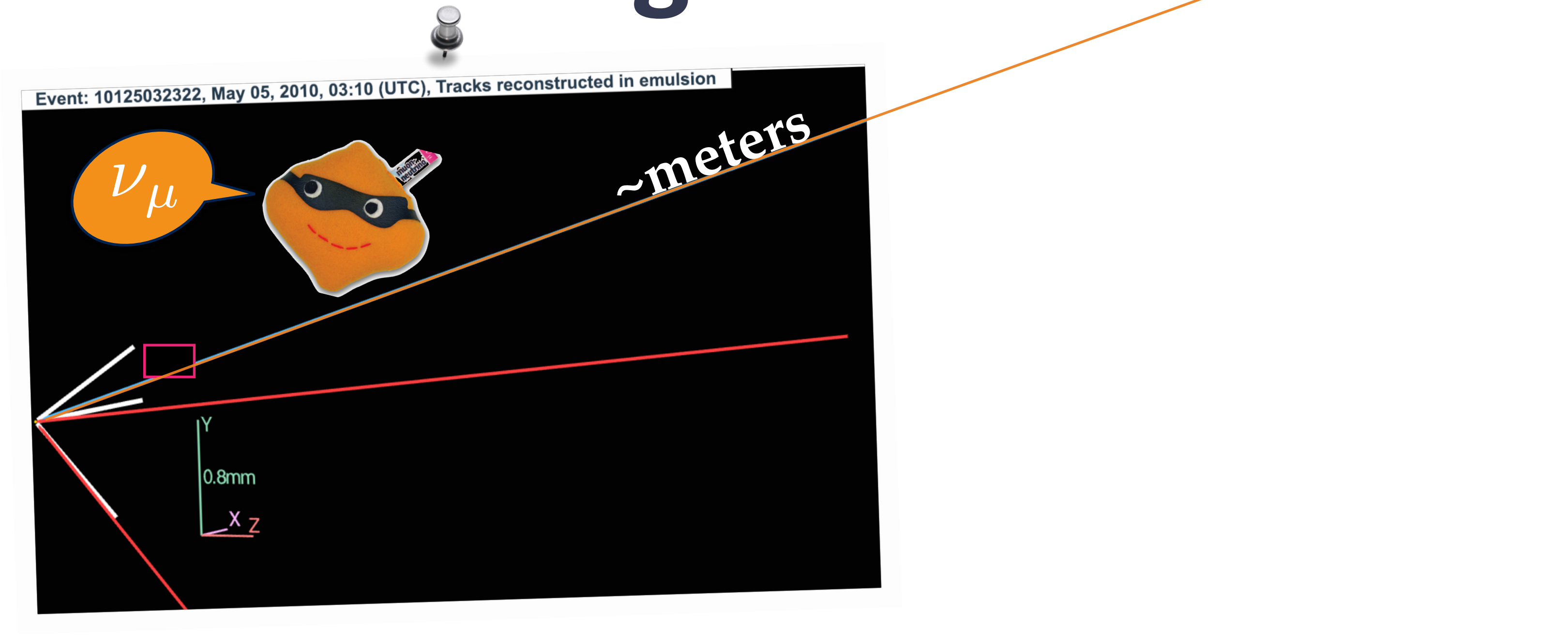

Recognize neutrinos

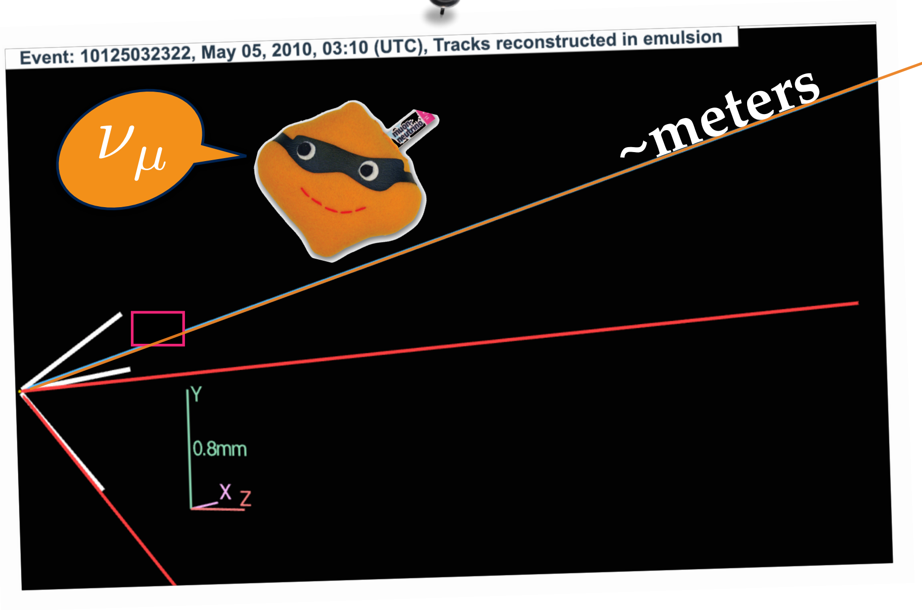

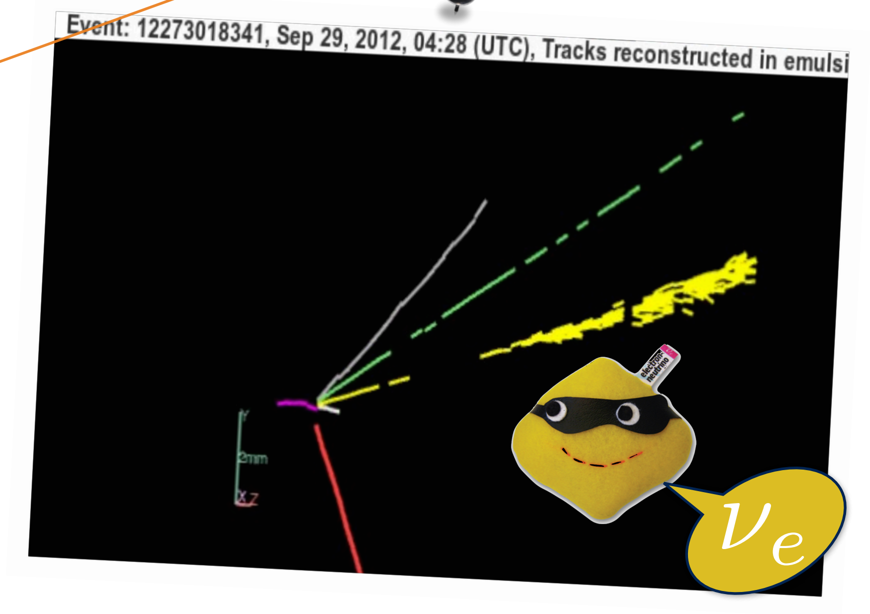

Recognize neutrinos

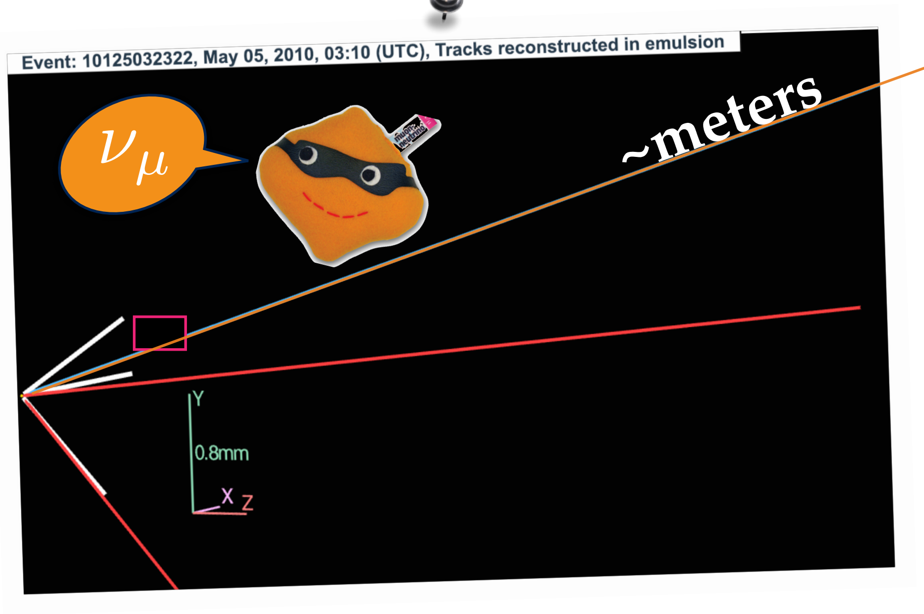

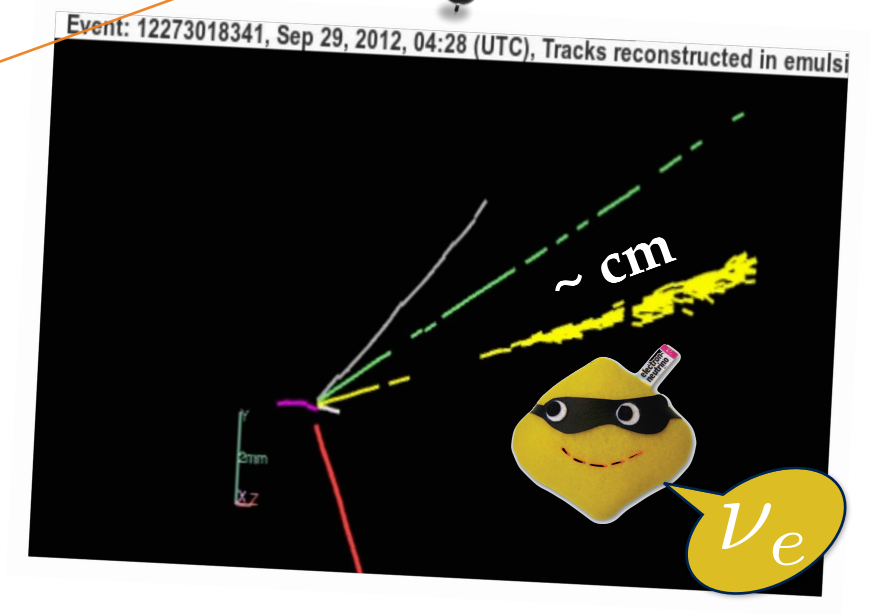

Recognize neutrinos

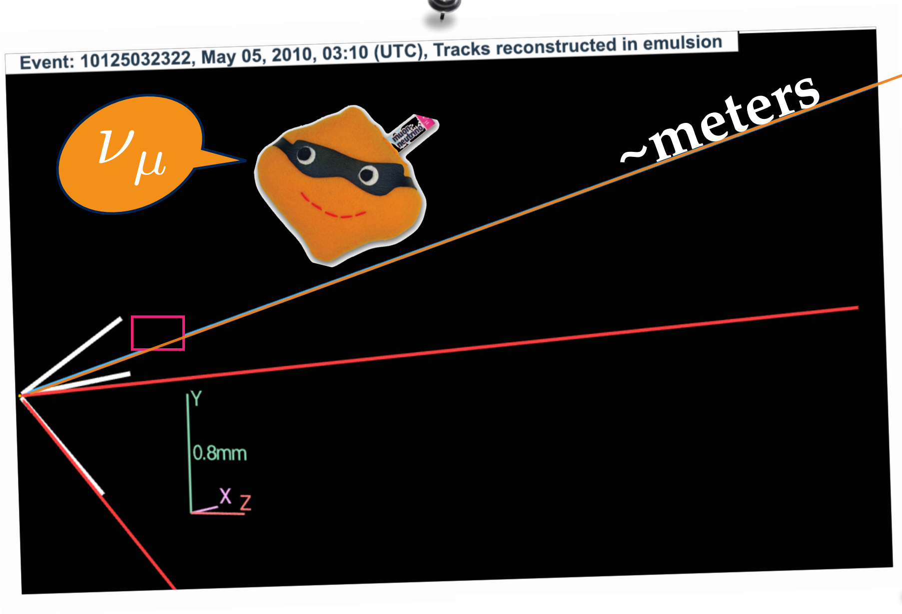

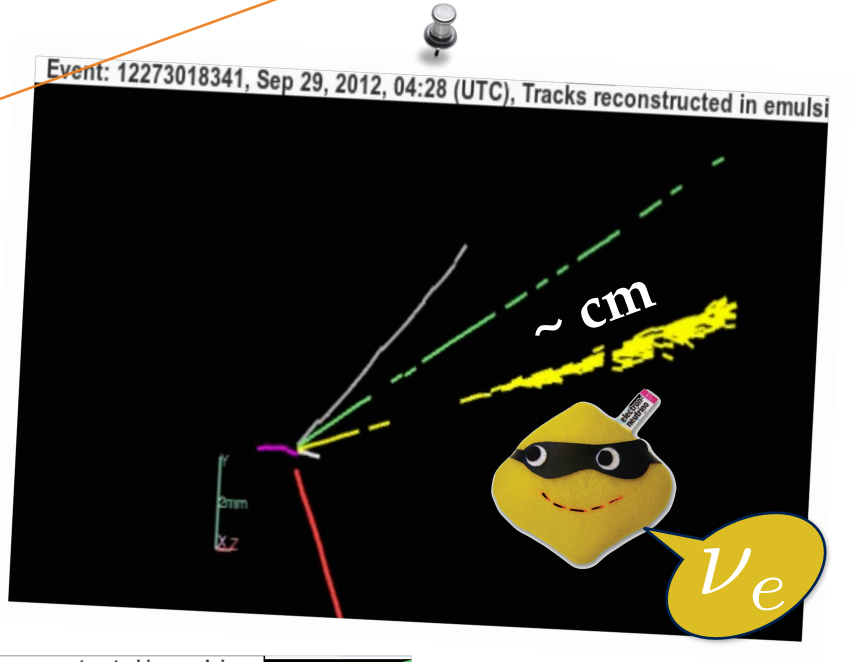

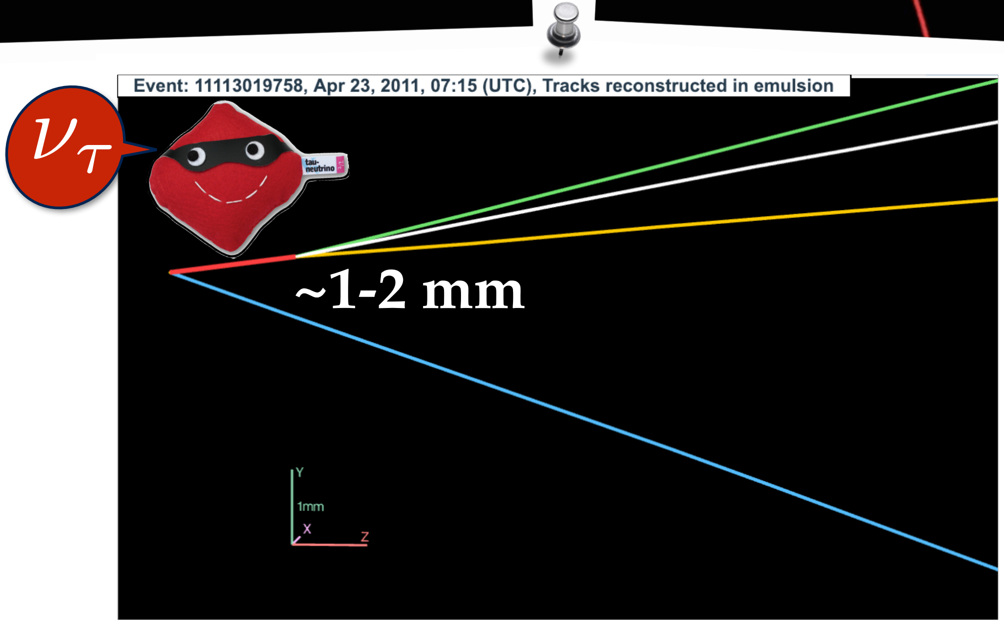

Momentum measurement by the multiple Coulomb Scattering

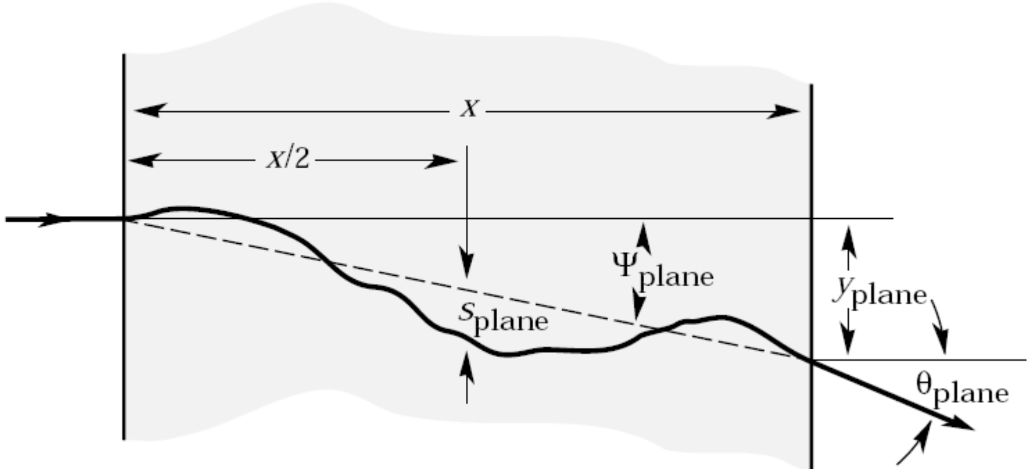

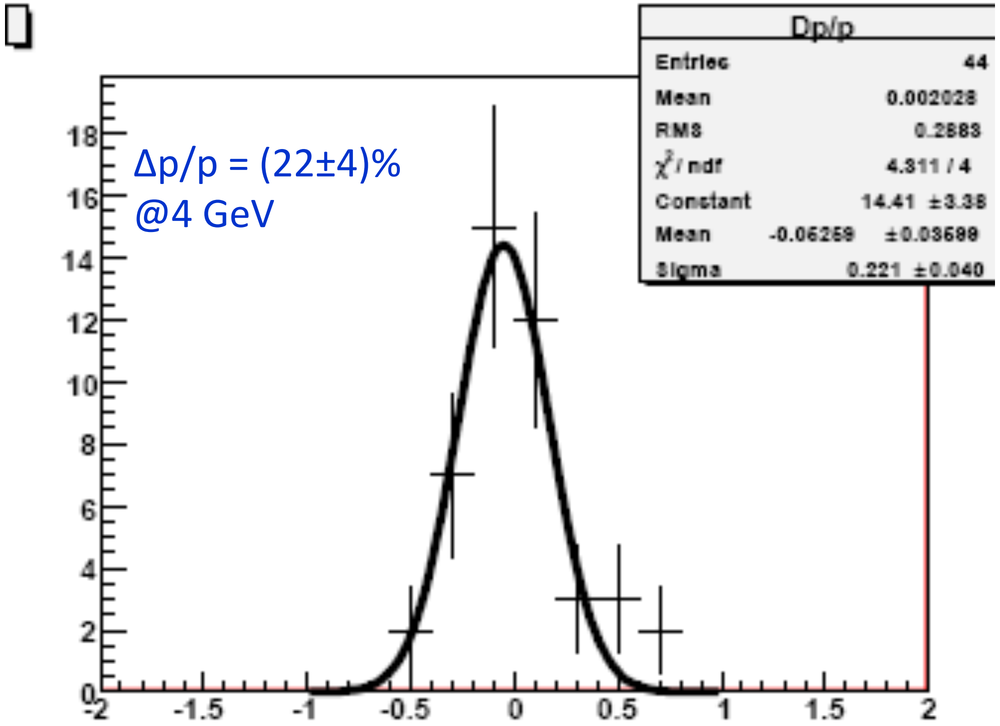

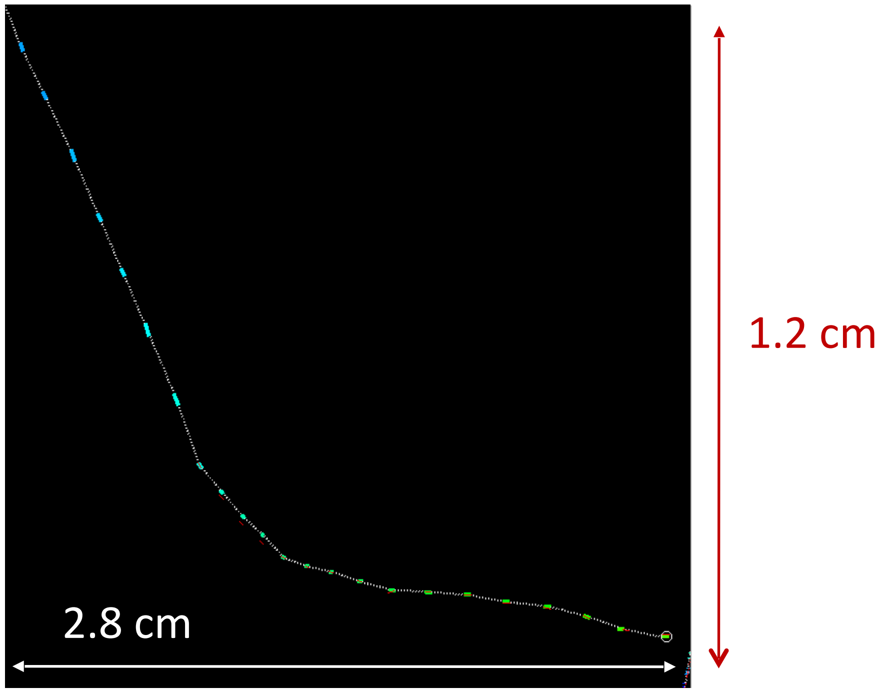

$$\theta_0 = \frac{13.6\ \text{MeV}}{\beta c p}\, z\, \sqrt{x/X_0}\Big[1 + 0.038 \ln(x/X_0)\Big]$$

High sampling calorimeter with >5 active layers per X_0

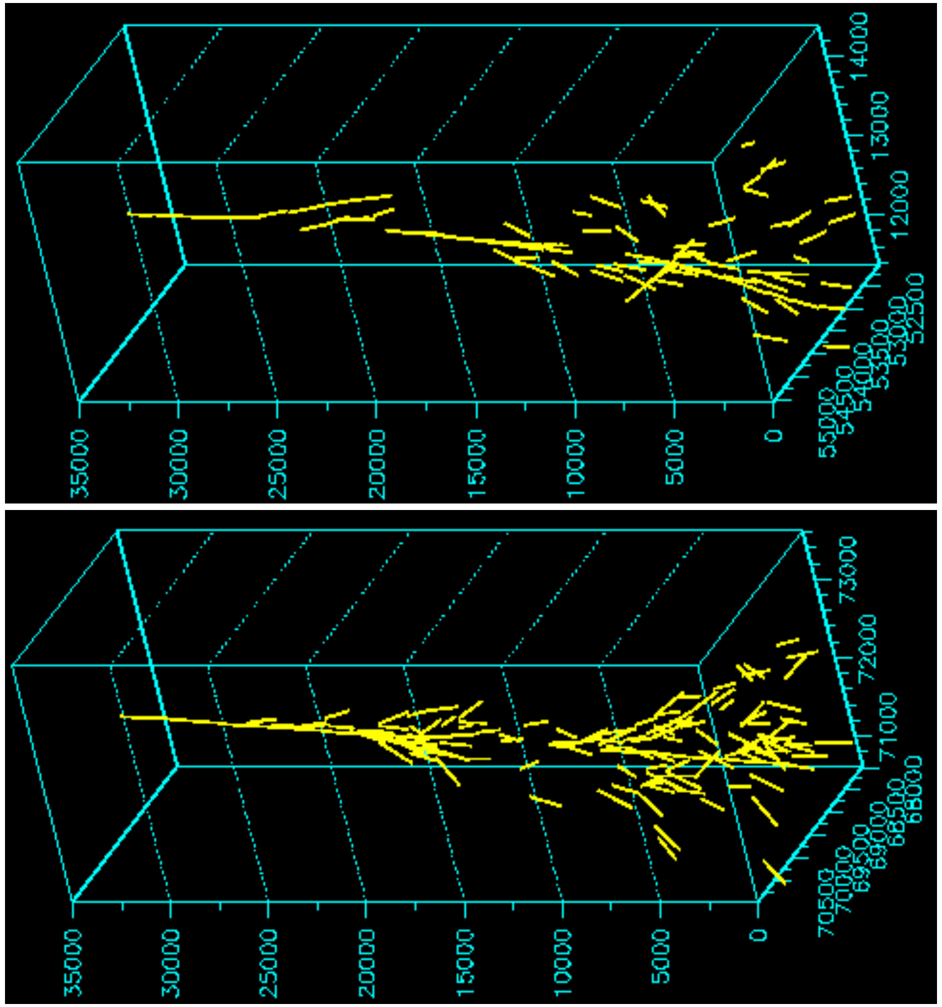

$$\frac{\Delta E}{E} \sim \frac{0.2}{\sqrt{E}}$$

5 X_0

The first tau neutrino candidate

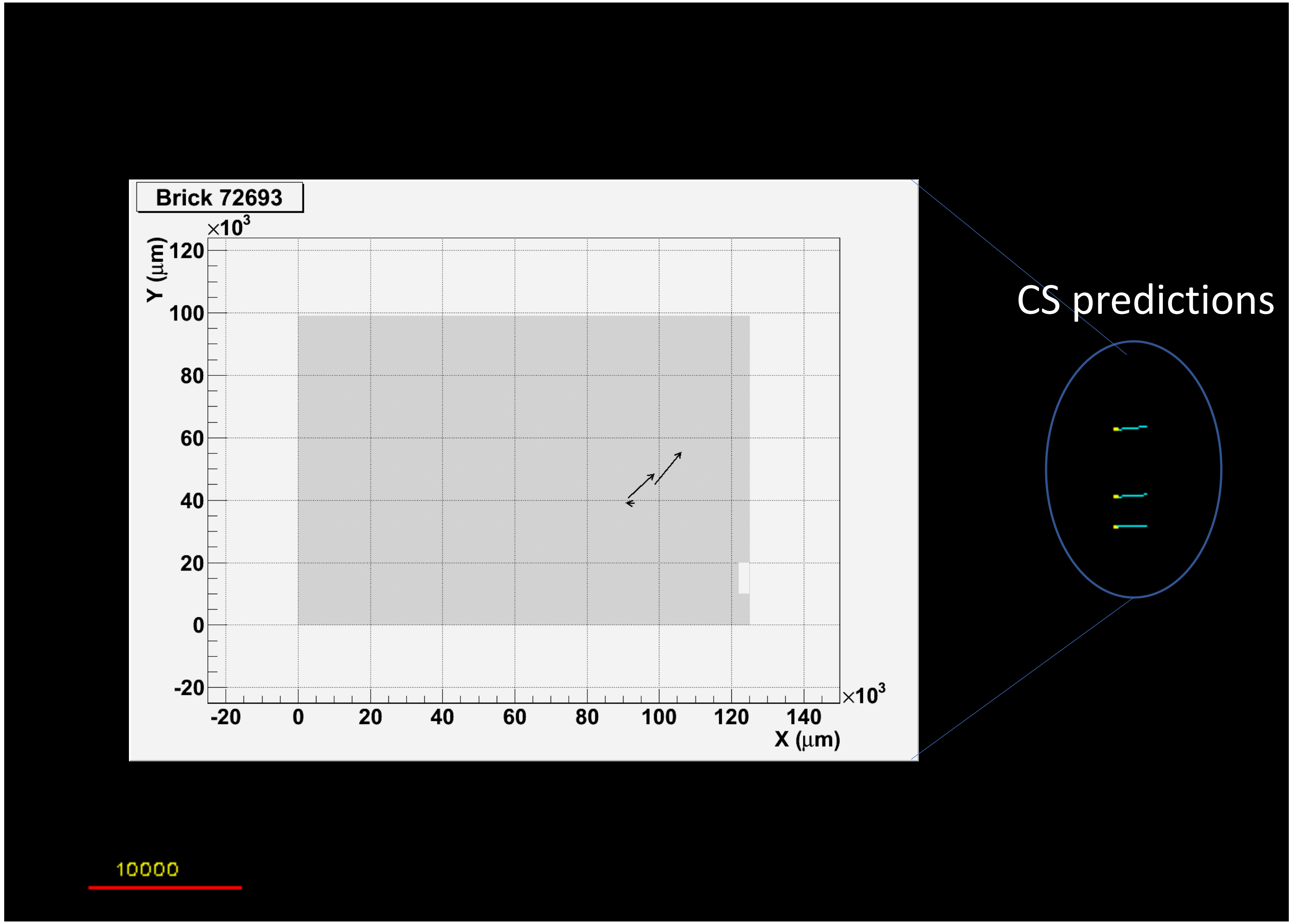

The first tau neutrino candidate

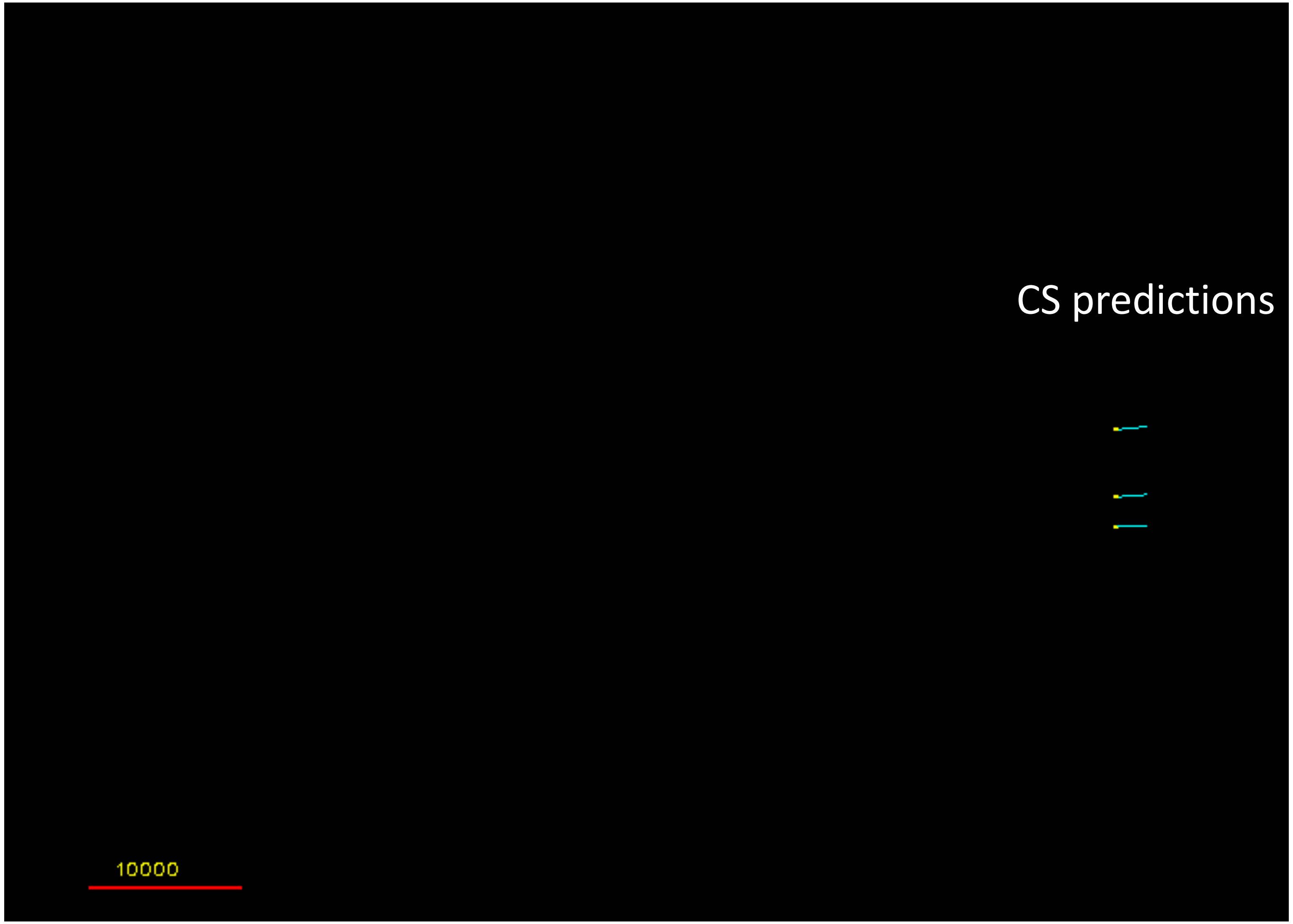

The first tau neutrino candidate

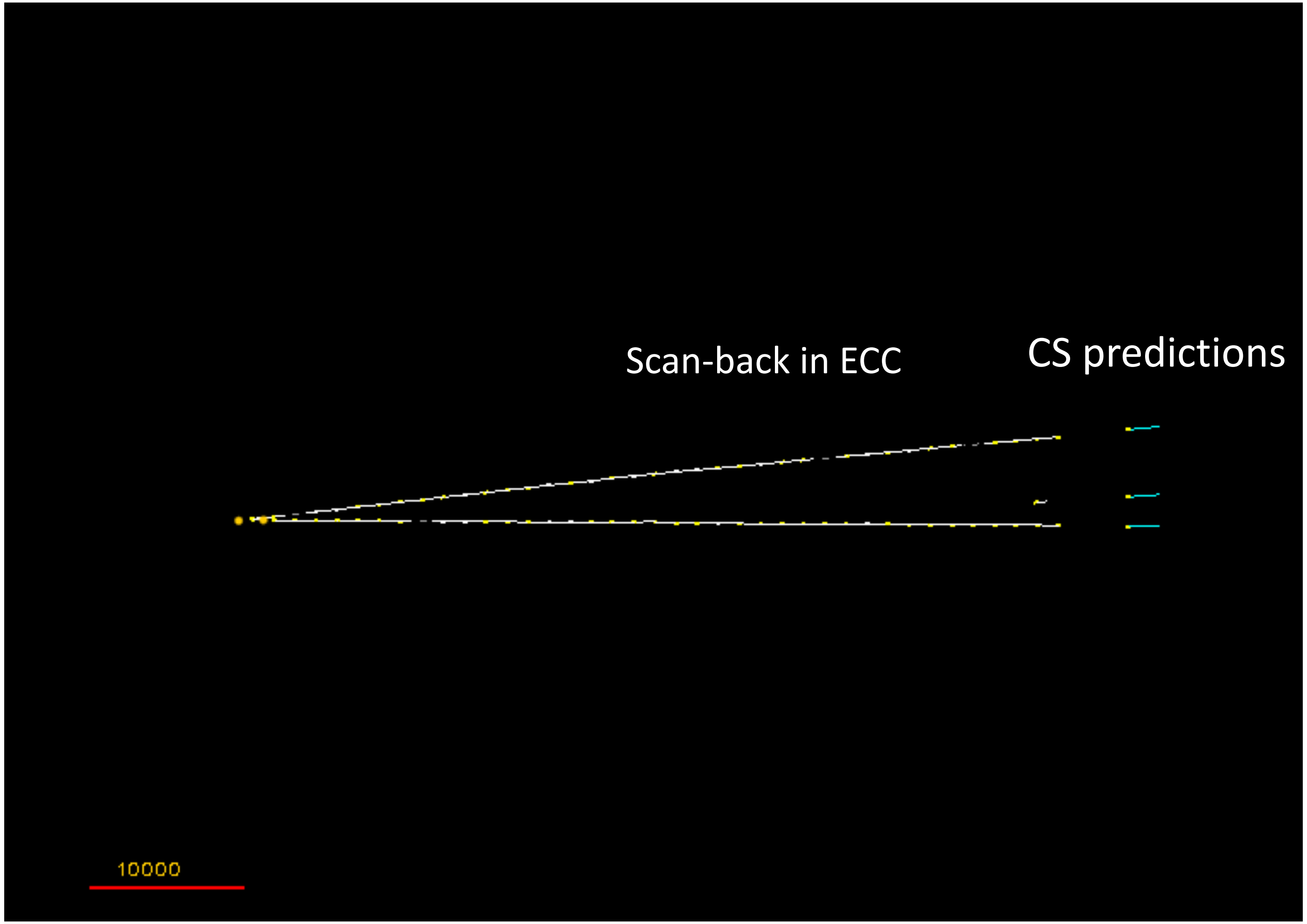

The first tau neutrino candidate

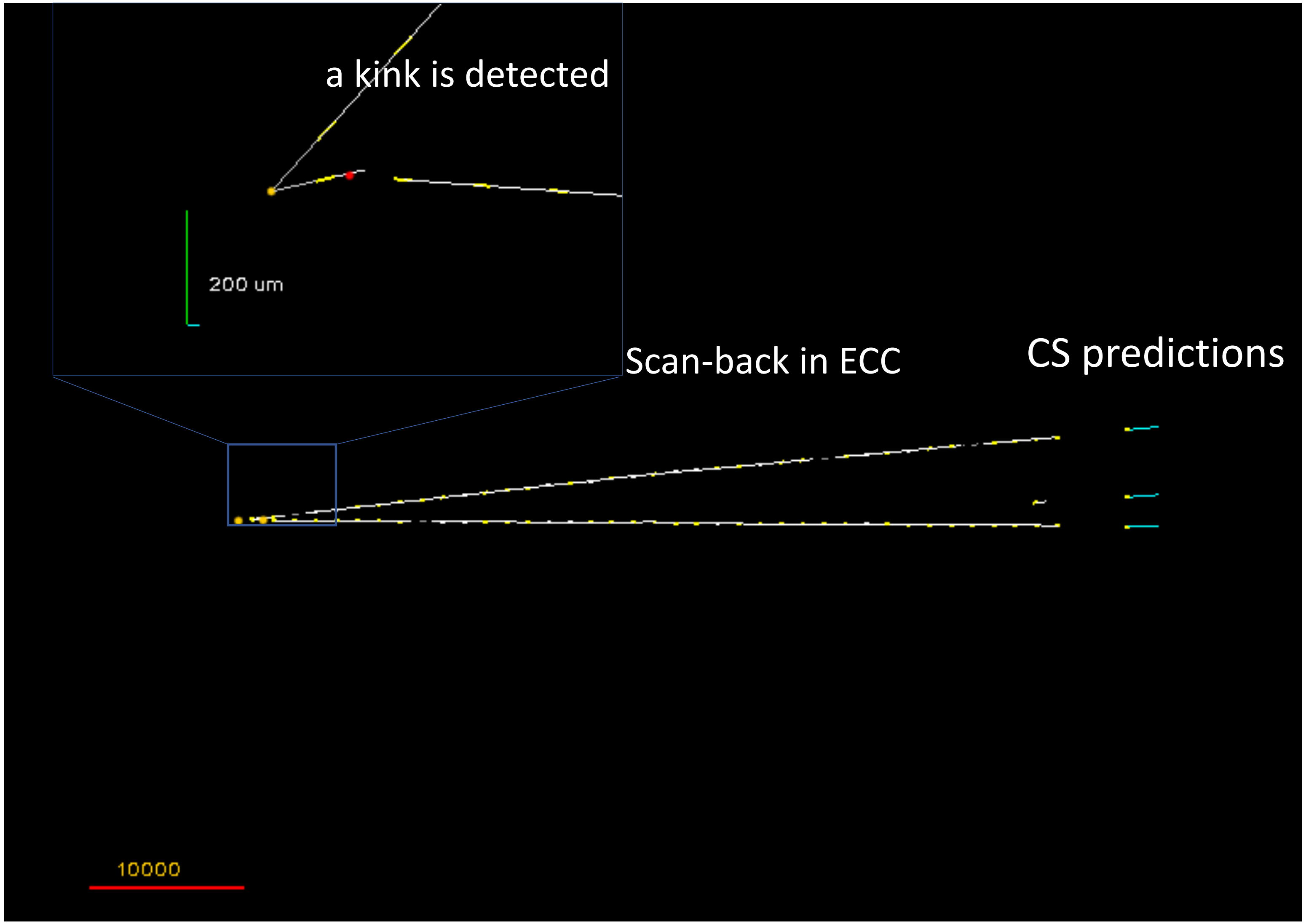

The first tau neutrino candidate

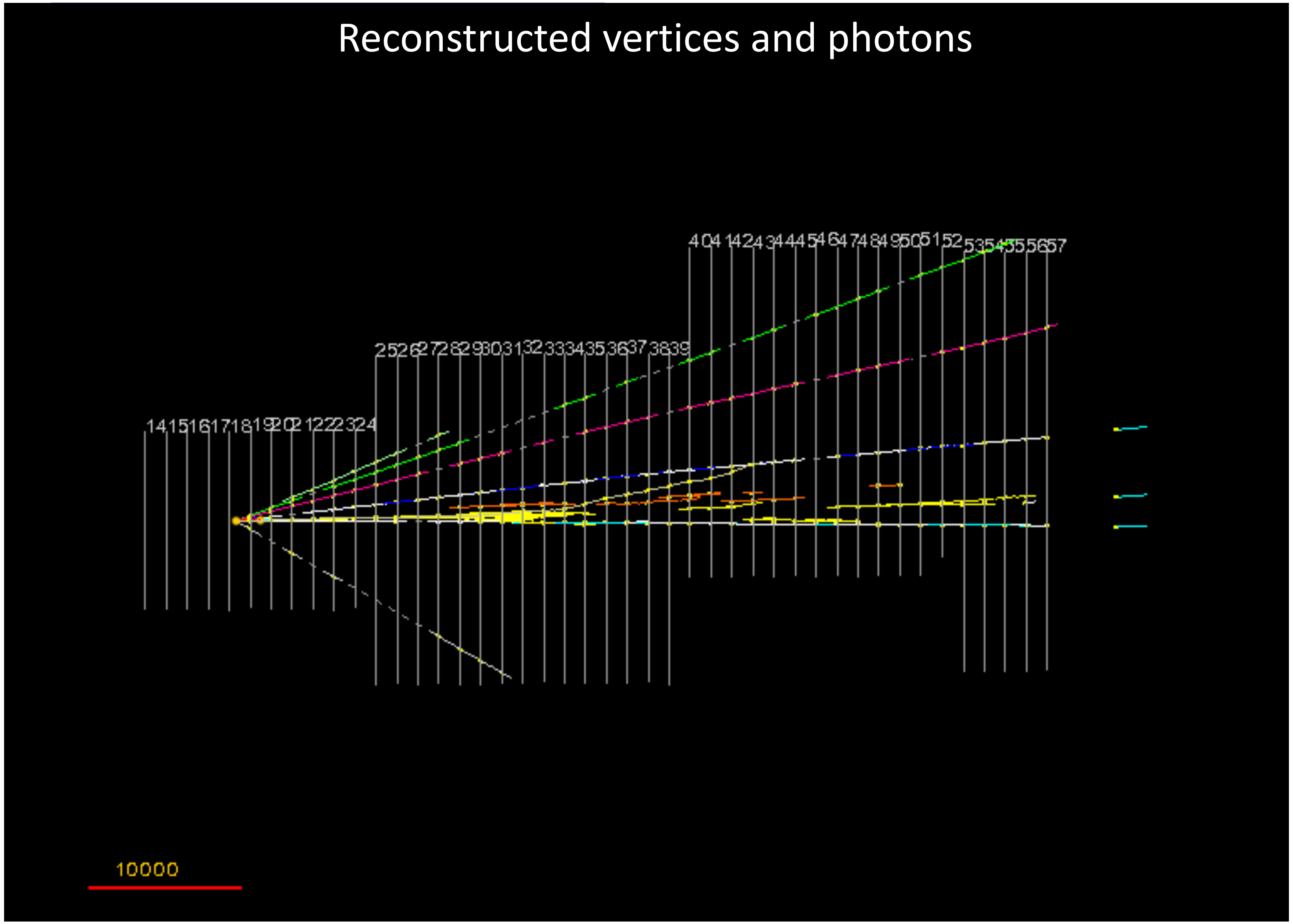

The first tau neutrino candidate

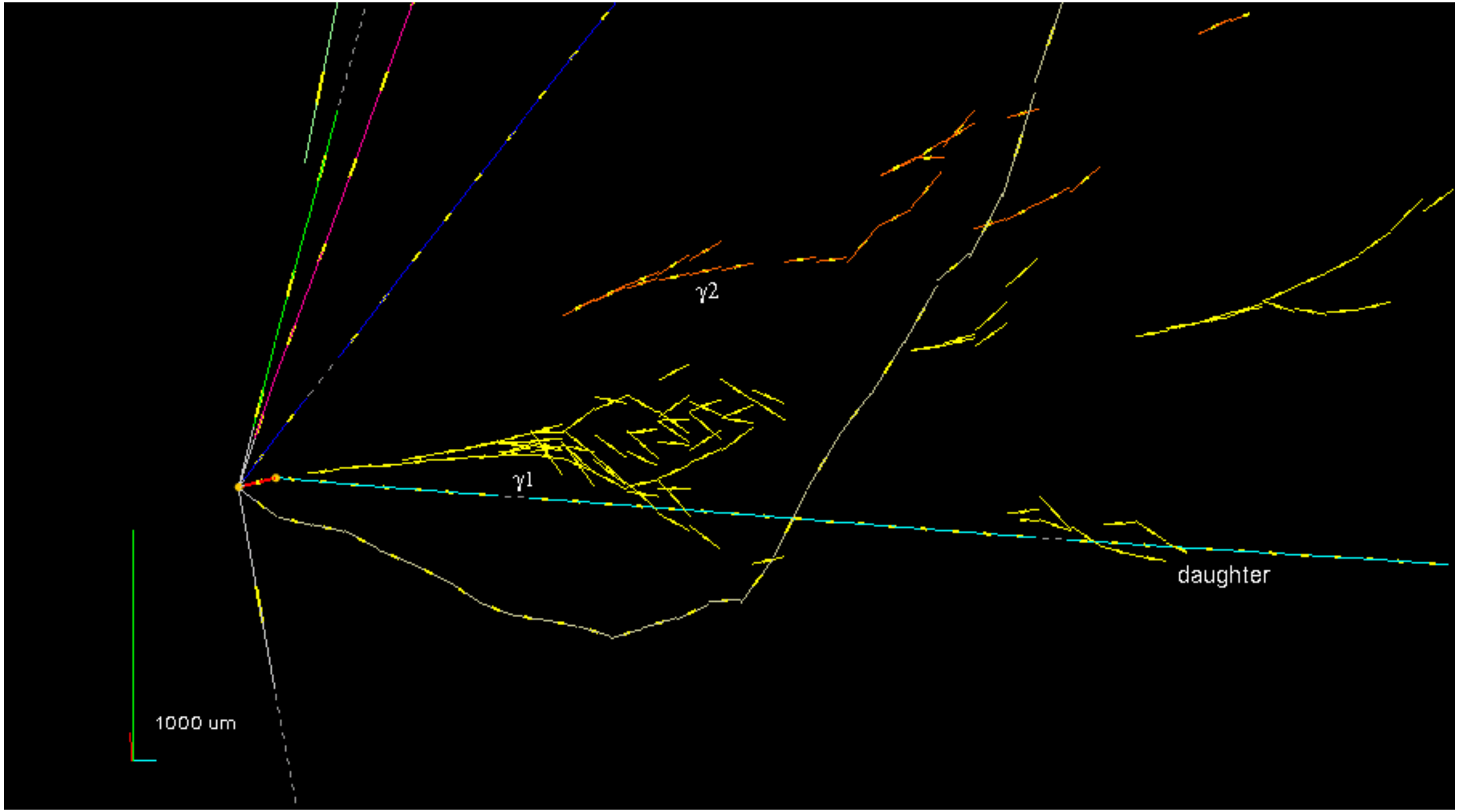

The first tau neutrino candidate

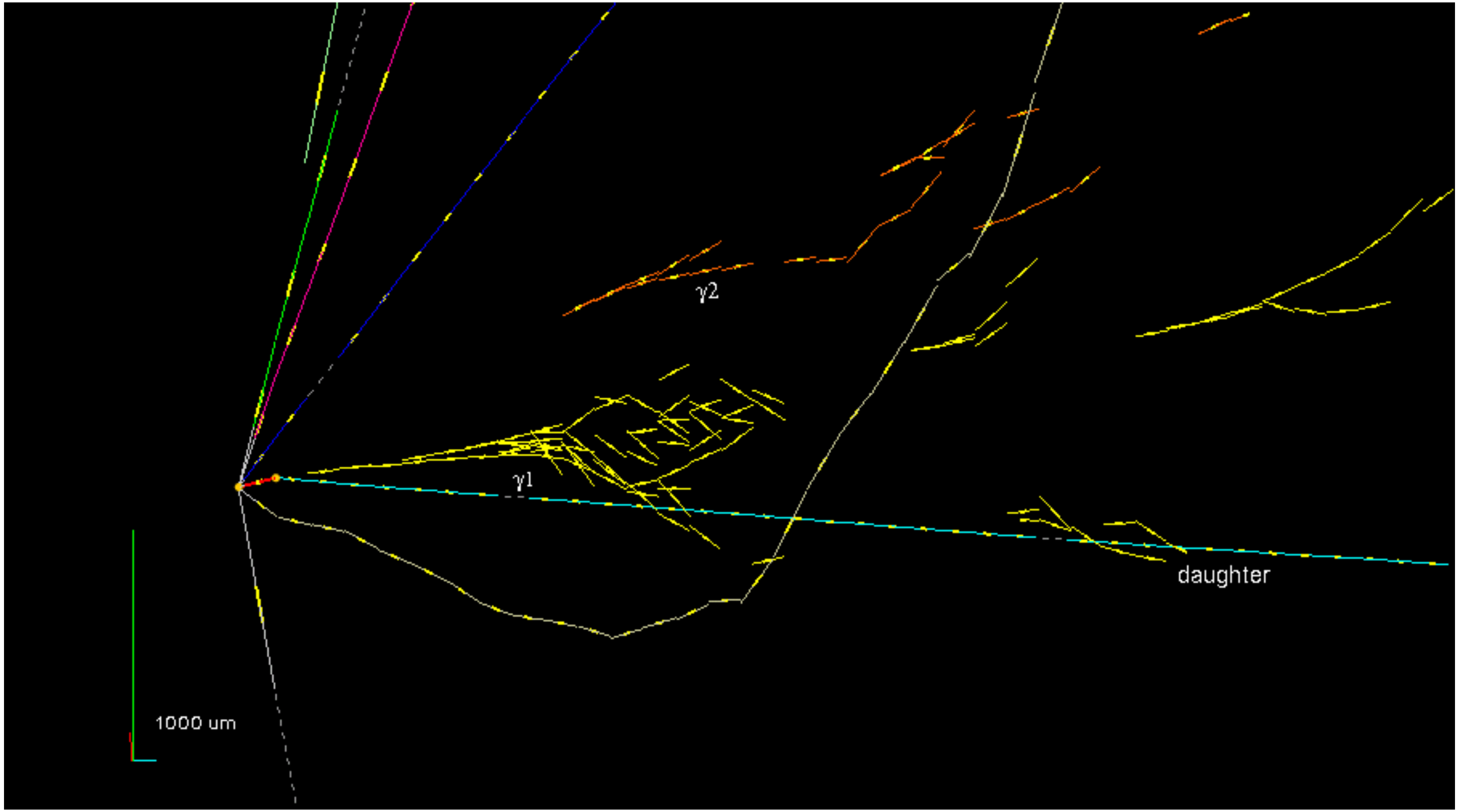

The first tau neutrino candidate

$\tau^- \rightarrow \rho^- \nu_\tau$

$\rho^- \rightarrow \pi^0 \pi^-$

$\pi^0 \rightarrow \gamma\gamma$

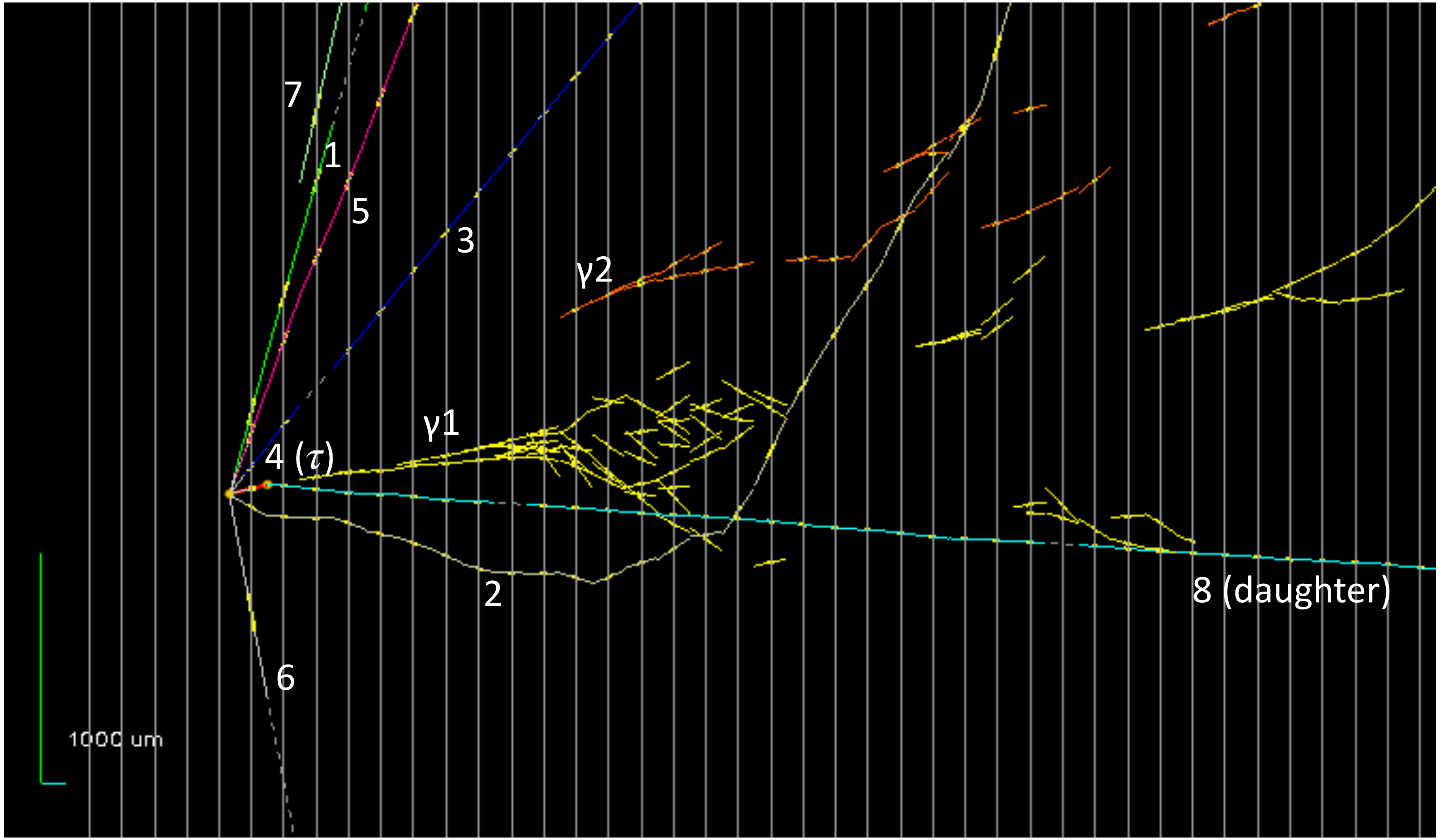

Particle identification by following the track along its path

Assess the muon/hadron nature of the particle

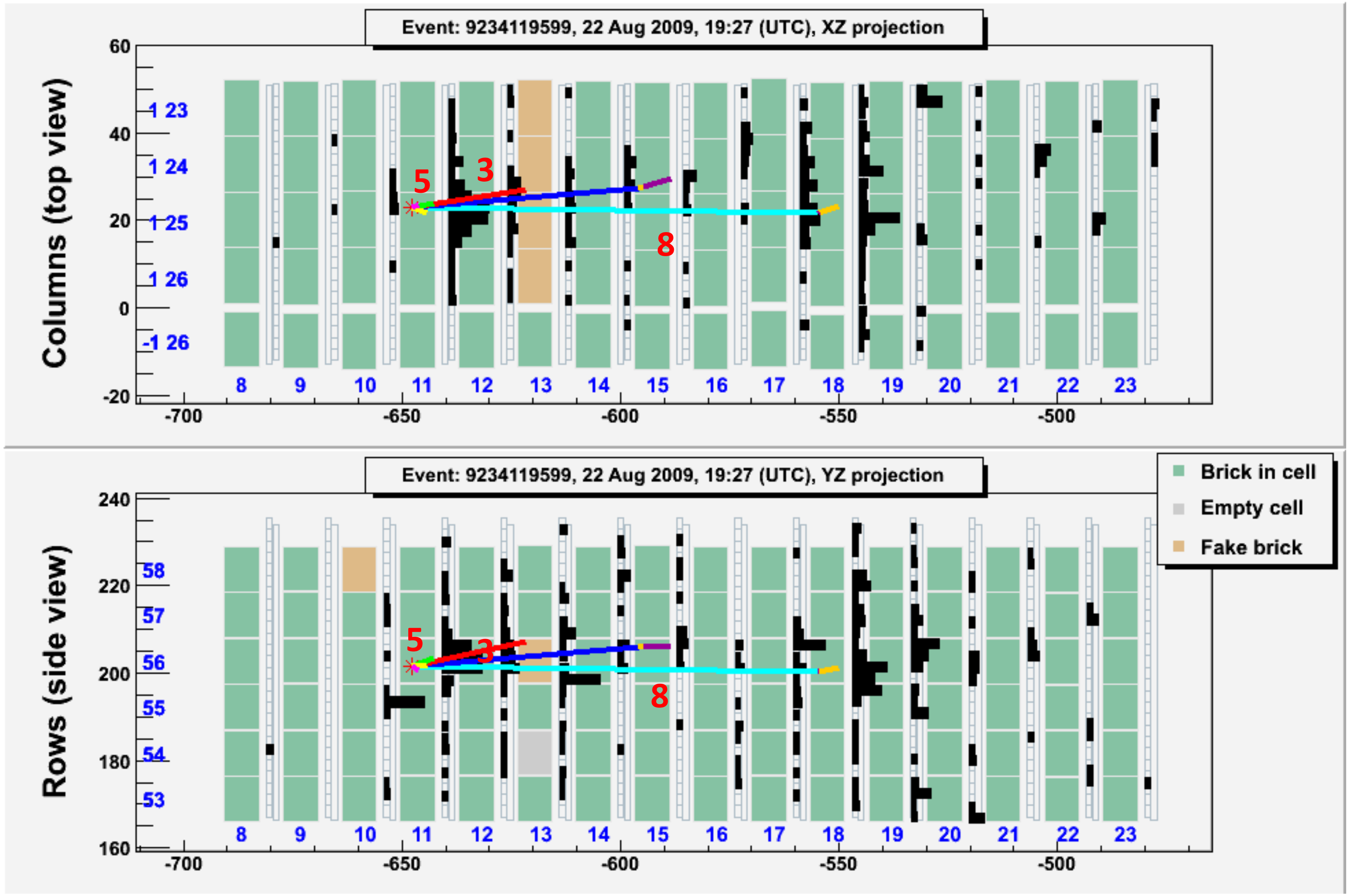

Kinematical variables measured in emulsion

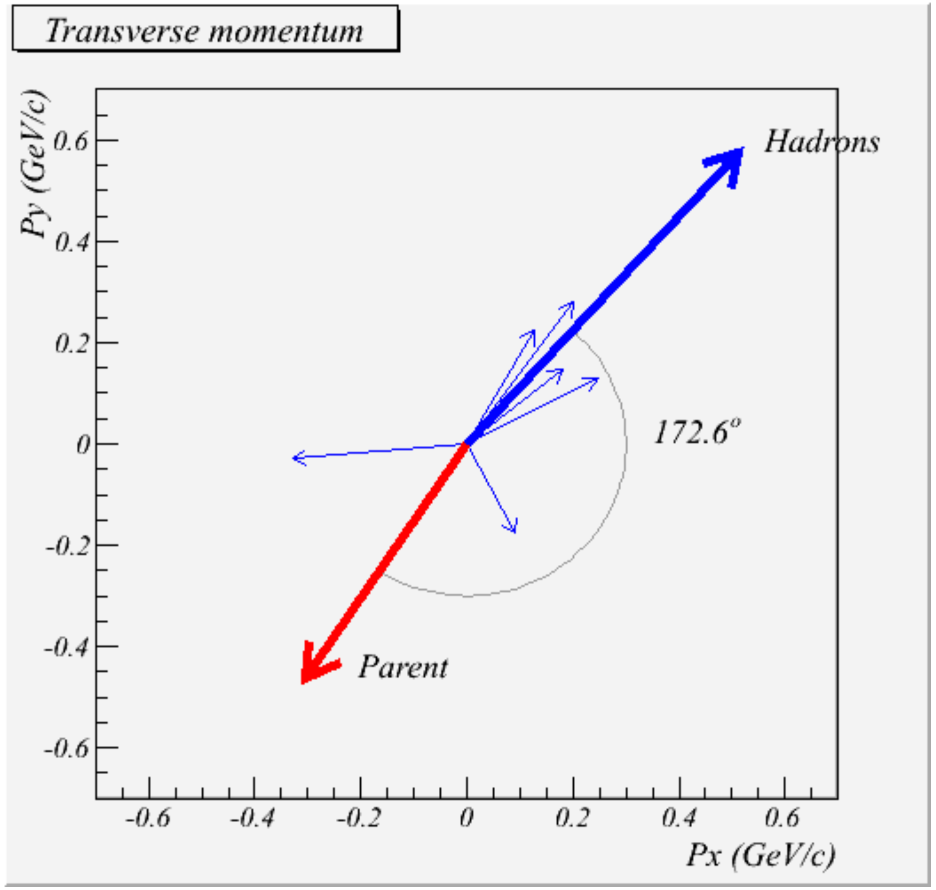

Variable	Measured value
kink (mrad)	**41 ± 2**
decay length (μm)	**1335 ± 35**
P daughter (GeV/c)	**12^{+6}_{-3}**
Pt (MeV/c)	**470^{+230}_{-120}**
missing Pt (MeV/c)	**570^{+320}_{-170}**
φ (deg)	**173 ± 2**

OPERA final results

2015

PRL **115,** 121802 (2015) PHYSICAL REVIEW LETTERS week ending 18 SEPTEMBER 2015

Discovery of τ Neutrino Appearance in the CNGS Neutrino Beam with the OPERA Experiment

- 5 events observed, discovery with 5.1 sigma significance

2018

PHYSICAL REVIEW LETTERS **120,** 211801 (2018)

Editors' Suggestion Featured in Physics

Final Results of the OPERA Experiment on ν_τ Appearance in the CNGS Neutrino Beam

- 10 events observed, discovery with 6.1 sigma significance
- First measurement of Δm^2 in appearance mode
- First cross-section measurement
- First direct observation of the leptonic number of ν_τ

Open data

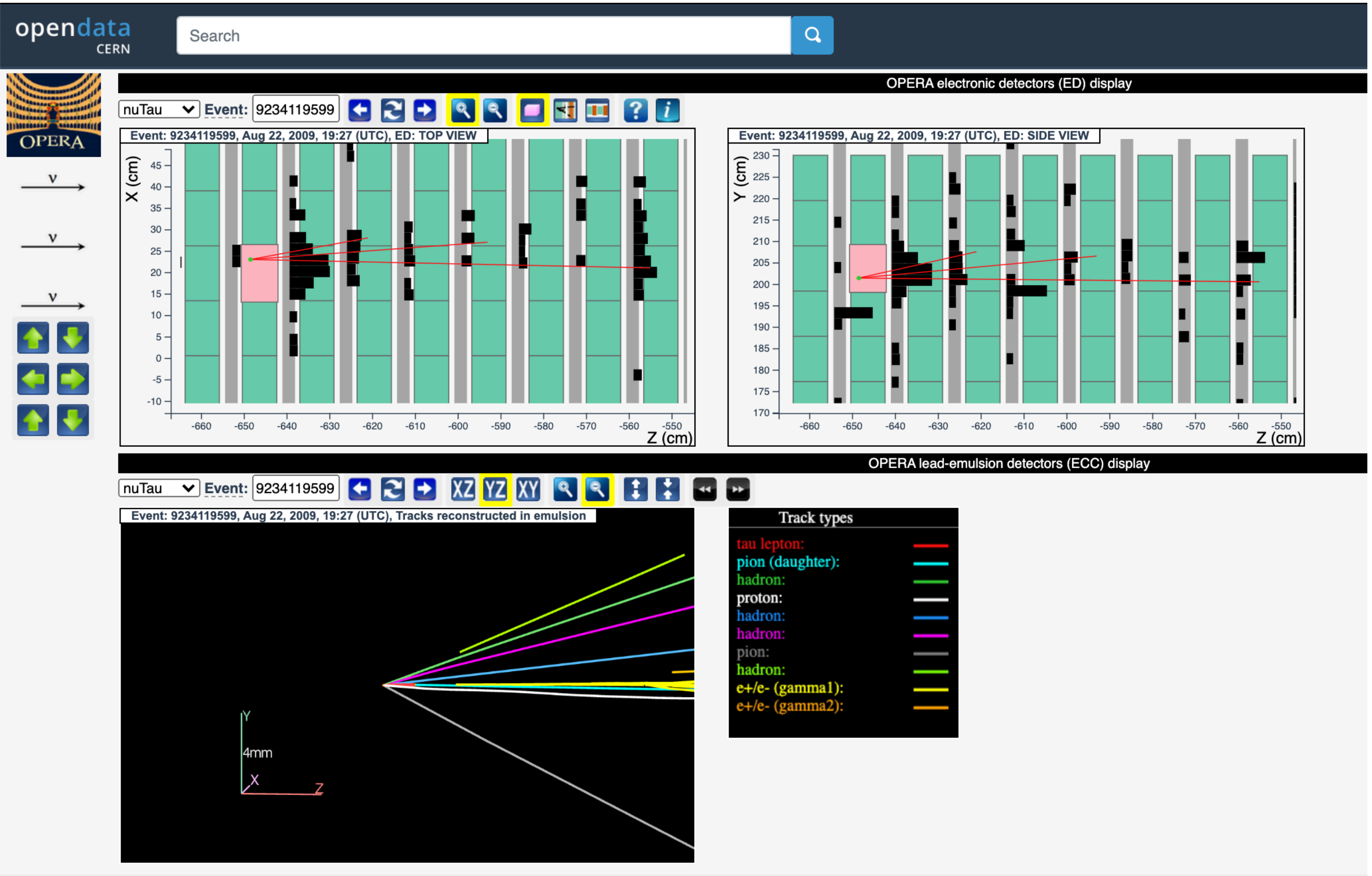

opendata.cern.ch

SCIENTIFIC DATA

OPERA tau neutrino charged current interactions

N. Agafonova[1], A. Alexandrov[2], A. Anokhina[3], S. Aoki[4], A. Ariga[5], T. Ariga[5,6], A. Bertolin[7], C. Bozza[8], R. Brugnera[7,9], A. Buonaura[2,10], S. Buontempo[2], M. Chernyavskiy[11], A. Chukanov[12], L. Consiglio[2], N. D'Ambrosio[13], S. Dallmeier-Tiessen[38] G. De Lellis[2,10,38], M. De Serio[14,15], P. del Amo Sanchez[16], A. Di Crescenzo[2,10], D. Di Ferdinando[17], N. Di Marco[13], S. Dmitrievsky[12, *], M. Dracos[18], D. Duchesneau[16], S. Dusini[7], T. Dzhatdoev[3], J. Ebert[19], A. Ereditato[5], R. A. Fini[15], F. Fornari[17,20], T. Fukuda[21], G. Galati[2,10,*], A. Garfagnini[7,9], V. Gentile[22], J. Goldberg[23], S. Gorbunov[11], Y. Gornushkin[12], G. Grella[8], A. M

*corresponding author(s): Sergey Dmitrievsky (dmitr@jinr.ru) and Giuliana Galati (giuliana.galati@na.infn.it)

Abstract

The OPERA experiment was designed to discover the ν_τ appearance in a ν_μ beam, resulting from neutrino oscillations. The detector, located in the underground Gran Sasso Laboratory, consisted of a nuclear photographic emulsion/lead target with a mass of about 1.2 kt, complemented by electronic detectors. It was exposed, from 2008 to 2012, to the CNGS (CERN Neutrinos to Gran Sasso) beam, an almost pure ν_μ beam with a baseline of 730 km, collecting a total of $18 \cdot 10^{19}$ protons on target. The OPERA Collaboration eventually assessed the discovery of $\nu_\mu \to \nu_\tau$ oscillations with a statistical significance of 6.1 σ by observing ten ν_τ candidate charged current interactions. The corresponding data sets have been published on the Open Data Portal at CERN. In this paper, a detailed description of the ν_τ data sample is provided in order to be handled and analysed by a wide range of users.

SND@LHC (SCATTERING AND NEUTRINO DETECTOR)

The SND@LHC experiment

- Colliders offer a novel laboratory for neutrinos: high ν flux in the unexplored energies of ~(10^2-10^3) GeV

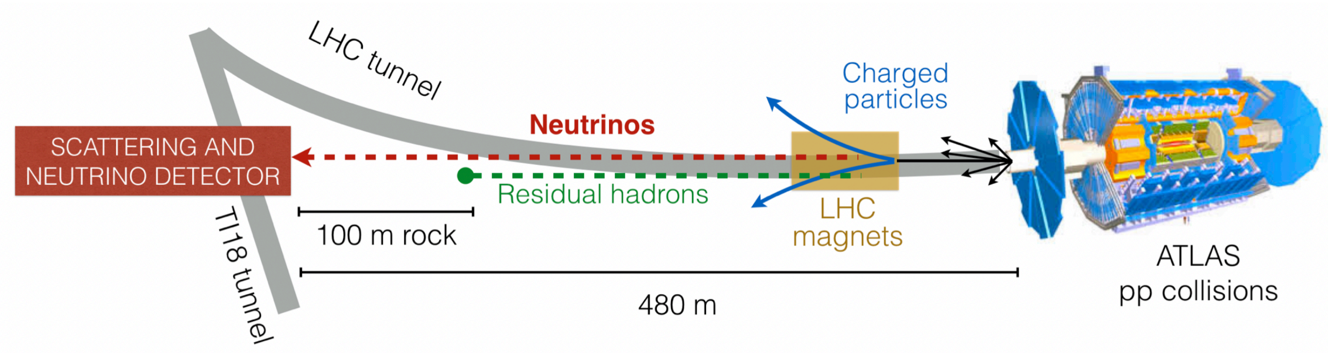

- New experiment: **Scattering and Neutrino Detector at the LHC**
  - Measures neutrinos from the LHC at an angular acceptance of 7.2<η<8.4
  - Designed to distinguish all neutrino flavours

Experiment timeline

August 2020
LETTER OF INTENT

January 2021
TECHNICAL PROPOSAL

March 2021
APPROVAL BY CERN RESEARCH BOARD

July 2022
FIRST MUONS FROM IP1 MEASURED


September 2021


December 2021


March 2022

SND@LHC Detector

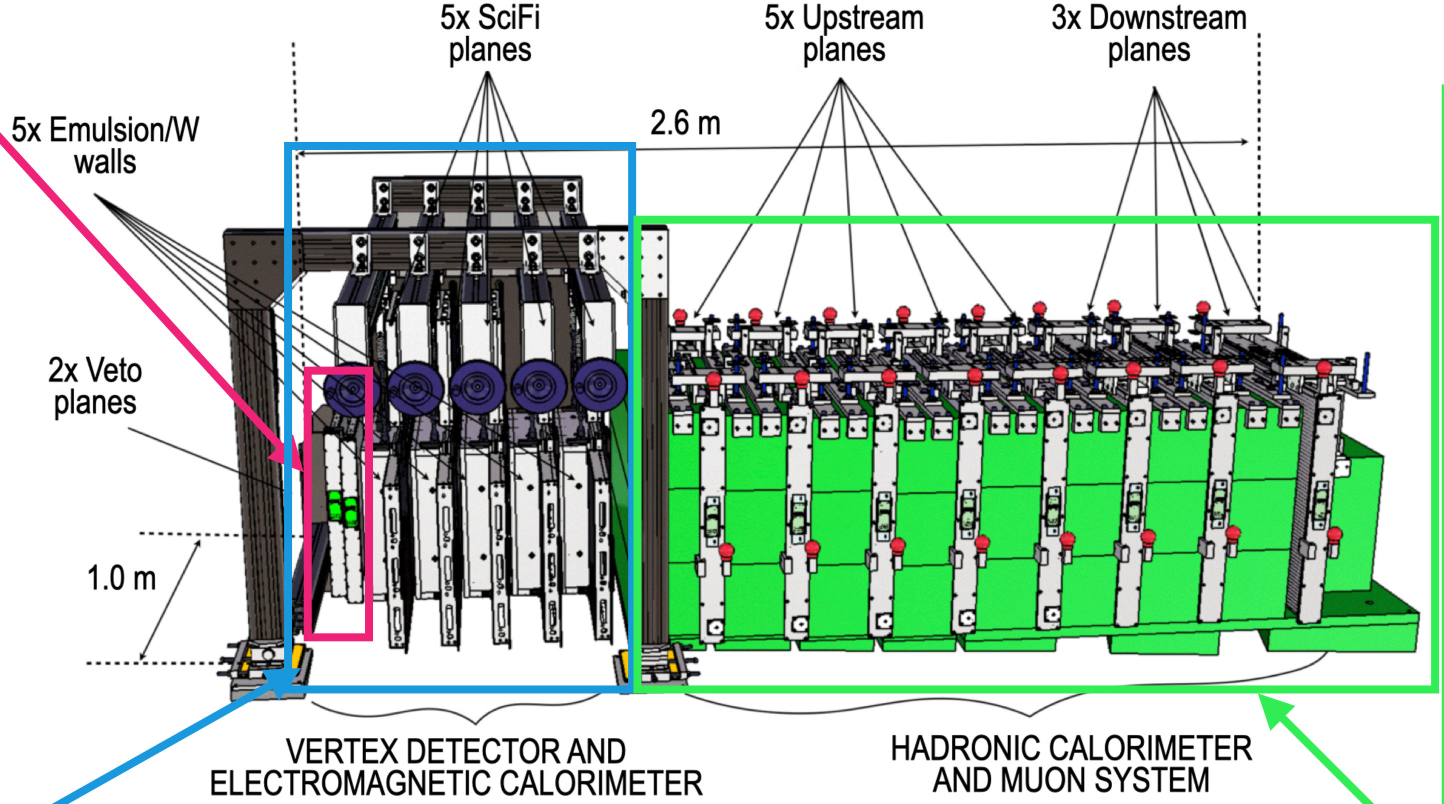

Veto

- Two planes of scintillating bars
- Tags charged particles as they enter

Muon System and HCAL (~10λ)

- Scintillating bars interleaved with iron walls, sampling every λ
- Timing, muon ID, and energy measurement
- Higher granularity in downstream stations for muon tracking

Vertex detector and ECAL (~40X_0)

- Emulsion Cloud Chambers (ECC) with tungsten for ν identification via precise vertexing
- Scintillating Fiber (SciFi) planes provide timing and calorimetric information

2022 Luminosity

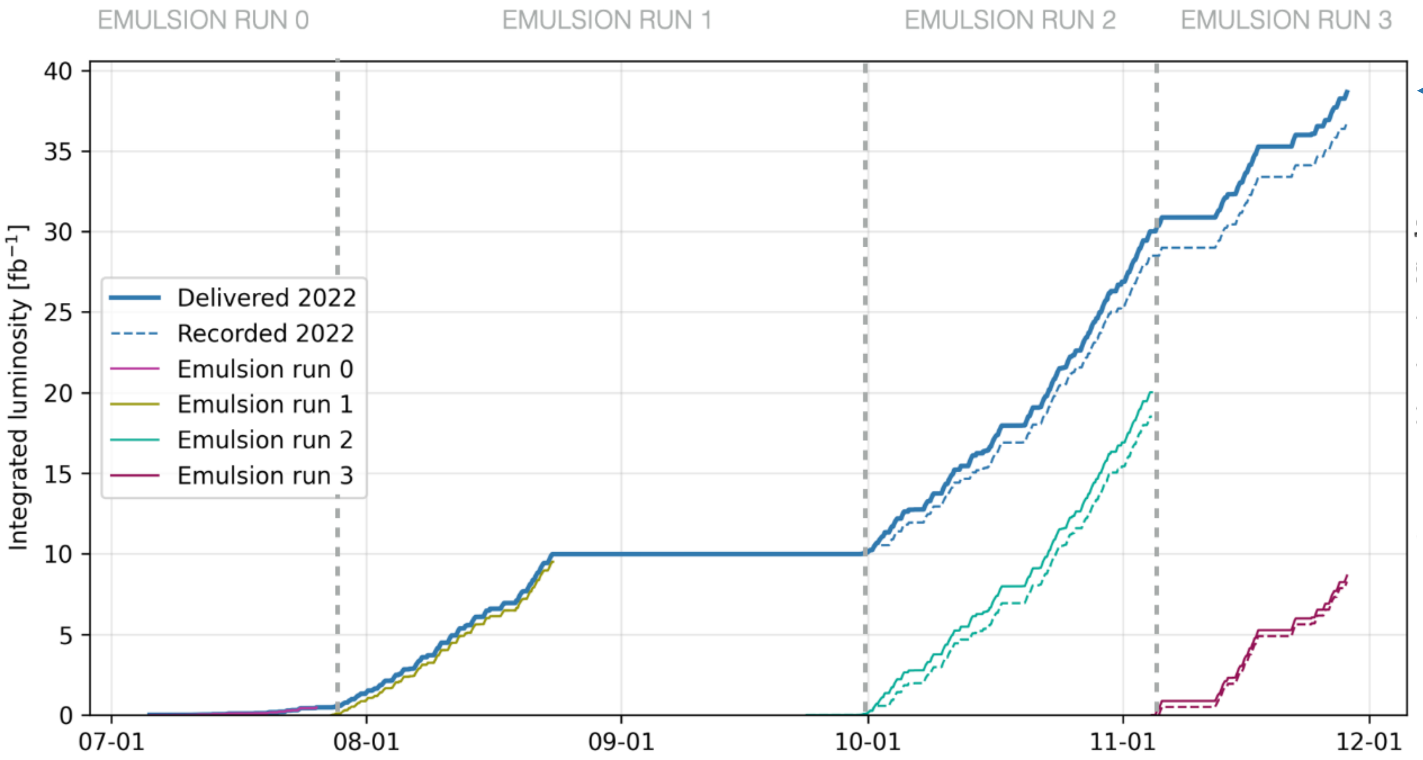

38.6 fb^{-1}

Start beam commissioning
First stable beams @6.8TeV
End of run

2022	Jan	Feb	Mar	Apr	May	Jun	Jul	Aug	Sep	Oct	Nov	Dec	INSTRUMENTED TARGET MASS	INTEGRATED LUMINOSITY
EMULSION RUN0													39 kg	0.46 fb^{-1}
EMULSION RUN1													807 kg	9.5 fb^{-1}
EMULSION RUN2													784 kg	20.0 fb^{-1}
EMULSION RUN3													792 kg	8.6 fb^{-1}

DAQ and event reconstruction

- Triggerless data acquisition
- Two-phase event reconstruction:

➡ **First phase**: online with electronic detectors

  - Identify ν candidates
  - Tag muons (Muon system)
  - Measure energy (SciFi & HCAL)

➡ **Second phase**: offline with nuclear emulsion films

  - Extract, develop, scan, and analyse emulsion data
  - Reconstruct ν primary and secondary candidates
  - Match nuclear emulsion films and electronics reconstruction

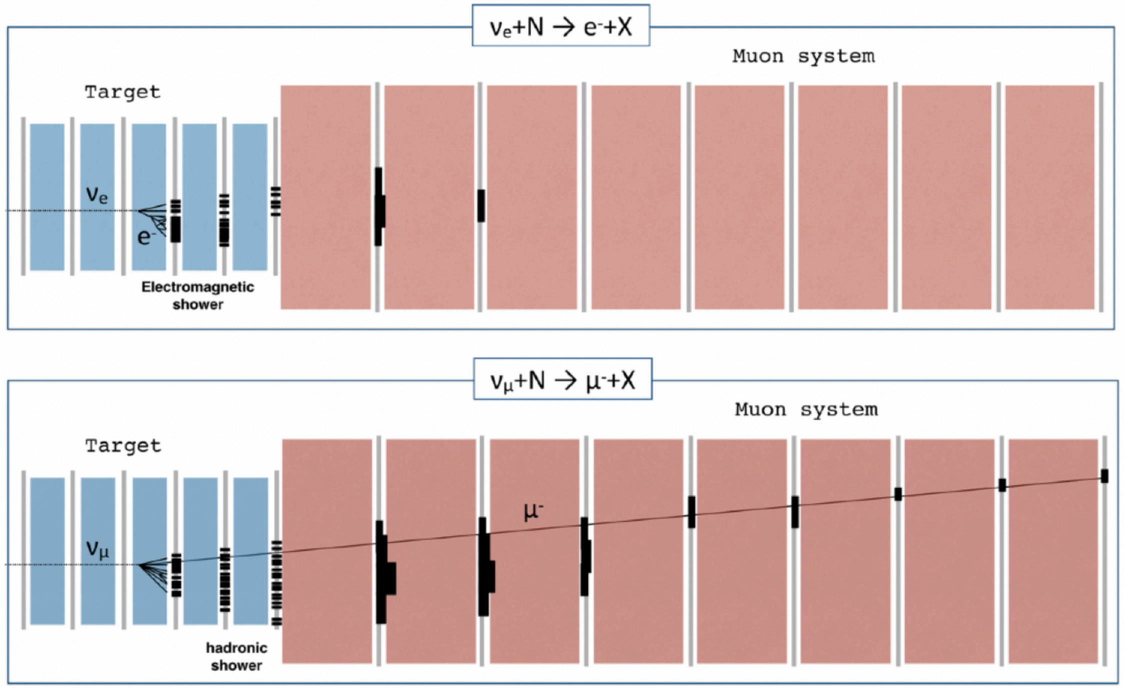

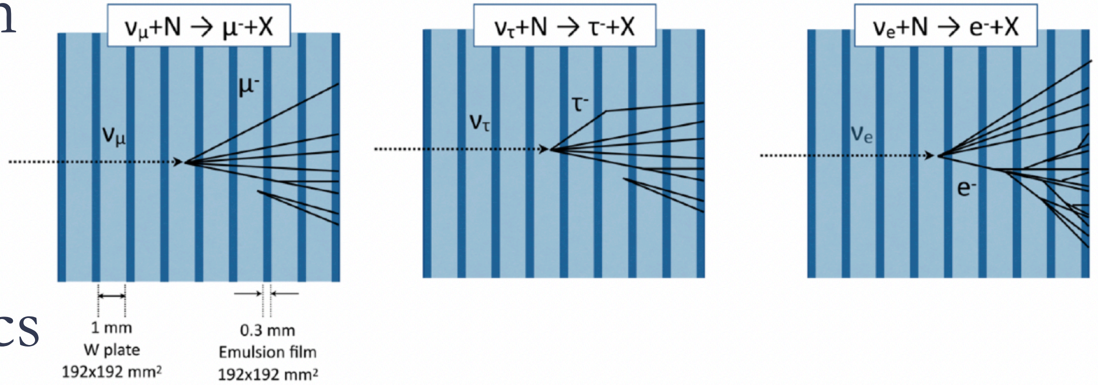

SND@LHC experimental difficulties

- Scan and analysis of nuclear emulsion data is on-going, for the moment in 4 scanning labs (Napoli, Lebedev, Bologna, CERN)
- Reconstruct neutrino interactions in an environment with a high density of traces ($\sim 5x10^5$ part/cm^2)

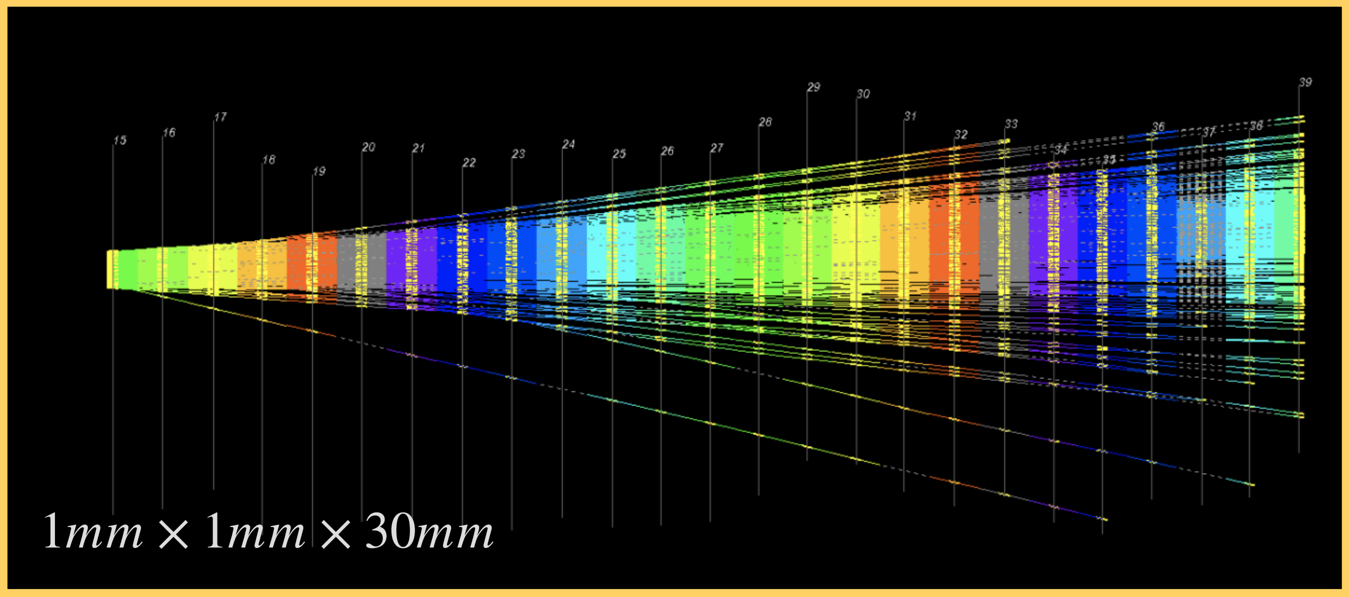

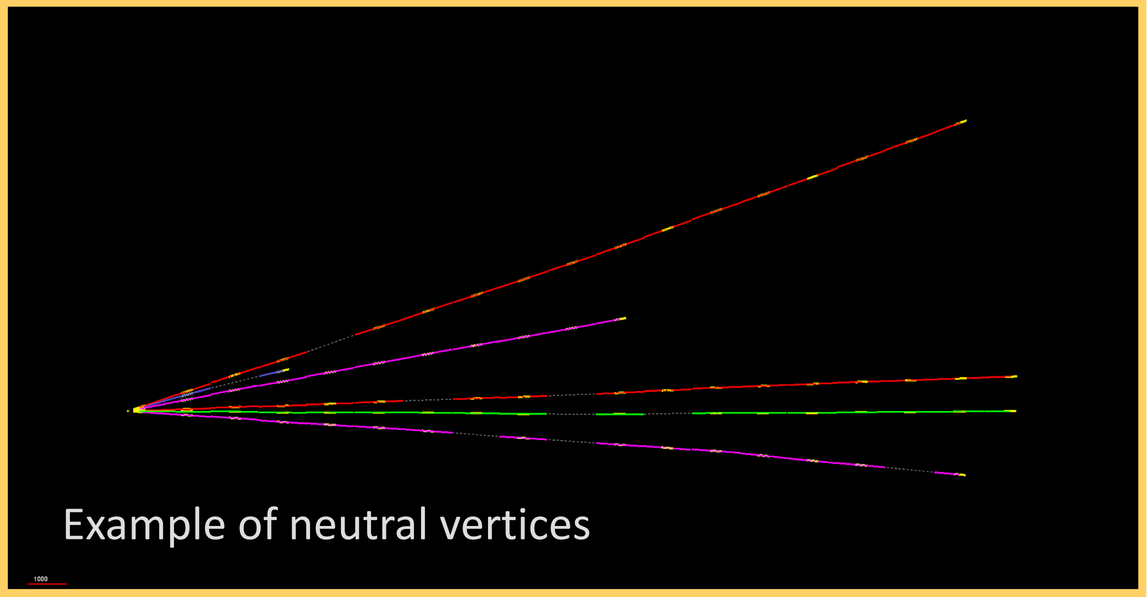

Measured track density: $\sim 10^5$ cm^{-2}

SND@LHC experimental difficulties

- Distinguish the signal (neutrino interactions) from those due to the background of neutral particles and muons

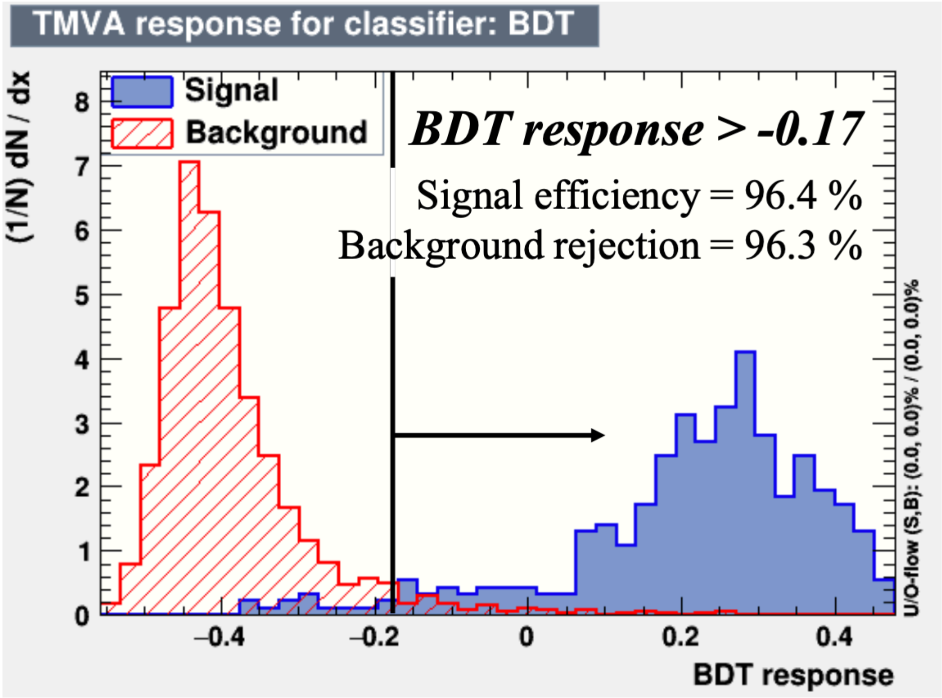

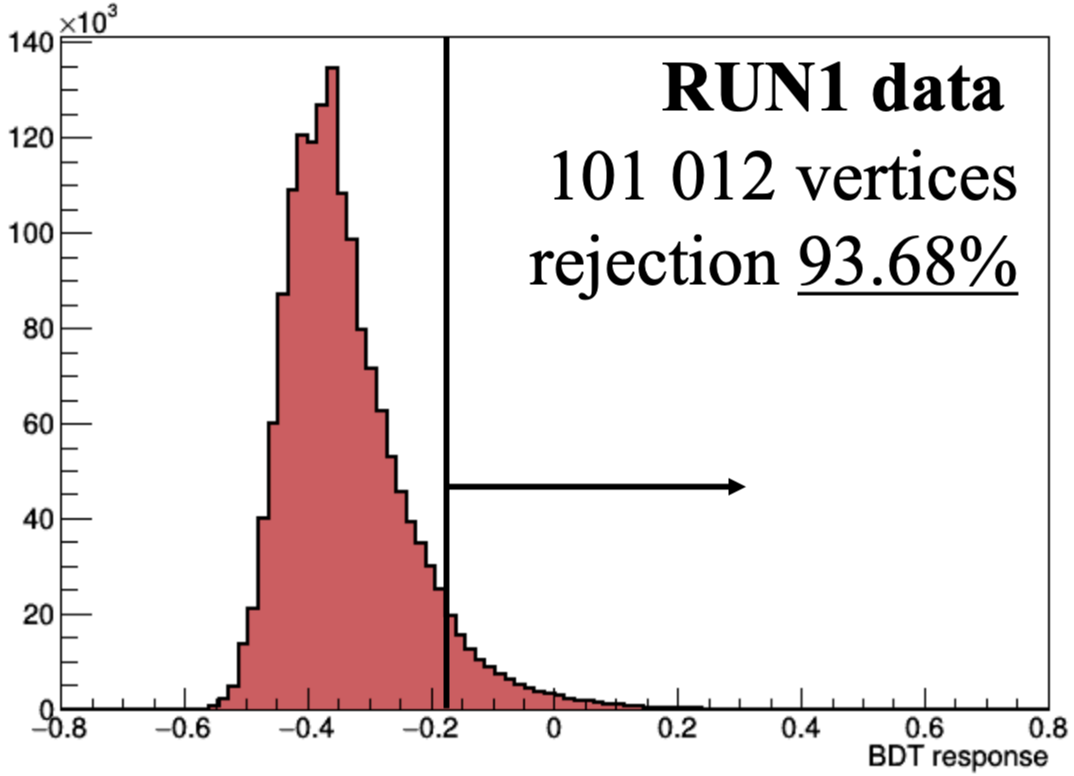

MUON RADIOGRAPHY

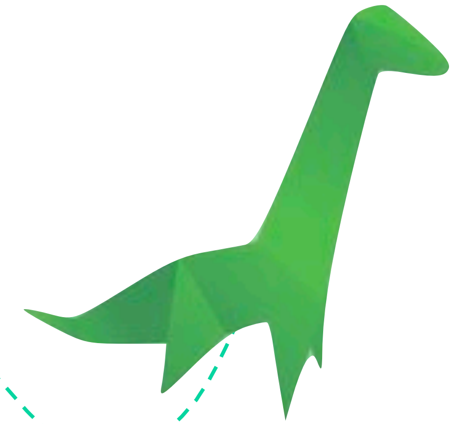

Very special radiographs

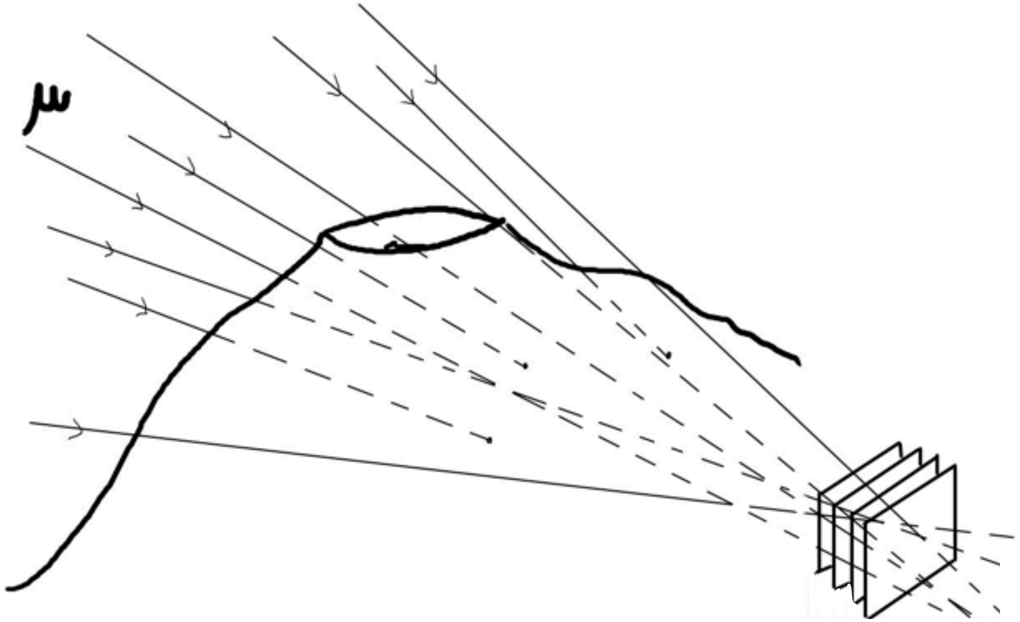

Very special radiographs

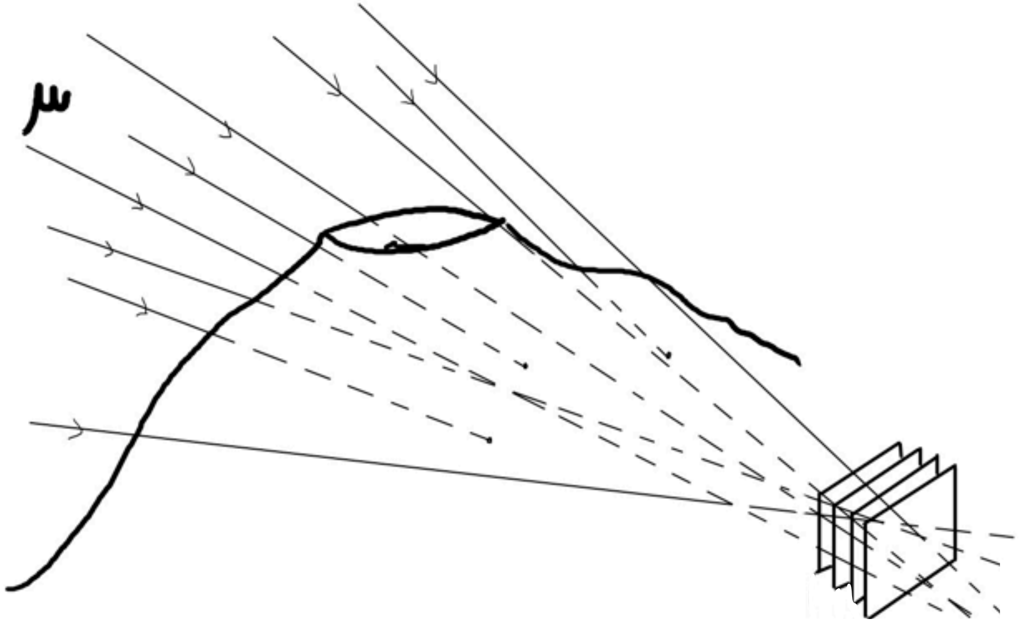

Muon Radiography

Stromboli Volcano

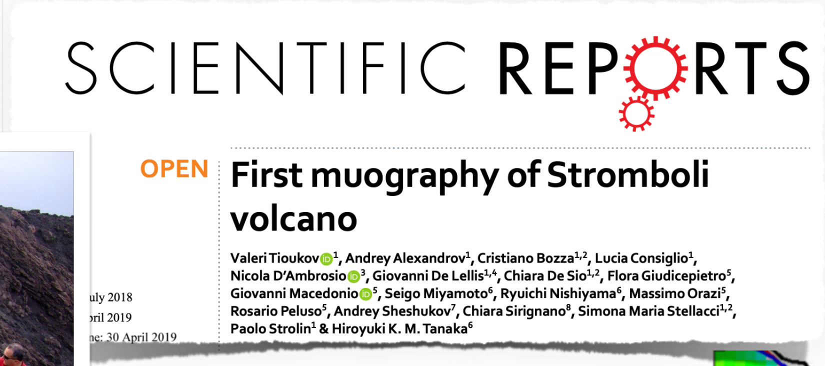

SCIENTIFIC REPORTS

uly 2018
ril 2019
ne: 30 April 2019

OPEN

First muography of Stromboli volcano

Valeri Tioukov[1], Andrey Alexandrov[1], Cristiano Bozza[1,2], Lucia Consiglio[1], Nicola D'Ambrosio[3], Giovanni De Lellis[1,4], Chiara De Sio[1,2], Flora Giudicepietro[5], Giovanni Macedonio[5], Seigo Miyamoto[6], Ryuichi Nishiyama[6], Massimo Orazi[5], Rosario Peluso[5], Andrey Sheshukov[7], Chiara Sirignano[8], Simona Maria Stellacci[1,2], Paolo Strolin[1] & Hiroyuki K. M. Tanaka[6]

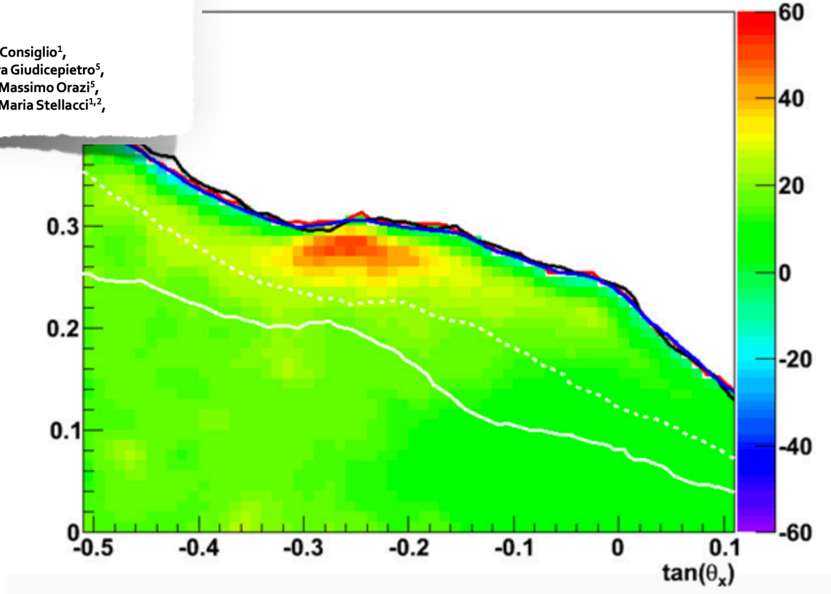

Muon Radiography

Stromboli Volcano

SCIENTIFIC REPORTS

OPEN

First muography of Stromboli volcano

Valeri Tioukov[1], Andrey Alexandrov[1], Cristiano Bozza[1,2], Lucia Consiglio[1], Nicola D'Ambrosio[3], Giovanni De Lellis[1,4], Chiara De Sio[1,2], Flora Giudicepietro[5], Giovanni Macedonio[5], Seigo Miyamoto[6], Ryuichi Nishiyama[6], Massimo Orazi[5], Rosario Peluso[5], Andrey Sheshukov[7], Chiara Sirignano[8], Simona Maria Stellacci[1,2], Paolo Strolin[1] & Hiroyuki K. M. Tanaka[6]

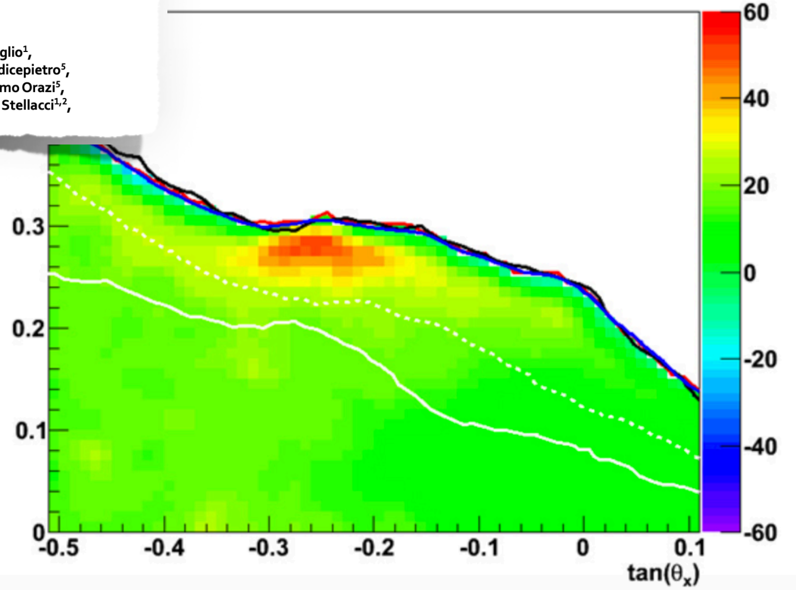

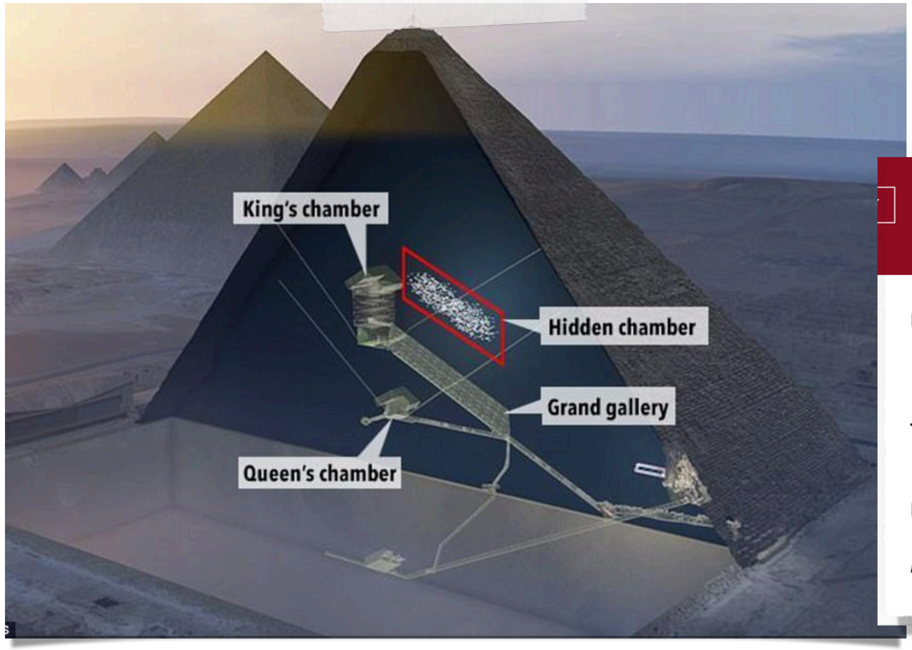

nature
International journal of science

Letter | Published: 02 November 2017

Discovery of a big void in Khufu's Pyramid by observation of cosmic-ray muons

Kunihiro Morishima, Mitsuaki Kuno [...] Mehdi Tayoubi

Nature **552**, 386–390 (21 December 2017) | Download Citation

Muon radiography at "Sanità" district (Naples, Italy)

Using a nuclear emulsion detector in an archaeological site in the "Sanità" district in Naples we clearly observed the known structures as well as some unknown ones

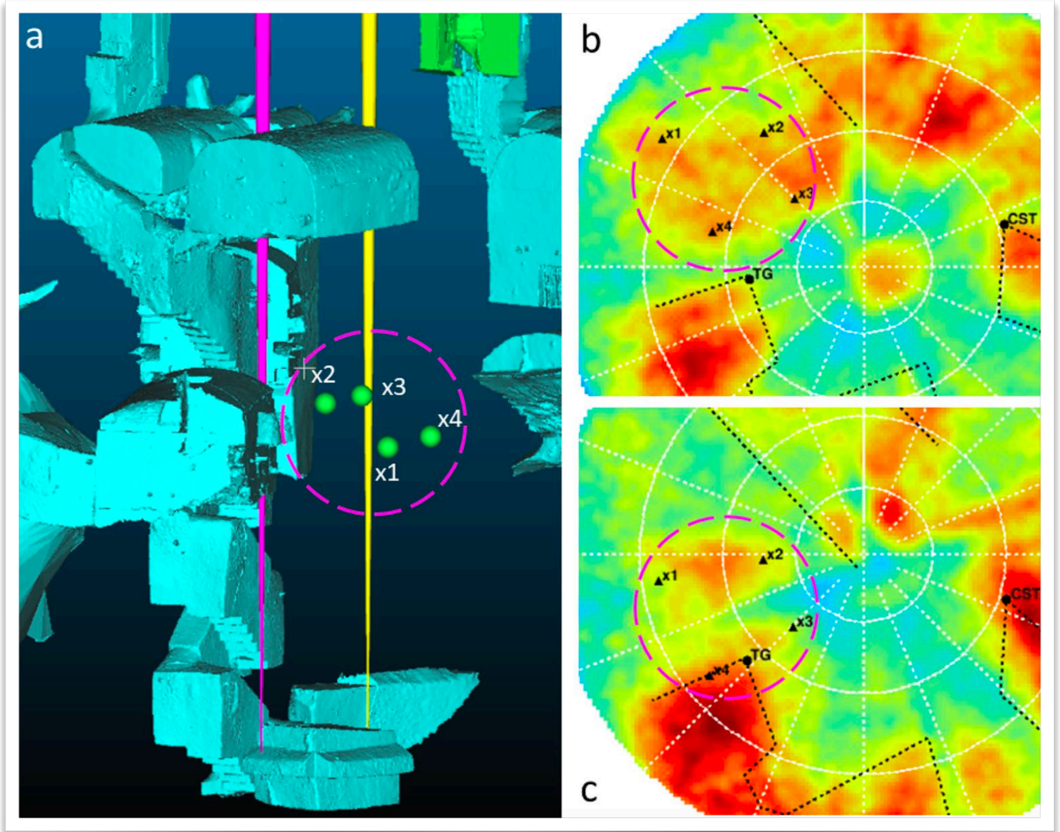

One of the new structures observed is compatible with the existence of a hidden burial chamber, currently inaccessible!

scientific reports

Explore content ⌄ About the journal ⌄ Publish with us ⌄

nature › scientific reports › articles › article

Article | Open Access | Published: 03 April 2023

Hidden chamber discovery in the underground Hellenistic necropolis of Neapolis by muography

Valeri Tioukov, Kunihiro Morishima, Carlo Leggieri, Federico Capriuoli, Nobuko Kitagawa, Mitsuaki Kuno, Yuta Manabe, Akira Nishio, Andrey Alexandrov, Valerio Gentile, Antonio Iuliano & Giovanni De Lellis

Scientific Reports **13**, Article number: 5438 (2023) | Cite this article

FOOT
(FragmentatiOn Of Target)

Few words on Hadrontherapy

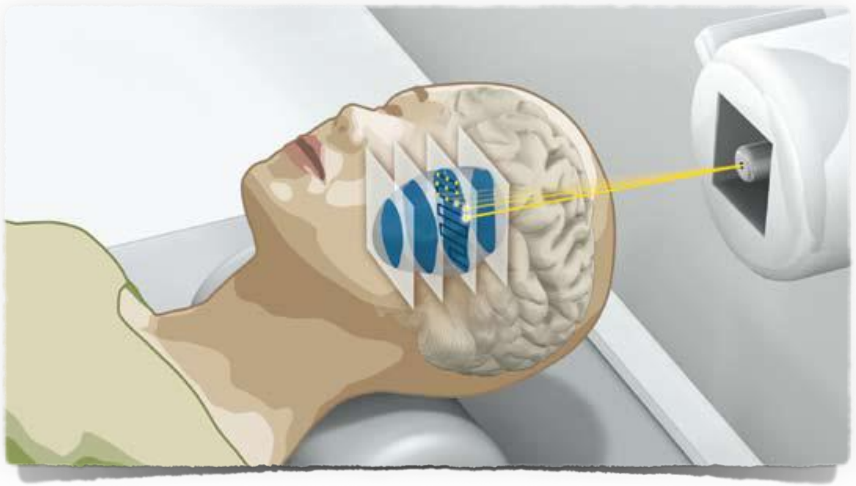

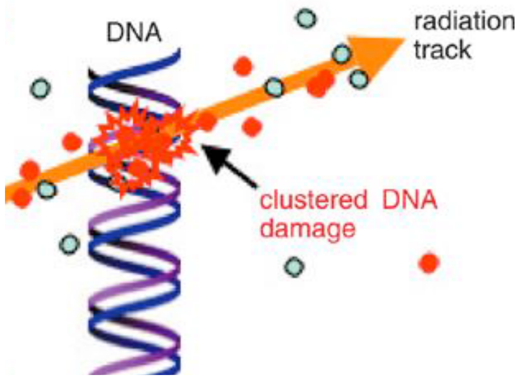

Few words on Hadrontherapy

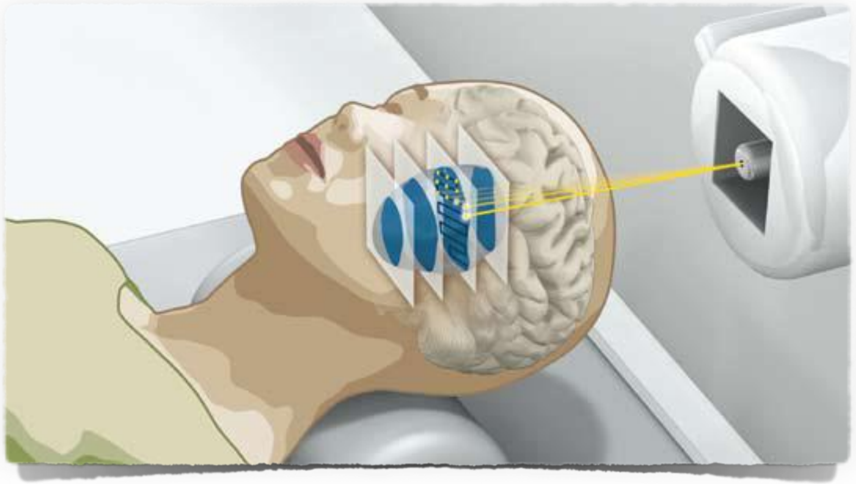

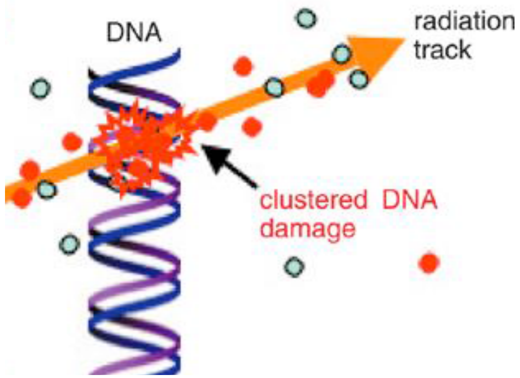

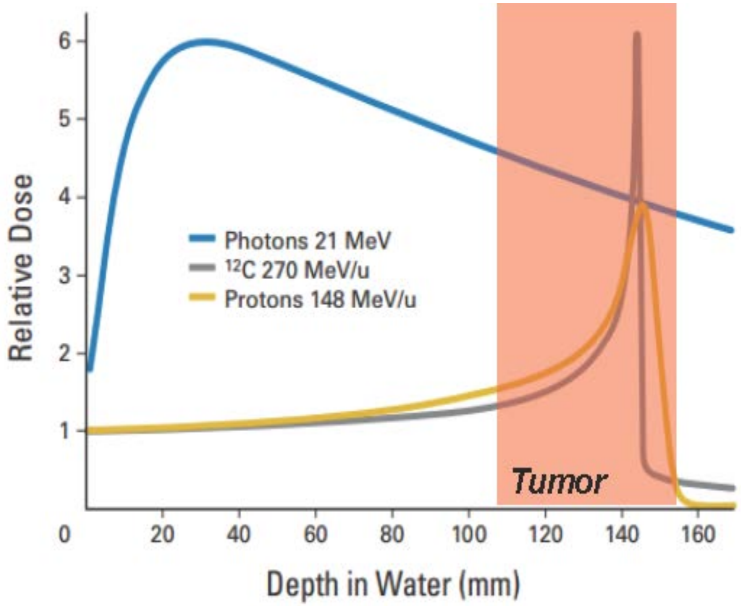

Few words on Hadrontherapy

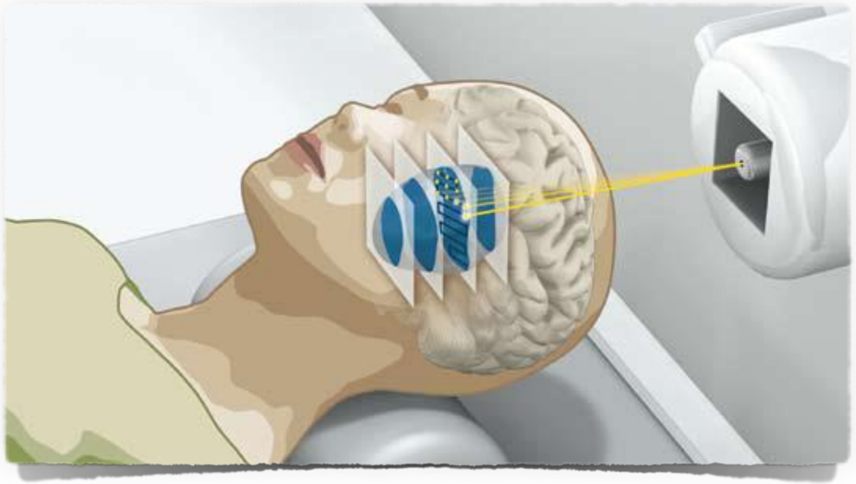

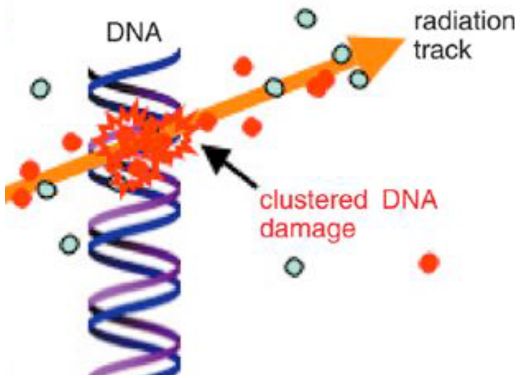

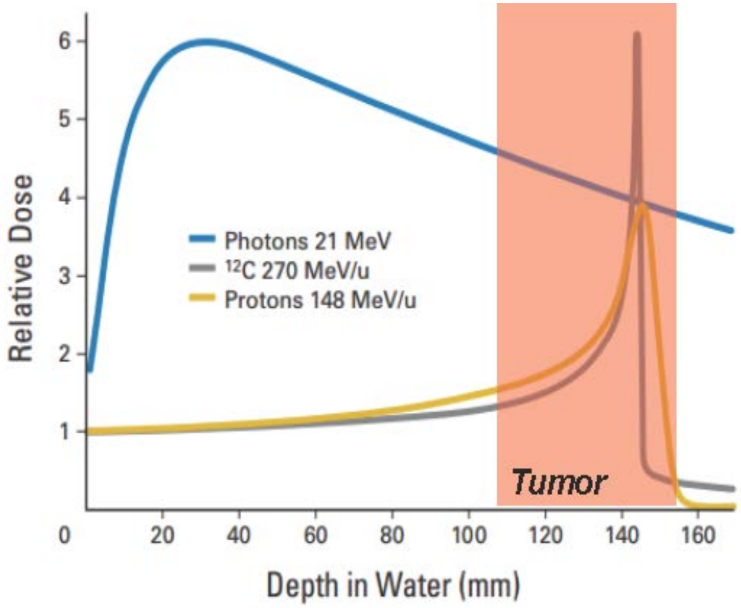

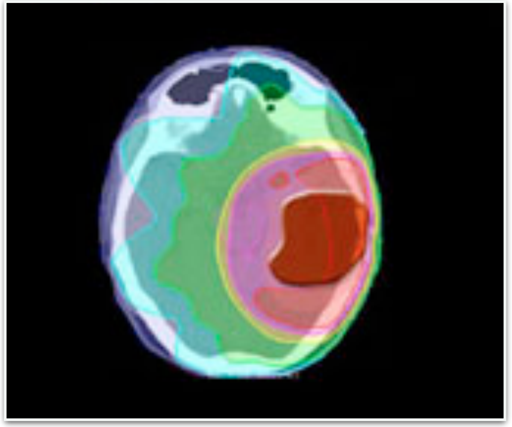

CONVENTIONAL RADIOTHERAPY

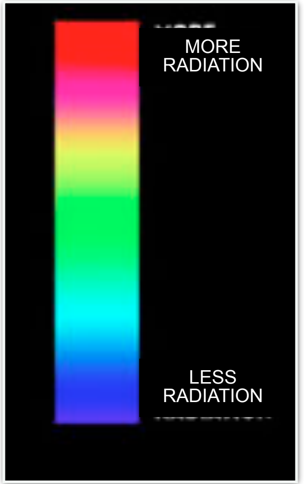

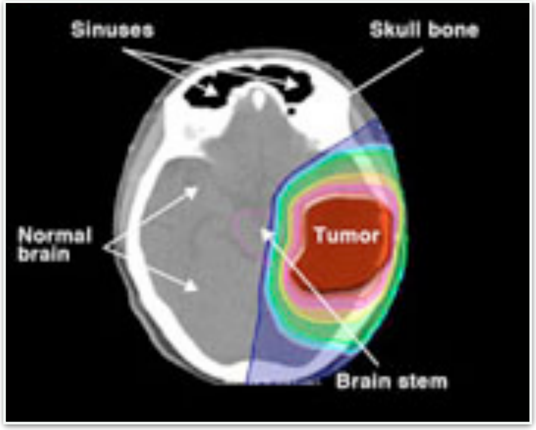

CHARGED PARTICLE THERAPY

Few words on Hadrontherapy

Lack of data on the fragmentation cross section of beams used for hadron therapy

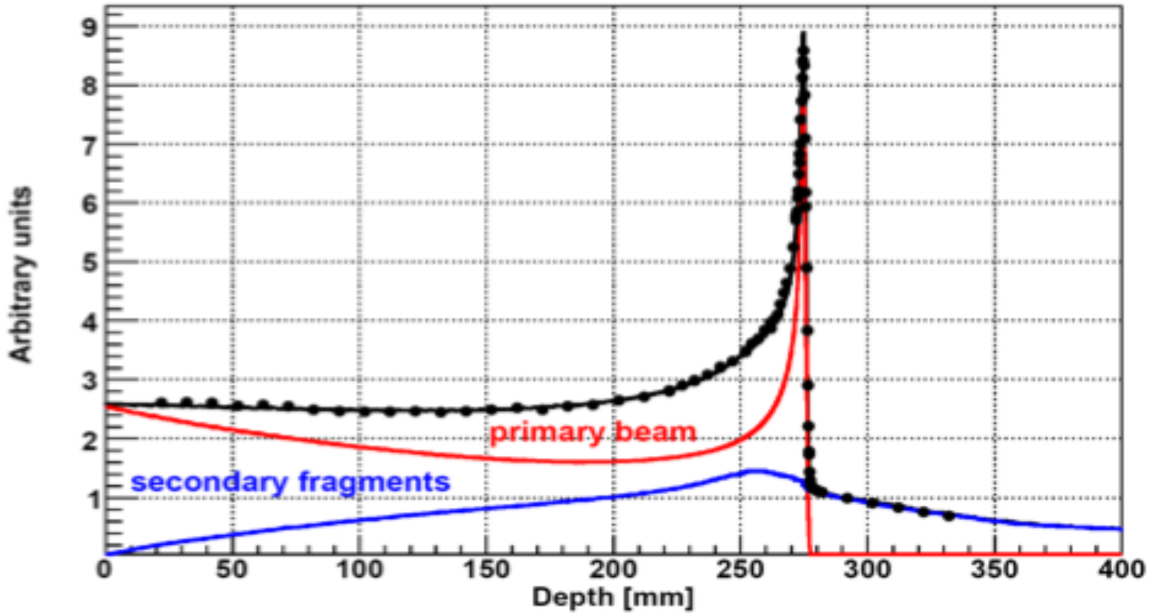

Exp. Data (points) from Haettner et al, Rad. Prot. Dos. 2006
Simulation: A. Mairani PhD Thesis, 2007, Nuovo Cimento C, 31, 2008

The FOOT experiment

Set up $Z \leq 3 \Rightarrow$

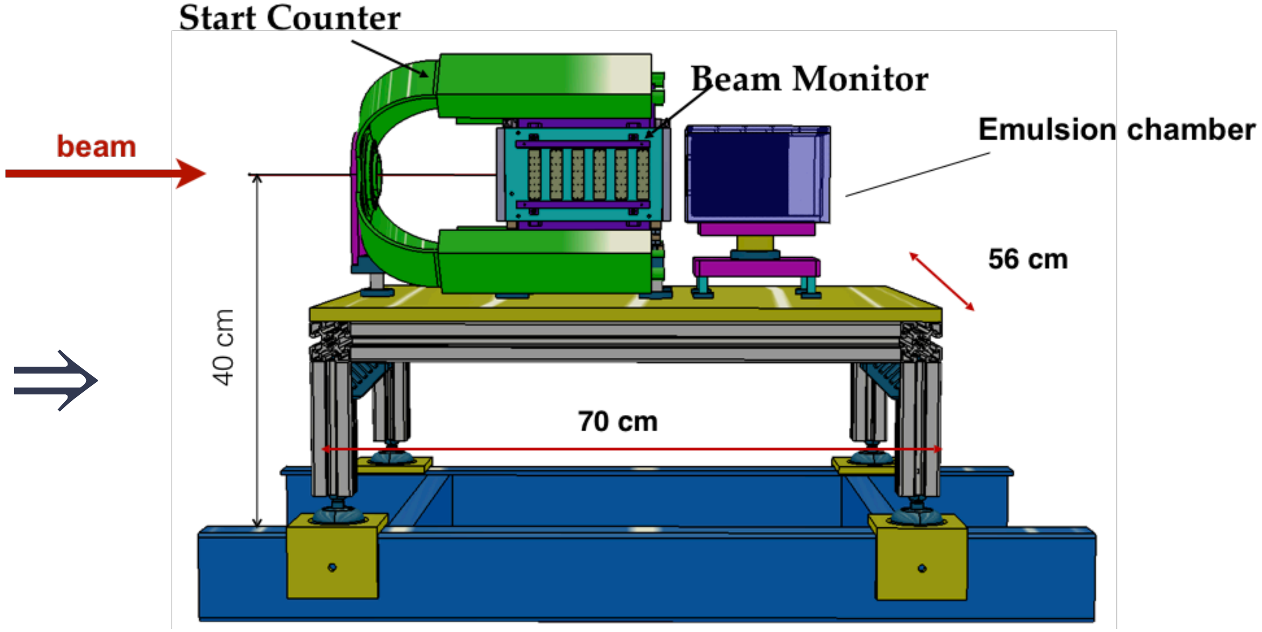

The FOOT experiment

Set up $Z \leq 3 \Rightarrow$

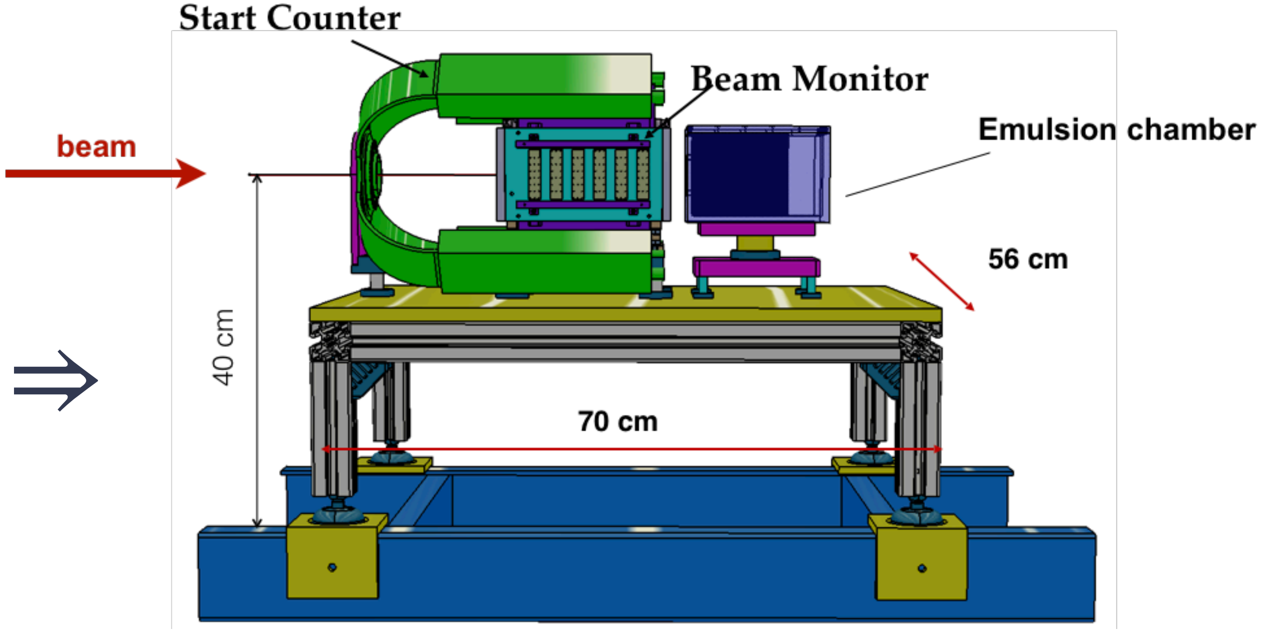

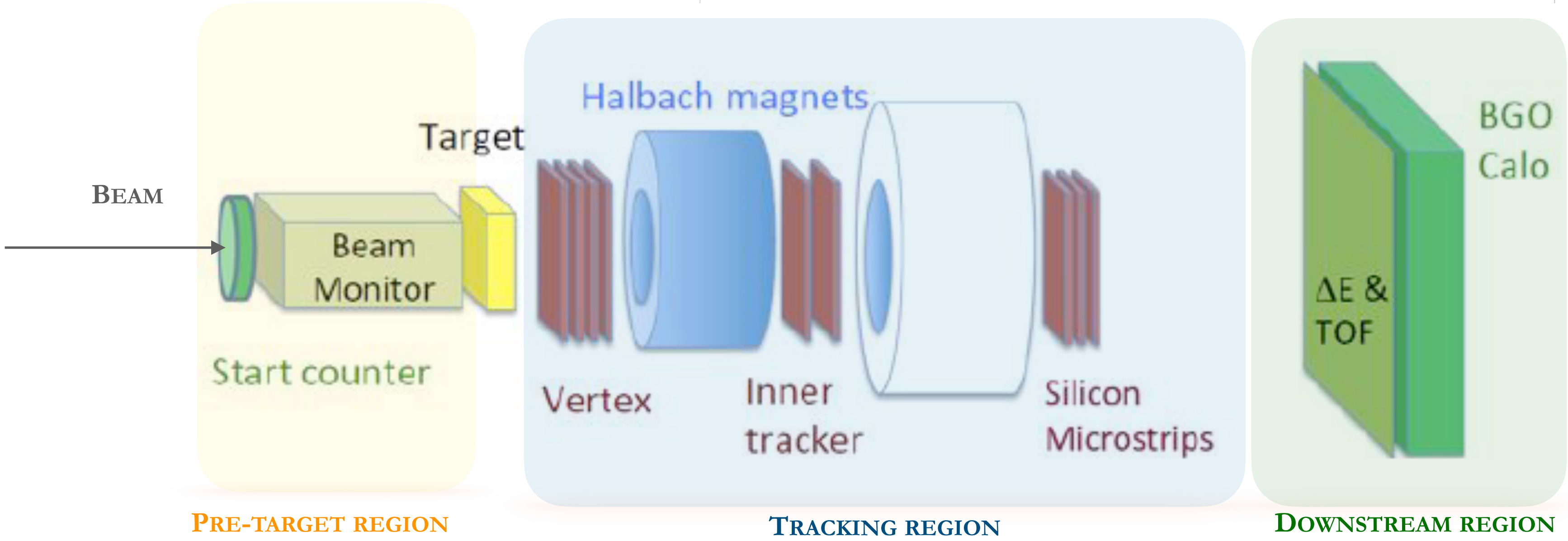

$\Leftarrow$ Set up $Z \geq 3$

Nuclear emulsions spectrometer

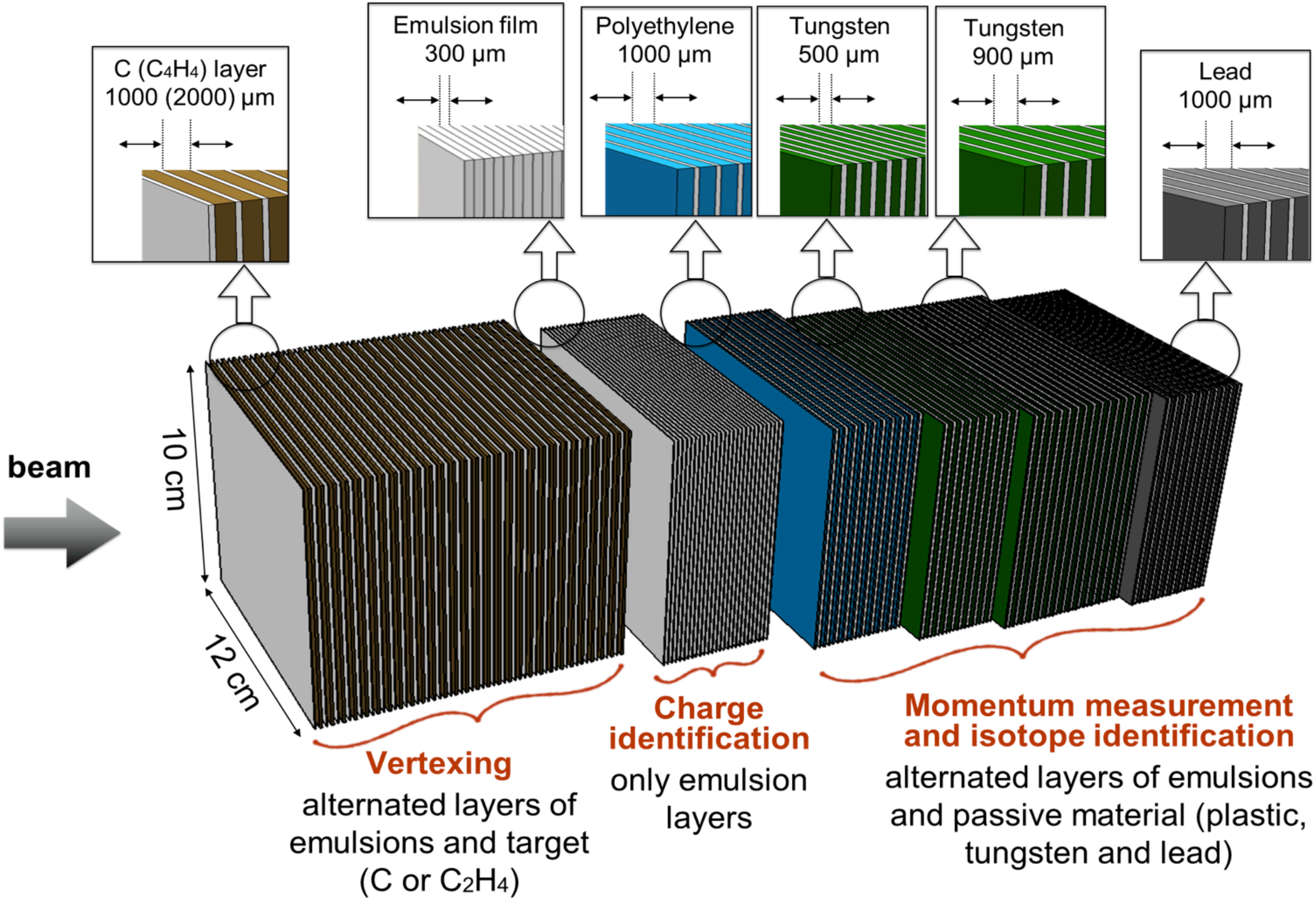

Data taken @ GSI (Darmstadt) 2020

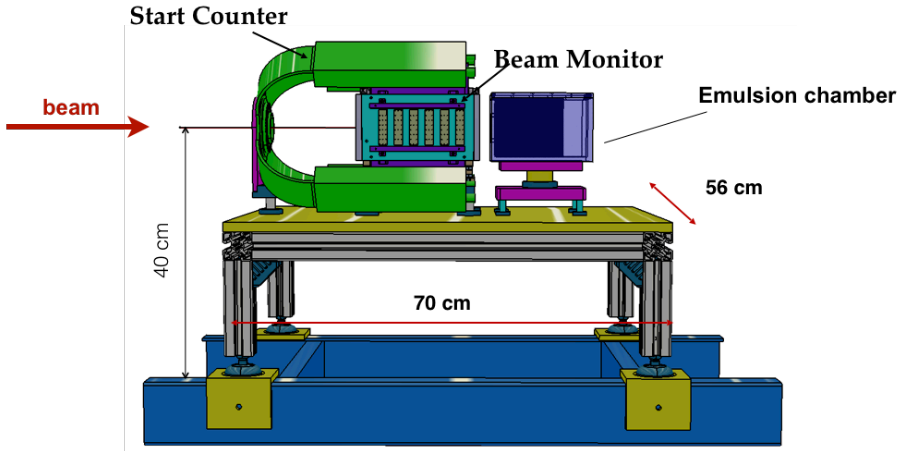

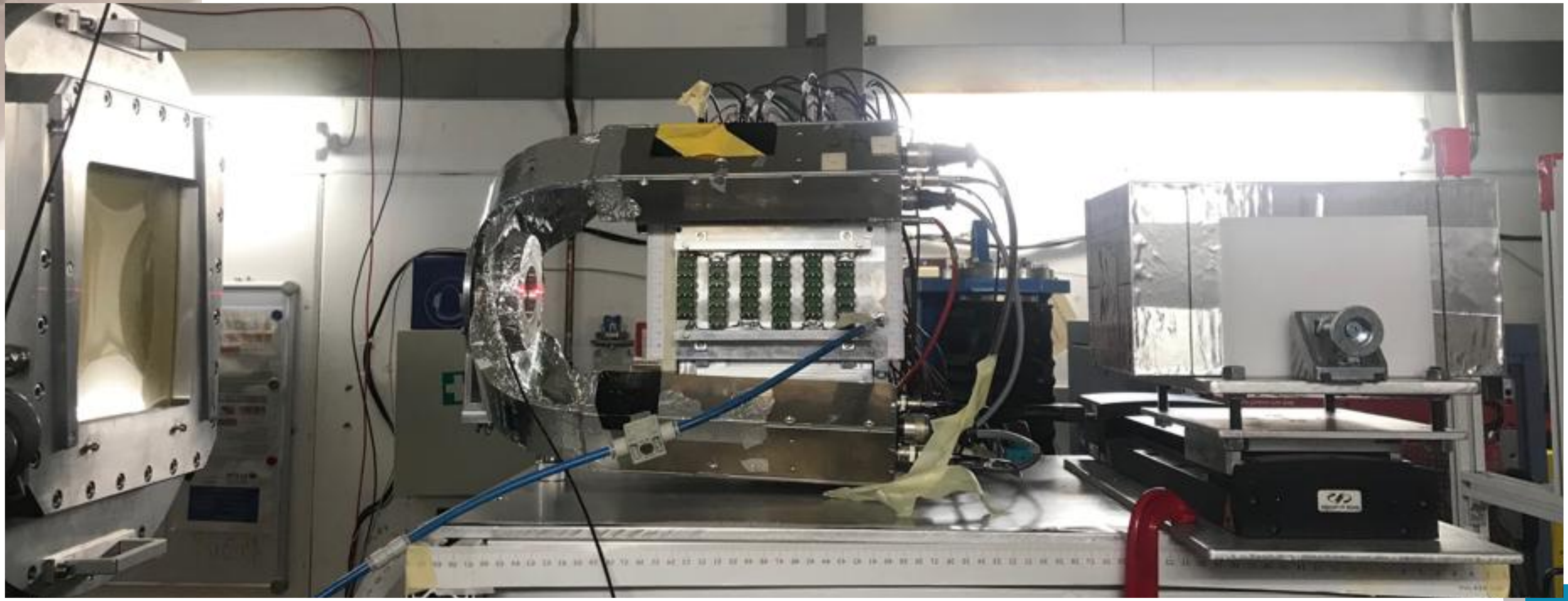

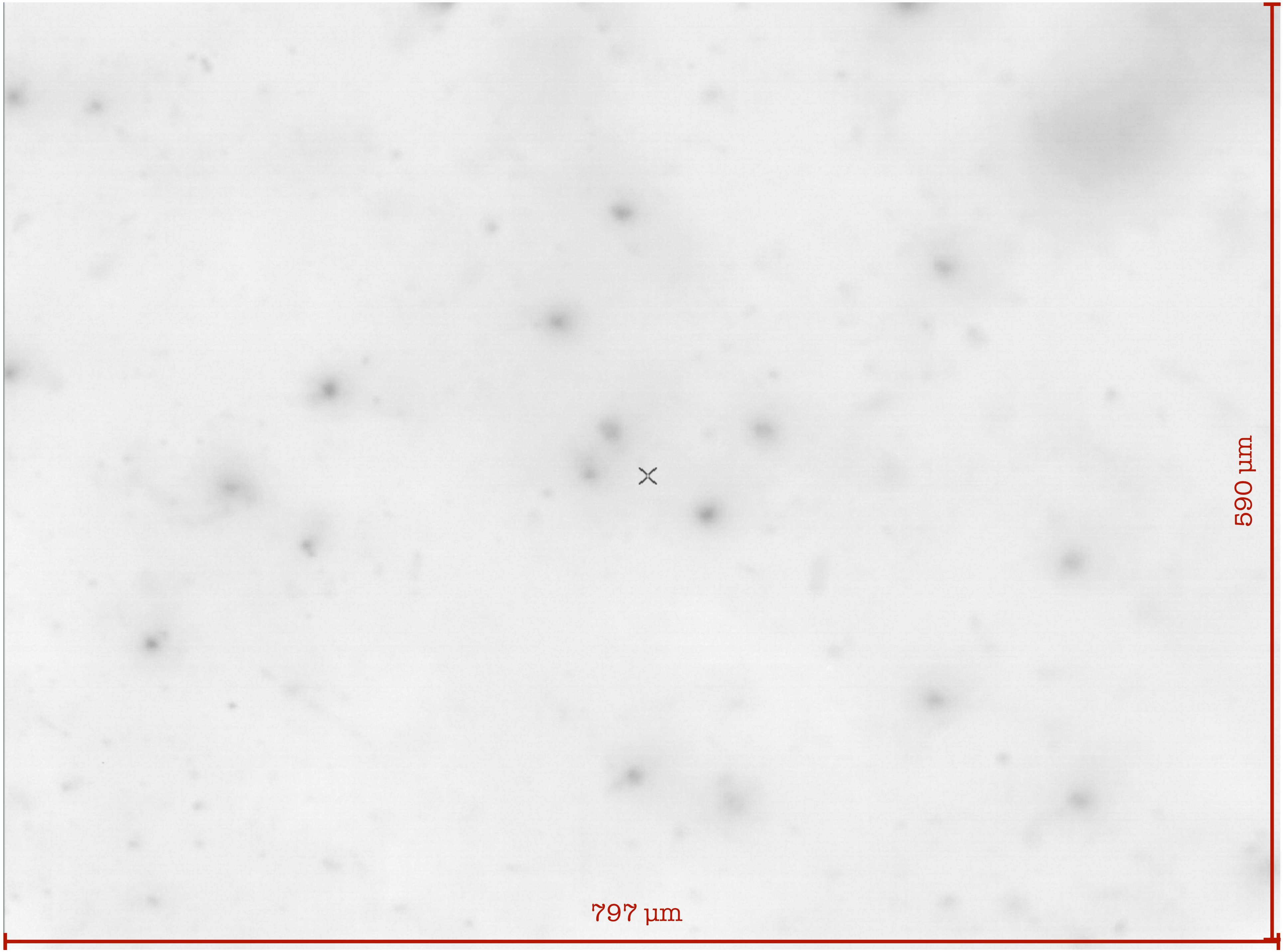
590 µm
797 µm

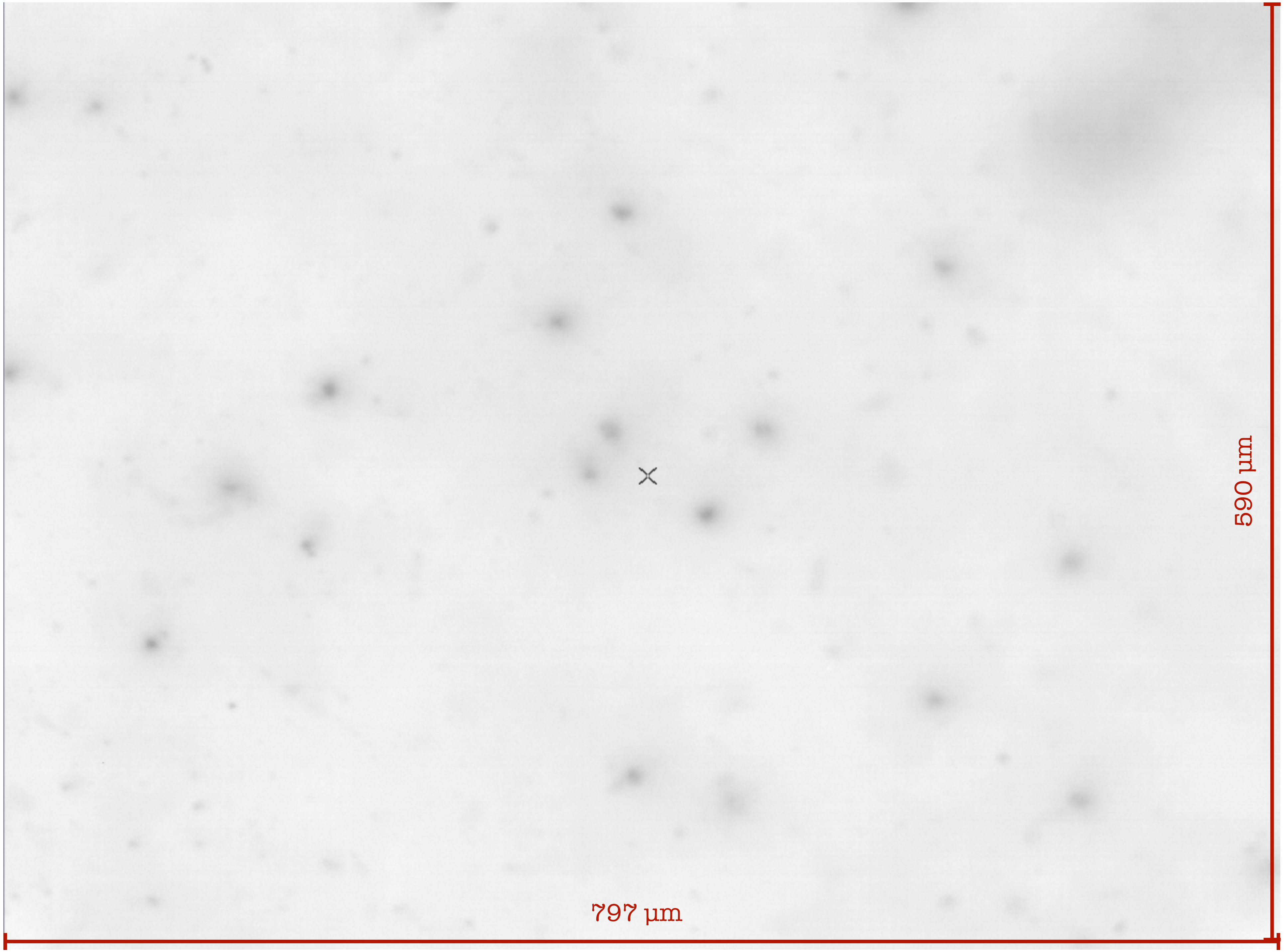
590 µm
797 µm

Study of interactions

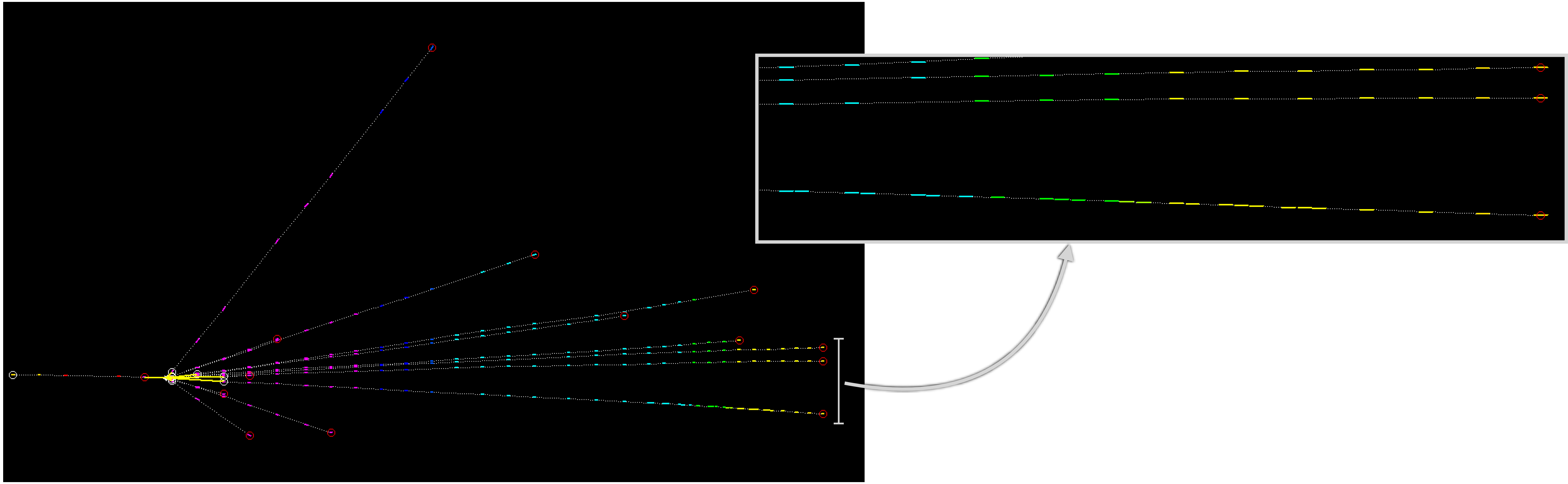

Charge measurement

- Nuclear emulsion response is proportional to the energy loss of particles over a certain dynamic range: grain density is proportional to the particle's specific ionization
- Highly ionizing particles saturate nuclear emulsion's response
- A procedure based on different thermal treatments can extend the dynamical range of the emulsions to overcome the saturation effects
- Each thermal treatment erase totally or partially the track’s segments, depending on its ionization

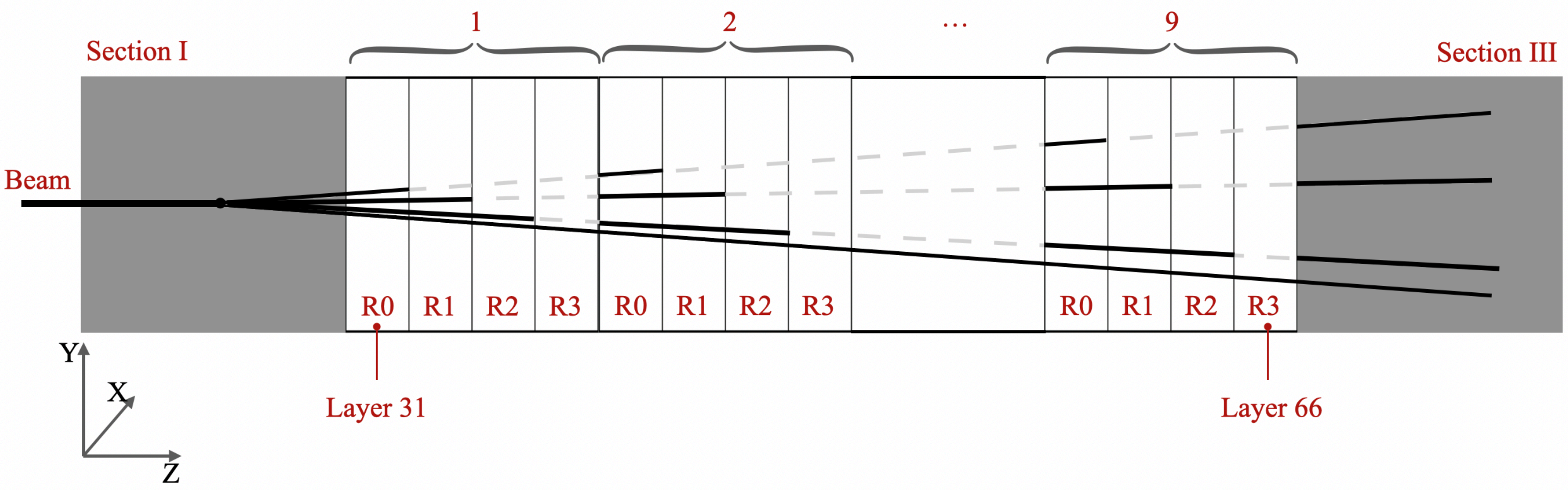

- **R0:** Not thermally treated
- **R1:** 24 h at **T1=28°C** and RH = 95%
- **R2:** 24 h at **T2=34°C** and RH = 95%
- **R3:** 24 h at **T3=36°C** and RH = 95%

Charge measurement

- Cut-based approach to distinguish MIP cosmic rays and Z≤2

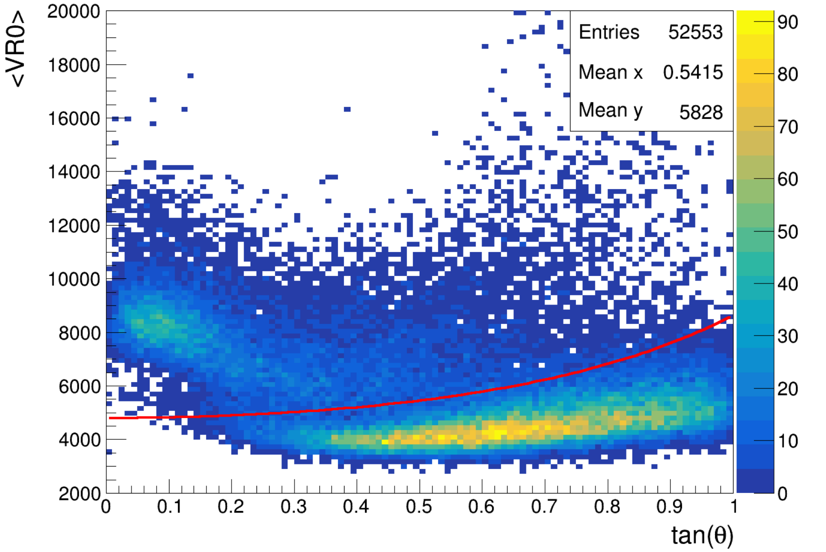

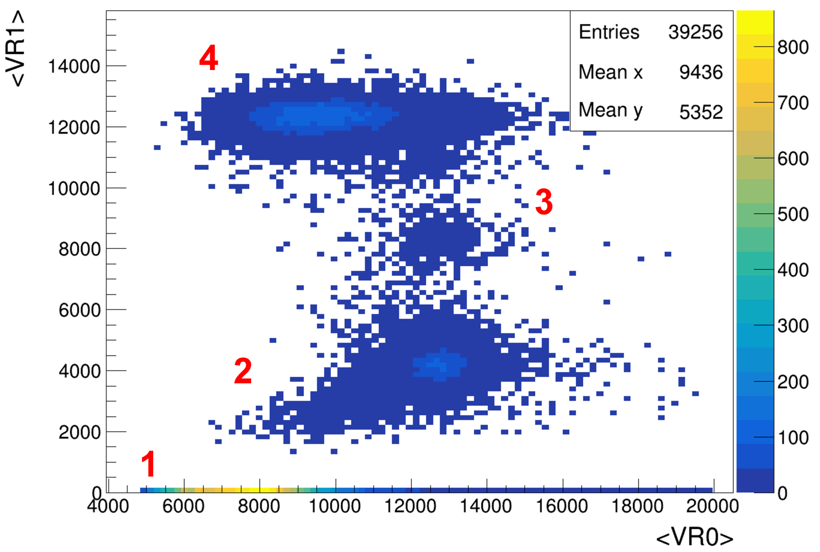

- Principal Components Analysis to distinguish Z≥2 fragments

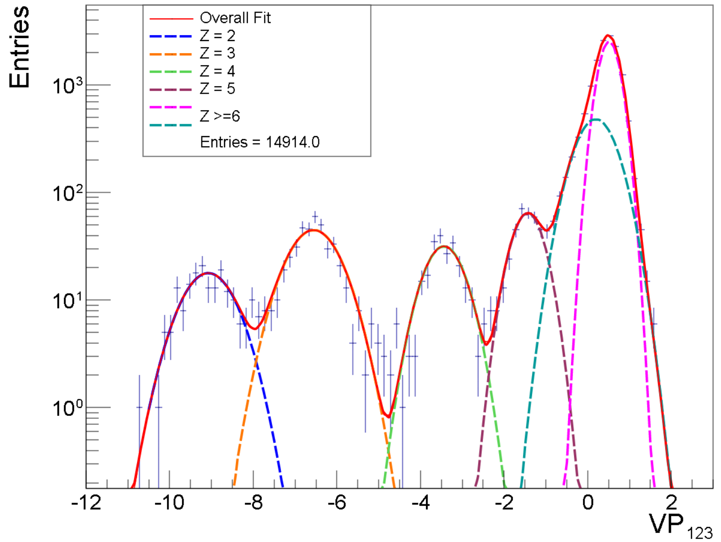

NEWSdm

Search for dark matter… underground

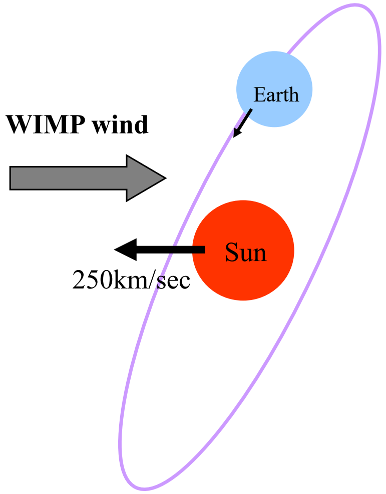

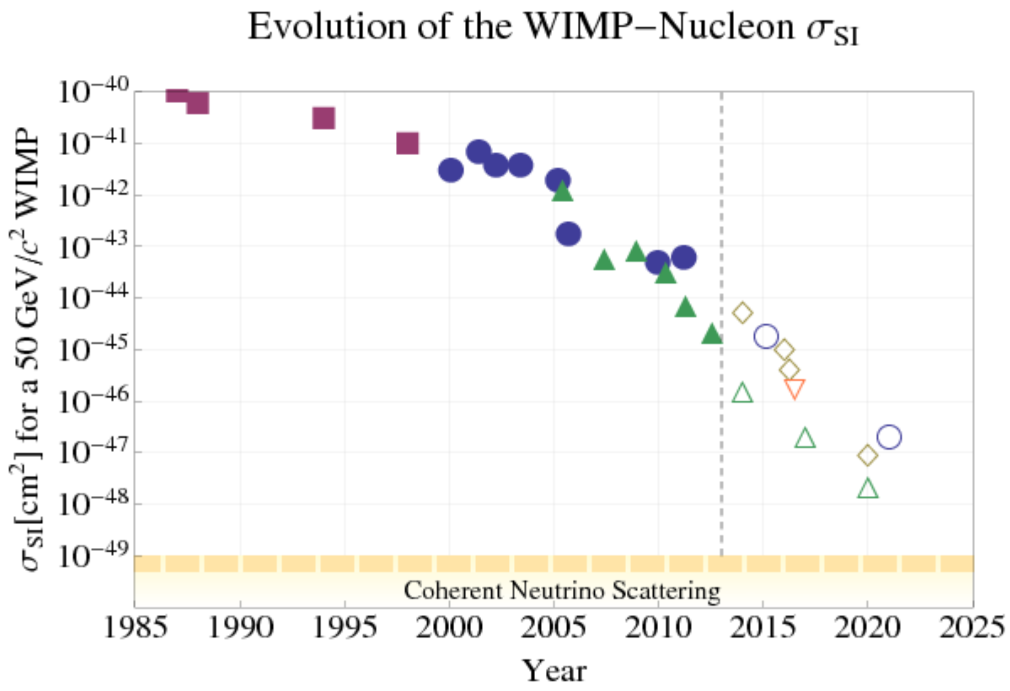

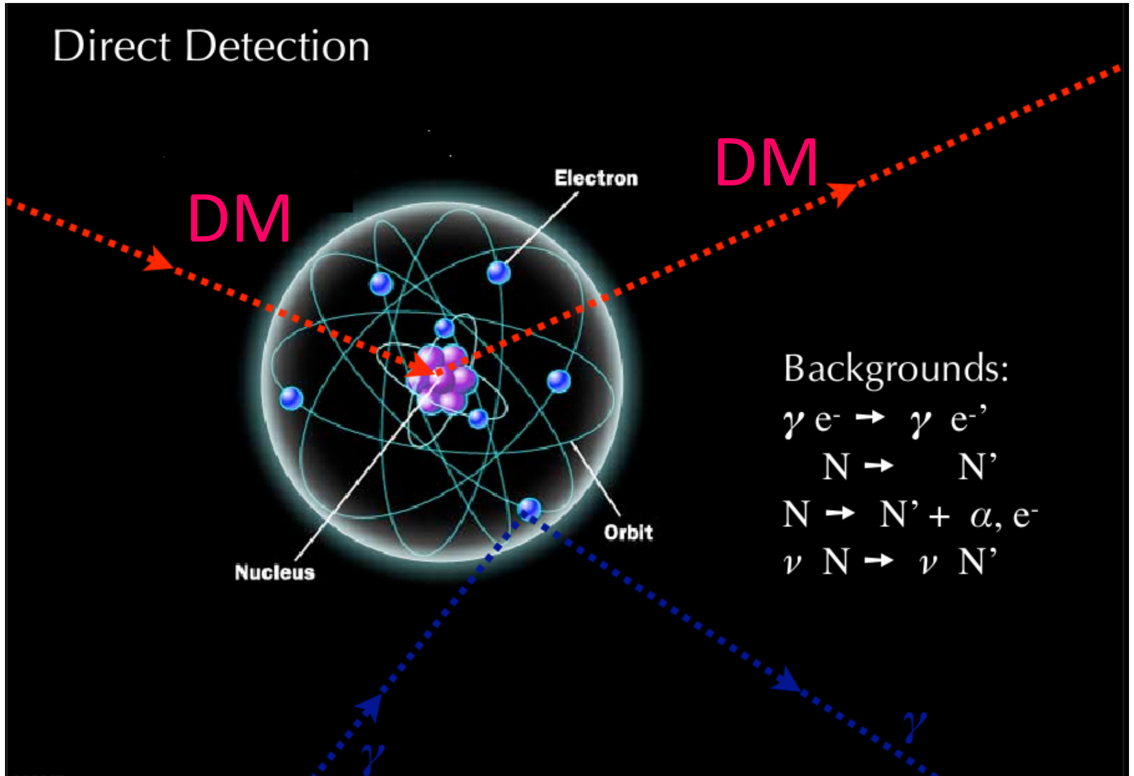

Search for dark matter… underground

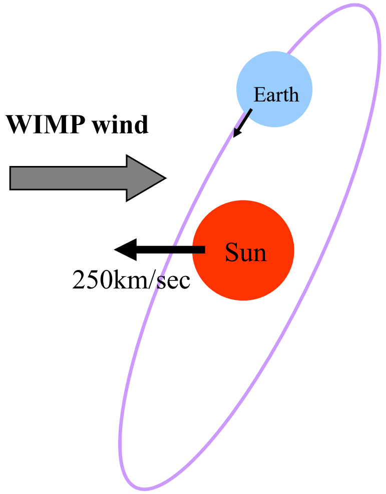

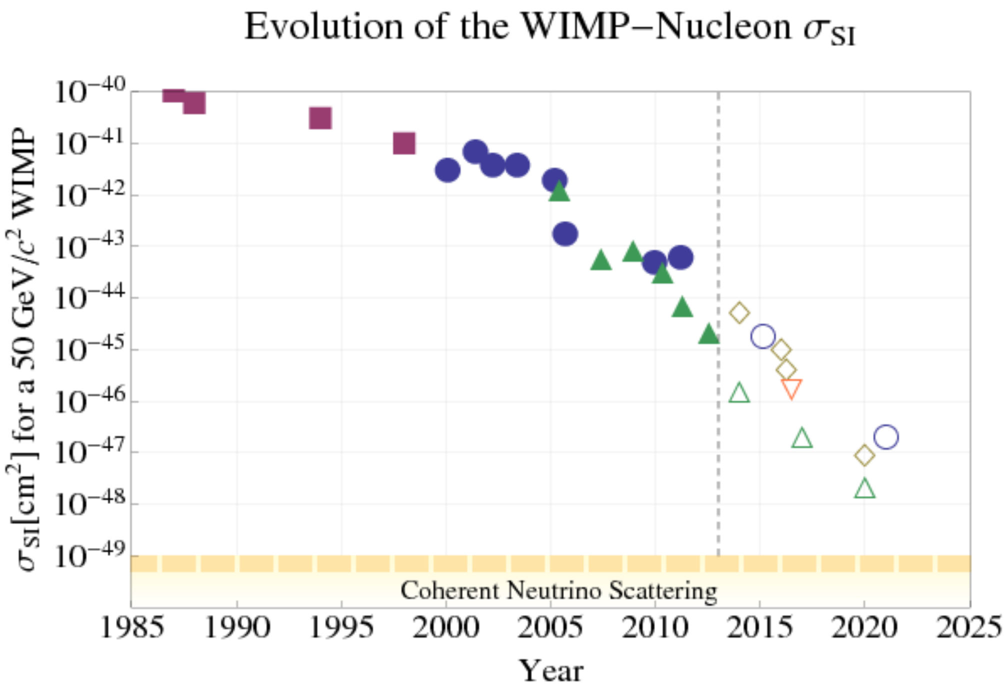

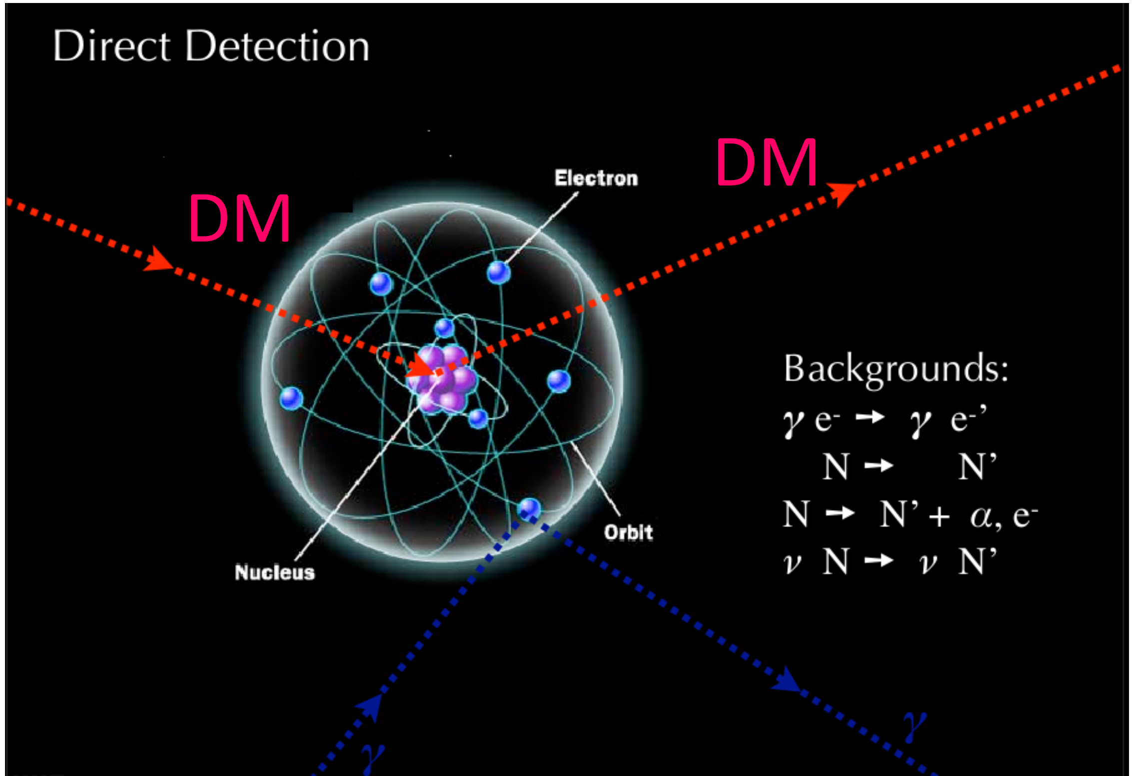

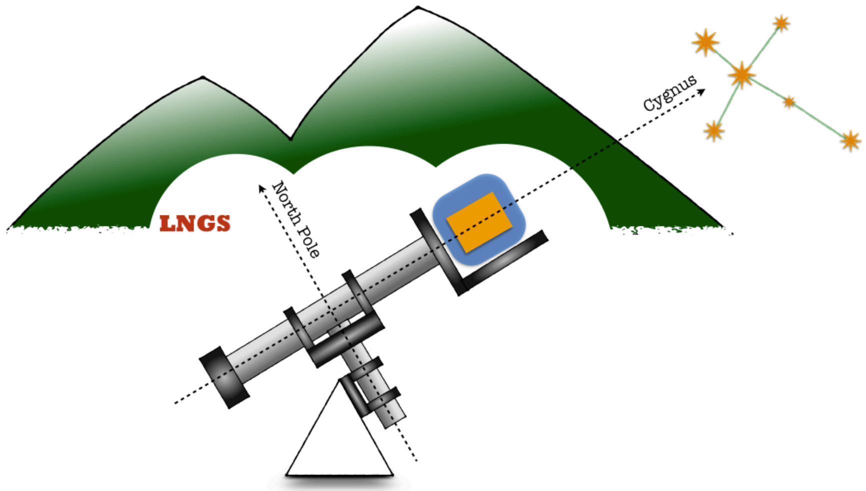

Nuclear recoils induced by galactic dark matter scattering in the emulsion

heavy nuclei: Ag, Br, I
light nuclei: C, O, N, H, S

Element	Mass Fraction
Ag	0.44
Br	0.32
I	0.019
C	0.101
O	0.074
N	0.027
H	0.016
S	0.003

Each nucleus gives different contribution to the overall sensitivity

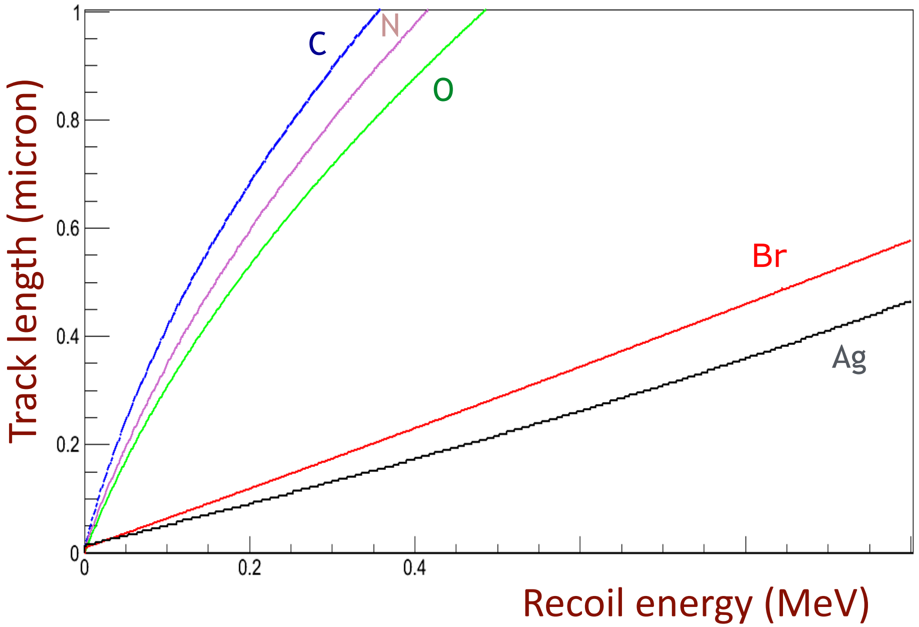

Range of recoil nuclei & WIMP Mass

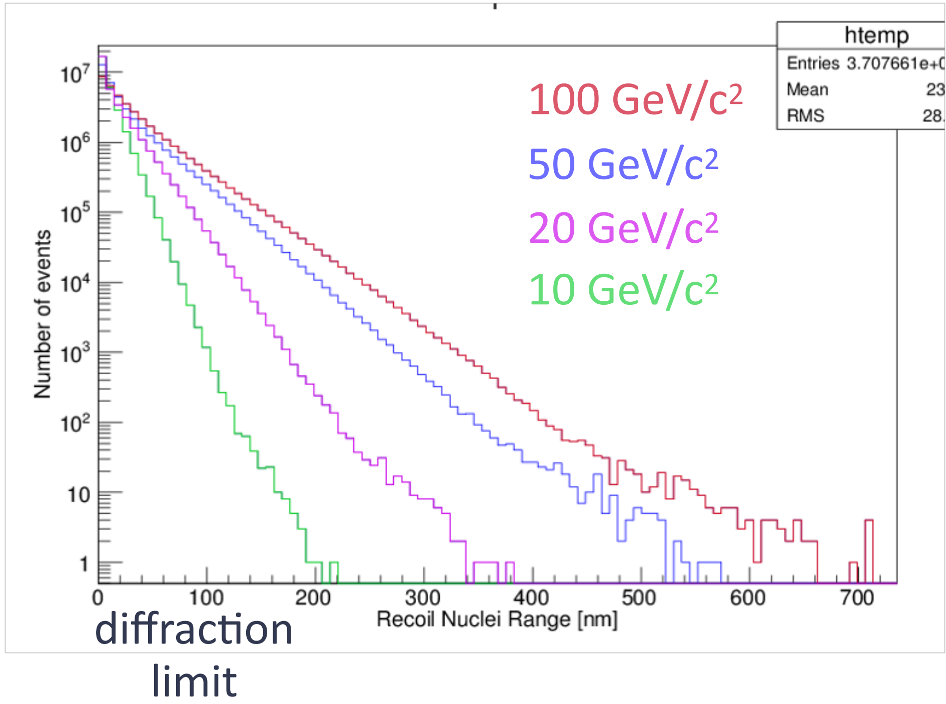

Lighter nuclei ⇒ longer range at same recoil energy ⇒ Sensitivity to low WIMP mass

Typical crystal size for a new type of emulsion film

NIT

Current emulsion sample

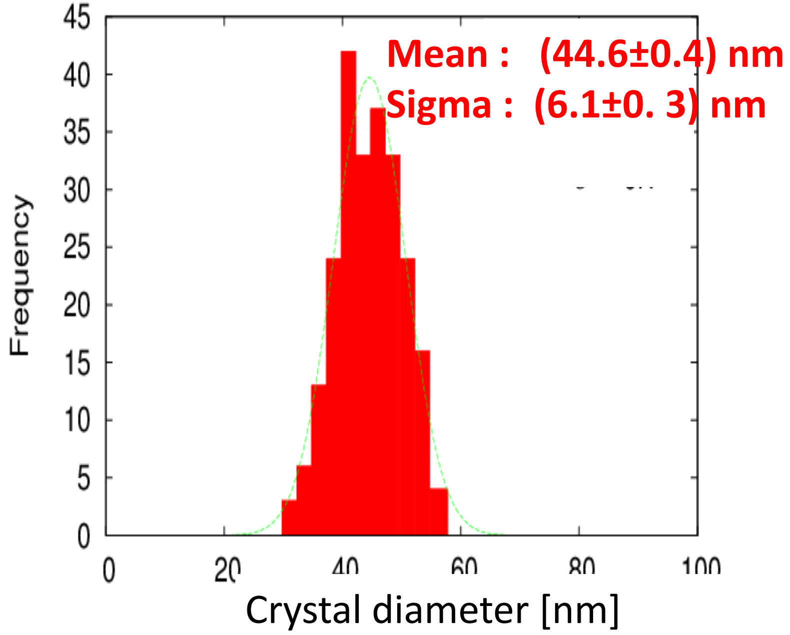

U-NIT

Finest grain emulsion

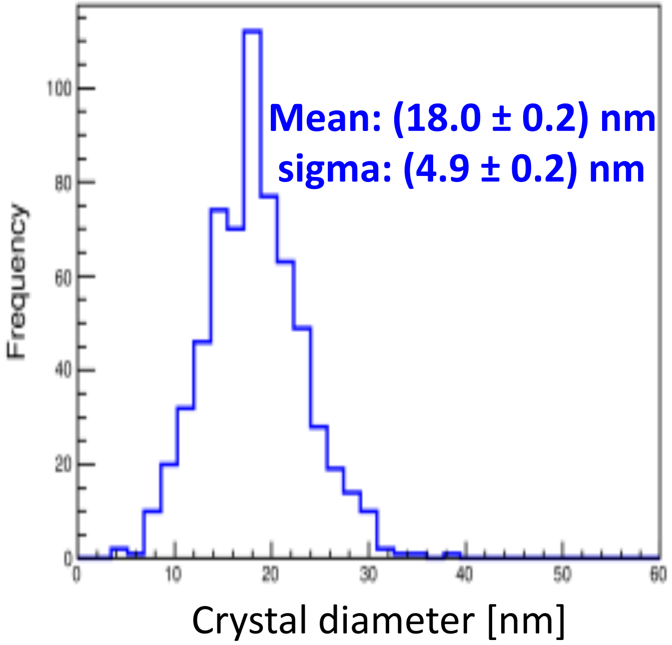

	NIT	U-NIT
AgBr density	11 AgBr/µm	29 AgBr/µm

Range threshold	Carbon Energy
200 nm	75 keV
100 nm	35 keV
50 nm	15 keV

Track identification

- Fast and completely automated optical microscopes
- Challenge: detect tracks with lengths comparable/shorter than optical resolution
- Baseline strategy: two-steps approach

STEP1: CANDIDATE IDENTIFICATION

Pros: Fast scanning profiting of the improvements driven by the OPERA experiment, dedicated measurement stations in each lab

Limit: Resolution with standard technologies ~200 nm

STEP2: CANDIDATE VALIDATION (Resonant light scattering)

Pros: Super resolution ~6 nm

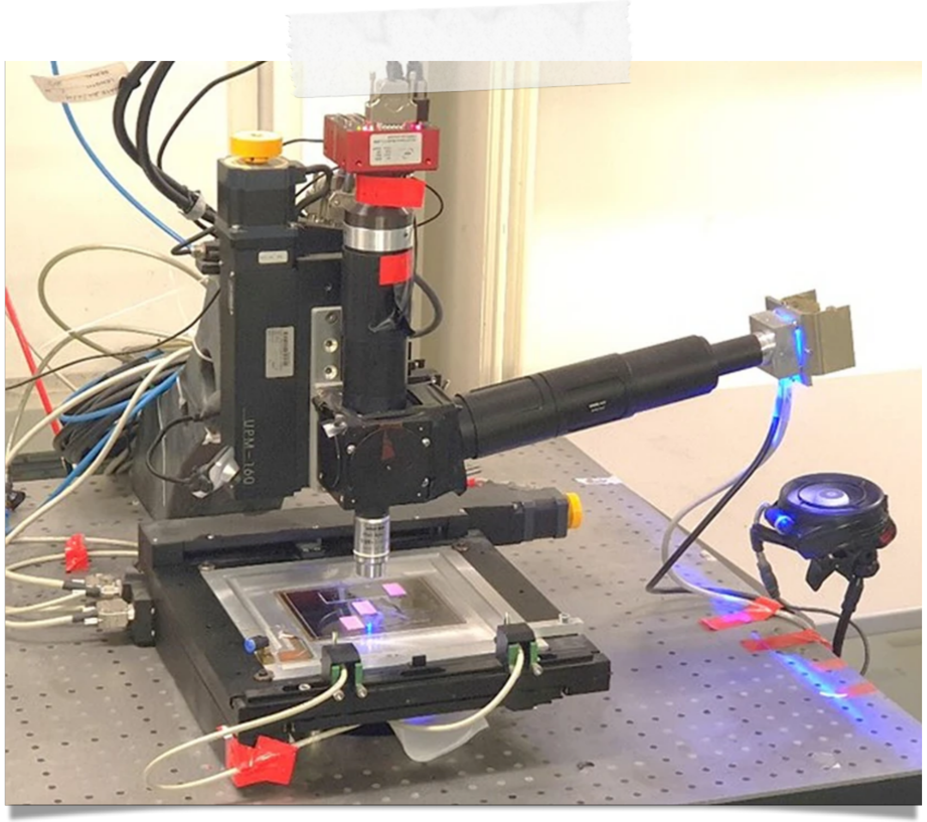

Step 1: Candidate Identification

- Scanning with optical microscope and shape recognition analysis
- Signal: clusters with elliptical shape: major axis along track direction
- Background: spherical clusters
- Automatic selection of candidate signals by optical microscopy
- Resolution 200 nm (one order of magnitude better than the OPERA scanning system), scanning speed 20 cm^2/h

Test using 400 keV Kr ions

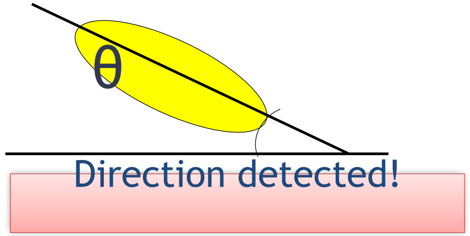

Nucl.Instrum.Meth. A680 (2012) 12-17

ANGULAR RESOLUTION:

$$\sigma^2 = \sigma^2_{intrinsic} + \sigma^2_{scattering}$$

$$\sigma = 360 \text{ mrad}$$

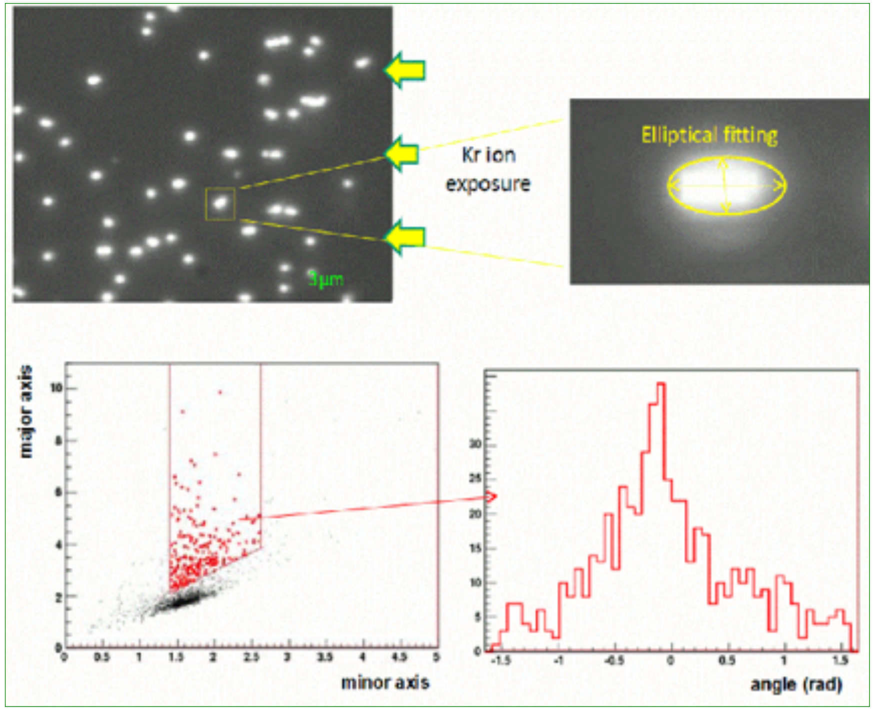

Step 2: Resonant Light Scattering

- Occurring when the light is scattering off a nanometric metallic (silver) grain dispersed in a dielectric medium (Applied Phys Letters 80 (2002) 1826)
- Sensitive to the shape of nanometric grains: when silver grains are **not spherical**, the resonant response depends on the polarization of the incident light.
- Each grain is emphasized at different polarization values

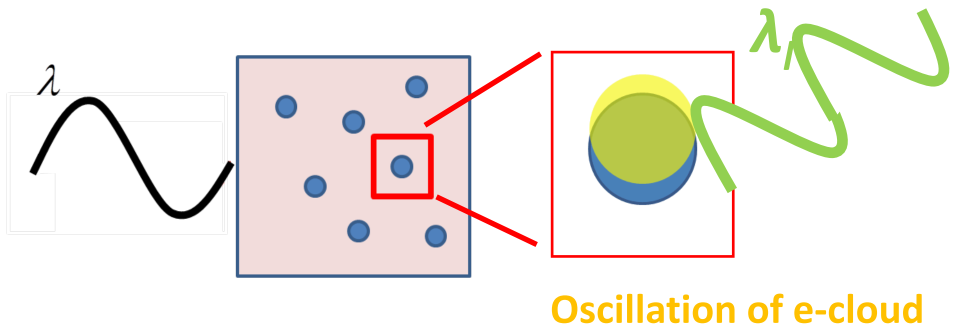

- Taking multiple measurements over the whole polarization range produces a displacement of the barycenter of the cluster
- Measure the displacement of cluster barycentre as a function of polarization angle (dx, dy)

Resonant light scattering: silver grains

TEM image of Carbon track after development

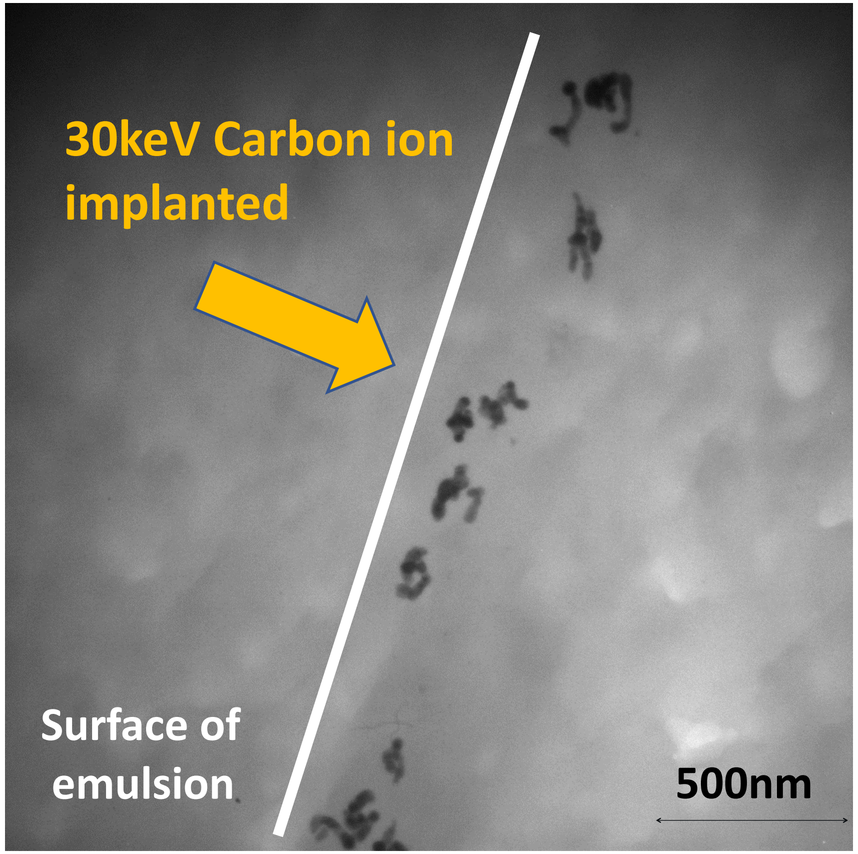

Different orientation

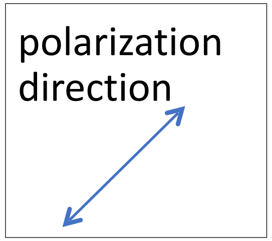

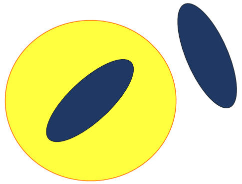

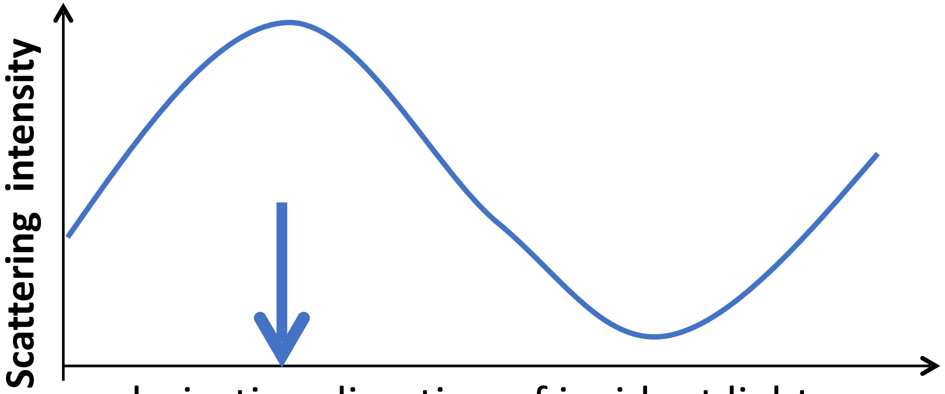

Optical response strongly depends
on the polarization of incident light

Resonant light scattering: silver grains

TEM image of Carbon track after development

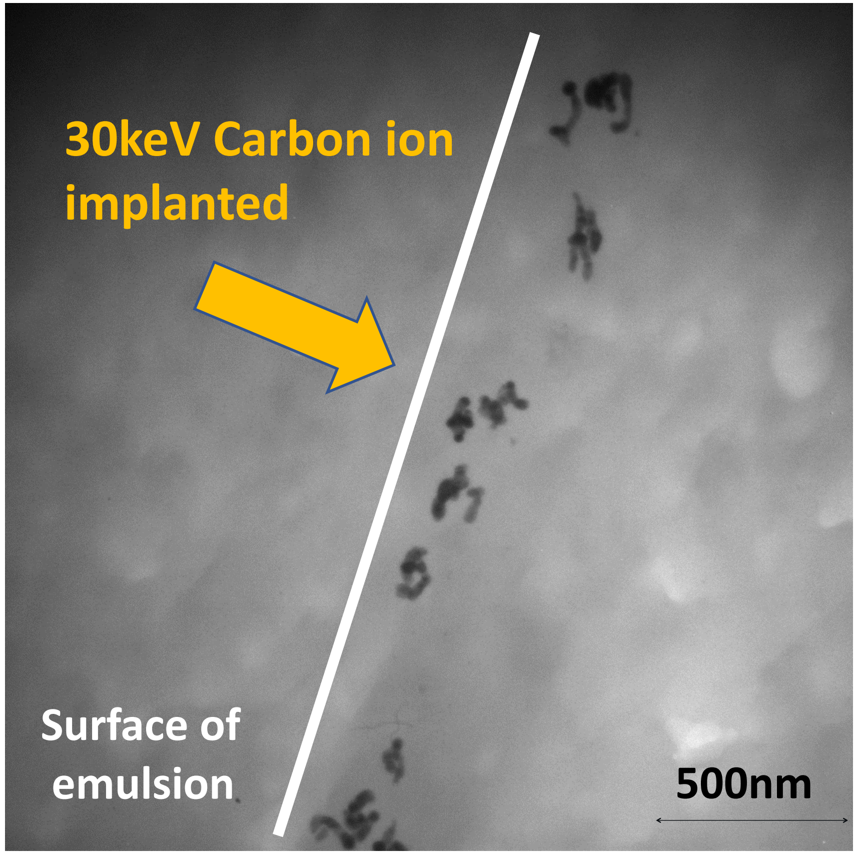

Different orientation

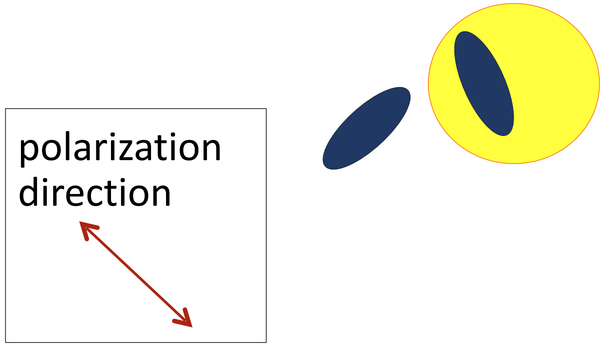

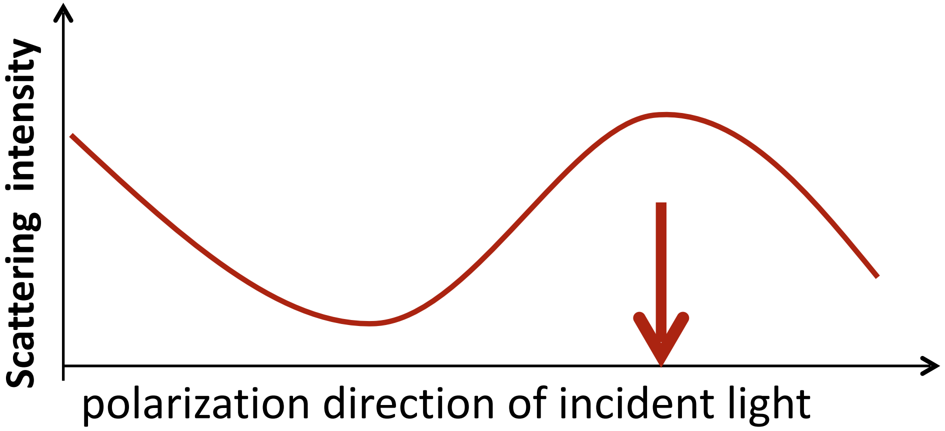

Optical response strongly depends on the polarization of incident light

Beyond the limits of diffraction

Background grain

Barycenter of the cluster

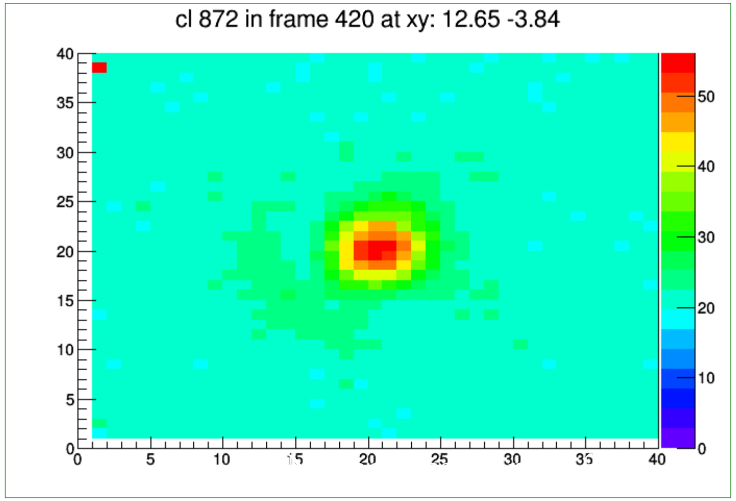

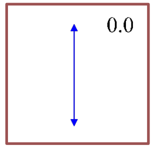

Polarization angle

Signal-like events (100keV C ion)

Max barshift

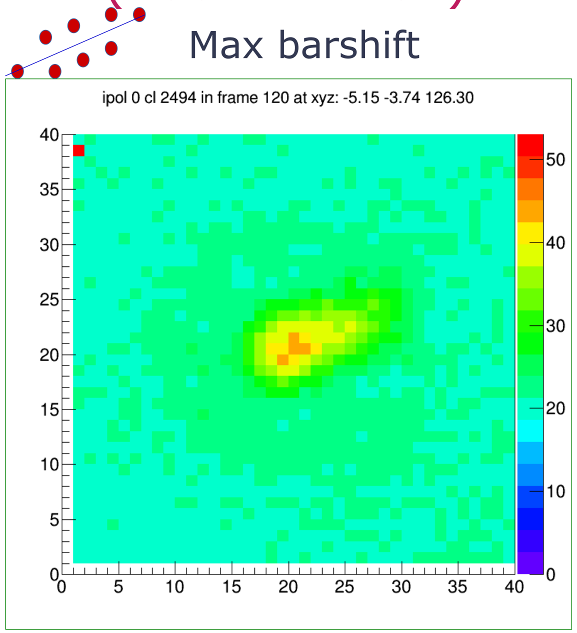

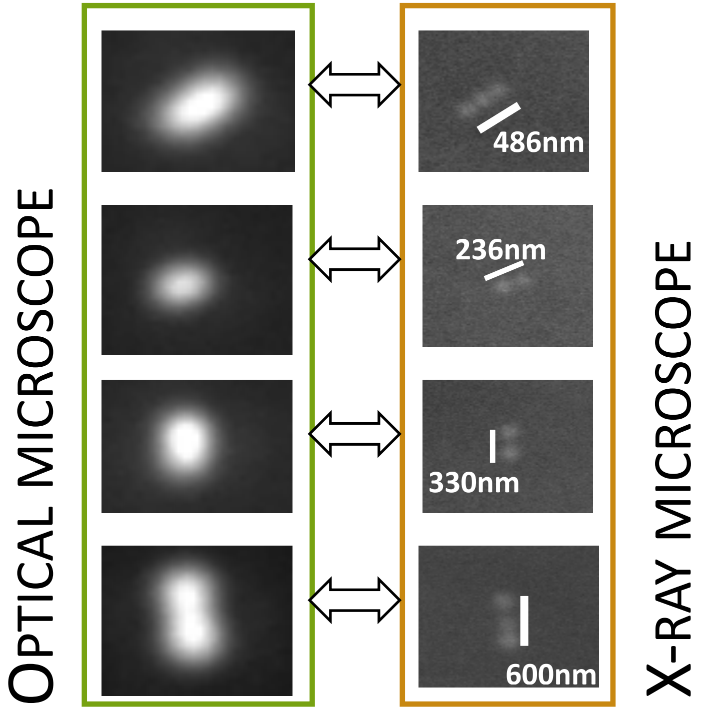

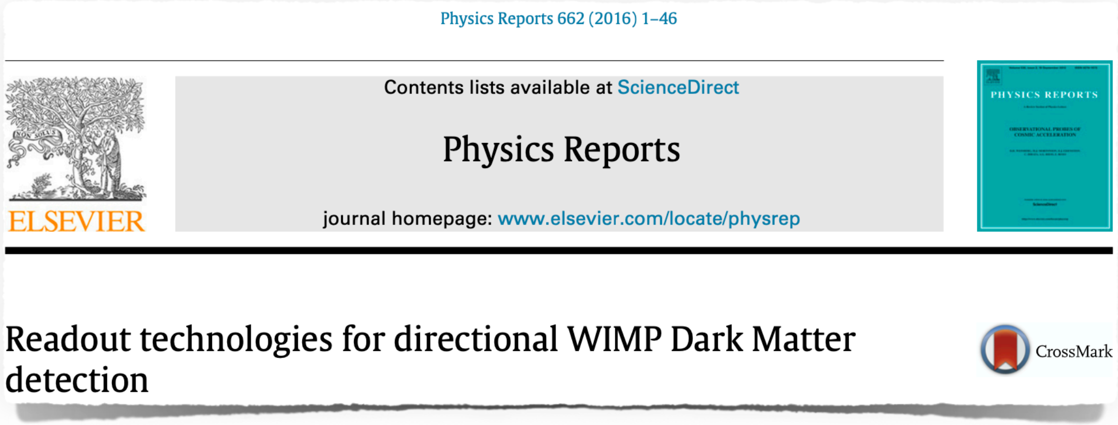

Physics Reports 662 (2016) 1–46

Contents lists available at ScienceDirect

Physics Reports

journal homepage: www.elsevier.com/locate/physrep

Readout technologies for directional WIMP Dark Matter detection

Beyond the limits of diffraction

Background grain

Barycenter of the cluster

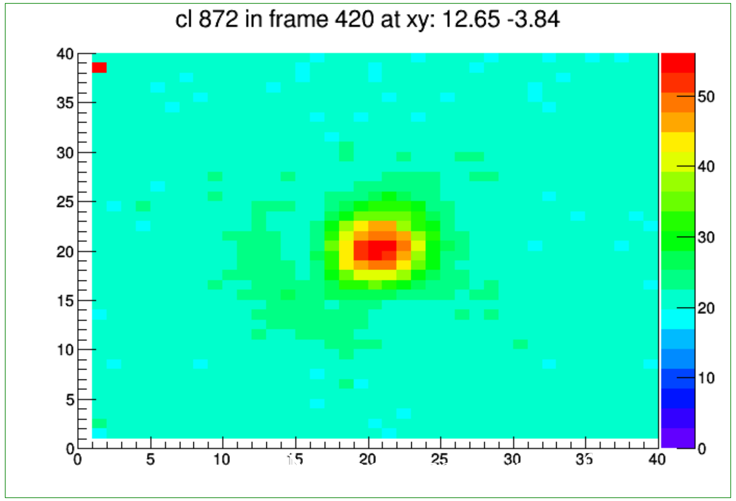

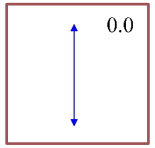

Polarization angle

Signal-like events (100keV C ion)

Max barshift

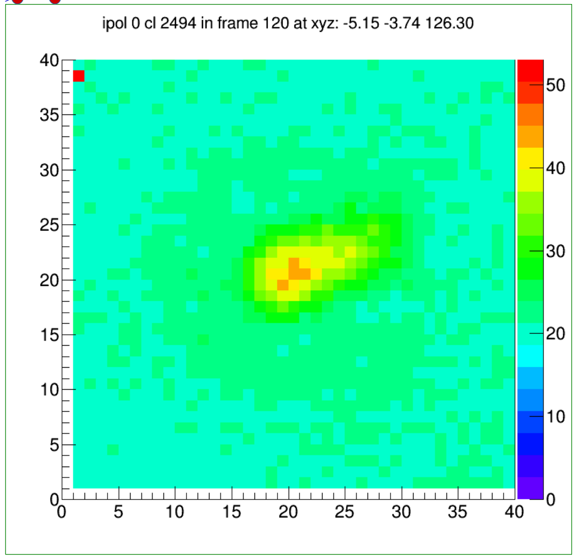

Optical microscope

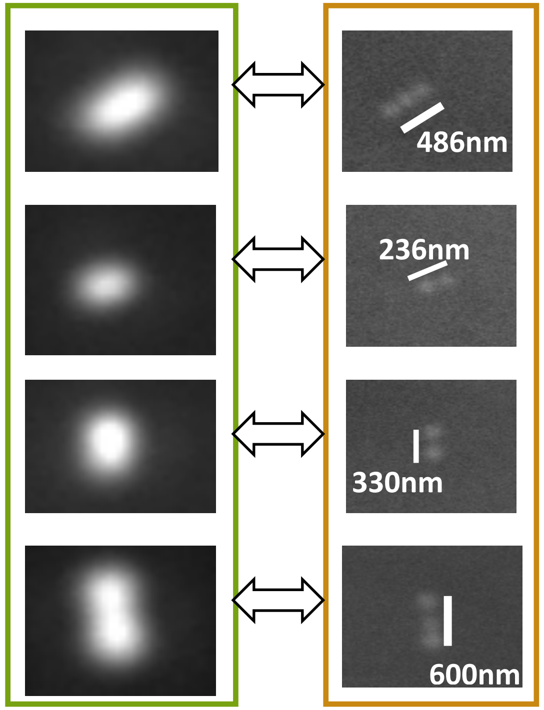

X-ray microscope

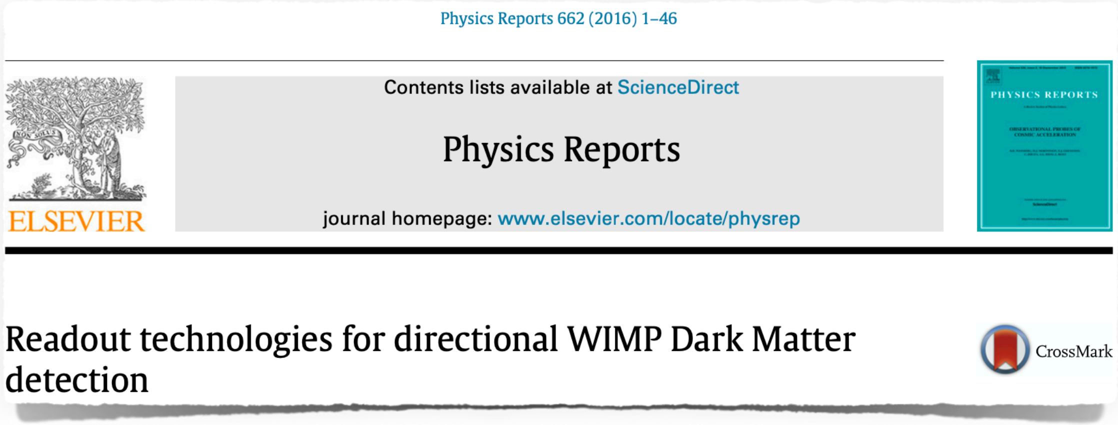
Physics Reports 662 (2016) 1–46

Contents lists available at ScienceDirect

Physics Reports

journal homepage: www.elsevier.com/locate/physrep

ELSEVIER

Readout technologies for directional WIMP Dark Matter detection

CrossMark

Beyond the limits of diffraction

Background grain

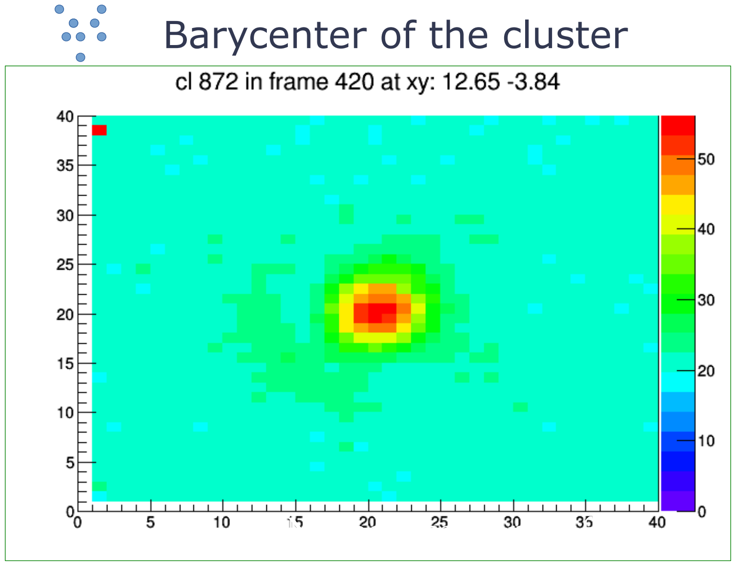

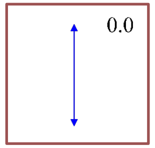

Signal-like events (100keV C ion)

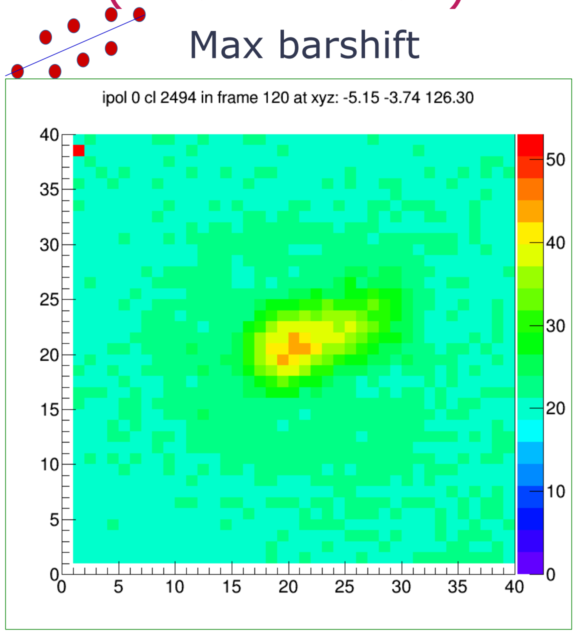

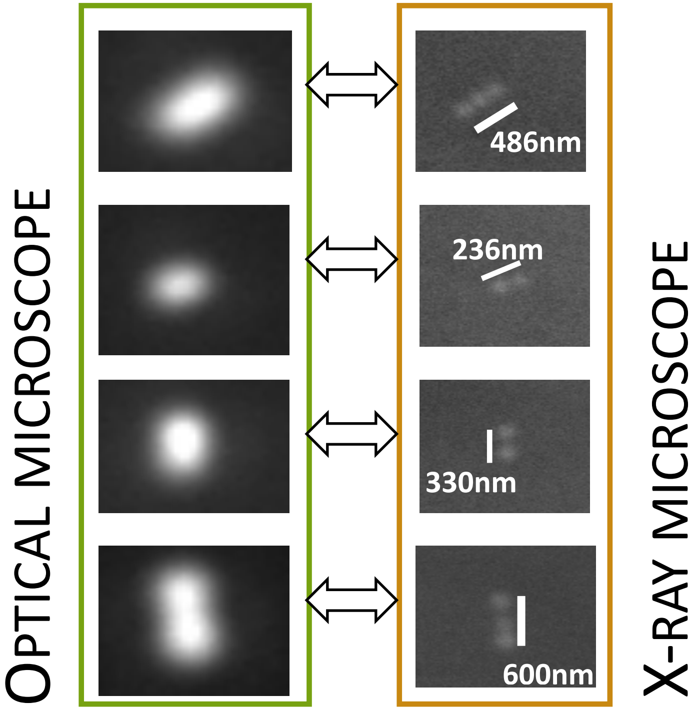

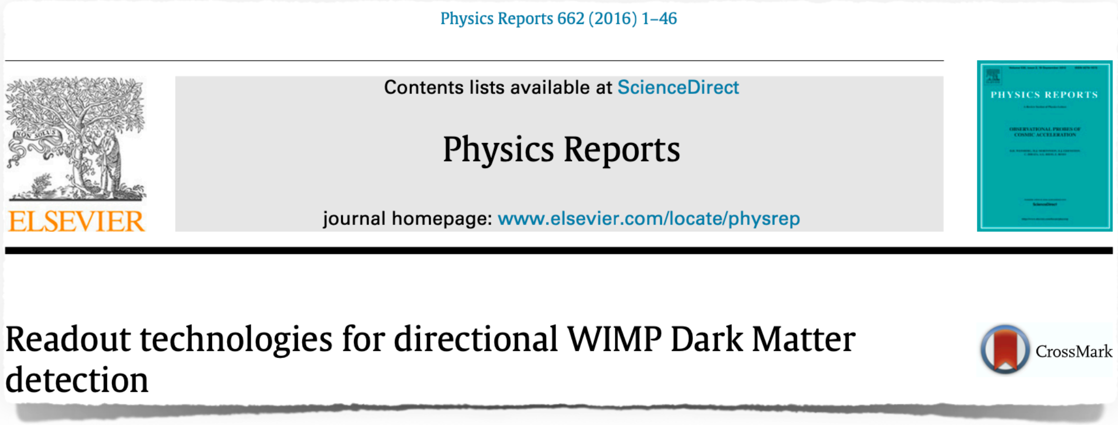
Physics Reports 662 (2016) 1–46

Contents lists available at ScienceDirect

Physics Reports

journal homepage: www.elsevier.com/locate/physrep

ELSEVIER

Readout technologies for directional WIMP Dark Matter detection

CrossMark

Beyond the limits of diffraction

Background grain

Barycenter of the cluster

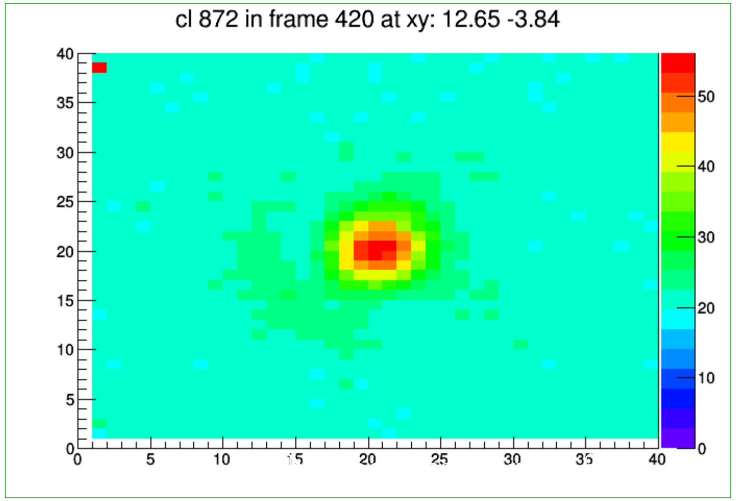

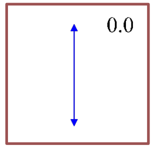

Polarization angle

Signal-like events (100keV C ion)

Max barshift

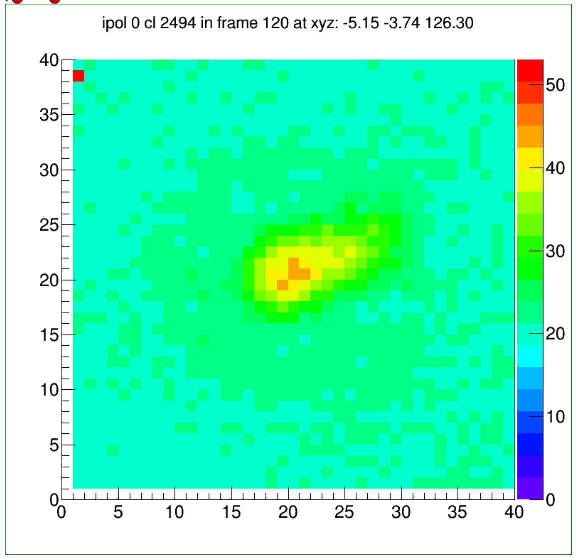

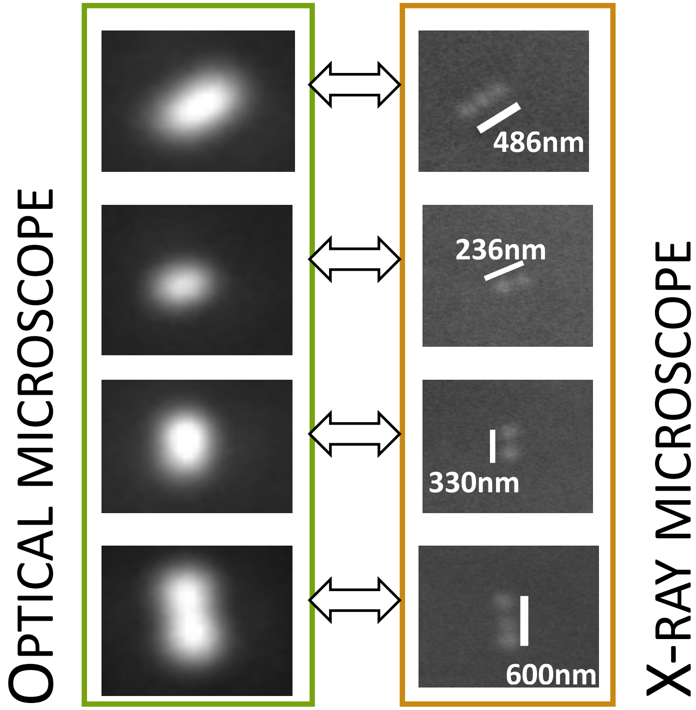

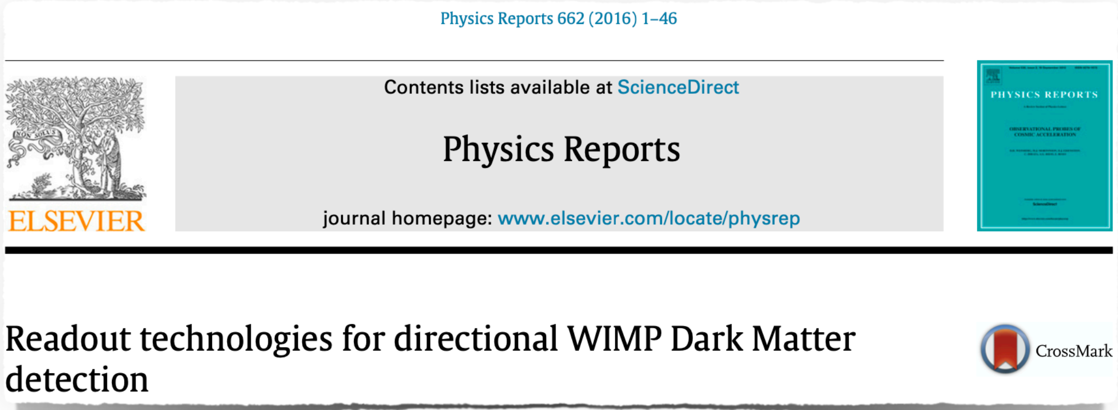
Physics Reports 662 (2016) 1–46

Contents lists available at ScienceDirect

Physics Reports

journal homepage: www.elsevier.com/locate/physrep

ELSEVIER

Readout technologies for directional WIMP Dark Matter detection

CrossMark

Two grains building up a track

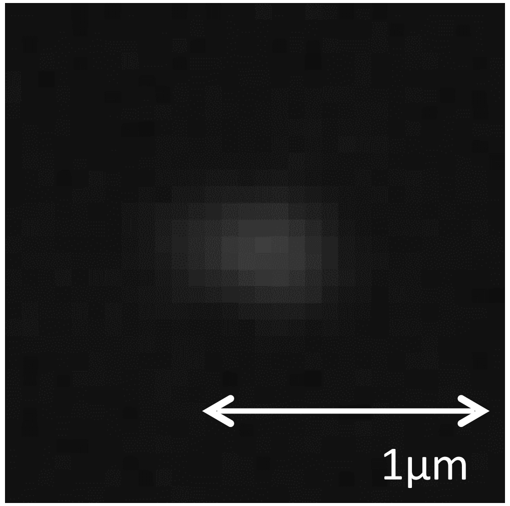

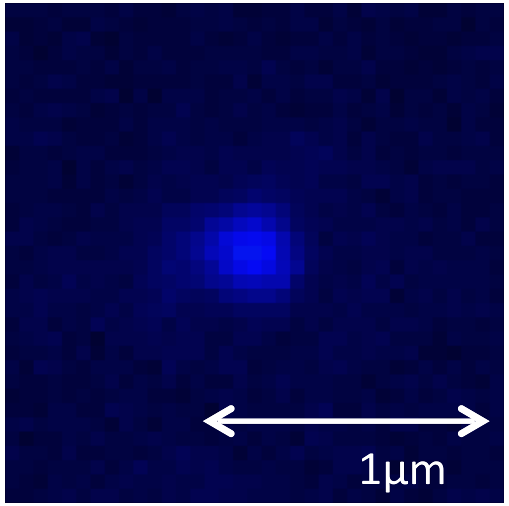

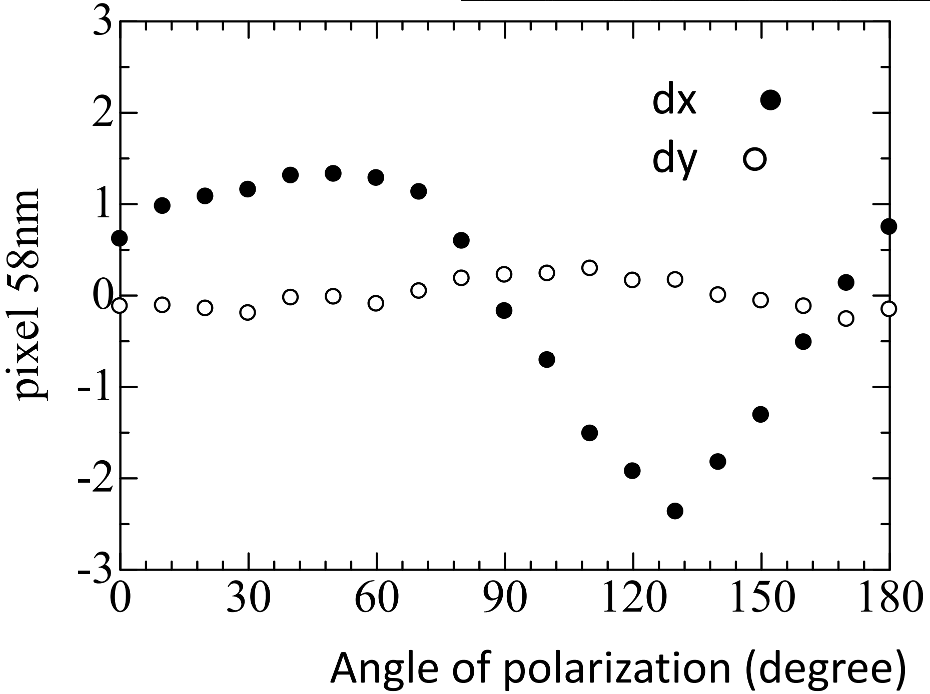

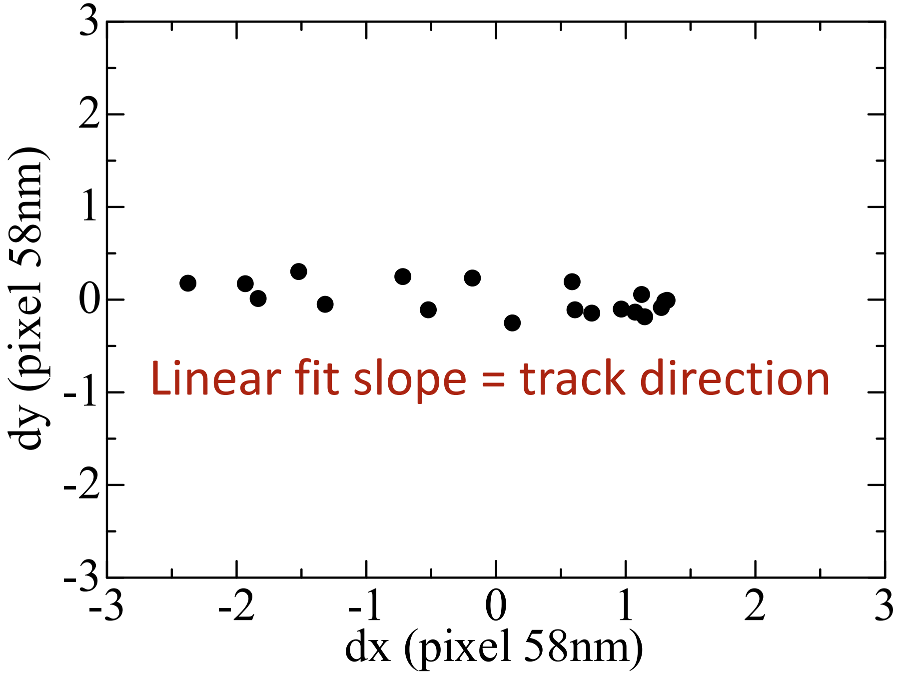

Two grains building up a track

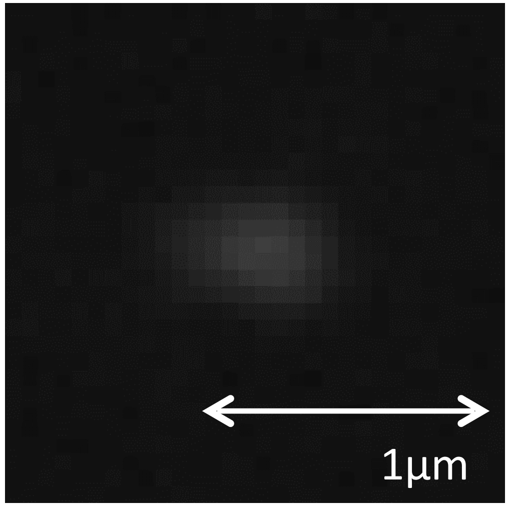

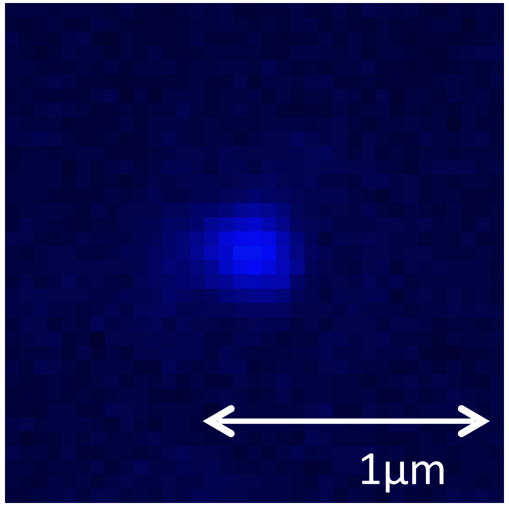

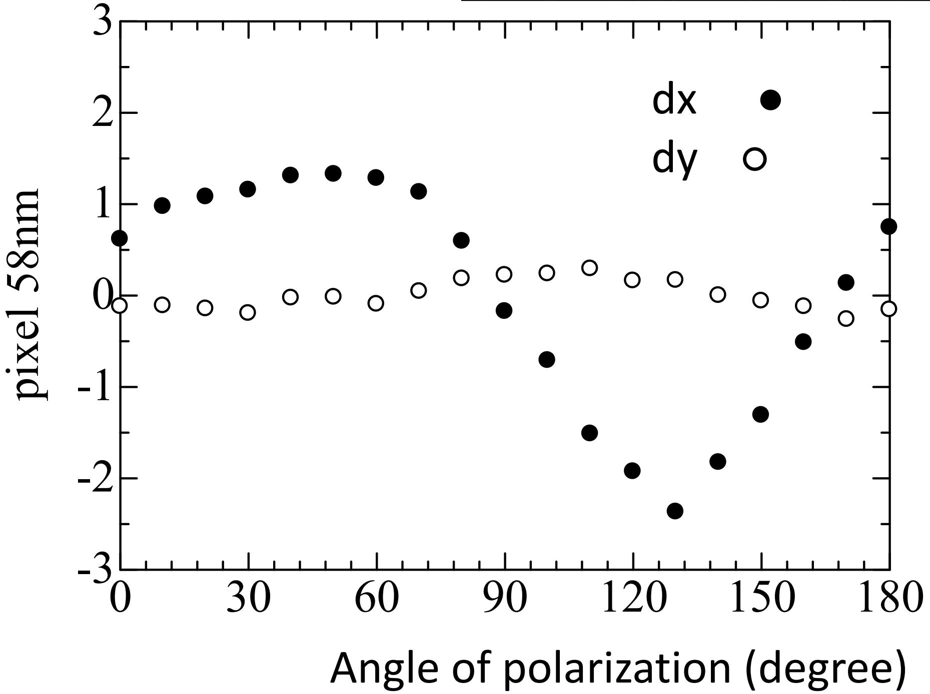

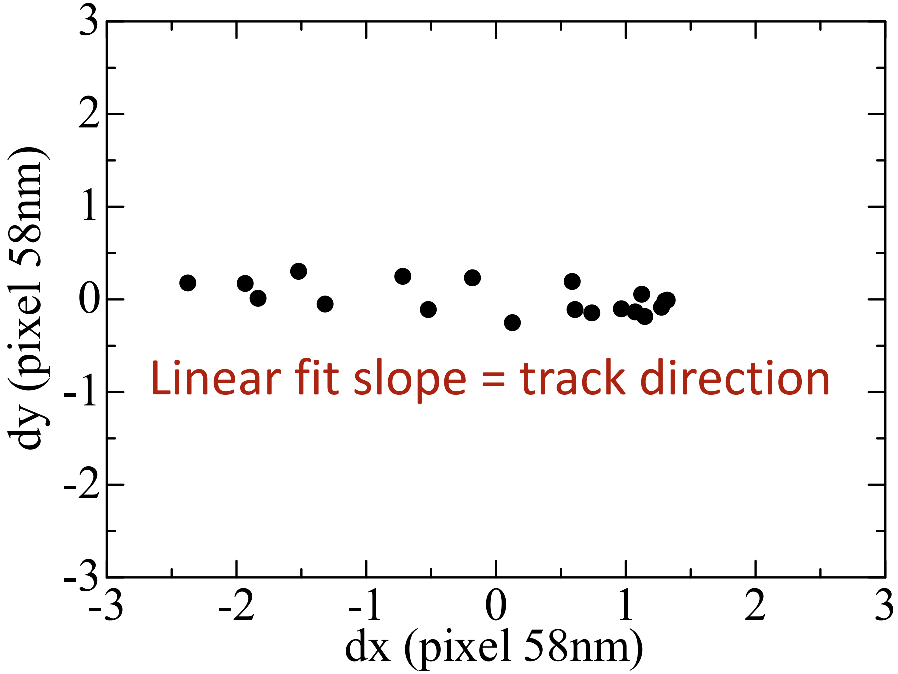

Single grain: accuracy

Ag 60nm

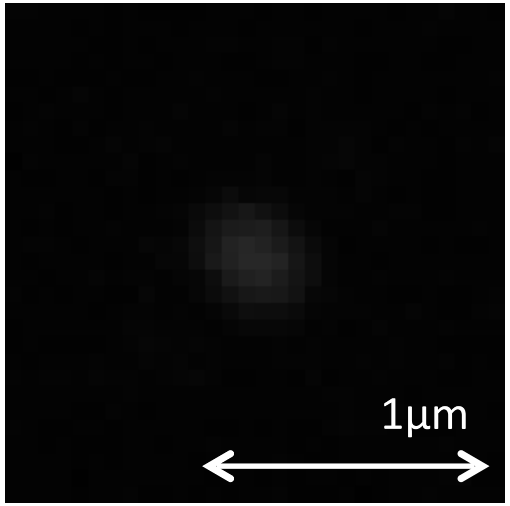

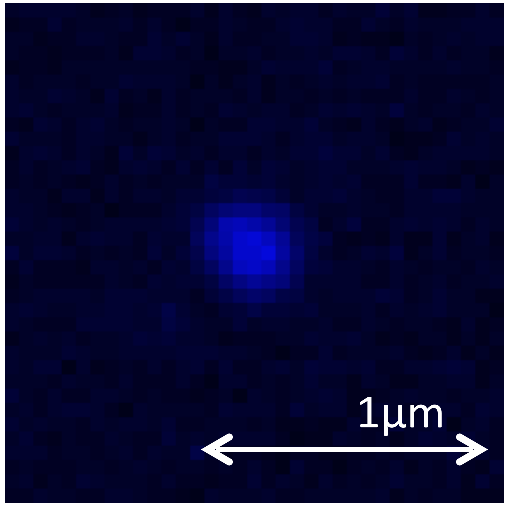

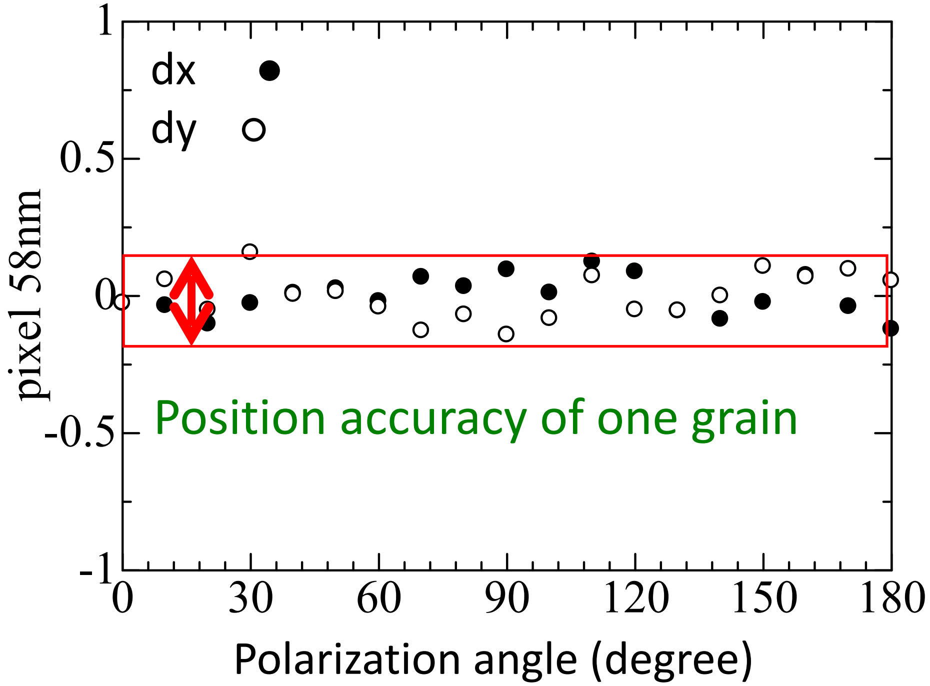

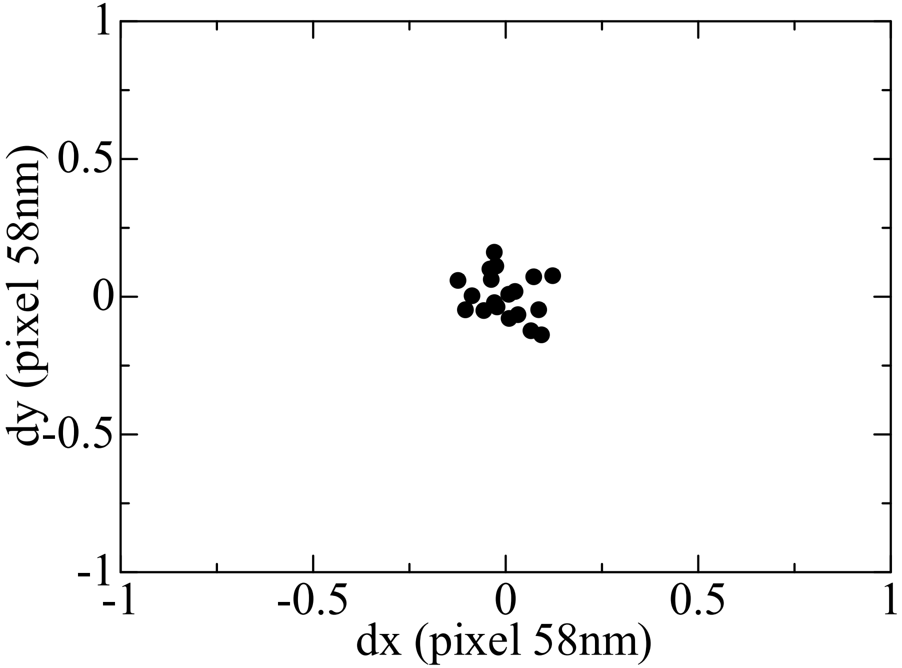

Single grain: accuracy

Ag 60nm

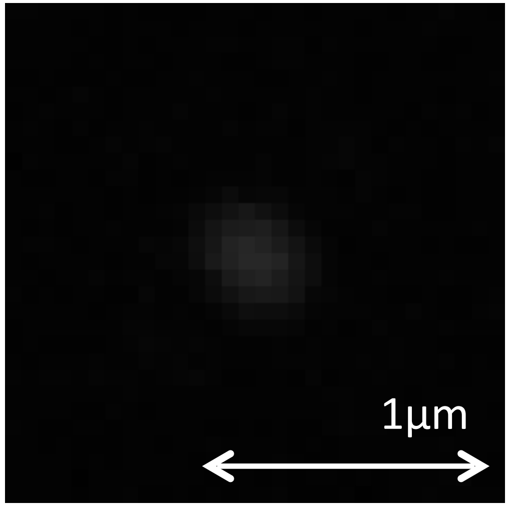

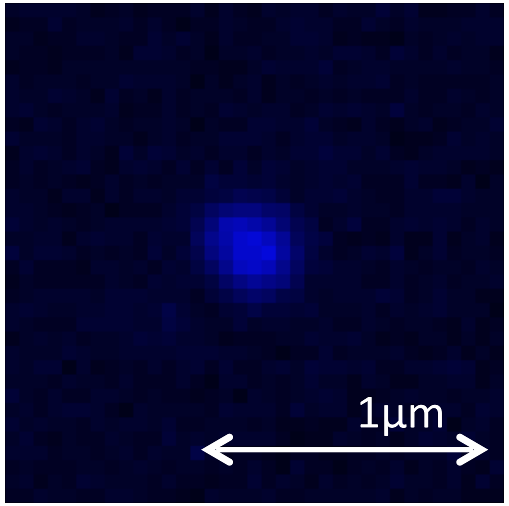

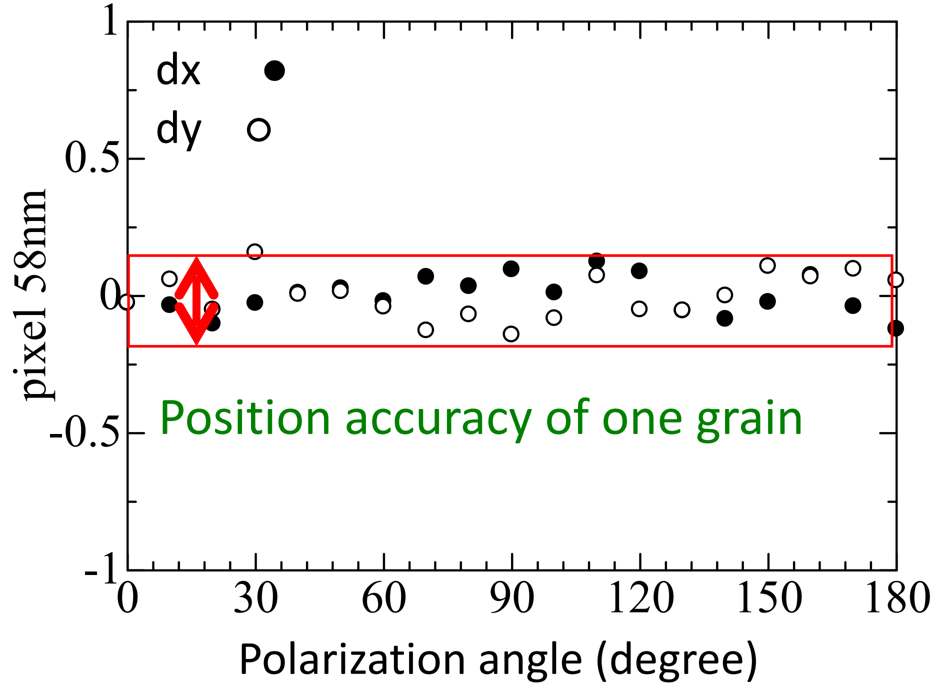

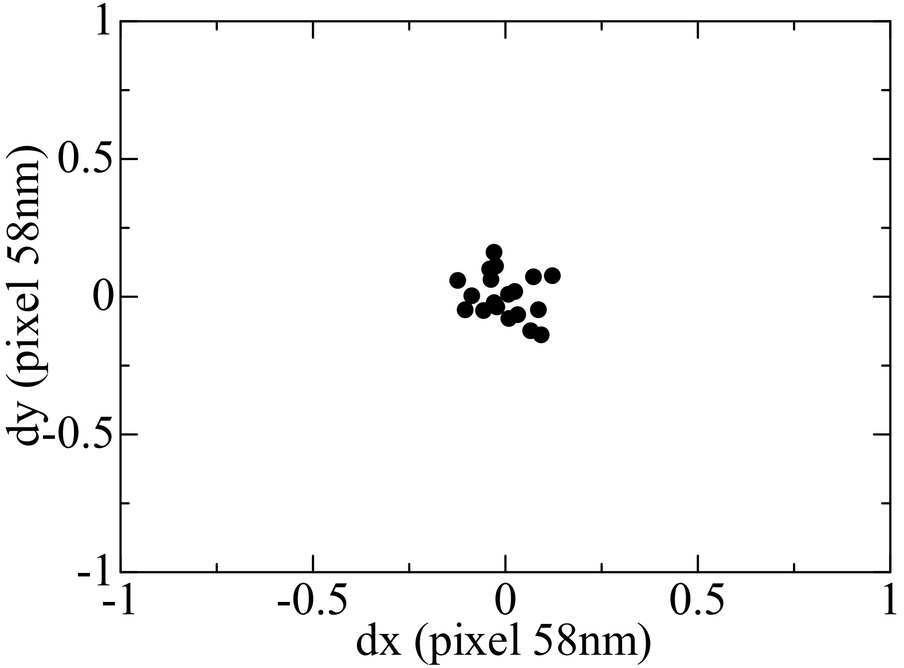

Super-resolution microscope

Int.Class	Appl.No	Title / Applicant	Ctr	PubDate / Inventor
1. WO/2018/122814		METHOD AND OPTICAL MICROSCOPE FOR DETECTING PARTICLES HAVING SUB-DIFFRACTIVE SIZE	WO	05.07.2018

Pub. No.: WO/2018/122814 **International Application No.:** PCT/IB2017/058544
Publication Date: 05.07.2018 **International Filing Date:** 30.12.2017

IPC: ***G02B 21/00*** (2006.01) ,***G02B 21/36*** (2006.01)

Applicants: **ISTITUTO NAZIONALE DI FISICA NUCLEARE** [IT/IT]; Via Enrico Fermi, 40 00044 Frascati (rM), IT

Inventors:
DE LELLIS, Giovanni; IT
ALEXANDROV, Andrey; IT
TIOUKOV, Valeri; IT
D'AMBROSIO, Nicola; IT

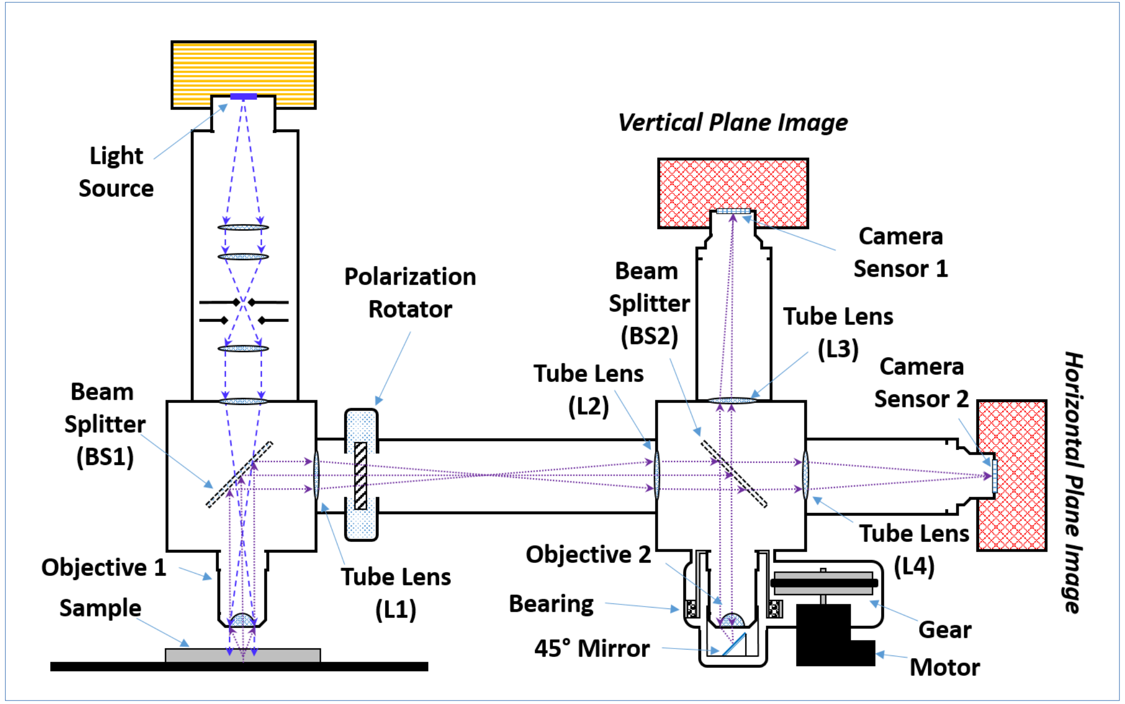

Breakthrough!

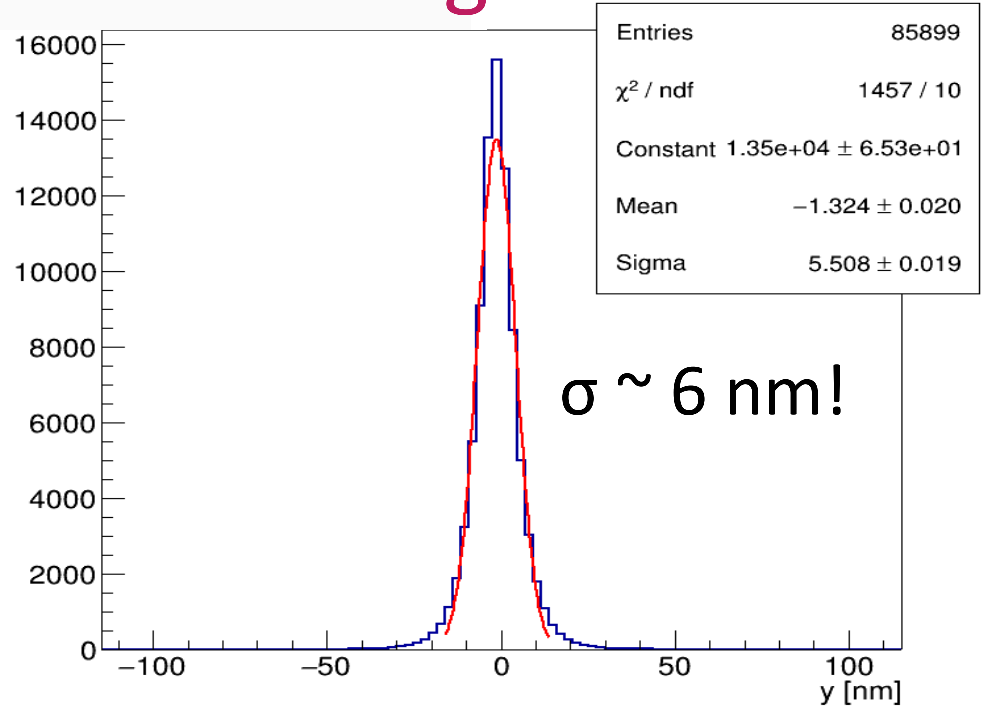

Measurement of track slope and length beyond optical resolution

Results for 100keV C-ions: Horizontal ions, signal-like events

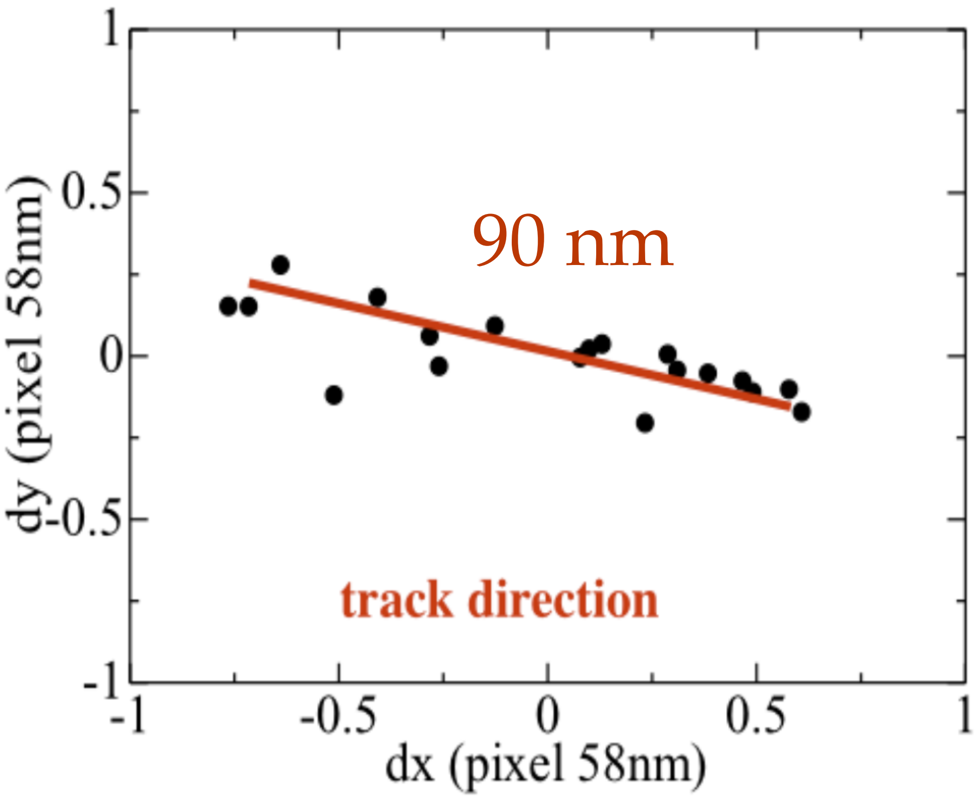

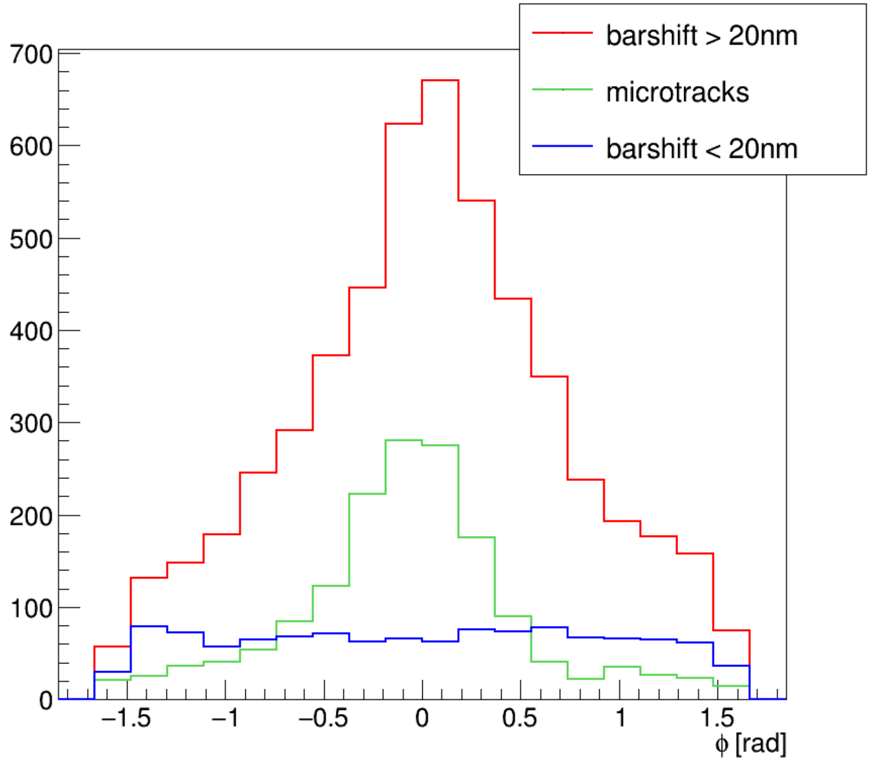

- Barycenter displacement > 20 nm (Displaced)
- Barycenter displacement ≤ 20 nm (Non-displaced)

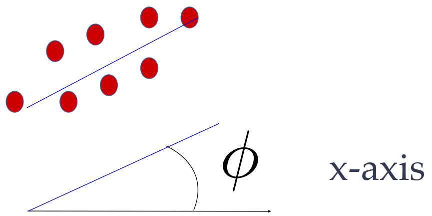

Color representation

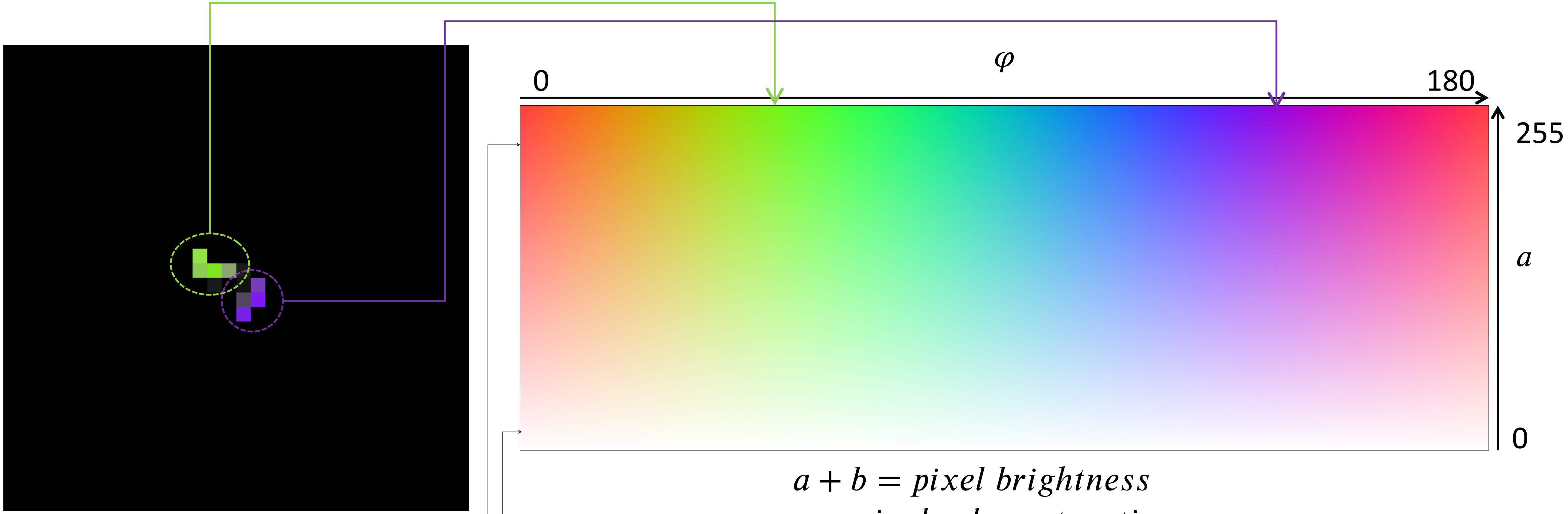

$$a + b = pixel\ brightness$$
$$a = pixel\ color\ saturation$$
$$\varphi = pixel\ color$$

Non-metallic or spherical NPs
Silver grain filaments

Super resolution imaging

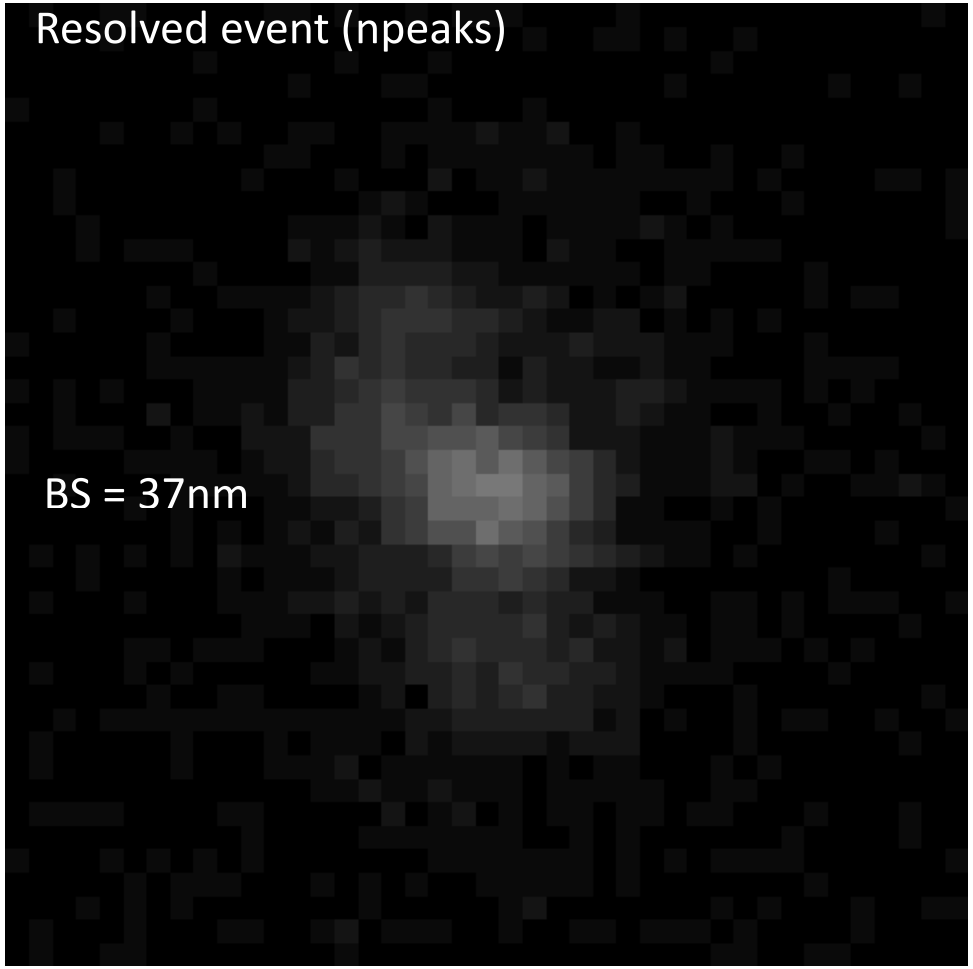

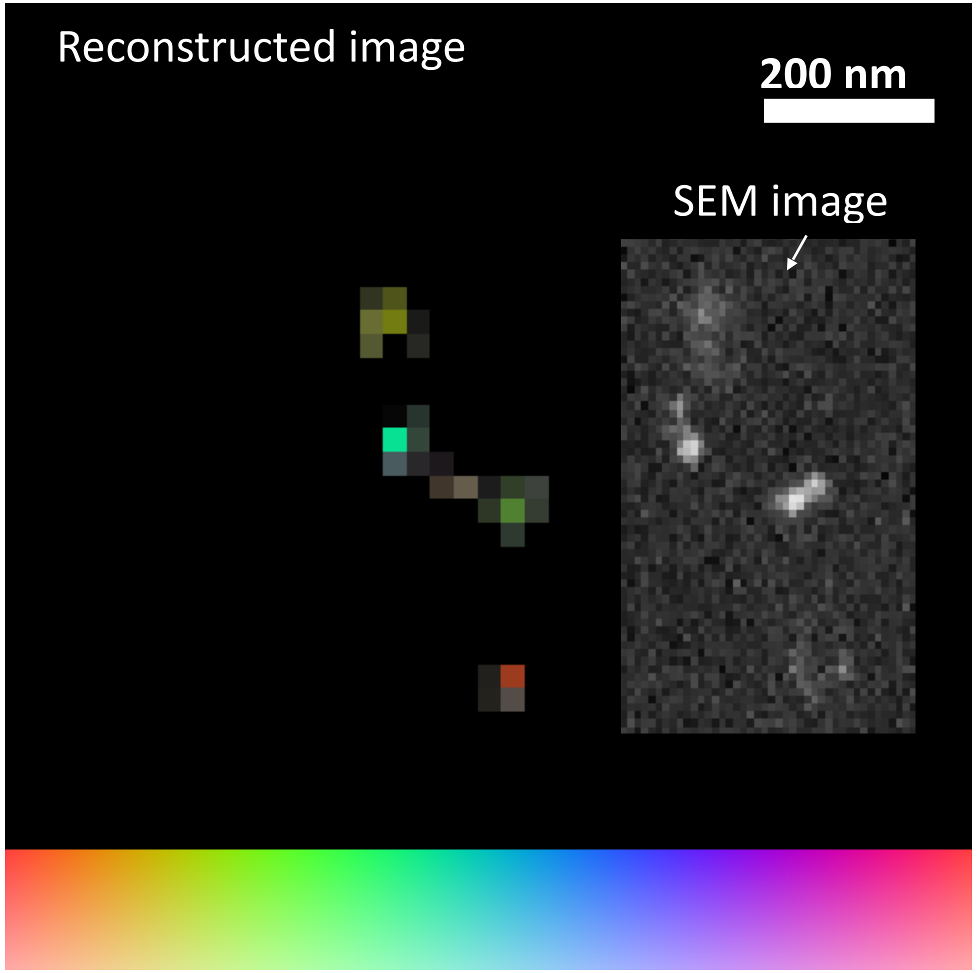

Super resolution imaging

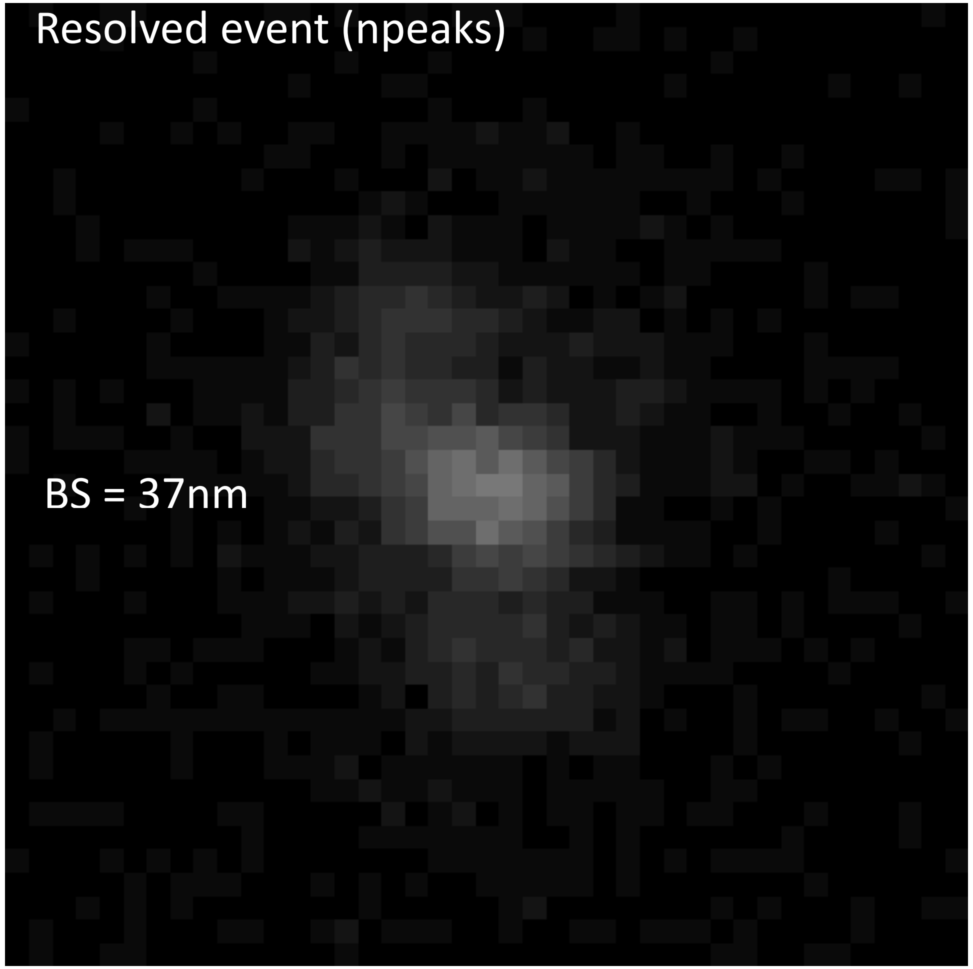

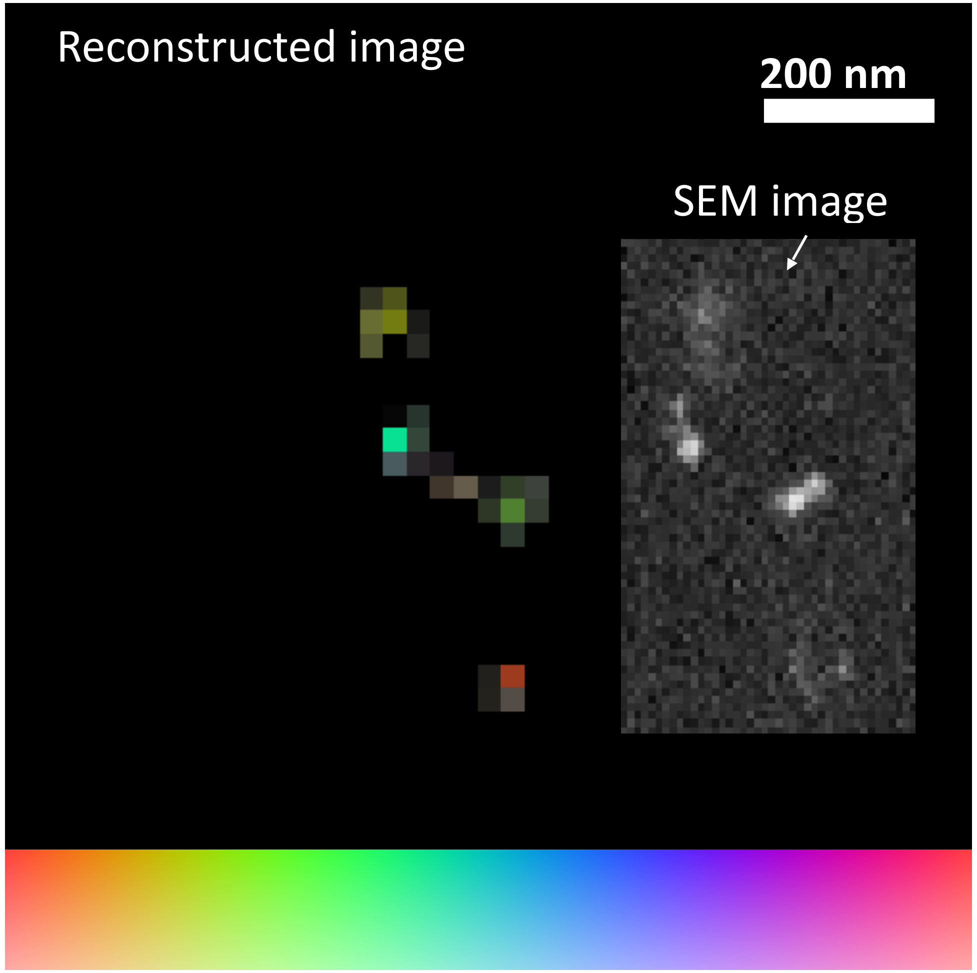

Super resolution imaging

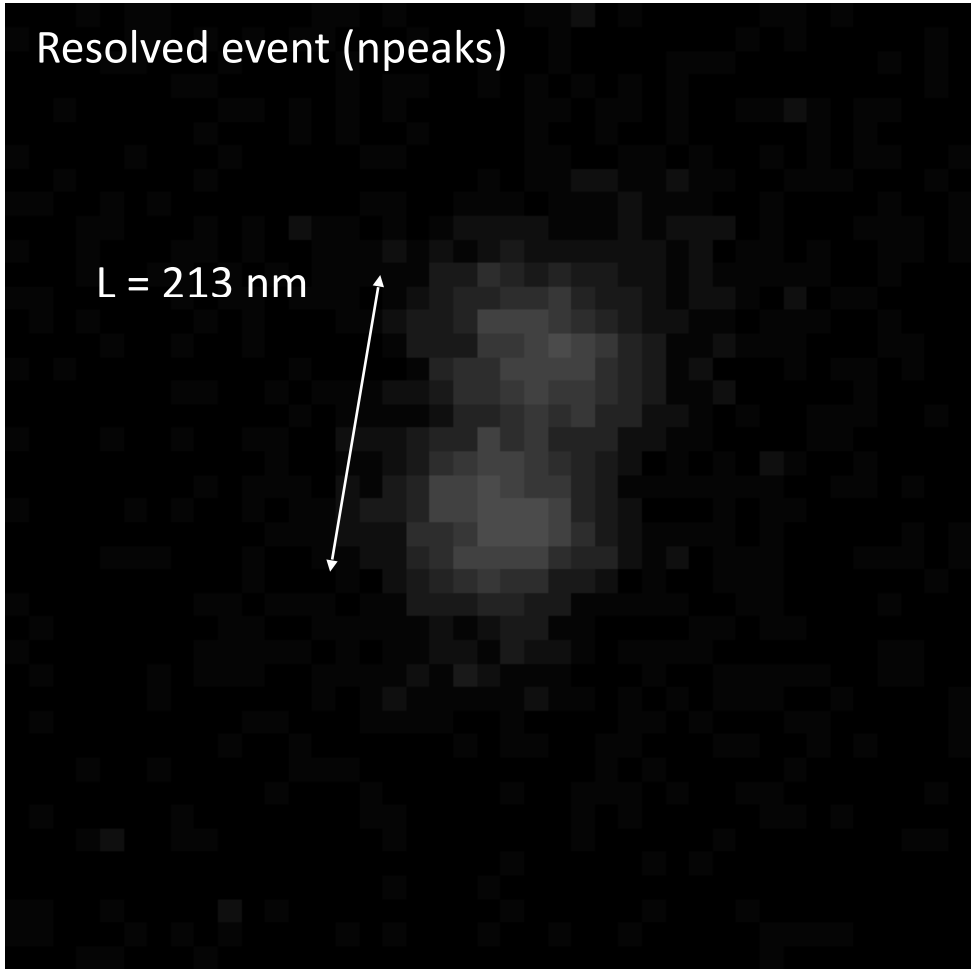

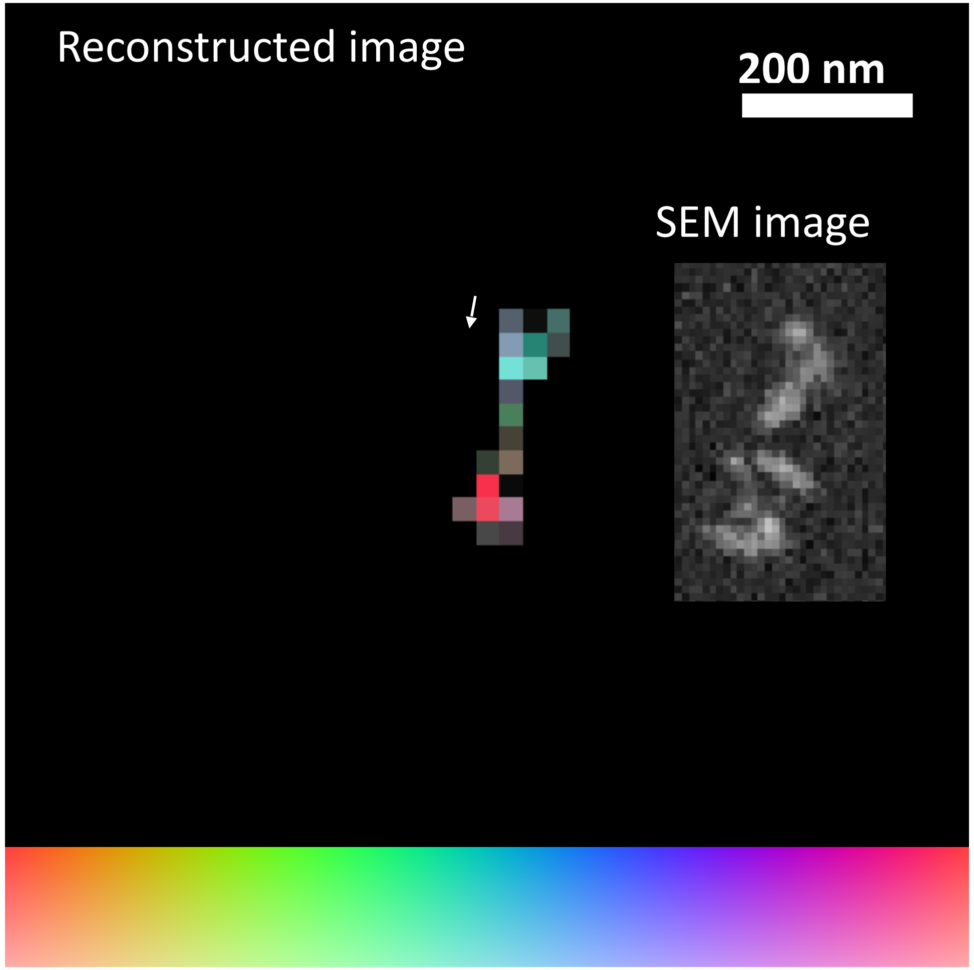

Super resolution imaging

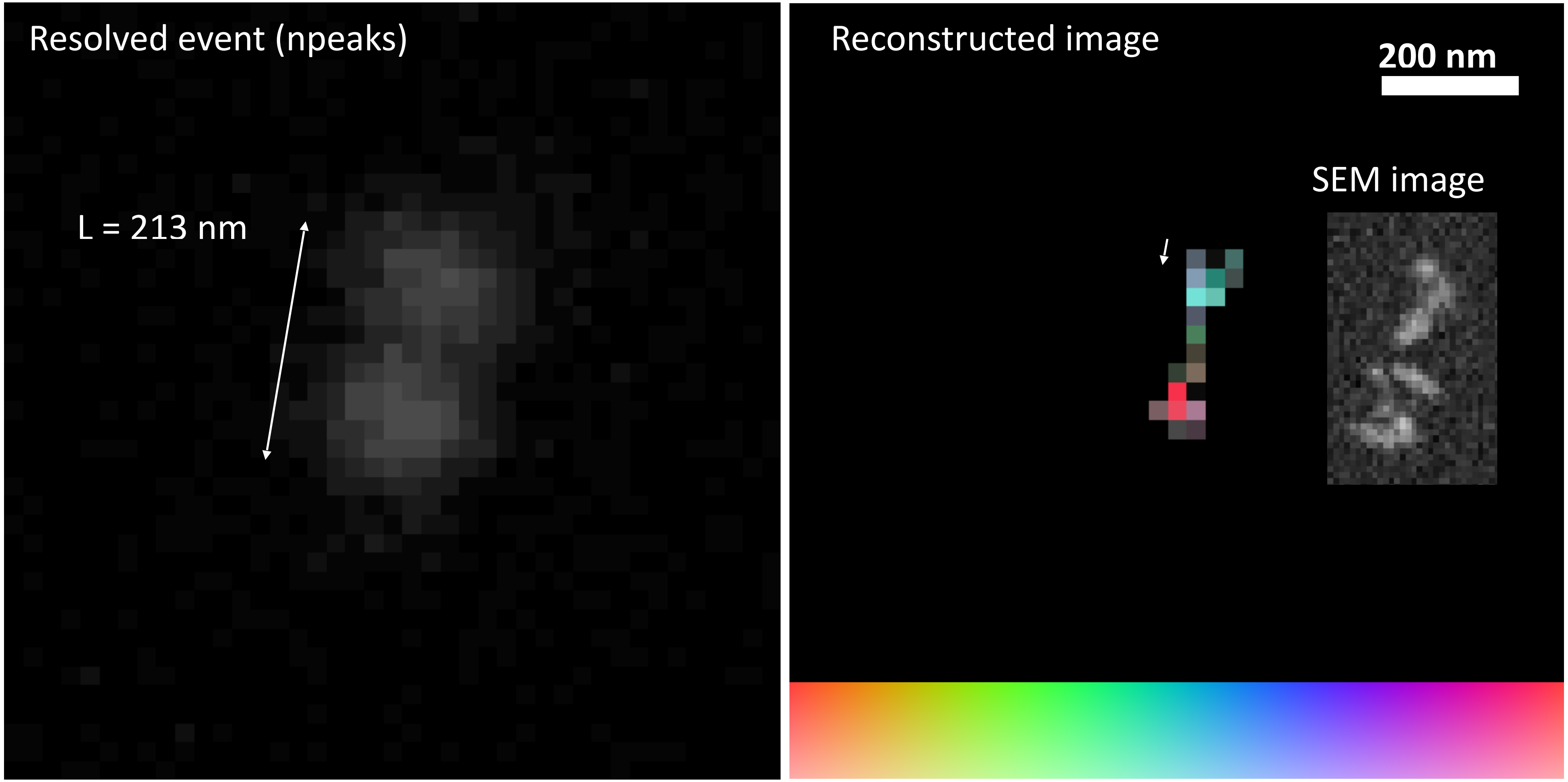

Super-resolution with plasmon analysis

R = 45 nm → blue
H = 80 (120) nm → green (red)

Annu. Rev. Phys. Chem. 58 (2007) 267-297

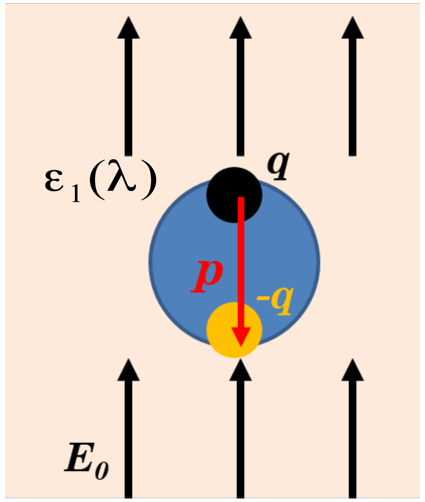

dipole in metallic particle

dipole moment

$$p = 4\pi\varepsilon_m a^3 \frac{\varepsilon_1(\lambda) - \varepsilon_m(\lambda)}{\varepsilon_1(\lambda) + 2\varepsilon_m(\lambda)} E_0$$

resonance

$$\varepsilon_1(\lambda_l) + 2\varepsilon_m(\lambda_l) \approx 0$$

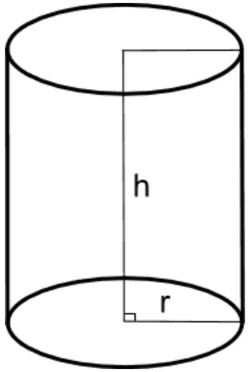

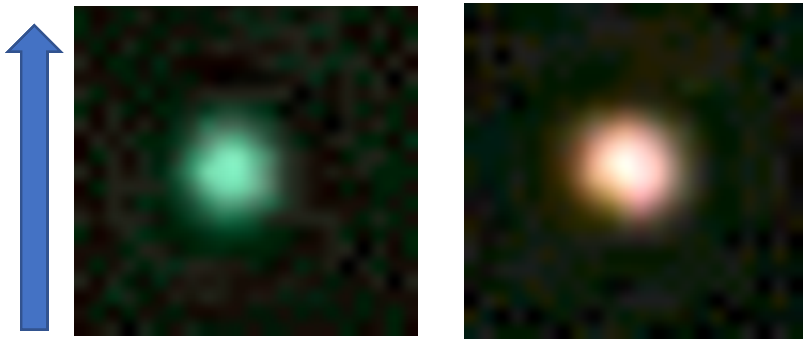

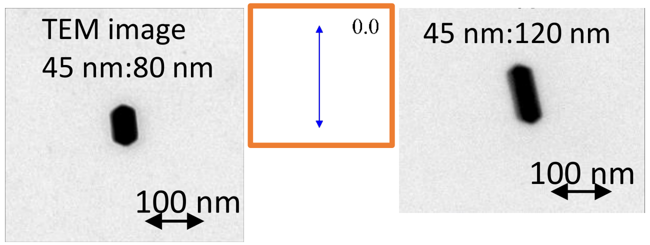

Appl. Phys. Lett. 80, 1826 (2002)

Ag grain size → resonance wavelength

metallic particle

Super-resolution with plasmon analysis

R = 45 nm → blue
H = 80 (120) nm → green (red)

Annu. Rev. Phys. Chem. 58 (2007) 267-297

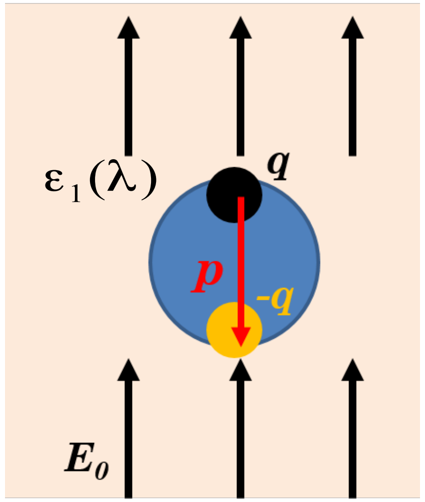

dipole in metallic particle

dipole moment

$$p = 4\pi\varepsilon_m a^3 \frac{\varepsilon_1(\lambda) - \varepsilon_m(\lambda)}{\varepsilon_1(\lambda) + 2\varepsilon_m(\lambda)} E_0$$

resonance

$$\varepsilon_1(\lambda_l) + 2\varepsilon_m(\lambda_l) \approx 0$$

Appl. Phys. Lett. 80, 1826 (2002)

Ag grain size → resonance wavelength

metallic particle

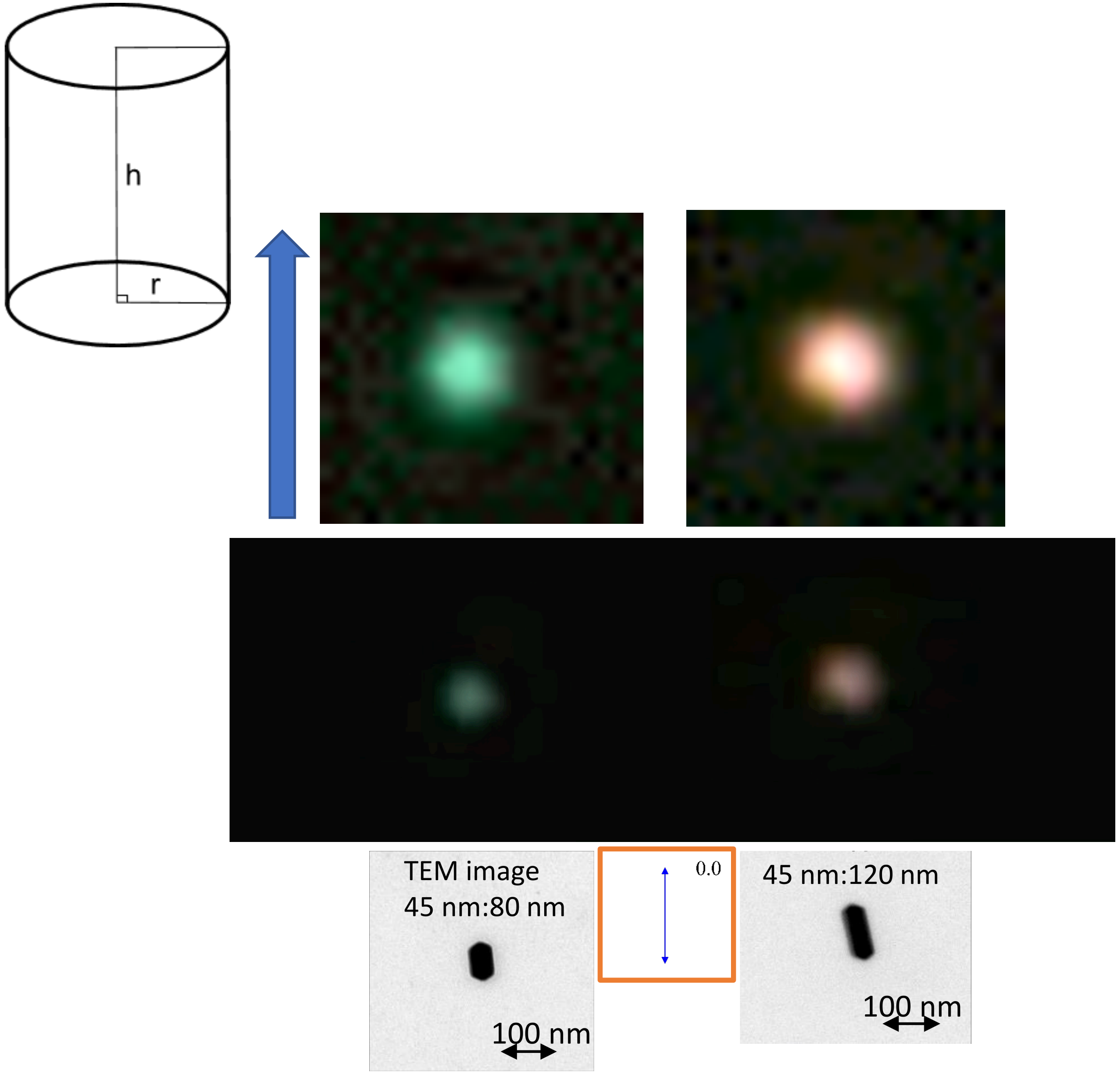

Super-resolution with plasmon analysis

40 nm diameter

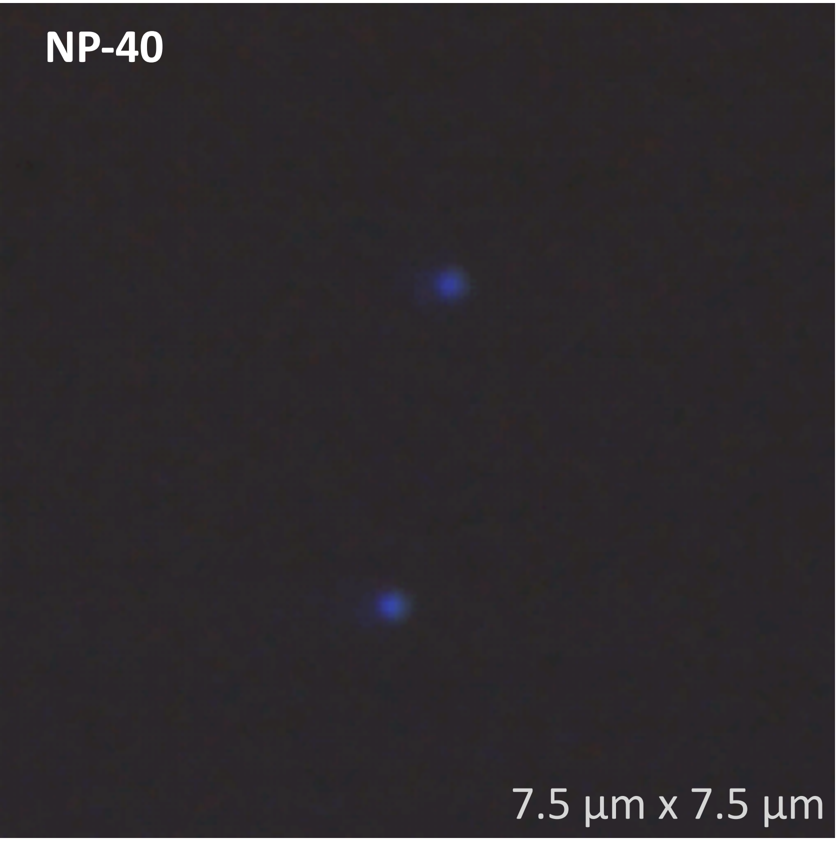

40 nm diameter, 80 nm height

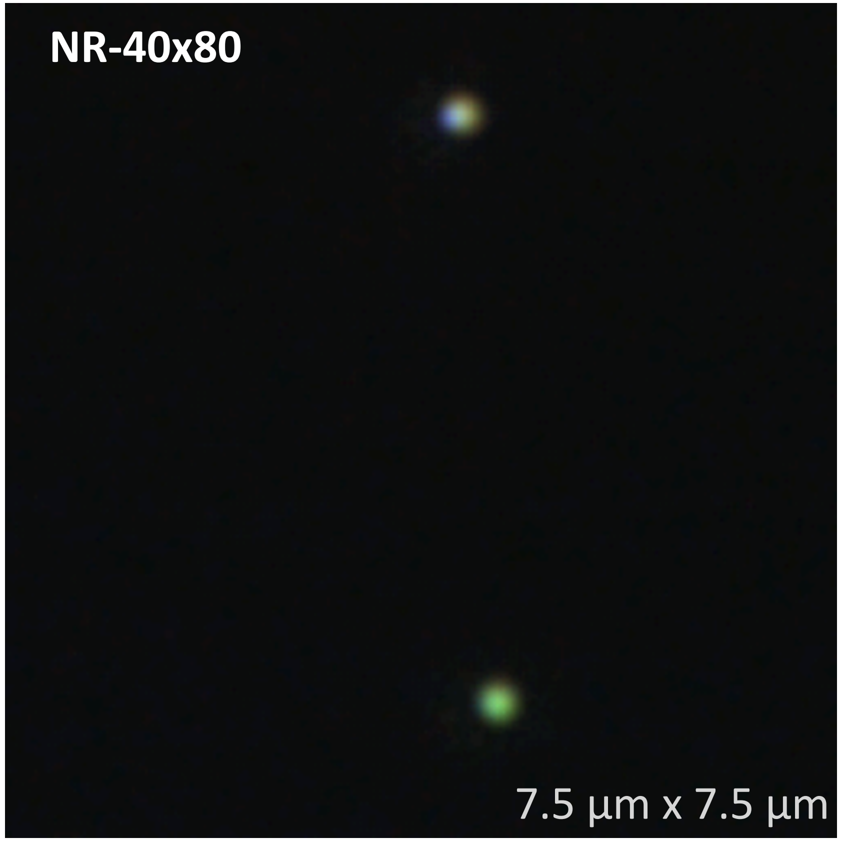

40 nm diameter, 120 nm height

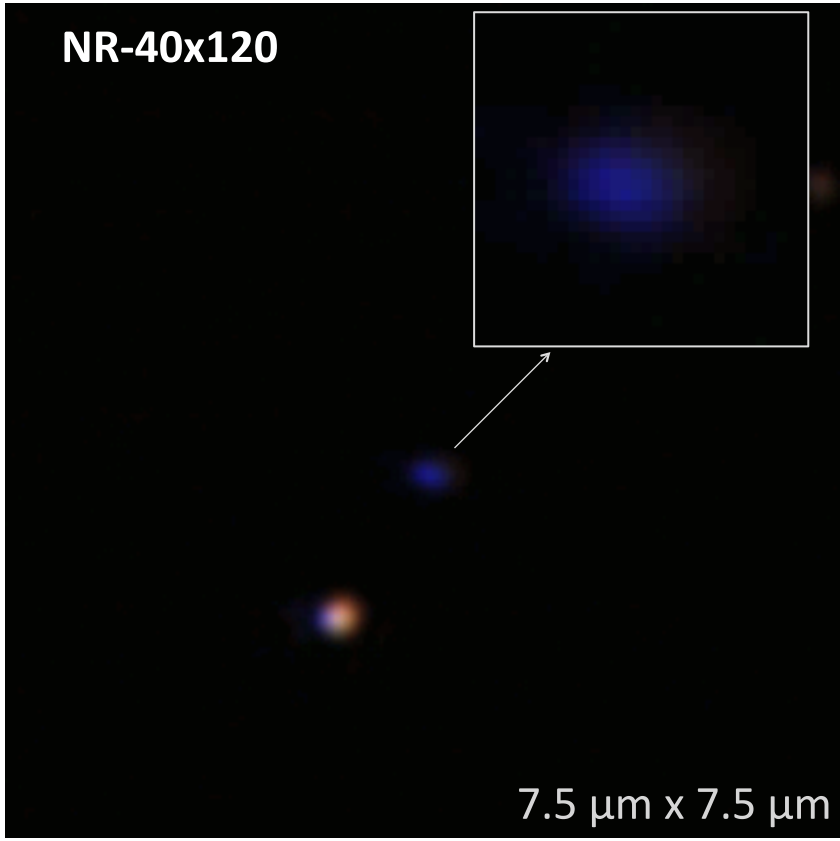

Super-resolution with plasmon analysis

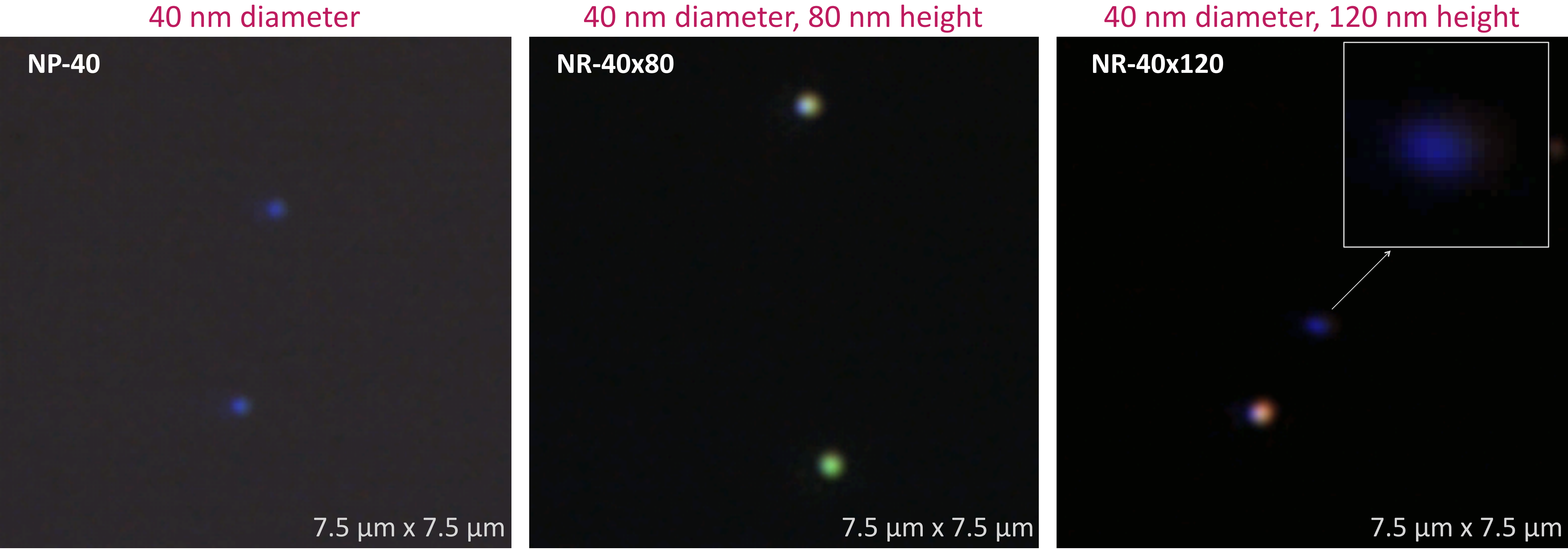

Super-resolution with plasmon analysis

Bragg peak: end of the track

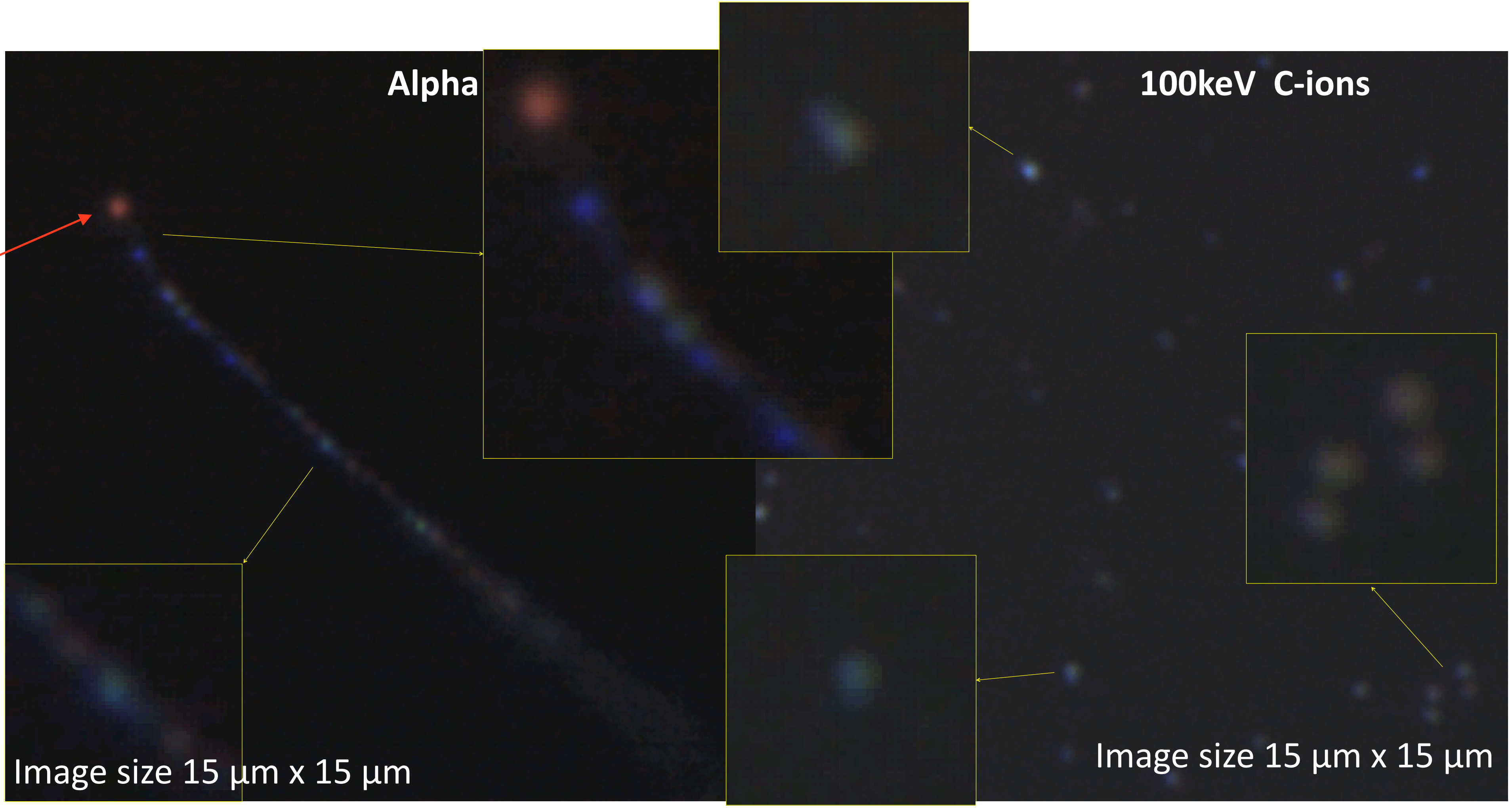

Super-resolution with plasmon analysis

Bragg peak: end of the track

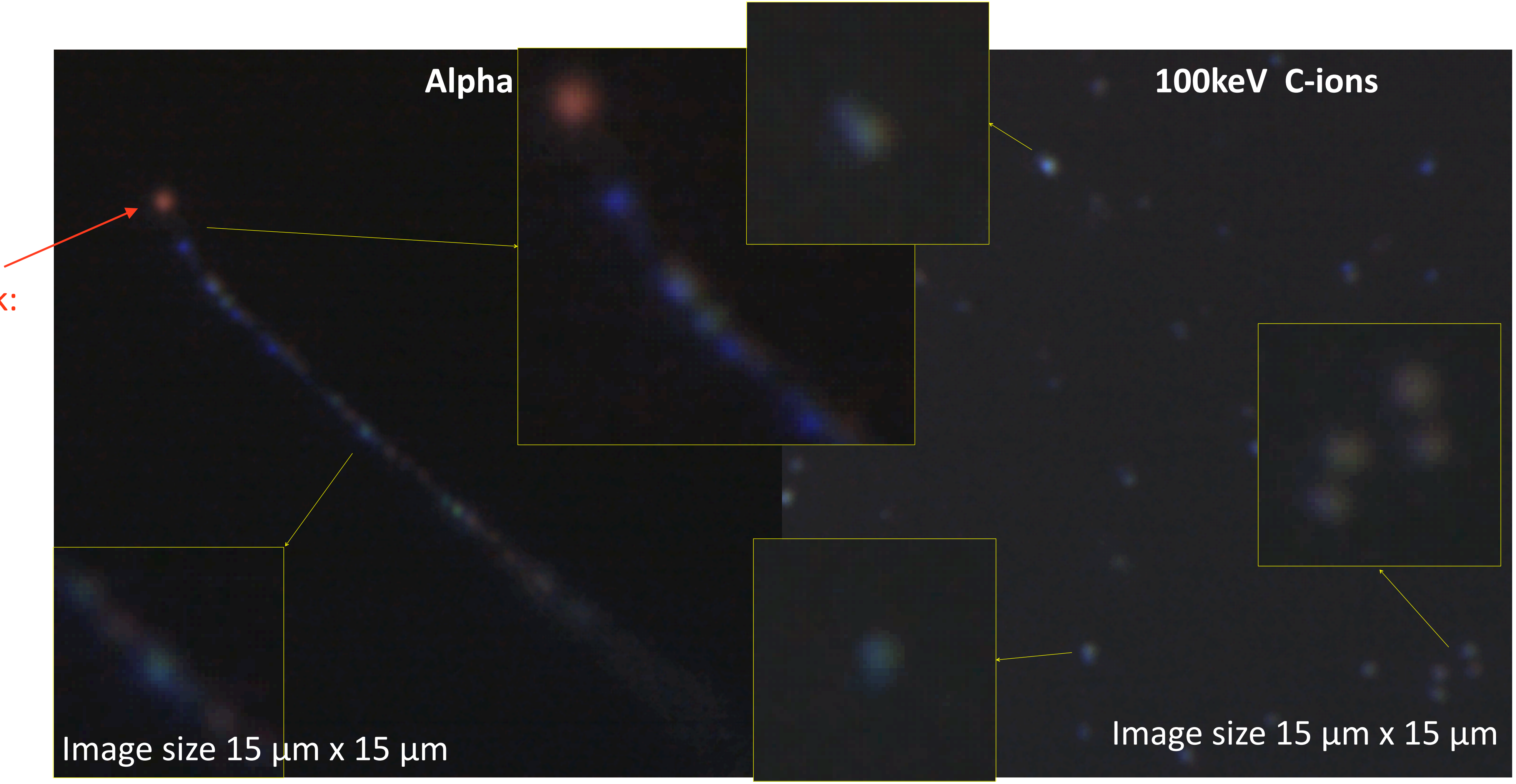

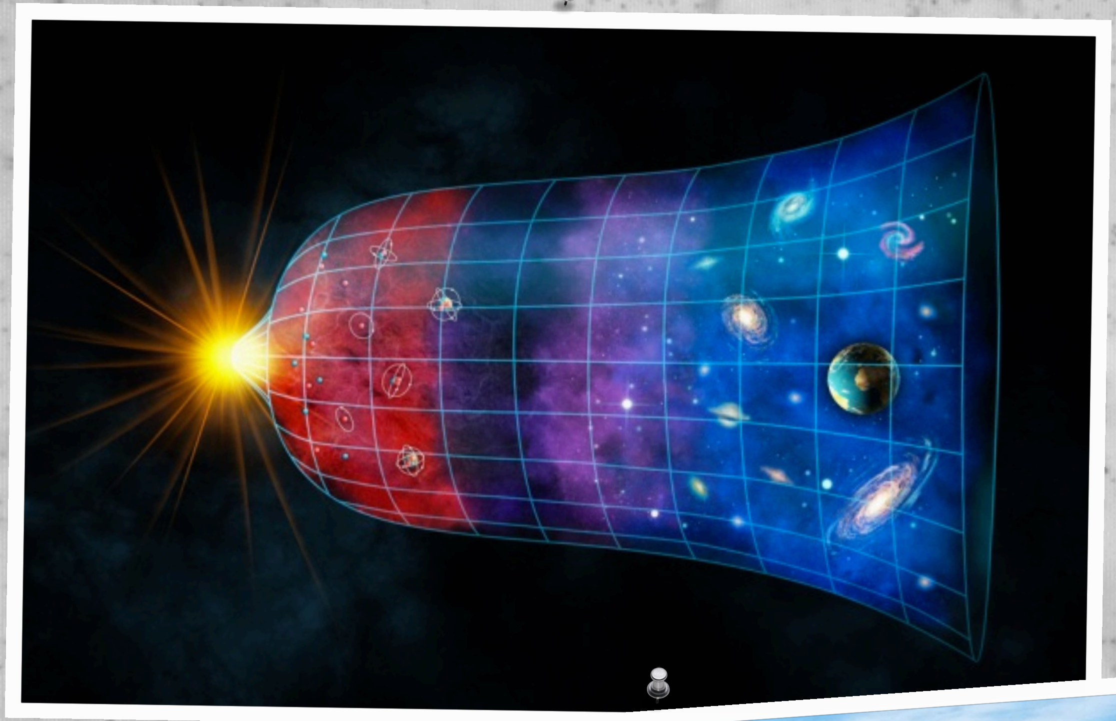
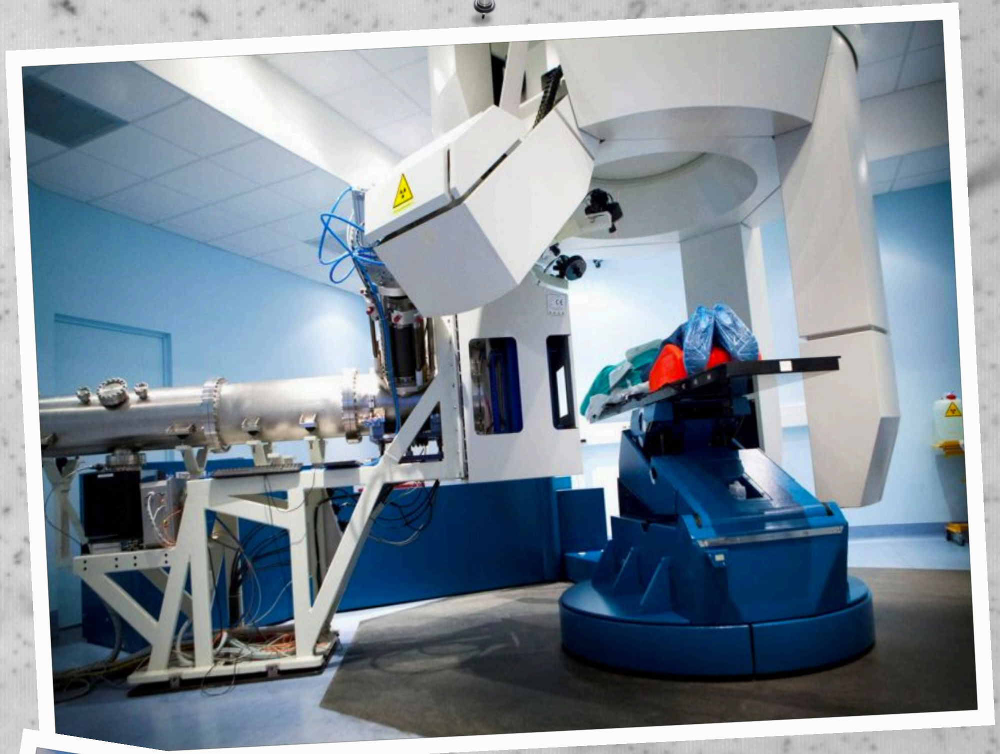

THANK YOU!

A few textbook references

- P.H. Fowler, D.H. Perkins and C.F. Powell, The study of elementary particles by the photographic method, Pergamon Press (1959).
- W.H. Barkas, Nuclear research emulsion, Academic Press, New York, 1973.
- Tadaaki Tani, Photographic Science, Advances in Nanoparticles, J-Aggregates, Dye Sensitization, and Organic Devices, Oxford University Press (2011), ISBN: 9780199572953.
- G. De Lellis et al., Nuclear Emulsions, vol. 21B1 of Landolt-Bo¨rnstein Series: Detectors for Particles and Radiation (Springer International Publishing AG, 2011). 2019 Edition being printed

backup slides

Summary of measurement performance

Observable	Method	Range	Notes
τ (lifetime)	Flight length, $<\vartheta>$	$10^{-16} \div 10^{-11}$ s	
Momentum	MCS	0.5 ÷ 10 GeV	pion
Momentum	range	<500 MeV	
Energy	Shower counting, calorimetry	1÷ 20 GeV	electron
Z (charge)	Ionization	1÷ 6	nuclei
A (mass number)	Range, MCS	1÷ 12	nuclei
Kinetic energy	Nanometric range	≥30 keV	Carbon
e/π^0 separation	γ conversion	No threshold	
μ/π separation	Range, topology	No threshold	Dense material

NEWSdm detector

Technical Test Installed in Underground Gran Sasso INFN Laboratories (Hall B) in June 2019

Simulation of 10kg Exposure

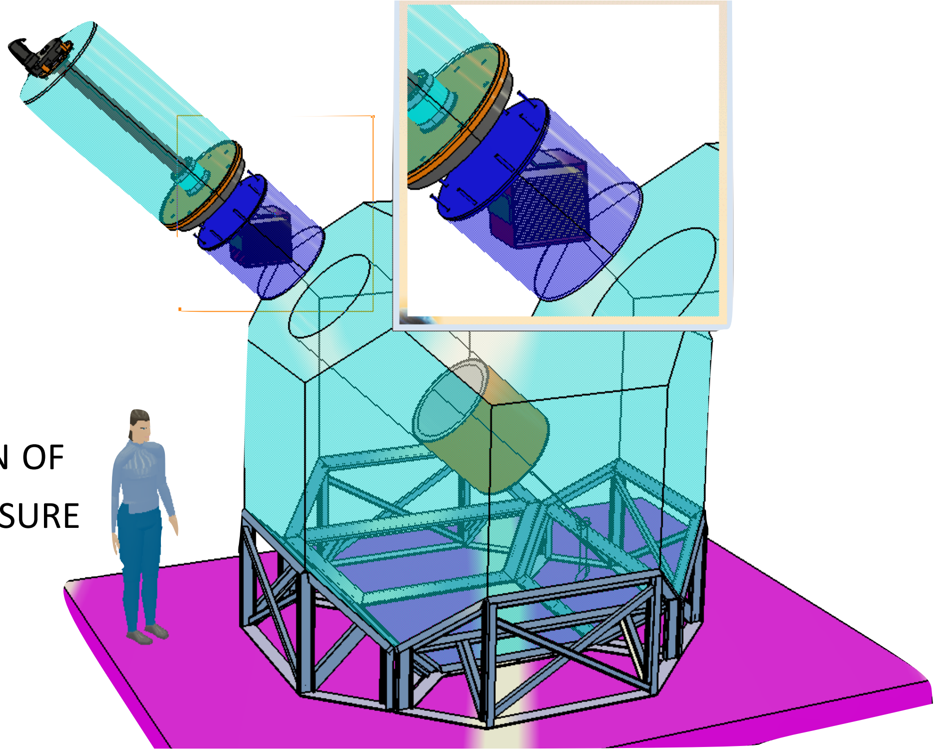

Resonant light scattering

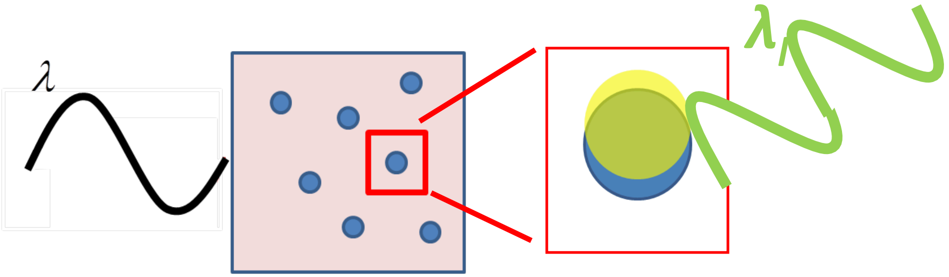

Nano-metal in medium $\boldsymbol{\varepsilon_d}$ Oscillation of e-cloud

$$E_l = \frac{3\varepsilon_d(\lambda)}{\varepsilon_m(\lambda) + 2\varepsilon_d(\lambda)} E_0$$

E_l intensity inside the metal

$$\varepsilon_m(\lambda_l) + 2\varepsilon_d(\lambda_l) \approx 0$$

$\boldsymbol{E_l}$ is resonance enhanced

Scattering spectrum depends on the light polarization and on the grain shape

H.Tamaru et al ., Applied Phys Letters 80, 1826 (2002)

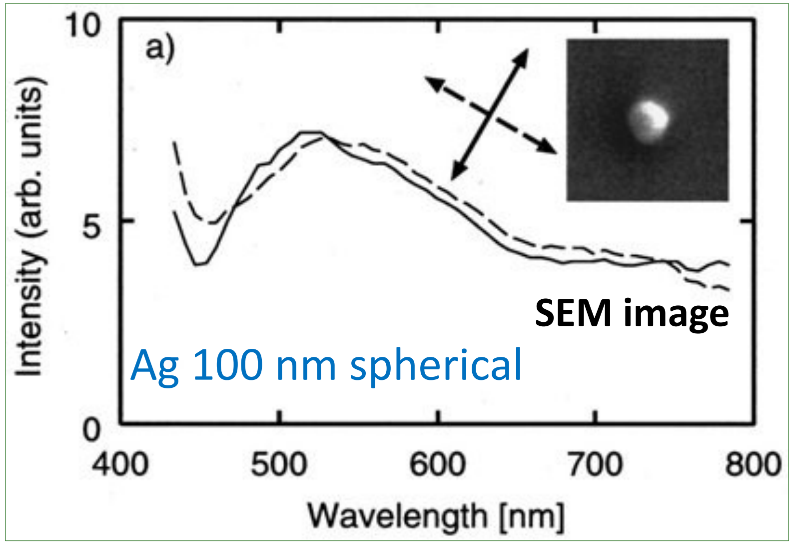

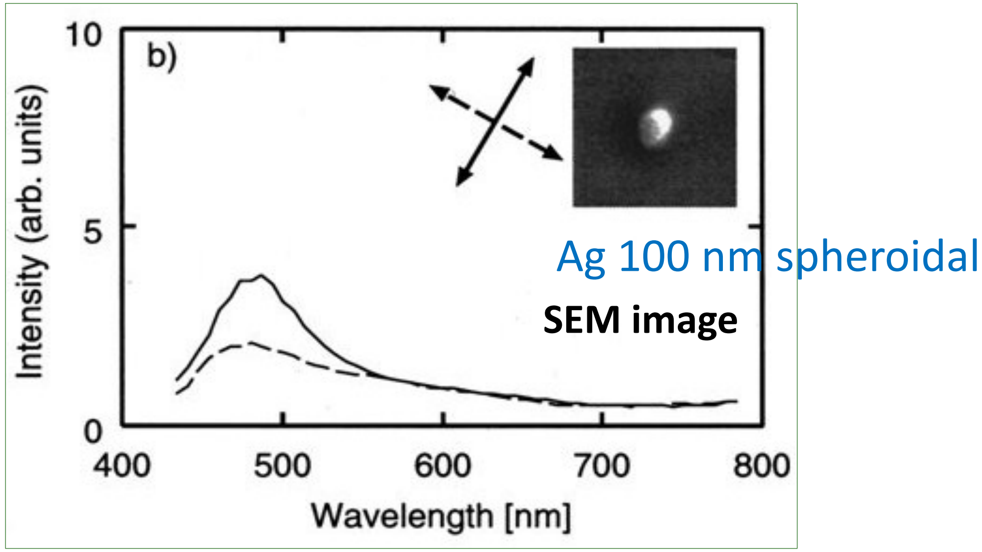

The polarization dependence of the resonance frequencies strongly reflects the shape anisotropy